Root Area Transition Zone – RATZ and Reduction O&M cost of WT blades

EUDP project 64015-0602 – Final Report

Date: 22-03-2019

Authors: Find Jensen[1], Margrethe Werk[1], Andrei Buliga[1], Theodoros Pardalakis[1], Christian Berggreen[2], Jacob Waldbjørn[2], John D. Sørensen[3], Yi Yang[3], Torben Lindby[4], Rune Kirt[5], Søren Horn[6], Lars J. Nissen[7], Mads Lübbert[7], Johnny Plauborg[8], Christian Løjtved[9], Birgit Junker[10], Nicolas Quievy[11], Hans Møller[12], Rikke Balle[13], Daniel Nies[14], Kai Grigutsch[15], Amilcar Quispitupa[16]

1: Bladena
2: DTU Mechanical Engineering
3: AAU Civil Engineering
4: LM Wind Power
5: Kirt x Thomsen
6: Guide2Defect aps
7: DIS Engineering
8: Total Wind
9: ECC
10: E.ON
11: Engie
12: EWII
13: Vattenfall
14: Nordex
15: UL (former DEWI OCC)
16: DNV G

List of Abbreviations

AAU	Aalborg University
AEP	Annual Energy Production
CBM	Condition-based Maintenance A maintenance strategy that recommends maintenance actions based on the information on the current damage severity.
CSSD	Cross Section Shear Distortion
CVI	Close Visual Inspection A close examination by visual and/or tactile means of an installation, assembly or specific item to detect damage, failure or irregularity.
DC	Damage Category Damage category is used to quantitatively characterize a damage by its size
EUDP	Energy Technology Development and Demonstration Program
FEM	Finite Element Method
G2D	Guide 2 Defect A database that contains various blades' failures, obtained from inspection reports. The failures are organized in different categories
GVI	General visual inspection A general examination by visual means of an interior or exterior area, installation, assembly or specific item to detect obvious damage, failure or irregularity.
ISP	Independent Service Provider
LE	Leading Edge The front side of the cross section that is facing the wind

LTT	Leading Towards Trailing The direction which points from the leading edge towards the trailing edge
NDT	Non-destructive testing Non-destructive testing is commonly used to localize and size defects in structures. The detection ability for the NDT method is defined as a function of a defect size, through probability of detection curves.
NREL	National Renewable Energy Laboratory
PM	Preventive Maintenance PM is the planned maintenance of plant infrastructure and equipment with the goal of improving equipment life by preventing excess depreciation and impairment.
PoD	Probability of Detection The probability of detection is used to quantify the ability of a non-destructive testing procedure for detecting a damage with a given size. For wind turbine blades, there are a few non-destructive testing procedures that are usually used.
O&M	Operation and Maintenance
RATZ	Root Area Transition Zone The zone between the root of the blade and the max chord area
TE	Trailing Edge The back side of the cross section
TTL	Trailing Towards Leading The direction which points from the trailing edge towards the leading edge
WP	Work Package
WT	Wind Turbine

Bladena
Universitetsparken 7
DK-4000 Roskilde
www.bladena.com

Table of Contents

Bladena
Universitetsparken 7
DK-4000 Roskilde
www.bladena.com

1 Project details

Project title	Root Area Transition Zone – RATZ and Reduction of O&M cost of WT blades	
Project identification (program abbrev. And file)	RATZ Project	
Name of the program	EUDP	
Project managing company/institution (name and address)	Bladena ApS, Universitetsparken 7, 4000 Roskilde, DK Project manager: Find Mølholt Jensen Mail: fmj@bladena.com	
Project partners	AaU Civil Engeneering DTU Mechanical Engineering Vattenfall E.ON Statkraft Engie EWII Total Wind A/S Blaest	DEWI OCC DNV GL Nordex LM Wind Power Guide2Defect Kirt x Thomsen DIS ECC
Bladena CVR	34208433	

1.1 Acknowledgement

Bladena and partners would like to acknowledge the Energy Development and Demonstration Program (EUDP) for financial support under the grant number: 64015-0602 RATZ Project. Furthermore, acknowledgement goes to LM Wind Power who has donated a LM58.7m blade to be used in the full-scale test and demonstration performed in the project.

Bladena
Universitetsparken 7
DK-4000 Roskilde
www.bladena.com

2 Short description of project objective and results

2.1 English version

The main objective of the RATZ project has been to develop and demonstrate the performance of the Floor™ technology which is intended to strengthen the root transition zone of wind turbine blades and thereby mitigate the risk of damages, defects and failures in this region. Three blades have been tested with and without the Floor™ technology.

1. Full-scale testing of an SSP34m blade at Blaest
2. Full-scale testing of an LM58.7m blade at Blaest
3. Large-scale testing of an SSP34m blade at DTU Mechanical Engineering

The full-scale tests confirmed that critical damages in this region may in fact occur during edgewise fatigue testing and that the use of the Floor™ technology is able to stop the damage progression. Further, the results confirm the findings from field inspections and from theoretical predictions using advanced software tools.

The second main objective of the project has been to develop methods to evaluate and optimize O&M costs. This part of the project has involved representatives from the entire value chain of the wind industry - WTOs, OEMs, certification bodies, ISPs, solution providers and universities - have all come together.

The WTO Blade Group Network has participated actively during the project meetings, workgroups and seminars. Focus has been on how to incorporate combined loading test scenarios in the certification process and how to use NDT methods to detect damages.

During this project, transverse cracks were studied with the conclusion that they are highly connected to panel bending. The large-scale testing performed at DTU showed that torsional load that arises from the combination of simultaneous edge and flapwise loading on wind turbine blades, increases the out-of-plane bending of the trailing edge pressure side panels in the max chord area with 57%. This finding is of key importance since it most likely is the main reason why so relatively many transverse cracks are found in the field on blades in operation.

2.2 Dansk Version (Danish version)

Det primære formål med dette RATZ projekt har været at udvikle og demonstrere effekten af Floor™-teknologien, som tilsigter at styrke rod transition zonen på vindmøllevinger og derved mindske risikoen for skader, defekter og svigt i denne region. Tre vinger er blevet testet med og uden Floor™-teknologien.

Bladena
Universitetsparken 7
DK-4000 Roskilde
www.bladena.com

1. Fuldskalatest af en SSP34m vinge hos Blaest
2. Fuldskalatest af en LM58,7m vinge hos Blaest
3. Storskalatest af en SSP34m vinge hos DTU Mechanical Engineering

Fuldskalatestene bekræftede, at kritiske skader kan faktisk opstå under kantvise udmattelsestests, og det ved brug af Floor™-teknologien er muligt at stoppe skadesudviklingen. Derudover bekræfter resultaterne fundene fra feltundersøgelser og fra teoretiske analyser udført ved brug af avancerede software-værktøjer.

Det andet hovedformål med projektet har været at udvikle metoder til at evaluere og optimere O&M udgifter. Denne del af projektet involverede repræsentanter fra hele værdikæden inden for vindmølleindustrien - WTO'er, OEM'er, Certificering, ISP'er, løsningsudbydere og universiteter er alle gået sammen.

Vingegruppenetværket af vindmølleejere har deltaget aktivt under projektmøder, arbejdsgrupper og seminarer. Fokus har været på, hvordan man kan inkorporere kombinerede belastningstestsscenarier i certifikationsprocessen, og hvordan man kan bruge NDT-metoder til at opdage skader.

Gennem projekte, er transversale revner blevet analyseret og konklusionen er at disse er relateret til panel bøjning. Stor-skalatesten udført på DTU viste at vridnings laster som opstår fra en kombination af kant og flapvise laster på vindmøllevinger, øger ud-af-plan bøjning af bagkant tryk på side panelerne i maks korde området med 57%. Denne opdagelse er et hovedresultat, da det sandsynligvis er hovedårsagen til hvorfor så relativt mange transversale revner er fundet i felten på vinger i drift.

Bladena
Universitetsparken 7
DK-4000 Roskilde
www.bladena.com

3 Executive summary

In this project focus is on the Root Area Transition Zone (RATZ or Root-Transition zone). The Root-Transition zone features a complex geometry with tapering panels in different directions. This makes the trailing edge transition zone vulnerable to out-of-plane deformations especially on medium-sized to large blades. Field damages in the trailing edge transition zone have been observed and documented under blade inspections and damages resulting in repeated repairs occuring in the same blade region during blade certification testing [1].

The continuous increase in size has a significant impact on blades' structural integrity, and as blades grow longer, the edgewise root bending moments increases with the power of 4 due to the increase in weight, if the theoretical scaling laws are used. The theoretical scaling laws imply that the blade mass is scaled up with a power of three, when the blade length increases [1], [2]. In practice, the industry has managed to optimize the blade weight, while the edgewise loading is scaled up by a power of around 3.5. However, since the annual energy production is scaled up by a power of two, a significant challenge arises for very large blades in terms of failure, especially at the root-transition-zone.

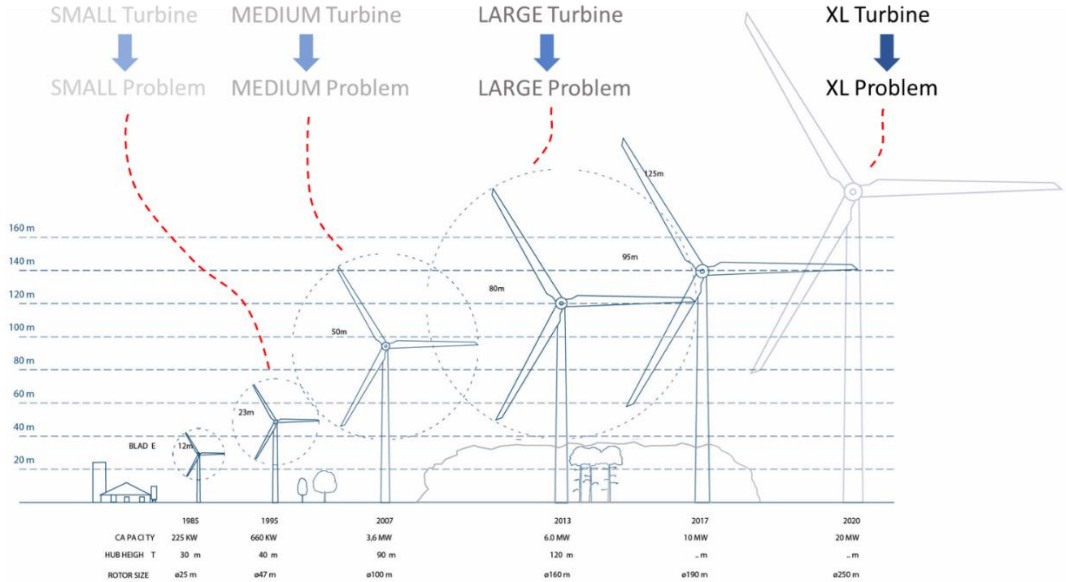

Figure 1: As blades grow in size the structural failure modes become rapidly more critical.

The challenges in the trailing edge root-transition zone is expected to grow as blades grow in length and weight. The LM58.7m blade tested in this project can already be considered a

Bladena
Universitetsparken 7
DK-4000 Roskilde
www.bladena.com

small to medium-sized blade. When the blades increase in length, the need for a solution to accommodate the increased forces in the Root-Transition zone is required.

The RATZ project has demonstrated proof-of-concept for the Floor™ technology. Bladena will seek to implement the Floor™ solution in new-designs of blades working together with manufacturers and in selected cases as a retrofit solution in blades that have experienced serious defects during operation. The Floor™ solution offers a significant structural enhancement of the trailing edge transition zone. In fact, similar enhancements have already been deployed for many years in other industries, such as ship building. Having achieved a stronger Root-Transition zone several opportunities open-up to reduce production costs and/or increase energy output.

In Figure 2 the Floor™ technology owned by Bladena [3].

A) The Floor™ technology

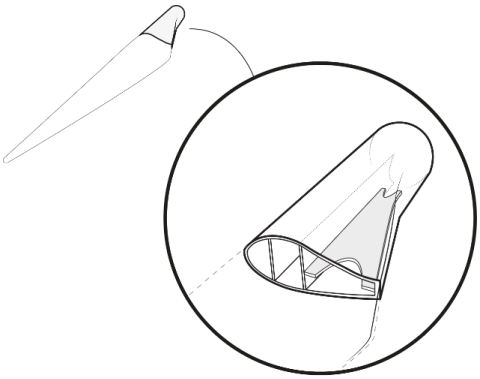

B) Floor™ installed in an SSP34m blade.

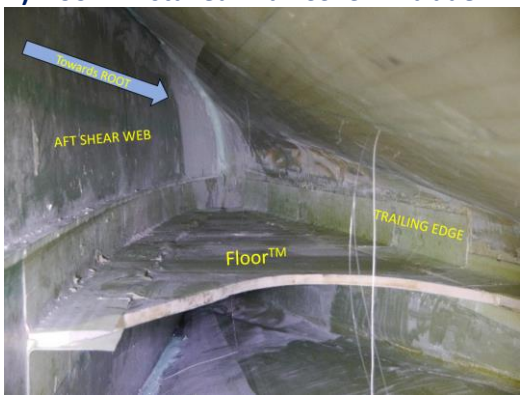

C) Floor™ installed in an LM58.7m blade.

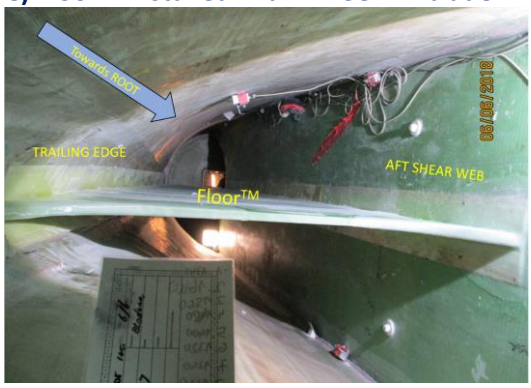

Figure 2: A) The Bladena Floor™ technology works as a horizontal shear web installed between the aft shear web and the trailing edge on the Root-Transition zone of a wind turbine blade. B) Floor™ is retrofitted in an SSP34m blade. It can be seen how the aft shear web spans out and connects with the trailing edge/blade root. C) Floor™ is retrofitted in an LM58.7m blade. The retrofitted Floors™ in the SSP34m blade and the LM58.7m blade are used for demonstration purposes in the RATZ project [4] [5] [6].

Bladena
Universitetsparken 7
DK-4000 Roskilde
www.bladena.com

The Floor™ supports the complex geometry in the Root-Transition zone and reduces local deformations of bending in the trailing edge panel. The Floor™ solution adds a small amount of material to the weight. However, the increased structural strength - provided by the Floor™ - implies that material can be taken out of the blade panels, the net result being that the collective mass amount will be reduced. With less material in the blade the production cost is expected to be reduced, without including the cost of the extra element and extra joint. Therefore, it is expected that manufacturers will be interested in discussing cost-out projects with Bladena, using the Floor™ technology.

The structural reinforcement of the Root-Transition zone would allow for a wider max chord design, thereby increasing power output of the wind turbine. The increased aerodynamic output is not part of this project, but theoretically it should be possible to increase the AEP with up to 6%, see Figure 3.

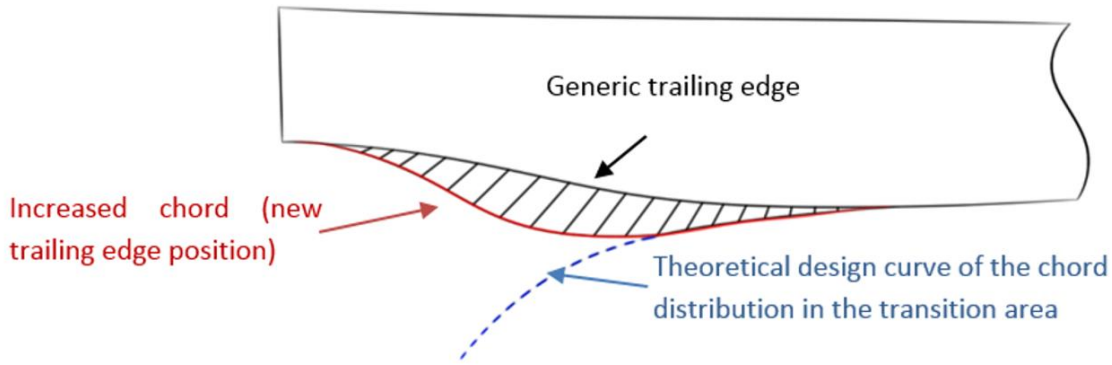

Figure 3: The max chord itself can be increased in width and/or the max chord can be moved closer to the blade root. Both solutions will result in a higher AEP.

Together with LM Wind Power and Blaest (Blade test center in Aalborg, Denmark) Bladena has carried out a full-scale test on an SSP34m blade and an LM58.7m blade with edgewise fatigue loads [4] [6]. The first blade to be tested was the SSP34m blade and in Figure 4 the damage developed during test in the Root-Transition zone can be seen.

Bladena
Universitetsparken 7
DK-4000 Roskilde
www.bladena.com

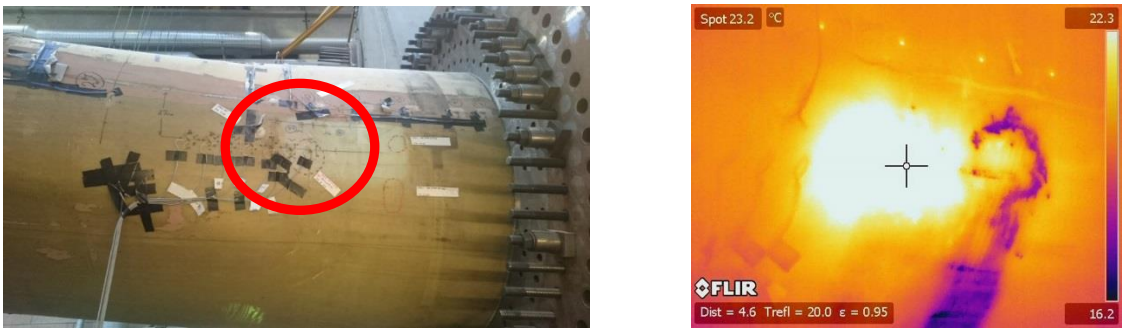

Figure 4: Left: Damage on the SSP34 blade, observed by visual inspection. Right: Thermographic photo of the same damage. The temperature at the damage location has been greatly increased.

The LM58.7m blade was severely over-tested to obtain the TE damage needed to demonstrate the function of the floor. Thus, the blade has shown sufficient strength to pass certification test load level. The blade performance was monitored by visual inspection and thermographic inspection performed by Blaest as well as Ultra Sound Scanning performed by Force Technology. Damages developed during fatigue in the predicted area in trailing edge transition zone, see Figure 5.

A)

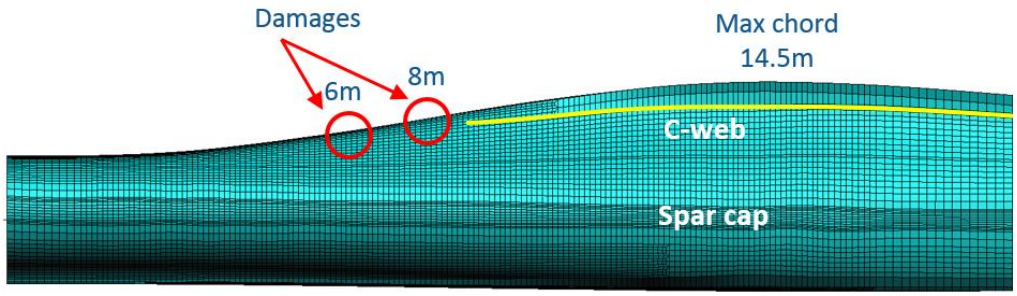

B)

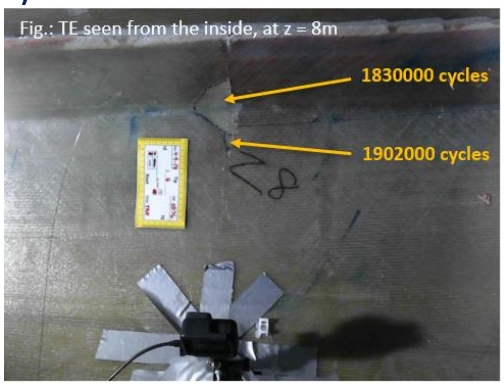

C)

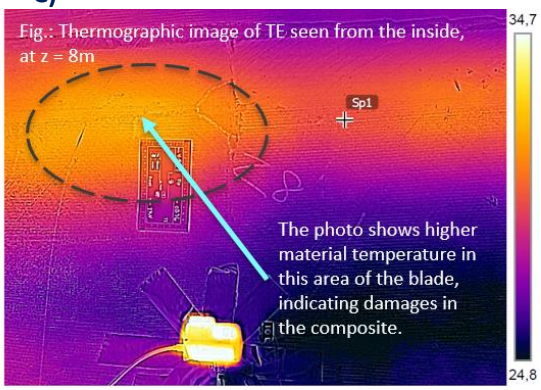

Figure 5: A) The FEM model of an LM58.7m blade shows the blade from root to beyond max chord. Damages at the trailing edge of the LM58.7m blade were found at 6m and 8m from the blade root. B) Visual inspection of the blade shows damage grows on the LM58.7m blade tested in Blaest with high fatigue loads. C) Thermographic inspection confirms activity inside the blade material resulting in heated areas.

Bladena
Universitetsparken 7
DK-4000 Roskilde
www.bladena.com

After damages had been observed in the LM58.7m blade, the Floor™ was installed in the blade and the edgewise fatigue loading was continued for another 1 million cycles. During this extended testing, the progression of the damage was stopped, demonstrating that the Floor™ prevents damage growth in the trailing edge transition zone region.

As part of the standardization work package a full-scale test with a high static combined loading (combination of flap- and edgewise load) has been performed on the LM58.7m blade, see Figure 6.

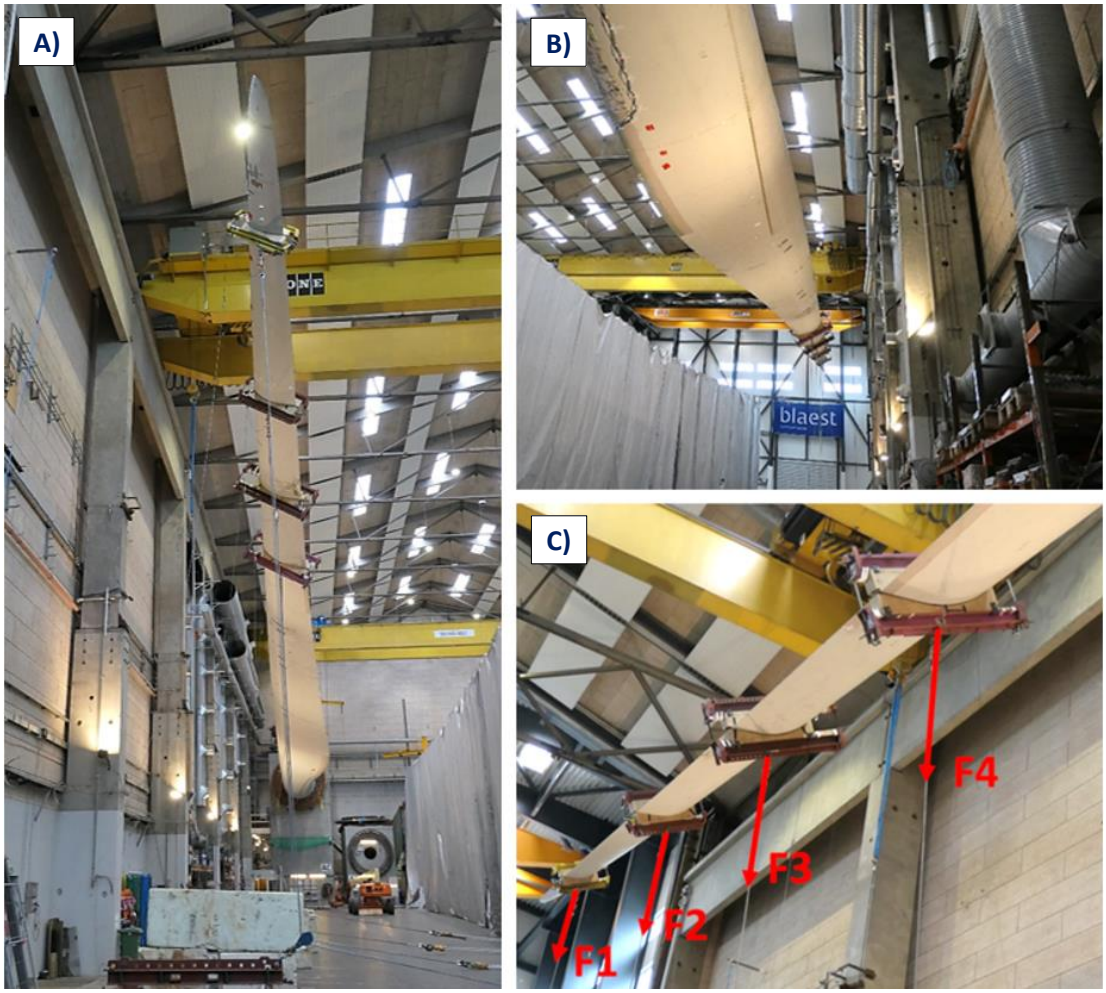

Figure 6: A) and B) The full LM58.7m blade can be seen with clamps in the outer 40% of the LM58.7m blade. The blade is angled to accommodate the combined edge/flap load towards the floor. C) Red arrows are showing the force directions working on the clamps (by means of wires).

Combined loading is intended to simulate the real-life extreme load scenario of the blade. The principle of the combined loading test is included in “Owners Requirements” criteria, which a group of large WTOs are working on now. Today, the certification test requirements

Bladena
Universitetsparken 7
DK-4000 Roskilde
www.bladena.com

do not require tests with combined loading. The purpose of the combined static test was to see if a medium-sized blade as the LM58.7m can withstand a static combined high load. The test setup has included the criteria, that the blade had to be able to locally deform freely as it would under field operation. The LM58.7m blade succeeded in maintaining its structural integrity during a series of combined loading tests. This shows that it is a feasible task to demand combined load testing of wind turbine blades as part or add-on to the certification process.

At DTU Mechanical Engineering an extensive sub-structural test of a 15m blade section of an SSP34m blade has been performed in the DTU Structural Lab test facilities at DTU Lyngby Campus. In addition to the fatigue testing of a blade section with and without the Floor™, the large-scale test has also been used to apply an advanced loading setup consisting of hydraulic actuators applied at the cut blade cross section, see Figure 7. This setup allows mimicking of a range of extreme and advanced loading conditions, which can be challenging to apply in conventional full-scale blade test centres, especially for large blades. The basic large-scale test setup can be seen in Figure 7.

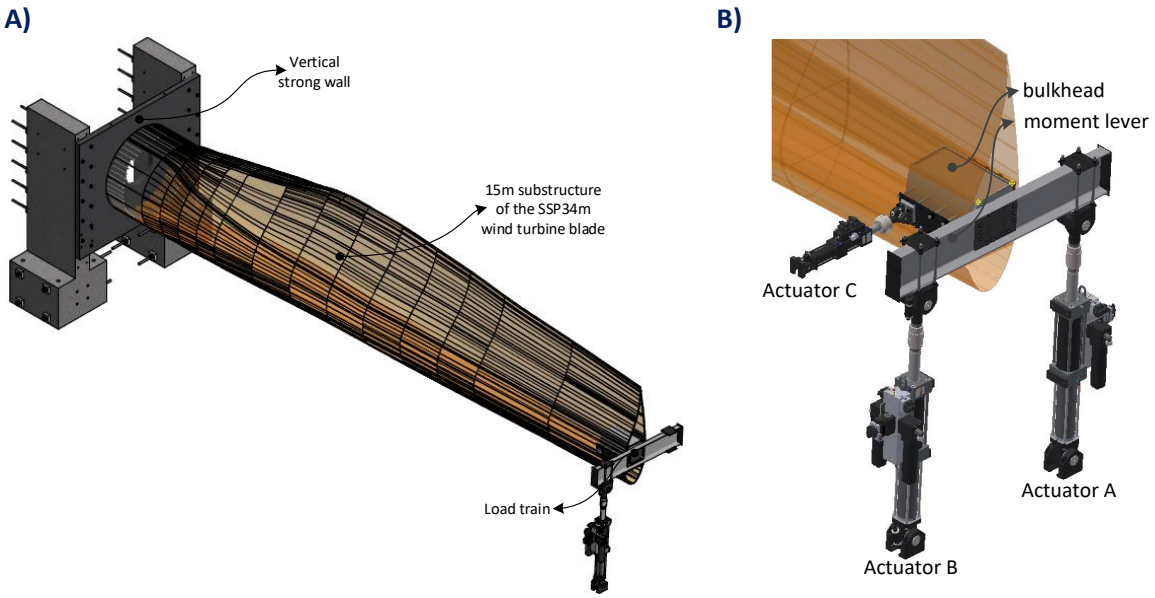

Figure 7: A) The 15m blade section of an SSP34m blade is fixed at the root from two concrete towers connected with an anchor plate. B) At the 15m blade section, three actuators are connected to the blade using an insert into the spar-box of the blade. The actuators can introduce any combination of edgewise, flapwise and torsional forces on the blade.

The large-scale method of limiting the blade testing to the inner structural section of the blade and the mechanical load application method using structural actuators will possibly prove to be a big advantage for test centres regarding future testing of large blades. By only testing the inner structural blade section, three immediate advantages are prominent:

Bladena
Universitetsparken 7
DK-4000 Roskilde
www.bladena.com

1) It will be easier and more cost effective to handle a blade section than a full blade.
2) The mechanical load application using structural actuators can apply any combination of edgewise, flapwise and torsional loads. This is not possible with conventional exciter-based fatigue loading.
3) The inner structural blade section is where most critical blade damages develop, due to the root-bending moment scales up faster than the mass increases and therefore, it is the root/transition zone that needs to undergo extensive testing.

Furthermore, on a longer time perspective, the possibility to apply any combination of loads at the blade cross-section using structural actuators, as seen in Figure 7, will make it possible to apply advanced hybrid testing technology for blade testing, where the outer part of the blade is simulated by a numerical model with potentially any loading condition applied. The simulation model, representing the outer blade region in a hybrid test, is actively controlling the structural actuators using input from sensors applied on the inner blade section being physically tested by the actuators. Hybrid testing will therefore make it possible to test a blade section under any arbitrary loading on the full blade. The hybrid testing technology has also been a part of the RATZ project, where the technology has been further developed for blade testing. Further details have been documented in academic journal papers.

Defects and damages in the transition zone may during operation develop and ultimately result in failures requiring exchange of the blade. Proactive and preventive inspections and maintenance can be a cost-effective approach to mitigate defects and damages. With the aim to develop methods and tools to minimize the costs for inspections, maintenance, repairs and replacement of wind turbine blades, the work in the Cost and Reliability work package has mainly been related to the package 'Optimized cost and risk solution' as illustrated in Figure 8.

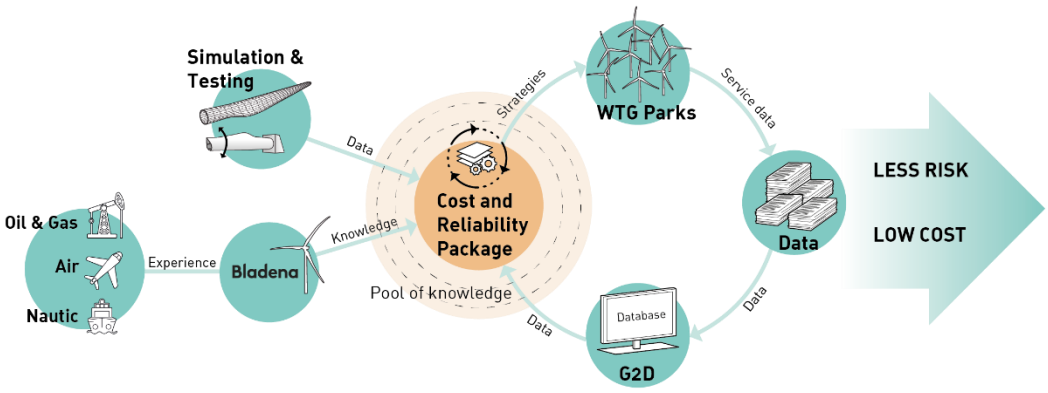

Figure 8: The motivation behind the Cost and Reliability package. A specific issue can have different solutions and strategies to obtain the best outcome in terms of technical but also cost efficiency. The development of the package aims to process an issue with respect to technical assessment and cost and risk performance, in order to offer the user an optimized strategy both in technical terms but also in cost and risk.

Bladena
Universitetsparken 7
DK-4000 Roskilde
www.bladena.com

RELIABILITY is an important part of the Cost and Reliability work package. Development of cracks and damages as function of time is subject to uncertainty, and therefore a probabilistic model is needed to describe this random behaviour. Two approaches have been considered in this project, namely a probabilistic fracture mechanics approach, and a reliability model based on a discrete Markov Chain modelling. The Markov Chain model has the advantage that it can easily be related to the discrete damage categorization used by many wind turbine owners. The disadvantage is that such a model only approximately can represent time-invariant uncertainties, e.g. model uncertainties, which on the other hand is possible by the more complicated probabilistic fracture mechanics model. A methodology is developed to calibrate the transition probabilities in the Markov Chain model using theoretical considerations from fracture mechanics and data from the inspection database Guide2Defect. Using the Markov Chain reliability model, it is possible to simulate lifetime realizations of cracks / damages which can be used for decision making as described in the following.

A framework for cost-optimal decision making with respect to planning of inspections and maintenance is developed and implemented for illustration in a tool. The approach is that different strategies for inspection type and time intervals and for maintenance/repair/replacement are selected, see Figure 9. For each of the strategies a generic COST mode is available for cost related to inspections, downtime, repairs, etc. The theoretical basis for the approach is the so-called pre-posterior Bayesian decision making which is used in other industries such as for Oil&Gas offshore platforms for cost-optimal planning of inspections.

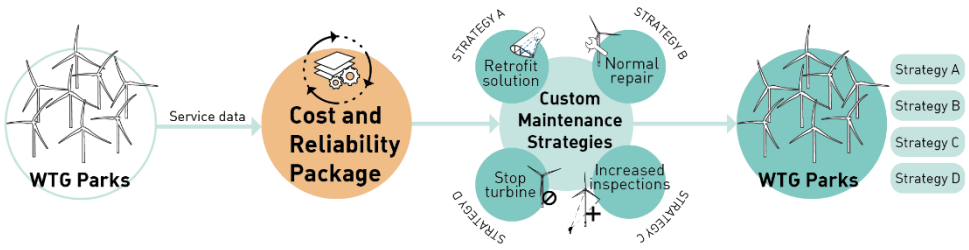

Figure 9: The Cost and reliability package receives data from the wind turbine fields through Guide2Defect The Cost and reliability package can be used to estimate the most cost optimal strategies for specific wind turbine fields. Bladena gather knowledge not only from the wind industry but also from other industries such as oil and gas, the aircraft and the marine industry. The structural knowledge from Bladena are part of the building tools in the Cost and reliability package.

Combining simulations of a large number of realizations of potential damages / cracks with the selected strategies for inspections and repairs and the cost models the expected total costs in the remaining lifetime can be estimated, and the optimal strategy is the one with the lowest expected costs.

Bladena
Universitetsparken 7
DK-4000 Roskilde
www.bladena.com

Case studies illustrating the potentials of the cost and reliability package is developed. Some of the applications of the package are to support decisions on which inspection method to choose accounting for the cost and reliability of the inspection method, how long inspection time intervals can be used without increasing the maintenance costs too much, and which maintenance and repair strategy to use. It is also possible to simulate a strategy where no inspections and no maintenance are performed, and thereby estimate the Value of Information (VoI) obtained by a selected inspection and maintenance strategy.

In addition to data sets of inspected damages with associated repairs, theoretical deterministic models based on fracture mechanics, able to predict the damage size and criticality, can also be used both to predict the criticality of a specific damage at a certain point in time for a single blade, but when combined with reliability and risk analysis such models can be used to develop probabilistic damage assessment procedures, which are generic and able to be applied for any blade type and operational profile.

The work associated with damage tolerance in the RATZ project has been aimed at two different main focus areas, but where all activities have been on a preliminary investigative level. The focus areas include:

1) Doing preliminary investigations on the use of fracture mechanics for the analysis of damage tolerance for design of new blades, as well as damage assessment of blades in operation exposed to in-service damage, linked to new blade design standards from DNV-GL 2015, which have opened up for an optional use of fracture mechanics [7]. The actual work in the RATZ has been aimed at determining suitable fracture characterization methods for sandwich face/core interfaces (as an example), as well as developing analysis models and validating these models against component and full-scale tests in close cooperation with the work package on sub-component/structural test.
2) Initiating work on simplified fracture mechanics based models, which are sufficiently simple, so that they can be used in connection with reliability and risk analysis. The work has been carried out in cooperation with the work package on cost and reliability analysis and has been initiated based on existing analytical fracture models from the literature and are still on-going.

Bladena
Universitetsparken 7
DK-4000 Roskilde
www.bladena.com

4 Project objectives

4.1 Main project objectives and implementation

The main activities in the RATZ project include five areas:

1. Test and demonstration of the Floor™ technology
2. Standardization and combined loads
3. Fracture mechanics modelling and testing
4. Cost and reliability strategy development
5. Knowledge platform for the value chain

Test and demonstration of the Floor™ technology

The main objective in the RATZ project has been to demonstrate the Floor™ technology as a solution to structural challenges in the root area transition zone. Two wind turbine blades, a 34m blade from SSP and a 58.7m blade from LM Wind Power, have been tested at Blaest test center. Both blades have been tested in edgewise fatigue tests with and without the Floor™ installed.

Furthermore, a second SSP34m blade has been tested in the large-scale test facilities (DTU Structural Lab) at DTU Mechanical Engineering in at DTU Lyngby Campus. This blade was also tested with and without Floor™. This blade was also exposed to fatigue loads but the testing also included several different load combinations.

The objective of the three fatigue blade tests has been to demonstrate that the Floor™ significantly reinforces the transition zone in blades, which constitute a challenging part of the blades. Further, to demonstrate that the Floor™ prevents fatigue damages in the blade shells, and if such damages have already occurred the installation of the Floor™ as a retrofit solution will prevent any further growth of these damages.

The actual Floor™ solution that was installed in the SSP34m blade and the LM58.7m blade required early product development of the Floor™ prototypes. The product development includes the design of the Floor™ and the optimal position of the Floor™ in specific blades. This work has been heavily supported by FEM simulations.

Standardization and combined loads

As blades increase in size the demand for complex (realistic) loading under the certification process increases significantly. Motivated by current IEC rules, where combined loading is not demanded for certification tests of wind turbine blades, two types of blades have been tested

Bladena
Universitetsparken 7
DK-4000 Roskilde
www.bladena.com

with combined loading, both with static and fatigue loads. The objective has been to develop and evaluate new load application methods for both static and fatigue testing. A 15m SSP34m blade section was tested with a complex (realistic) fatigue load scenario taking both edgewise, flap wise and torsional loads into account. A LM58.7m blade was tested with a combination of high static loading and the blade only had load clamps in the outer region of the blade, which allow for free movement of the blade profile in the inner part of the blade.

The main objective of the large-scale test has been to develop a new test setup which demonstrate that only the inner part of a blade is needed in order to reach the realistic cross-sectional deformations, e.g. bending of trailing edge panels. Out-of-plane panel deformations generate critical peeling stresses in bond lines and interlayer stresses between layers such as the sandwich face sheet and the sandwich core material. This way of testing a wind turbine blade is expected to be used by commercial test centers and manufacturers in the future.

As the second part of the standardization work package a relatively large blade, namely the LM58.7m blade, has been tested with combined static loading and a load application method with added torsion to the blade and allowed for free deformation in the inner structural part of the blade. The purpose of the test has been to show, that a large blade can be tested with high combined loading only applying loads in the outer region. This could therefore be a future add-on criterion to certification loading. The purpose of the test was further to evaluate the effect the newly developed way of applying the loading on the blade. The full-scale test was executed at in collaboration of Bladena, Blaest and LM Wind Power.

Fracture mechanics modelling and testing

To understand damage development in composite materials fracture mechanics is an indispensable tool. When it comes to wind turbine blades there are a strong need to understand the severity of damages identified during field inspection and in particular to obtain critical knowledge on the manners in which face sheet debonding or cracks in general will/ or will not develop to critical levels for the structural integrity of the blade. Fracture mechanics modelling and testing at DTU Mechanical Engineering have been used to investigate these questions.

As part of the large-scale test of the SSP34m blade, face sheet debonding in the trailing edge panels at the max chord area has been tested. Using a combined numerical and experimental approach, fracture mechanics has been used to estimate the growth rate of cracks for different sizes of debonded areas. Based on results from the fracture mechanics analysis, a debonded area was created and has been introduced in the 15m section of the SSP34m blade. With this approach by inclusion of fracture mechanics modelling and testing to gain

Bladena
Universitetsparken 7
DK-4000 Roskilde
www.bladena.com

knowledge on damage growth and apply these results as input for the Cost and Reliability package developed by AAU.

Cost and reliability strategy development

AAU has developed a framework for assessment of Cost and Reliability. The framework helps to minimize expenses for maintenance and repair and to develop improved decision making for maintenance strategies. Focus has been on the two key topics in the RATZ project: Structural challenges in the Root-Transition zone and Transverse cracks at trailing edge panels.

Knowledge platform for the value chain

The RATZ project has also included activities related to the dissemination of knowledge and awareness in the wind industry about the structural issues caused by the increasing size of wind turbine blades.

This work has identified the need to develop a set of additional criteria for the certification testing of large wind turbine blades. This work has been labelled “Owners Requirements” because the additional criteria are meant to be included in the specifications used by the WTOs when they purchase new blades. The combined static full-scale test of LM58.7m blade has been done in relation to Owners Requirements, and the large-scale fatigue testing with combined loads may one day replace the sub-component fatigue test program, which is also part of Owners Requirements.

4.2 Risk in the project

One of the first obstacles facing the project was to find a 60m blade for full-scale testing. LM Wind Power solved this challenge by donating a LM58.7m blade to the project and transport was arranged and paid by TotalWind. LM Wind Power also accepted to take the blade back after the testing was completed, hence the project has no cost on scrapping the blade.

Another challenge was the design of the Floor™ prototypes. The Floor™ technology is meant as a solution to be used in new-design of wind turbine blades. In this project the Floor™ solution was retrofitted in already produced blades. The Floor™ boundary (bondline towards the trailing edge) used in the LM58.7m blade in the edgewise fatigue test was not designed to withstand the high edgewise forces and in the first try, failure happened in the bondlines connecting the Floor™ to the trailing edge of the blade. The test was successfully completed after a mechanical connection was implemented, see Figure 14.

Bladena
Universitetsparken 7
DK-4000 Roskilde
www.bladena.com

4.3 Milestones

12 Technical milestones (TM) and 4 Commercial Milestones (CM) was defined prior to the project start and used to keep the momentum and direction of the project.

Technical Milestones		
TM1:	**Full-scale test of 34m blade without reinforcement completed (WP5)**	DONE
TM2:	**First retrofit of Floor done (WP9)**	DONE
TM3:	**Development of FEM models (WP6)**	DONE
TM4:	**O&M model runs with real data including catastrophic failures (WP12)**	DONE
TM5:	**Start testing blades with implemented floor (WP3)**	DONE
TM6:	**Animation #1 - Technical Problem Highlighted (WP11)**	DONE
TM7:	**Large-scale sub-structural testing of 15m blade section without reinforcement completed (WP4)**	DONE
TM8:	**Large-scale sub-structural testing of 15m blade section with reinforcement completed (WP4)**	DONE
TM9:	**Large-scale sub-structural hybrid testing of 15m blade section with reinforcement completed (WP4)**	DONE
TM10:	**Fracture mechanical characterization completed (WP7)**	DONE
TM11:	**Generic business case for each relevant market segment (WP12)**	DONE
TM12:	**Software tool (WP12)**	DONE
Commercial milestones		
CM1:	**Identification and handling of market barriers for Floor Solution (WP10)**	DONE
CM2:	**Animation #2 - Solution Presented (WP11)**	DONE
CM3:	**Guideline in Lifetime Prediction (WP1)**	DONE
CM4:	**Guideline: How to use the new DNV GL Guideline with Fracture Mechanics (WP7)**	Replaced*

*CM4 has been replaced with two fracture mechanic workshops and an artificial damage introduced on a SSP34m blade in Lyngby.

The project has followed the project plan except for three months delay. The delay was caused by the fact due to the fact that the RATZ partner/company TotalWind went into bankruptcy during the project. This problem was solved when another company volunteered to do the work of TotalWind. As a result, another company able to install the Floor™ in the LM58.7m blade had to be found.

Bladena
Universitetsparken 7
DK-4000 Roskilde
www.bladena.com

5 Project results and dissemination of results

The five main areas in the RATZ project are the following:

1. Test and demonstration of the Floor™ technology
2. Standardization and combined loads
3. Fracture Mechanic modelling and testing
4. Cost and Reliability strategy development
5. Knowledge platform for the value chain

Below the activities and key results under each area will be highlighted and explained.

5.1 Test and demonstration of the Floor™ technology

The Root-Transition zone, defined as the geometric transitions from the round blade root to the aerodynamic blade profile, has shown to be a structurally challenging area of a wind turbine blade. This is because of the complex geometry with tapering panels in different directions and with double-curved properties

The Root-Transition zone is shown in Figure 10 as well as a retrofitted Floor™.

A) **B)**

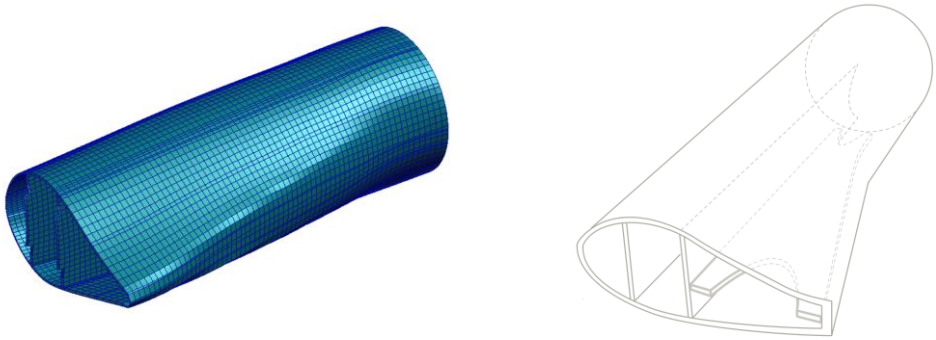

Figure 10: A) The Root-Transition zone of a wind turbine blade can be seen to be the transition between the round blade root and aerodynamic blade profile, typically ending before max chord. B) The Floor™ are designed to be retrofitted in the Root-transition zone of a wind turbine area between the aft shear web and the trailing edge. Here can be seen the first prototype of a Floor™ retrofitted in the SSP34m blade.

Further, the transition zone is where the edgewise shear forces are at their maximum, see Figure 11.

Bladena
Universitetsparken 7
DK-4000 Roskilde
www.bladena.com

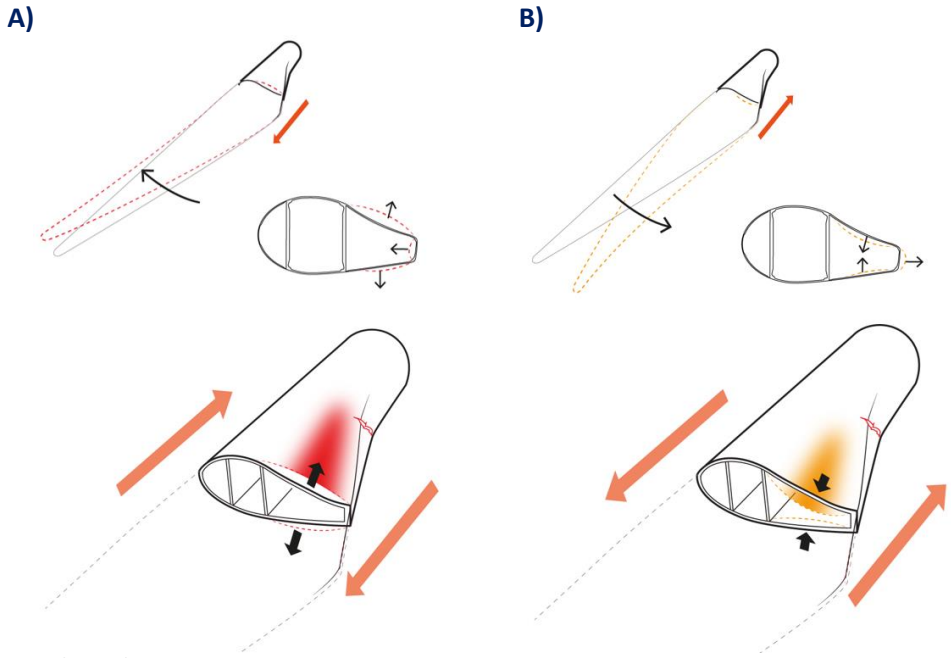

Figure 11: In A) and B) the two outer positions of a blade in edgewise fatigue is shown. The edgewise fatigue loading of a wind turbine blade will result in both global and local deformations. In the figure the high shear forces in the blade Root-Transition zone are marked with orange arrows and the local deformations out-of-plane are shown with black arrows. A crack due to fatigue can be seen forming in the trailing edge of the Root-Transition zone.

Damages and structural collapses in the Root-Transition have already been documented in the field and under blade testing. In the future, this is expected to be an even more severe challenge because as blades scale up in length, the edgewise root bending moments increases with the power of 4 due to the increase in weight, when the mass scales up with a power of 3.

To demonstrate the performance of the Floor™ technology and the positive effect of the Floor™ solution in the Root-Transition zone, three wind turbine blades have been tested in fatigue with and without the Floor™ technology:

1. Full-scale testing of a SSP34m blade with fatigue loads at Blaest
2. Full-scale testing of a LM58.7m blade with fatigue loads at Blaest
3. Large-scale testing of a SSP34m blade with fatigue loads at DTU

The Floor™ technology is intended to strengthen the Root-Transition zone of wind turbine blades and thereby mitigating the risk of damages and failures in this region. Both full-scale tests and the large-scale fatigue test confirmed that critical damages in this region may in fact occur during edgewise fatigue testing, and that the use of the Floor™ technology is able to stop the damage progression. The test results confirm the findings from field inspections and from theoretical predictions using advanced software tools.

Bladena
Universitetsparken 7
DK-4000 Roskilde
www.bladena.com

Key results from the blade tests will be highlighted in the next sections. For more information on the two full-scale tests, see Appendix D and Appendix E.

Floor™ product development

The Floor™ product was originally meant to be a part of new-designs for large wind turbine blades. In the RATZ project the tested Floors™ have been designed essentially as retrofit solutions. The Floor™ designs have been supported by FEM simulations and retrofitted in two SSP34m blades and one LM58.7m blade, see Figure 12.

A) Floor™ prototype #1
SSP34m blade, Blaest

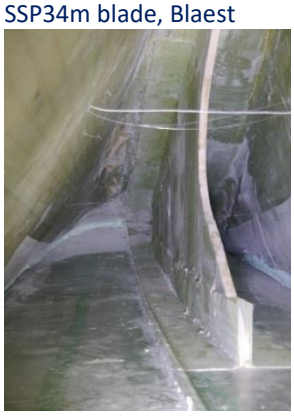

B) Floor™ prototype #2
SSP34m blade, DTU

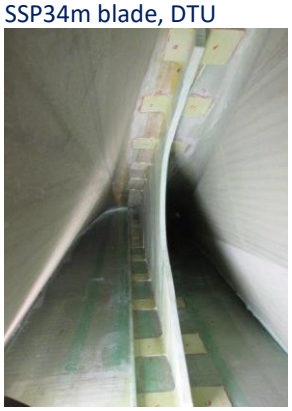

C) Floor™ prototype #3
LM58.7m blade, Blaest

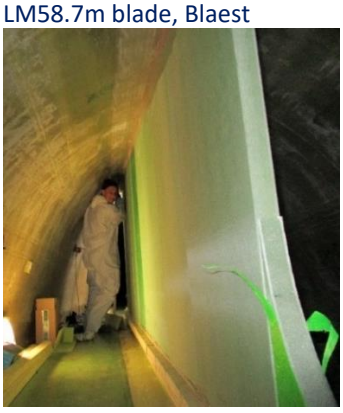

Figure 12: A) and B) Prototype #1 and #2 are both designed to be retrofitted in a SSP34m blade. For each prototype, experience is gathered and used in the design for the next prototype. C) The Floor™ prototype are retrofitted in the LM58.7m blade which are almost twice as long as the SSP34m blade.

Three Floors™ has been designed, retrofitted in blades and tested in fatigue during the RATZ project. The largest Floor™ was 6m long and installed in the LM58.7m blade, see Figure 12c and Figure 13.

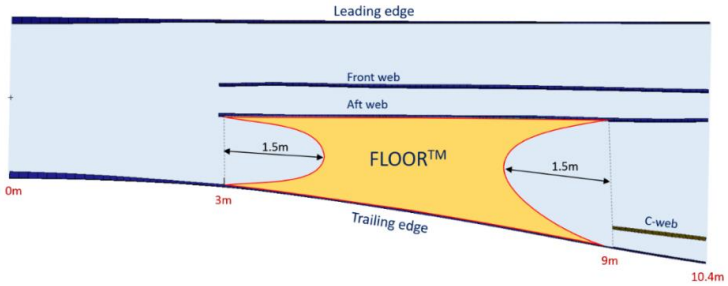

Figure 13: The Floor™ in the LM58.7m blade started 3m from blade root and ended just before the start of the C-web 9m from blade root. In each end of the Floor™ a "fish-mouth" was introduced to prevent local stress concentrations.

Bladena
Universitetsparken 7
DK-4000 Roskilde
www.bladena.com

Full-scale edgewise test of LM58.7m blade with fatigue loads

The Floor™ boundary (bondline towards the trailing edge) used in the LM58.7m blade in the edgewise fatigue test was not able to withstand the high edgewise forces and in the first try, failure happened in the bondlines connecting the Floor™ to the trailing edge of the blade, see Figure 14A.

Figure 14: A) The connection of the Floor™ to the trailing edge in the LM58.7m blade has disconnected from the trailing edge. In a video the gap marked by red lines can be seen opening and closing during the fatigue test. B) A mechanical solution with steel strips and bolts was implemented and the fatigue test continued.

The test was successfully completed after a correction of the design had been implemented, see Figure 14B.

The Floor™ is originally meant as a new-design product and the boundaries must be a part of the new blade design to withstand the high forces, so if the Floor™ should be used as a retrofit solution either the mechanical solution or an alternative connection need to be developed. In case this is chosen, an improved solution needs to be developed, e.g. a solution which does not contain any metallic parts.

In the other adhesive connection between the aft shear web and the Floor there was no problem. From both video documentation and measurements, it could be concluded that there was no visible or detectable deformation in this joint. Thus, the critical joint is only located in the trailing edge region. For more information on this full-scale test, with and without the Floor, see Appendix D.

Full-scale edgewise test of SSP34m blade with fatigue loads

A 34m blade from SSP-Technology was the first blade which was tested in the project. Edgewise dynamic loading was applied, see Figure 15.

Bladena
Universitetsparken 7
DK-4000 Roskilde
www.bladena.com

A)

B)

C)

D)

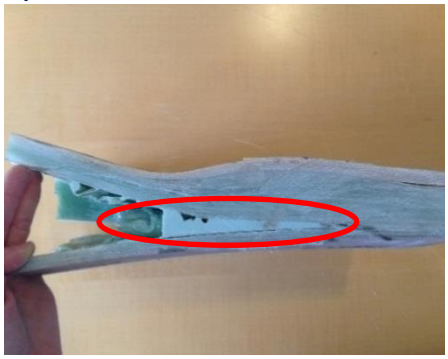

Figure 15: A) Edgewise fatigue test with a rotating mass placed midspan of the blade B) A damage was detected in the Root-Transition zone both by NDT-techniques and different sensors e.g. Strain gauges. The damaged area is marked with a red circle, which is impossible to see on the picture, but measurement, movie and cut-out of the blade afterwards, showed no doubt that a large area has been damaged. C+D) After the test was completed, the blade was cut up in pieces and it was confirmed that the other laminate was debonded for the load carrying structure.

The full-scale fatigue test showed the same damage development in the Root-Transition zone as tested on another SSP34m blade tested as part of a certification process in 2001, see Figure 16.

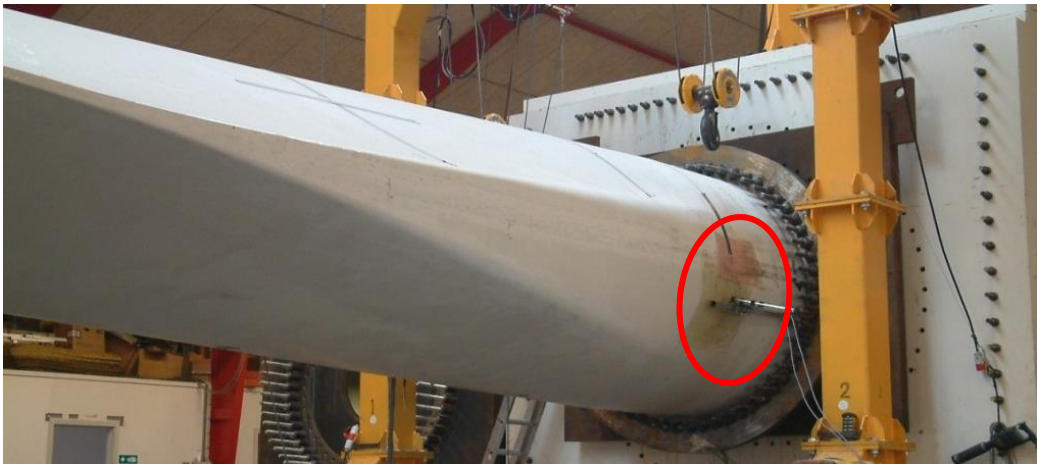

Figure 16: A SSP34m blade tested in a certification test in 2001 under similar load conditions. The damage which arose in the Root-Transition zone, marked by the red circle, was visible at the surface, after the blade had been repaired.

Bladena
Universitetsparken 7
DK-4000 Roskilde
www.bladena.com

The damage developed in in a similar way and in the same location, in two “identical´” blades, shown in Figure 15 and Figure 16. During a fatigue test -in a controlled test environment - the possibilities to observe damages are significantly higher, than if the blade is installed on a turbine. First, the blade is static during up tower inspection, and delaminated laminates will therefore bend outwards when loaded and cannot be seen. Also, noise originating from crack development, can obviously not been observed during up tower inspection, while during a fatigue test, noise from crack development is an important signal that crack is developing under the surface and between the layers. When noise was detected, a number of strain gauges were mounted in the damage area in order to measure the growth of the damage. This was done to ensure that the test would stop, before any catastrophic failure occurred in the blade in order to be able to initiate the next part of the experiment (with the Floor inserted). Before the blade could be cut-out Non-Destructive Testing (NDT) Inspection were used see Figure 17. Final confirmation of the damage was done after the testing was completed, by cutting the Root-Transition in pieces, see Figure 17.

Figure 17: NDT (Ultrasound) inspection was used to detect the size of the damage in the Root-Transition zone of the SSP34m blade.

The NDT inspection which was used to detect the damage below the surface was a method based on ultrasound.

When the damage was detected, and the size had grown to a size, where there was a risk for total collapse, a Floor was retrofitted, see Figure 18.

After installation of the Floor the damage stopped growing, which was the main objective of the demonstration testing.

Bladena
Universitetsparken 7
DK-4000 Roskilde
www.bladena.com

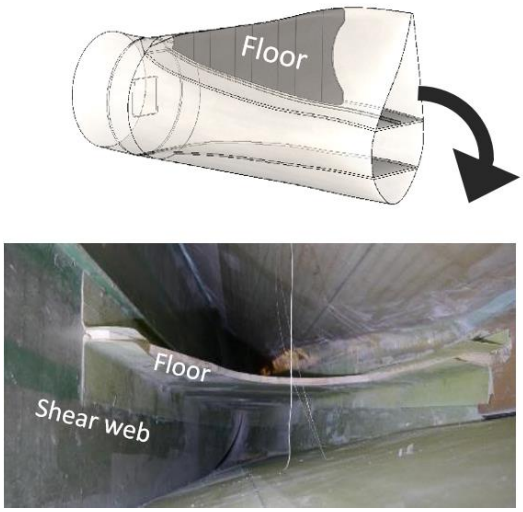

Figure 18: A Floor inserted in the SSP34m blade at Blaest after the damage in the Root-Transition zone has reached a critical level.

Fatigue driven damages

A fatigue driven damage in the trailing edge panel was noted during the full-sale test, see Figure 19.

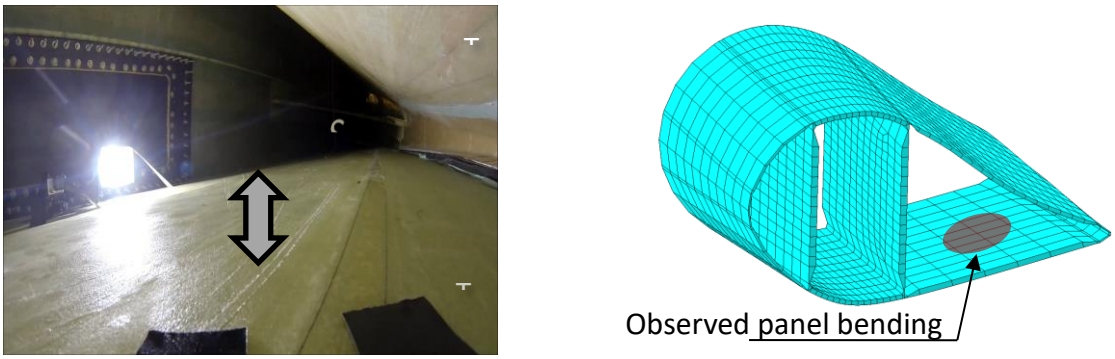

Figure 19: A clearly visible "damage" was visible during the fatigue test of SSP34m blade at Blaest.

The damage was identified as a sandwich face sheet debonding at the pressure side (inside face sheet) in the max chord region and could be identified only when the blade was subjected to the fatigue loads.

After an observation on the suction side panel at 6.5 meter from the root, it was depicted that there was an area where the panel deformed in a strange manner. In a video made during the test, an out-of-plane panel bending can be observed, see https://www.youtube.com/watch?v=LIK3-kPe0cY.

Bladena
Universitetsparken 7
DK-4000 Roskilde
www.bladena.com

After sectioning of the panel was performed, the face sheet debonding from the core was confirmed, see Figure 20.

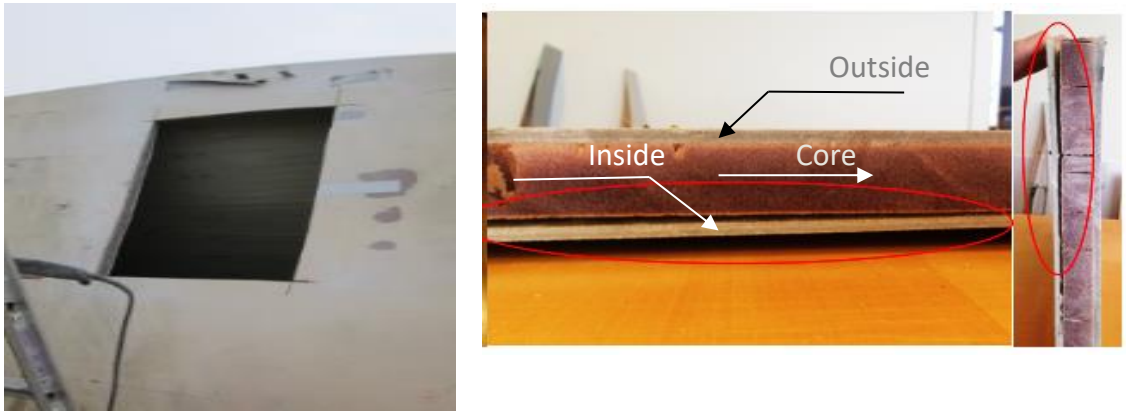

Figure 20: Cut-out from the Trailing edge (max chord area) of the SSP34m blade tested at Blaest. The damage was confirmed while the size of the damage had been increased.

This phenomenon (face sheet debonding due to bending) has been further investigated and tested in the Sub-component testing and Fracture Mechanics part of this report.

Large-scale testing of the SSP34m blade with fatigue load

One of the main limitations of full-scale blade testing is the capability to accommodate large blades and to trigger the relevant failure modes during testing. An alternative solution to full-scale fatigue testing has been investigated in this project. The alternative consists of using only the inner part of the blade (the structural part) and test this using a novel approach of load application. The main advantages are, reduced testing time and the possibility to trigger the relevant failure modes during early blade development.

The SSP34m blade was used, with and without the Floor with the aim being to test if the Floor technology has the capabilities to carry a combination of flap-, edge, and torsional loads. The test is performed using an advanced instrumented fatigue testing method under a multiaxial controlled testing configuration in the DTU Mechanical Engineering strong floor structural test facilities (DTU Structural Lab) at DTU Lyngby Campus. The following section includes more details on the load configuration. The pictures in Figure 22 illustrate the installation of the Floor in the SSP34m 15m section.

Bladena
Universitetsparken 7
DK-4000 Roskilde
www.bladena.com

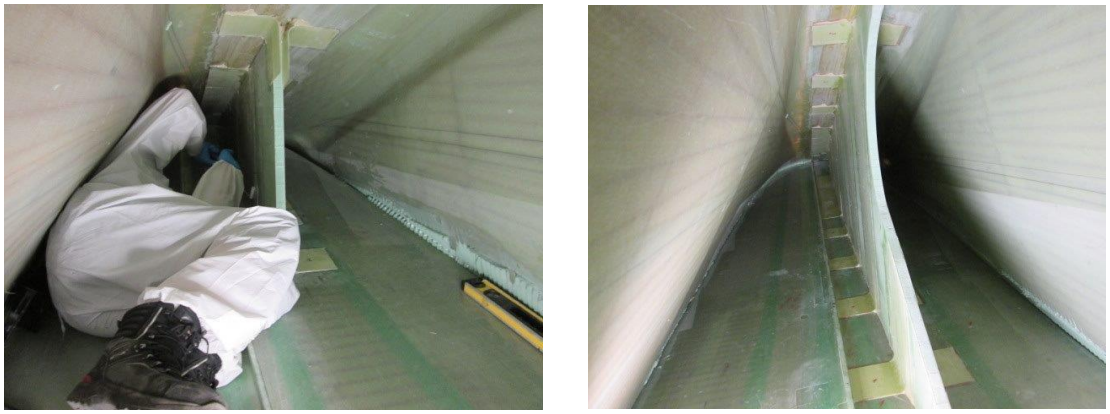

Figure 21: Floor installed in Root-Transition zone of a 15m section of aSSP34m blade.

Installation of the Floor™, also went relatively smoothly this time, since experiences were utilized from the first installation + full-scale testing. Furthermore, less material was used for this installation.

Standardization and combined load

The combined loading tests were done in Aalborg, at Blaest test center. From a fatigue perspective the testing to be carried out at DTU, a load configuration was used to assess the fatigue combined loading with torsional loads.

Sub-structural scale testing provides a service link between laminate and structural scale testing within the industry. This setup enables structural assessment of the root and transition zone, which exhibits structural failure as a direct impact of the increased size of wind turbine blades. This hypothesis is from an operational perspective, supported by the Wind Turbine Owners (WTOs) who report an increasing number of transverse cracks. Regardless of the blade make or model, the transverse cracks are located in the transition zone and max chord region. These cracks typically require extensive repairs up-tower or on the ground which leads to loss of AEP due to downtime. Hence, the need to identify the root cause of these blade damages in the design phase is critical.

An initial load configuration capable of triggering the pumping/breathing behaviour, which is believed to be the source of damages in the root area transition zone, was developed. This load configuration was applied for a predefined number of cycles through the fatigue driven multi-axial sub-structural test setup. Through three-dimensional digital image correlation, the pumping/breathing behaviour of the curved panels in the root area transition zone is quantified periodically.

Bladena
Universitetsparken 7
DK-4000 Roskilde
www.bladena.com

Current standardization rules do not demand combined loading, neither for static tests nor for fatigue tests. With the current testing methods, possible future demands from the certification bodies can be addressed.

Large-scale test of the SSP34m with torsion

At DTU the 15m inner blade section of a SSP34m blade has been subject to a number of combined loading scenarios following the edge fatigue testing with and without Floor™ was finished. The actuators applied at the end of the blade section (15m from blade root) facilitates any combination of edge, flap and torsional loads, see Figure 22.

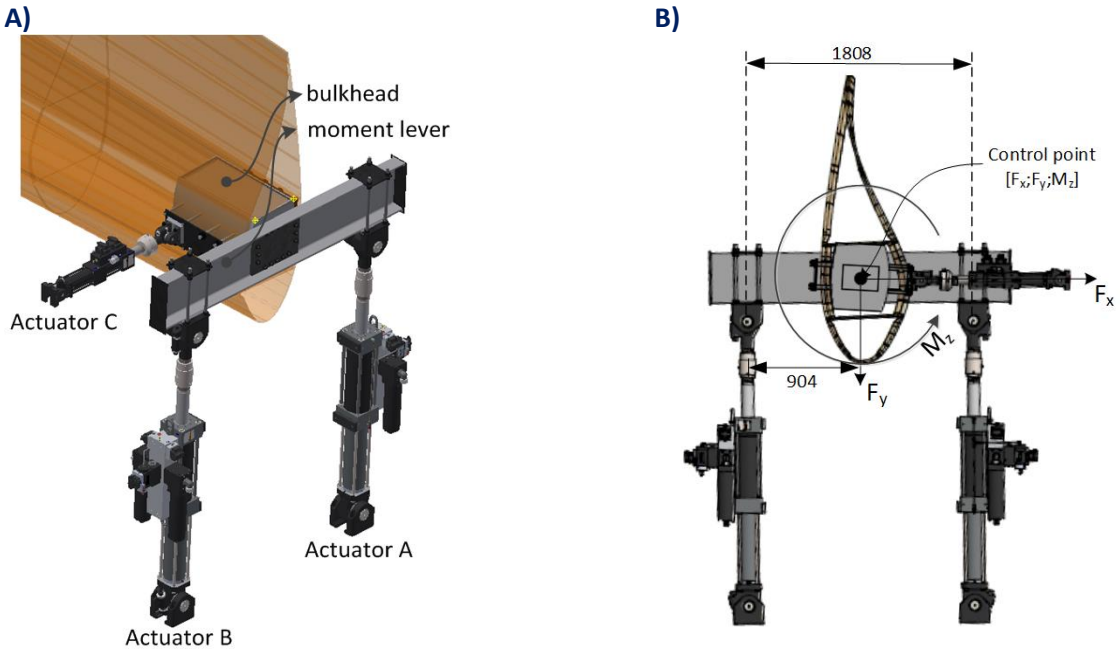

Figure 22: Large-scale test setup in DTU Structural Lab of the 15m SSP34m blade section. A) 3D view of the applied actuators at 15m from blade root. B) The active coordinate system and notation shows edgewise, flapwise and torsional directions.

A parameter study of combinations of edgewise and torsional forces has been performed. The evaluated results are the out-of-plane deformation with focus on the pressure side panel. The out-of-plane measurements were obtained with a full-field 3D DIC system (ARAMIS 12M). An in-depth description of the parameter study and results can be seen in Appendix C. The load combination found to be most critical in terms of pressure side panel out-of-plane deformation can be seen in Figure 23.

Bladena
Universitetsparken 7
DK-4000 Roskilde
www.bladena.com

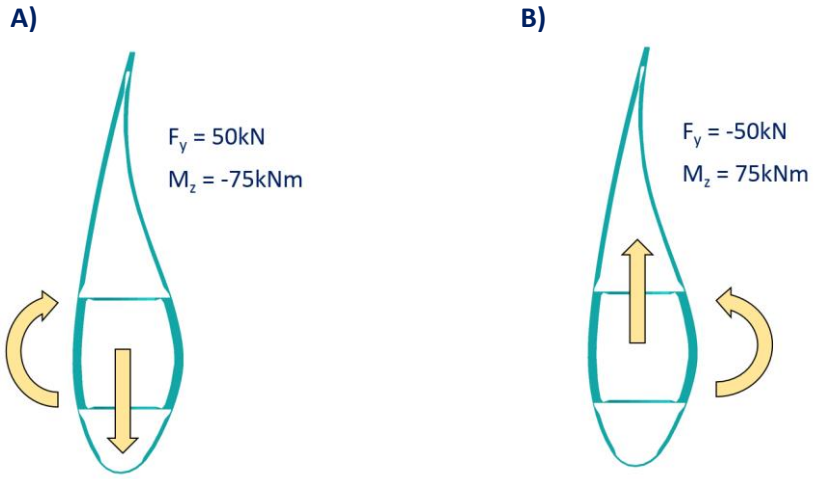

Figure 23: A) and B) are showing the two opposite load directions for the most critical combination of edge and torsional loads tested in the large-scale parameter study of the SSP34m blade section.

In Figure 24B the out-of-plane deformation for the pressure side mid-panel is shown.

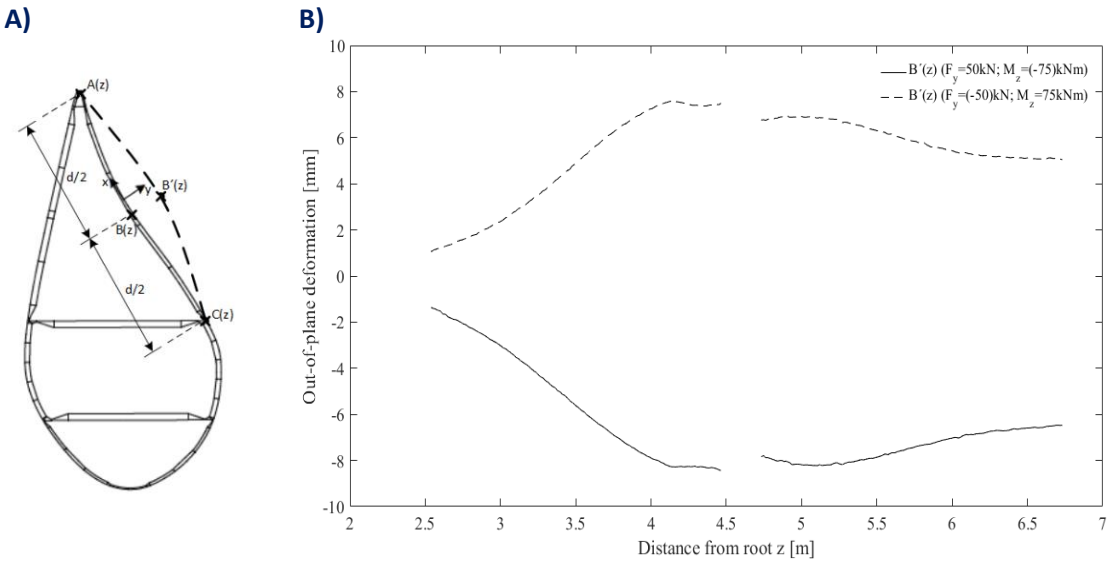

Figure 24: A) B'(z) denotes the out-of-plane direction for the pressure side mid-panel. B) The max chord is at 7m from blade root on a SSP34m blade. The graph is showing the out-of-plane deformation B'(z) for the pressure side mid-panel in the transition area of the SSP34m blade.

In Table 1 the out-of-plane deformation measurements for the critical load case described in Figure 23 are compared with the measurements from the corresponding load case without the torsion component. The torsion component increases the out-of-plane deformations with 58%.

Bladena
Universitetsparken 7
DK-4000 Roskilde
www.bladena.com

Table 1: Two load cases with the same edge load component but one with torsion and one without torsion are compared. The out-of-plane deformation increases with 58% when torsion is applied. See also Figure 22 and Figure 23 for definition of "positive edge" and "negative edge".

Out-of-plane deformation (B'(z)) [mm]			
Load direction	Edge	Edge + Torsion	Increase [%]
Positive edge	-5.27	-8.37	58.8
Negative edge	4.78	7.57	58.4

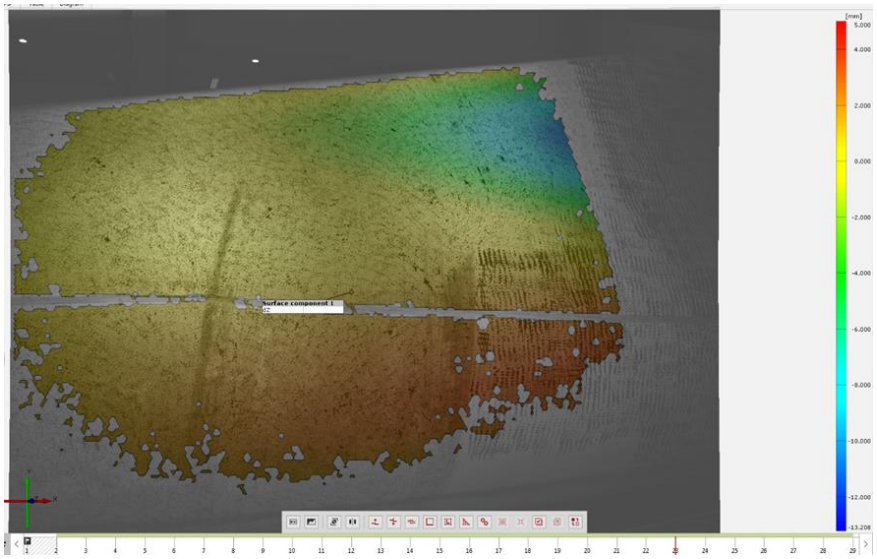

Figure 25: DIC result for the SSP34 for a load of +100kN

The loading on the 15m SSP34 blade has been compared to an equivalent load on a full SSP34m blade in FEM analysis, see Figure 27.

A combined loading scenario considering the flap wise loads at rated wind speed together with the edgewise loads is used in a base load for simulations of the full SSP34 blade. The edgewise loads are introduced in a distributed manner along the blade in the corners of the spar caps. Flap wise loads are introduced at ¼ distance from LE, where the aerodynamic center of the profile is located, in a distributed manner as well along the blade.

The substructure loads are introduced using a rigid bulkhead simulated using an RBE2 MPC, with an offset, to account for the eccentricity revealed through the substructure test.

Bladena
Universitetsparken 7
DK-4000 Roskilde
www.bladena.com

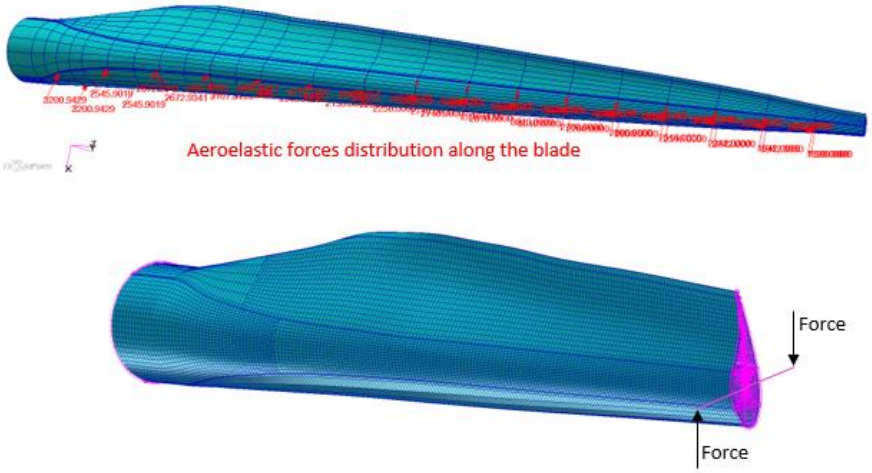

Figure 26: Load introduction technique. Top: Aeroelastic loading. Bottom: Sub-structural load configuration.

In both cases, the load introduction technique will not create stress concentration areas on the blade, that might interfere with the results.

Non-linear simulations are carried out and the out-of-plane bending of the panels in max chord and transition area are evaluated in the gauge area for both models, see Figure 27.

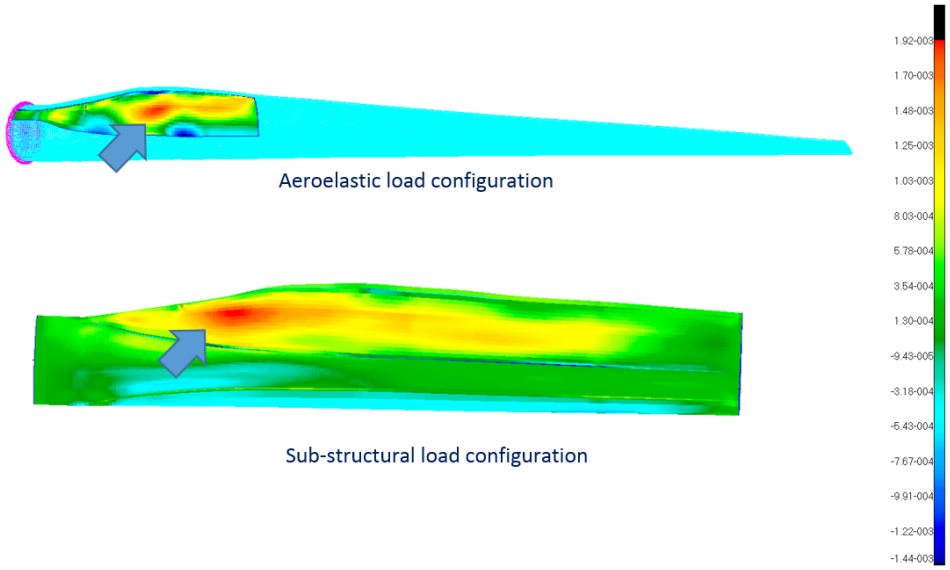

Figure 27: Comparison of the out-of-plane bending obtained on a full SSP34m blade when loaded with aeroelastic loads to a 15m SSP34 blade section using sub-structural load configuration. The colours refer to strain levels.

Figure 27 shows, that the method of applying cross-sectional loading and testing only the inner structural part of a wind turbine blade can be used instead of testing a full blade with combined fatigue loading.

Bladena
Universitetsparken 7
DK-4000 Roskilde
www.bladena.com

Large-scale test of the SSP34m with torsion loads

The method developed at DTU Mechanical Engineering for large-scale testing of wind turbine blades has the advantages of being able to be utilized for a wide variety of fatigue load cases. This includes the movement the blade would experience during field operation where a combination of loads is present, which results in torsional loads.

For a full blade these kind of fatigue loads have proven a difficult challenge for test centers, especially for the larger blades. But with large-scale blade testing only the inner structural section of the blade is tested. This is exactly the section of blades where most failures occur. At the same time, it will prove much easier to test a part of a blade that may be less than its full length than the full blade itself.

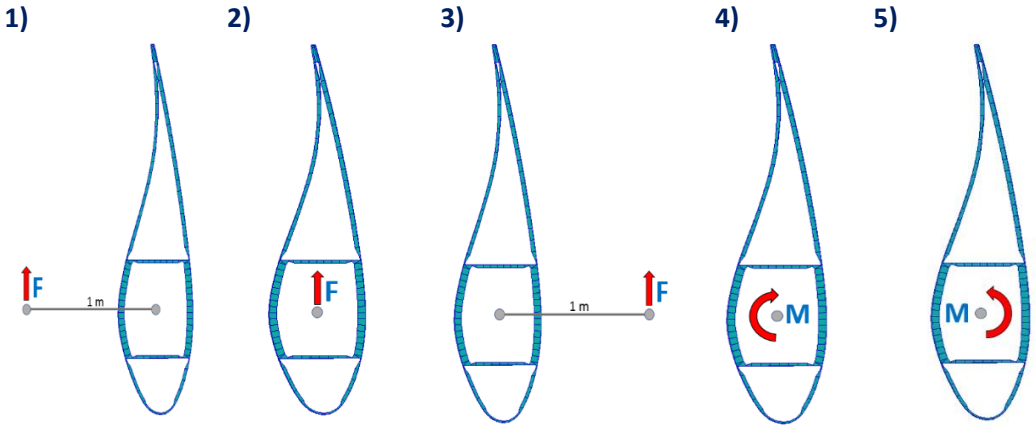

Figure 28: The figure is showing different load configurations possible to apply at the end of the 15m large-scale test of the SSP34m blade at DTU. 1) Force offset 1m towards pressure side. 2) Force, no offset. 3) Force offset 1m towards suction side. 4) Clockwise moment applied. 5) Counter clockwise moment applied.

Full-scale test of LM58.7m blade with combined load

The LM58.7m blade was also imposed under a full-scale static test with a static combined load. The blade withstood this amount of loading with no occurrence of failures. The forces applied during the static test are presented in Table 2, while a detailed description regarding the test setup and loading configuration can be found in RATZ - Data report: Full-scale test of LM58.7m blade with combined static loads [5].

Table 2: Applied loads at specific sections of the blade. All distances are from the blade root.

Blade section	Force applied [kN]	Force applied [Tn]
z = 39m	74	7.6
z = 44m	61	6.2
z = 49m	29	3.0
z = 55m	11	1.1

Bladena
Universitetsparken 7
DK-4000 Roskilde
www.bladena.com

Clamps/forces only applied on the outer 40% of the blade permitting the inner 60% to move freely in terms of local deformations as breathing, panel bending and cross-sectional distortion in shear - called Cross Sectional Shear Distortion (CSSD). Furthermore, buckling of the trailing edge must be changed when clamps are supporting the trailing edge. By only having the clamps placed in the outer region, they do not “disturb” the midspan area, where buckling usually is most critical. In Figure 29 the clamps are shown in two different load configurations. The two different positions are used in order to introduce torsion to the blade, which is expected to affect the overall deformational behavior of the blade, both in terms of breathing and CSSD.

Original load application:

Offset load application:

Figure 29: The same test was performed with and without and offset of the load application point towards trailing edge. In the figure is shown the wooden clamp at 49m from blade root with the two different load applications.

As it can be observed from Figure 30 and Figure 31. The loading offset, indeed, affects the structural response of the blade, as both the inclination angle as well as the individual panel deformation are maximized in case of the offset.

Bladena
Universitetsparken 7
DK-4000 Roskilde
www.bladena.com

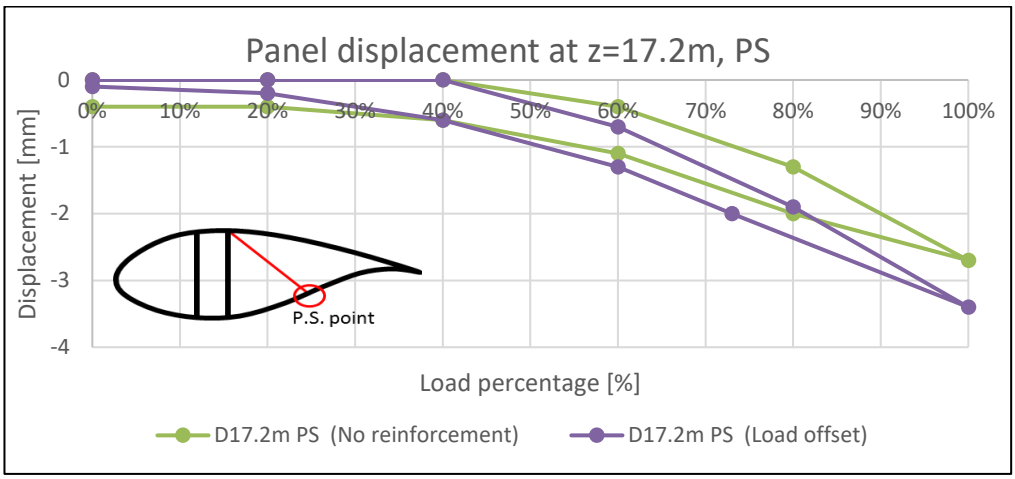

Figure 30: Effect of the load offset on the resulted deformation of the pressure side panel.

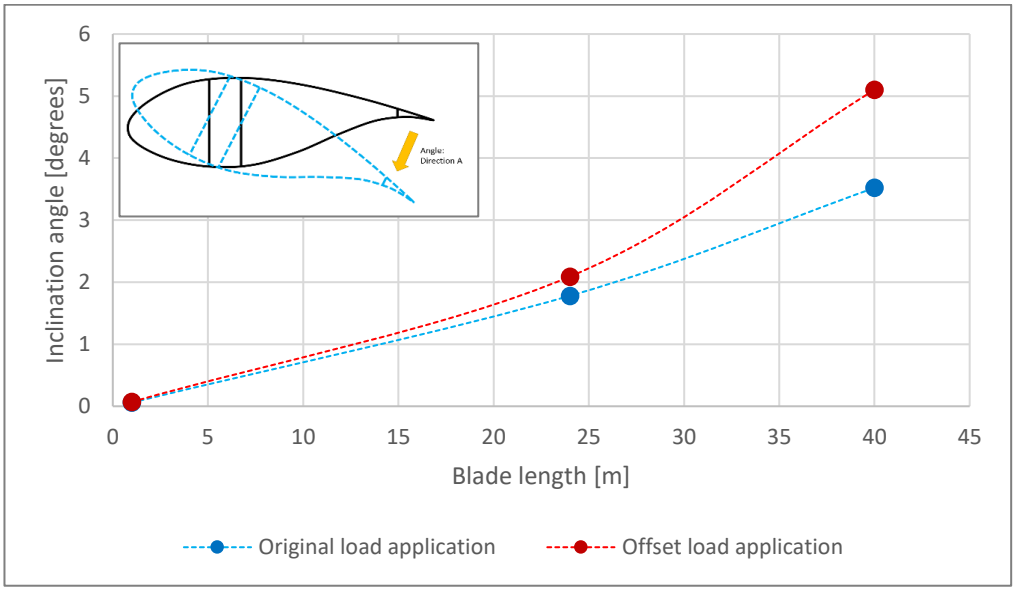

Figure 31: At the full test loads the angle inclinations have been measured for three cross sections , z=1m, z=24m and z=40m, marked by dots. In this figure the two load figurations "original load" and "offset load" are compared. It can be seen, that the offset load gives a higher inclination of the blade.

Under the scope of this project, a new measurement method was introduced aiming to capture the relative displacement of the suction and pressure side panels more accurately. As it can be depicted in Figure 32, two measurements are introduced connected at the pressure and suction side, while as a reference point the corner at the spar cap with the shear web is used. This is based on the assumption that due to the increased stiffness of the spar cap, the local deformation at that point are limited, thus only the individual movement of the two panels is captured.

Bladena
Universitetsparken 7
DK-4000 Roskilde
www.bladena.com

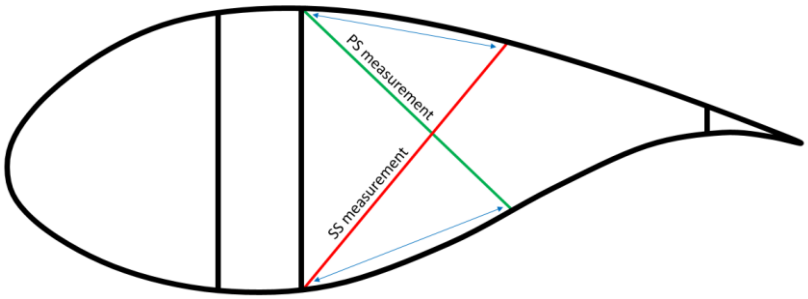

Figure 32: Measurement method, capturing the individual panel movement of both the pressure and suction side. The denoting of PS and SS measurements refer to the pressure and suction side respectively.

5.2 Fracture Mechanical modelling and testing

The need for accurate models for the evolution of debonding damage in sandwich panels is crucial to the understanding of the damage severity, its rate of propagation, and to formulate adequate maintenance strategies. In order to fully understand the behavior of a large structure in operation, one must first gain sufficient knowledge of smaller elements subjected to known load conditions. Linear Elastic Fracture Mechanics (LEFM) offers a valid tool to implement the fracture evolution laws in a simulated environment, but this requires that a series of tests on small coupons are performed and validated before being applied to large scale components with high complexity. The pyramid diagram represented in Figure 33 represents clearly the principles of this Building block approach.

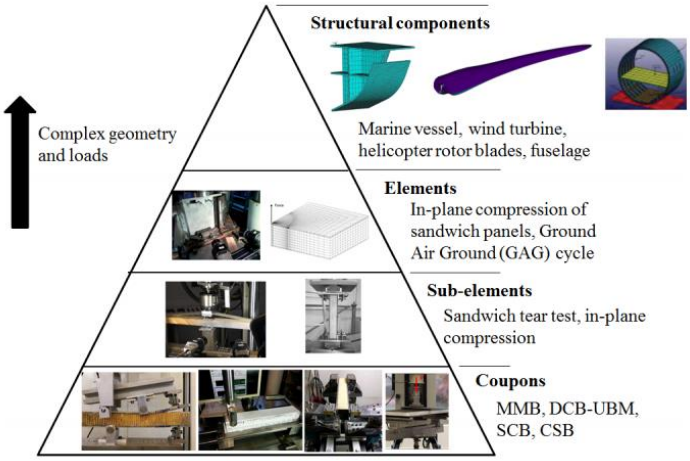

Figure 33: Building block approach: at the base, coupon tests are required to characterise a material and its failure modes, this information support the analysis of small elements with added complexity, one step above. Again, when sub-elements analyses are validated against experimental trials, this information are used to investigate one step above, and again until a full-scale analysis is developed to predict the behaviour of a real structure in operation.

Bladena
Universitetsparken 7
DK-4000 Roskilde
www.bladena.com

Coupon tests

Several tests have been proposed to evaluate the debonding of the face-core interface, the double cantilever beam loaded with uneven bending moments (DCB-UBM) is a method proposed by DTU to carry out tests at different load configurations in a convenient laboratory environment. A more detailed description of the numerical model principles and validations is reported in Appendix B.

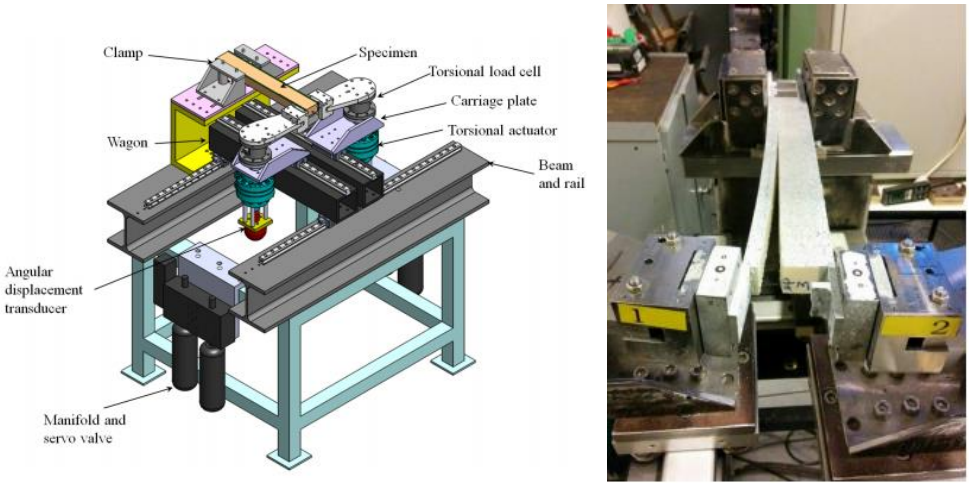

Figure 34: Schematics and example of a DCB-UBM test setup in operation. The independence of rotational moments applied to the two arms allows to test the debonding at the interface under several load modes (mode mixities).

A finite element model for the fracture mechanics is built and validated against experimental data and closed form solutions. The agreement between the results guarantees that the numerical model could be applied to more complex applications, where no known solution is available.

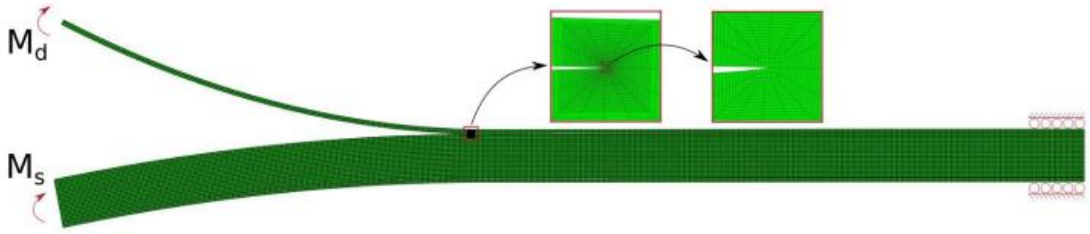

Figure 35: Detail of the DCB-UBM numerical model for the evaluation of the fracture toughness

Bladena
Universitetsparken 7
DK-4000 Roskilde
www.bladena.com

Small scale element tests

Small element level tests were also conducted. Rectangular shape specimens extracted from a curved section of a SSP34 blade were obtained, and these were loaded in static and fatigue mode on a standard four-point bending test rig. With the introduction of a known defect at the top face-core interface, it was possible to obtain the buckling of face sheet loaded in compression, thus replicate the breathing effects seen on the large-scale test described in 5.1. Tests indicate that the debond generates a reduction in the bending stiffness of the panel (Figure 36), which poses severe risks in the operation of blades and is suspected to be cause more severe types of damages like transverse cracks. It was also shown that cyclic loading is responsible and effective in the enlargement of the debonded zone. A validation of these experimental data is under investigation. For more in-depth of the work and theory of fracture mechanics in the RATZ project, see Appendix C.

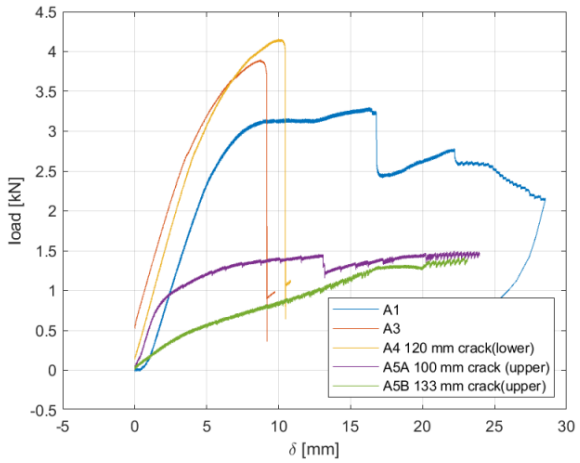

Figure 36: Static load four-point bending tests on SSP34 specimens, highlighting the loss in bending stiffness due to increase in the debonded area at the upper face having a net compressive load. Note that a crack in the lower face loaded in tension (A4) does not influence the behaviour of the beam and is equivalent to the pristine condition (A3).

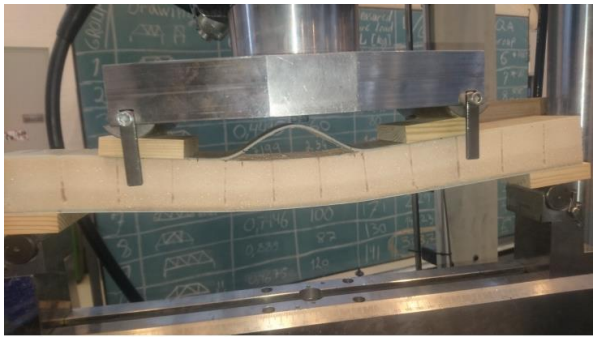

Figure 37: Detail of the face buckling under compressive state loading. This is phenomenon additionally lowers the bending stiffness of the setup

Bladena
Universitetsparken 7
DK-4000 Roskilde
www.bladena.com

Transverse cracks

Transverse cracks are frequent problem of varying severity on a wide selection of blade types. For that reason, the damage mechanism transverse cracks has been used in the RATZ project as a case study both for the Cost and Reliability package and as a study case for the fracture mechanical testing performed at DTU.

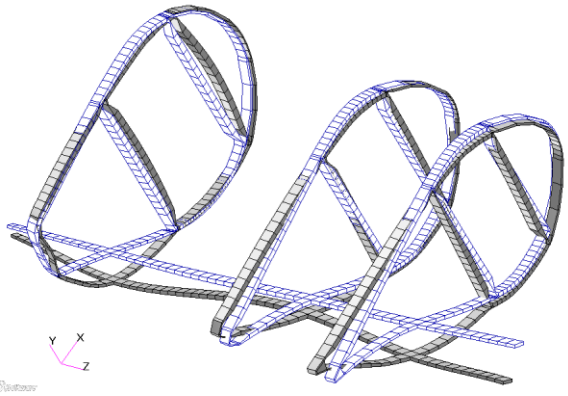

Figure 38: The figure shows three cross sections of a SSP34m FEM blade model. The undeformed blade elements are shown with white and the deformed elements are show with grey. The out-of-plane displacement for the pressure side panel varies along the blade. For the first and the last cross section in the figure, the out-of-plane displacement are larger than for the middle cross section.

Every month Bladena receives several reports about transverse cracks. An understanding of the cause of these failures is expected in the large scale testing of the SSP34 blade with skin debonding.

SSP34m blade large-scale test with skin debonding

The object of this setup is to validate the propagation of debond damage in the large-scale setup of the SSP34 blade section. At the root transition zone, a circular debonded zone of known area was introduced into a repair (Figure 39) at the interface between outer skin and core. This defect generates a weak zone where loads concentrations are present, which are in turn responsible for the propagation of the damage. By replicating the loads occurring during operation the same damages can be reproduced and a full understanding of the origin of transverse cracks in the panels is expected.

Digital image correlation technique is used to evaluate the displacement of the outer skin under loading and estimate the extent of the damaged zone, both these inputs are used to validate the full-scale numerical model (Figure 41).

Bladena
Universitetsparken 7
DK-4000 Roskilde
www.bladena.com

Figure 39: Debonded skin setup in SSP34 blade installed at DTU. On the right, a detail of the defect manufacturing highlighting the size of the defect introduced.

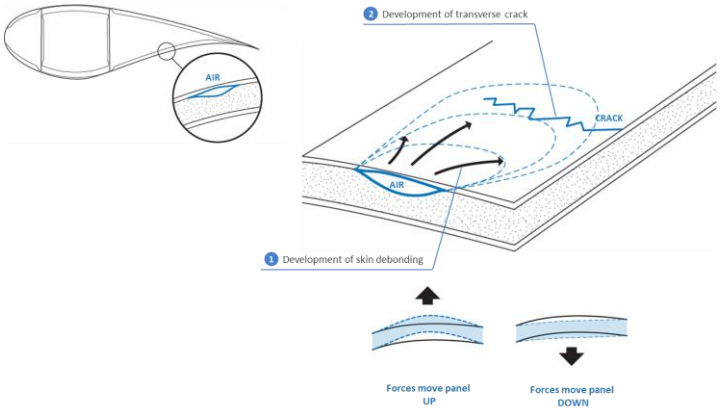

Figure 40: Hypothesis for the formation mechanisms of transverse cracks in blade panels. The initial debonded zone grow under cyclic loads until a critical size is reached, at which the skin starts to fracture due to high stress concentrations.

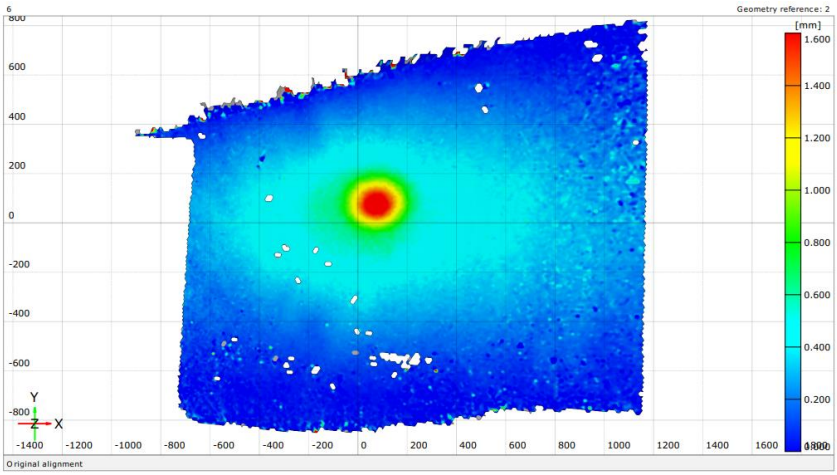

Figure 41: Surface contour plot of the out of plane deformation of the debonded area using Digital Image Correlation technique. The load applied on the backside of the top face shows the presence of a delaminated zone, although the precise extent of it is not clearly defined.

Bladena
Universitetsparken 7
DK-4000 Roskilde
www.bladena.com

5.3 Cost and reliability strategy development

The reliability model is linked to the Work Packages 4, 5 & 7 which focus on the investigation into failure mechanisms by means of the fracture mechanics studies and laboratory tests (at coupon level, at sub-component level or at full-scale level). The primary purpose of the reliability modelling is to develop and describe a probabilistic model as basis for reliability analyses and integrate the damage propagation model into the probabilistic model to simulate deterioration processes. Based upon this, a probabilistic damage propagation model is developed to simulate the stochastic process of damage propagation as either a continuous or a discrete function of time, which constitutes the basis of the reliability model. The Guide2Defect database provides in-history inspection records which are used to calibrate the parameters (e.g. transition probabilities in the reliability model) of the probabilistic damage propagation model. In the RATZ project, a five-level damage categorization scheme is used based on a similar categorization applied by blade designers, operators and owners. In the damage categorization scheme, the continuous damage propagation process is discretized into 5 damage categories, each of which covers a range of crack/defect sizes. Each realization of the stochastic damage propagation process is a discrete step-wise time realization (Figure 42).

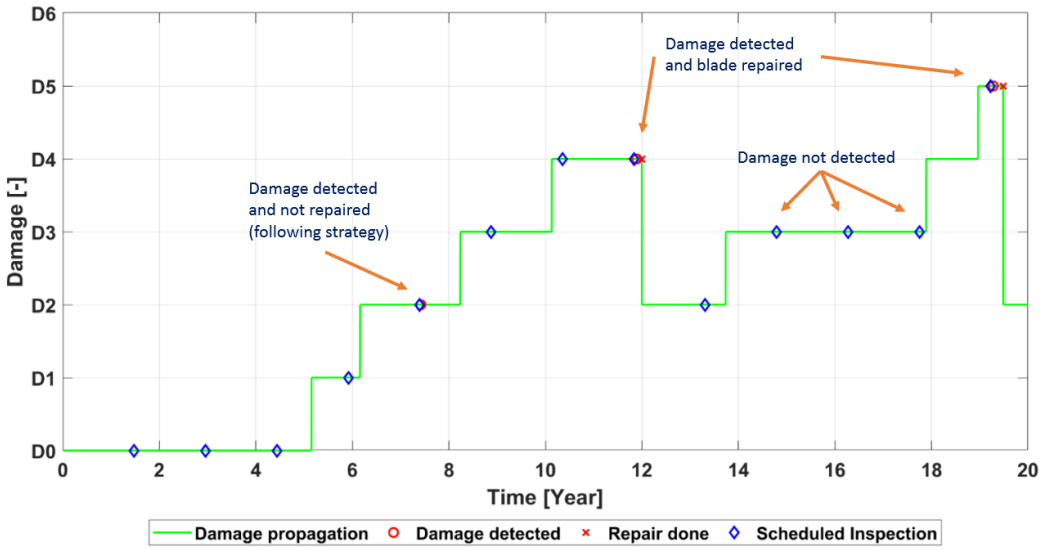

Figure 42: The figure shows one realization of a stochastic damage propagation. The damage state of the blade over time are shown by the green line. There will always be a probability for the damage state to jump to the next (more severe) level. At regular interval the blade is inspected (blue circles). A red circle marks the detection of a damage. Based on the chosen maintenance strategy only detected damage states of 3 or above are repaired (red cross). Not all damages are detected at inspection (due to the probability of detection). The Cost and Reliability package will create a high number (e.g. 5000) of realizations which are all a possible damage propagation outcome based on the input and the considered parameters and could all be shown as a slightly different version of this graph. Each realization corresponds with a probable cost over the blade lifetime and based on the mean values for all realizations an optimal maintenance strategy can be predicted.

Bladena
Universitetsparken 7
DK-4000 Roskilde
www.bladena.com

Figure 42 shows an example of a realization of the damage propagation process. The figure also shows inspections, which may result in detection or no-detection of a damage depending on the reliability of the inspection technique modelled the PoD (Probability of Detection) which in a probabilistic way models the probability that a damage (of a given size and a given type, e.g. internal, surface) is detected by the inspection. Further, the figure illustrates that if a defect/crack is detected then a repair may be performed depending on the user chosen maintenance strategy.

A simulation-based probabilistic damage propagation model is developed with the calibrated model parameters based upon the Guide2Defect database. Based upon this model, the stochastic damage propagation process can be simulated many times. One simulation can be considered as a realization of the stochastic damage propagation process, which is used as the basic input for decision-making and cost estimation. The output of the reliability model can provide a decision maker with the following information, see Figure 43:

- How long time it takes for an initial defect to propagate to a critical size, namely the lifetime before a corrective maintenance must be done;
- If the decision maker knows how severely the blade is currently damaged, how much longer is the damage to stay at the current damage state before it jumps to a more severe state, and when should non-destructive testing inspections be conducted, and some necessary preventive maintenance should be planned.

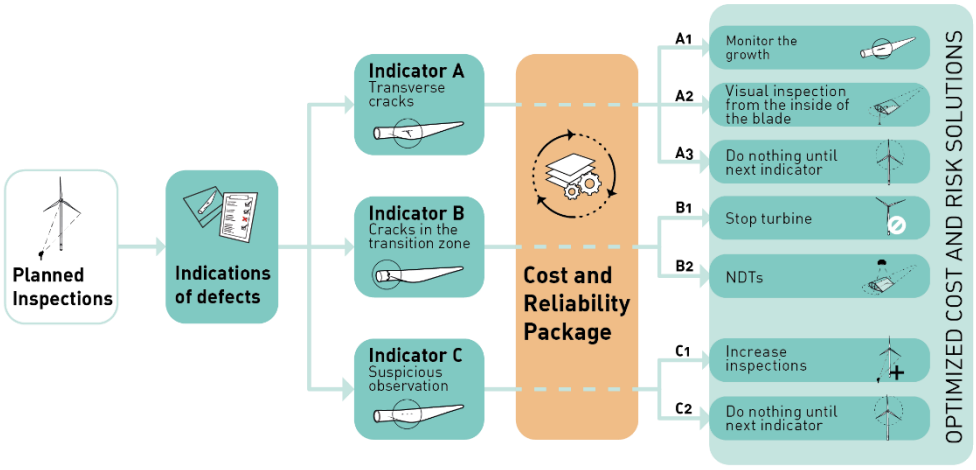

Figure 43: Data obtained through planned inspections lead to different defect indicators. However, a defect indication does not contain information regarding how severe the specific damage is. The cost and reliability package, through the different technical modules and probabilistic models, "filters" the various indicators and different actions are obtained depended on the severity of the damage.

The overall purpose of decision-making is to minimize the total expected operation and maintenance (O&M) costs. Generally, a decision maker should decide which inspection method should be used to inspect the blades; how often the inspections should be conducted; and if a damage of a specific damage severity is detected, what should be done. A maintenance strategy can provide the answers to these questions.

Bladena
Universitetsparken 7
DK-4000 Roskilde
www.bladena.com

The maintenance strategy constitutes the basis of the cost model. The actions that a decision maker takes depend upon the maintenance strategies. A maintenance strategy is usually composed of three fundamental aspects, namely the inspection method, the inspection intervals and some pre-defined decision rules on actions (e.g. repairs) to be done after the inspections have been performed. These fundamental aspects, like some basic building blocks used to construct a system, constitutes the main framework of a maintenance strategy. There are some possible options of each of these fundamental aspects for a decision maker to choose from. Possible options for each fundamental aspect can be freely combined with the options of the other two fundamental aspects. For example, one of possible inspection methods is combined with one of inspection intervals and one decision alternative, as illustrated in Figure 43 and Figure 44. This combination process is repeated until all the possible scenarios are covered. The probabilistic damage propagation model developed in reliability modelling is used to generate a number of realizations and based upon a large number of realizations the total expected costs is estimated as the mean of all costs associated with the simulated realizations. The total expected maintenance costs can be calculated based upon different combinations of inspection methods, inspection intervals and decision alternatives. The decision maker can choose the cost-optimal one and determine the inspection type and intervals accordingly.

Another important aspect of the cost model is to estimate the costs related to maintenance activities with the uncertainties considered. The maintenance costs are composed of logistic and inspection/repair costs.

The logistic-related cost is composed of the cost of waiting time, which for offshore wind turbines is due to waiting for an appropriate time weather window for repairing/replacing a blade, the vessel cost (daily rate or hourly rate) and the technician cost (daily rate or hourly rate). The costs for a vessel and technicians are slightly subject to the economic situation and can be considered constant in decision-making and cost estimation.

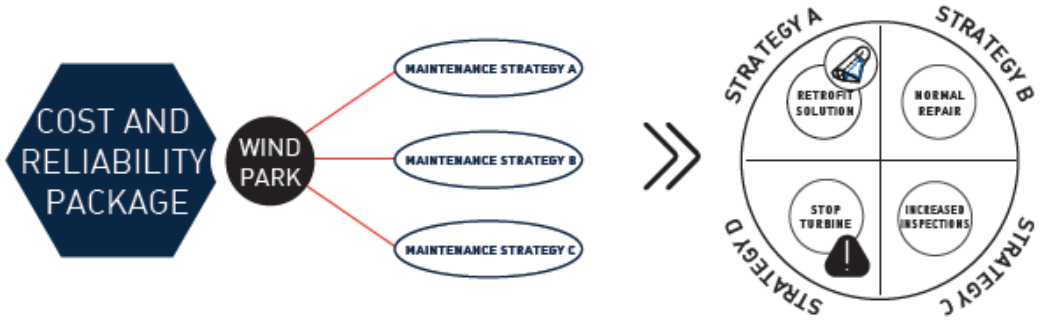

Figure 44: A specific issue can potentially have various solutions. The cost and reliability package, through the different modules, results to tailor-made maintenance strategies that are optimized in both cost and risk and offers the user the possibility to decide which strategy is optimum.

Bladena
Universitetsparken 7
DK-4000 Roskilde
www.bladena.com

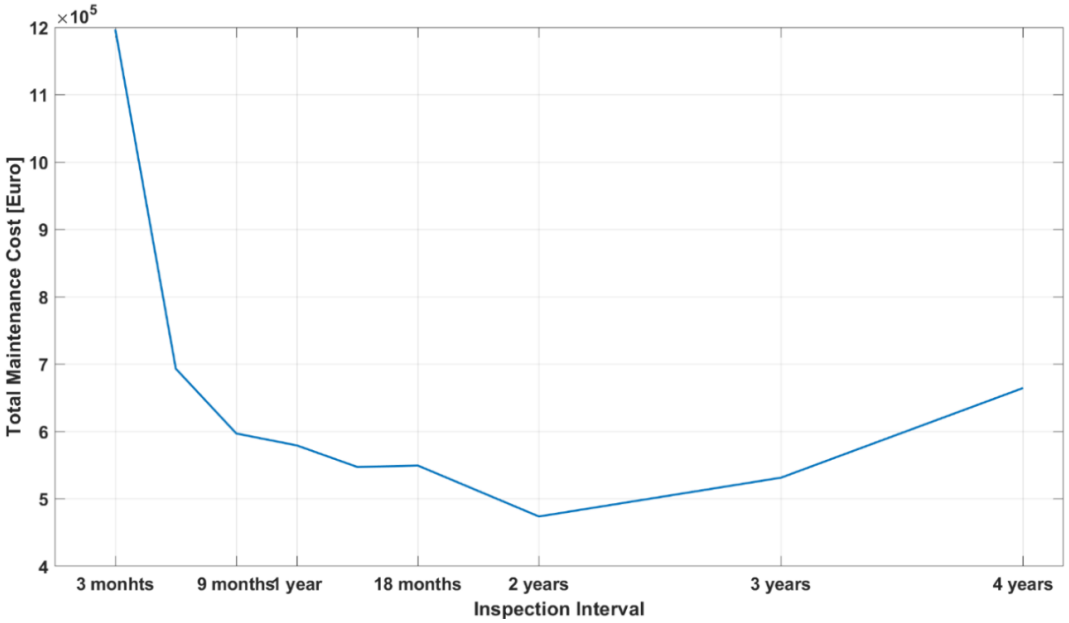

Figure 45: Cost Trend (corresponding to a specific maintenance strategy).

Figure 45 shows an example where the total expected cost for inspections and maintenance/repair is shown as function of the inspection time interval. In this example the cost-optimal decision is to choose an inspection time interval equal to 2 years. For more information on the Cost and Reliability activities and case studies, see Appendix B.

5.4 Knowledge platform for the value chain

The WTO Blade Group Network has participated actively during the project meetings, workgroups and seminars. Focus has been on how to incorporate combined loading test scenarios in the certification process and how to use of NDT to detect damages. This has been made possible by the number of partners from different areas of the wind industry value chain participation in the project and in close collaboration with the WTO Blade Group Network.

The strengthening of WTOs as a group to be reckoned with has an impact on the industry's and manufacturer's motivation to recognize blade damages and failures and the need to find solutions. In recent years awareness of blade damages not visible from the outside but starting inside the blade has had increased focus. In June 2018 a WTO seminar about Non-Destructive Testing (NDT) and how to apply NDT for blade inspections was held as part of this project.

Knowledge of blade damages has improved. One way of gathering damage knowledge is through the Guide2Defect (G2D) database which collect data from blade inspection reports

Bladena
Universitetsparken 7
DK-4000 Roskilde
www.bladena.com

delivered by the WTOs. The G2D database is a strong tool for statistical data on blade damages occurring at the field and are giving input to the Cost and Reliability package developed by AAU. Bladena adds knowledge of structural blade issues that based on blade scaling laws will only grow more critical in the future. All this are information for the WTOs to help them make plans and decisions according to strategies on how to run their wind turbine parks.

Further the objective of the project has been to develop methods to evaluate and optimize O&M costs. This part of the project has involved representatives from the entire value chain of the wind industry - WTOs, OEMs, certification bodies, ISPs, solution providers and universities - have all come together.

Dissemination of project results

The RATZ project has used a communication strategy to ensure that all partners and other interested parties had access to follow the project progress and results. This has been by use of professional visualization of project concepts from day one to the final stage and communication of results, e.g. in posters, figures and presentations. The project has a web project page and a web page with updated information and downloads. Additionally, four project News-Letters has been sent out as well as press releases. Naturally meetings between partners and work packages has been plenty as well as the Kick-off meeting, the Mid-Term meeting and the Final meeting.

As an important aspect to the project several workshops and seminars have been arranged during the 3-year project period e.g.:

- NDT-Seminar - Next Generation Inspection Methods
- 2 workshops on Fracture Mechanics
- 1-day seminar on Owners Requirements
- Several WTO seminars e.g. on the topic “Combined loading during full-scale test”
- Seminar on Cost & Reliability and damage database e.g. data from G2D-database

The seminars and workshop were mainly targeted the WTOs and providing a possibility for WTOs to gain knowledge and awareness of blade issues and to come with their input during discussions, which in turn has shaped the focus of the industry as well as the RATZ project.

A number of “tools” have been made in order insure an efficient communication between partners and industry in general. Two examples are presented below (Figure 46).

The Next Generation Inspection Reports (NGIR) have been developed in close correlations with WTOs to fit their needs for streamlined quality documentation on blade inspections and

Bladena
Universitetsparken 7
DK-4000 Roskilde
www.bladena.com

blade repairs. As part of the NGIR package an interactive photocard to be used in the field for easier and photo documentation has been designed. In the RATZ project the NGIR instructions (x3) and reports (x2) and the photocard (x1) have been wrapped up and used for a blade conference in Gothenburg in April 2017, see Figure 46.

Figure 46: The NGIR reports were initiated during the former EUDP project and wrapped up in the EUDP RATZ project in 2017. The NGIR reports were developed to streamline the documentation of blade inspection and repair and to ensure a high quality on inspection and repair report. The popularity of the NGIR reports amongst WTOs have been a motivating factor to continue the discussion and effort to improve shared communication in the wind business. LEFT: An open inspection manual is lying on the table. RIGHT: A interactive photocard is being used in the field during blade inspection.

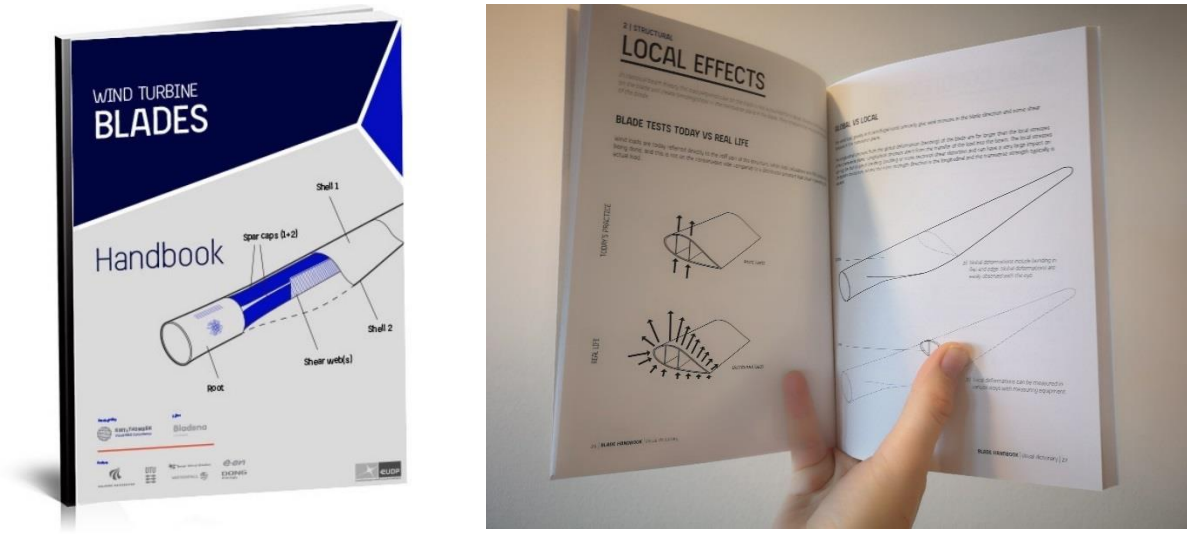

Figure 47: The Blade Handbook serves to streamline communication and understanding between different sections of the wind industry. LEFT: The Blade Handbook. RIGHT: Reading one of the chapters in the Blade Handbook.

RATZ Blade Handbook has been developed to streamline the way different sections in the wind industry understand and talk about blades, see Figure 47.

Bladena
Universitetsparken 7
DK-4000 Roskilde
www.bladena.com

6 Utilization of project results

Knowledge for understanding failure mechanisms in the Root-Transition zone under extreme fatigue loading has proven very valuable. Bladena's patented Floor™ solution has been demonstrated to address the challenges manufactures will have when blades grow larger. Bladena will continue the dialogue with manufactures on how to utilize the Floor™ Technology in new blade design. It is Bladena believe that it can be very difficult, maybe impossible, to design a cost-effective very large blade, without utilizing the Floor™ Technology. Since the trend in the industry is to develop and design larger blades and lower LCoE it is of key important to be able to develop cost-efficient and reliable blades. Also, the thorough understanding of the importance of representing torsional forces in future full-scale testing in order to get representative panel deformations, which e.g. cause transverse cracks on the trailing edge panel in the max chord area, has proven very important. Finally, the Large-scale sectional test method developed at DTU Mechanical Engineering, is expected to be used in commercial test centers in the future.

7 Project conclusion and perspective

7.1 Main conclusions from the RATZ project

Floor™ technology has been demonstrated

The Floor™ technology has been demonstrated to mitigate damages in the trailing edge transition zone of wind turbine blades. The Floor™ technology has been demonstrated on three blades, two of them on full-scale with edgewise fatigue loads, and one on large-scale with combined fatigue loading. In the two full-scale test, the test was started without any Floor™ reinforcement. In both test damages appeared and expanded in the root-transition zone. Then the Floor™ was installed and the damage progression stopped. NDT inspections of the blade in the root-transition zone gave a clear vision of the extent of the damage at the time of the individual inspection. The third blade, tested in the large-scale test facilities in DTU Structural Lab at DTU Lyngby Campus, the Floor™ was installed before the blade test. Also, this test successfully showed the effect of the Floor™, since no failure was observed neither in the transition zone or in the adhesive connection between the Floor™ and the blade structure.

Bladena
Universitetsparken 7
DK-4000 Roskilde
www.bladena.com

Standardization - Torsional loads increase risk of transverse cracks

During this project, transverse cracks were studied with the conclusion that they are highly connected to panel bending. The large-scale testing performed at DTU showed that torsional load that arises from the combination of simultaneous edge and flapwise loading on wind turbine blades, increases the out-of-plane bending of the trailing edge pressure side panels in the max chord area with 57%. This finding is of key importance since it most likely is the main reason why so relatively many transverse cracks are found in the field on blades in operation. Torsional loading and the resulting transverse cracks are not addressed in the certification based on full-scale testing, where torsional loads are not included.

Cost and Reliability

In the Cost and Reliability work package a reliability model is developed based on a discrete Markov Chain model closely linked to a five-step damage categorization scheme, utilizing information from fracture mechanics considerations and calibrated using inspection datafrom the Guide2Defect database. A generic cost model is developed including costs to inspections, maintenance, repair, replacements, downtime etc. The cost model is linked to the decision alternatives which are inspection type, inspection time intervals and maintenance/repair options. The cost-optimal decision is identified by a simulation based approach where the total expected lifetime costs are estimated and the decision alternative with the lowest costs is chosen. The procedure is illustrated by case studies which shows the large potentials of such a tool for providing decision support to wind turbine operators, owners and other parts of the value chain. Knowledge of blade damages has improved during the project, headed by Guide2Defect Aps which has a database, which collect data from blade inspection reports delivered by the WTOs. The G2D database is a strong tool for statistical data on blade damages occurring in the field and are giving input to the Cost and Reliability package developed by AAU.

WTO Blade Group Network

The WTO Blade Group Network has grown from 15 wind turbine owners to 37 and almost all the major WTOs are part of the network. The strengthening of WTOs as a group to be reckoned with has an impact on the industry and manufacturer's motivation to recognize blade damages and failures and the need to find solutions. The WTO-Blade Group Network often invite other participants from the value chain and especially the participating of RATZ-partners e.g. Blaest, DNV GL, DEWI OCC, Nordex and LM-Windpower have been participating in seminars with WTOs from the Blade Group Network. Most of the 37 WTO-members have been actively participating in project meetings, workshops and seminars arranged the last 3 years financed by this project. Focus has been on how to incorporate combined loading test

Bladena
Universitetsparken 7
DK-4000 Roskilde
www.bladena.com

scenarios in the certification process and how to minimize Operation and Maintenance costs by choosing the optimal maintenance strategy. In the past it has not been tradition to consider use of NDT to detect damages, which cannot be seen from surface, but with the increased knowledge this is now part of the consideration choosing the optimal inspection methods. Both the technical and the cost aspect have been addressed on seminars.

7.2 Future perspectives

Floor™

The Floor™ solution was originally meant to be a part of new-designs for large wind turbine blades. In the RATZ project the tested Floors™ have been designed essentially as retrofit solutions and it has been demonstrated on three blades that it is possible to install/retrofit a Floor™. In case this is done an alternative connection towards the trailing edge, need to be considered if the blades are large and the forces are very high. Bladena will also study the potential using the technology in a Cost-out project together with an actual case with a manufacturer(s). Also the increase in AEP, by increasing the width and position of the chord needs to be analysed more in detail on the actual design together with the manufacture(s).

Standardization - Torsional loads increase risk of transverse cracks

The loads in the root-transition zone drastically as blades grow in size and structural issues are expected to increase. The torsional loads will also increase significantly due to the higher tip deflection and the reacting aerodynamic forces in the other region where the tip deflection is highest. With the expanding understanding of loads and the root causes for structural failure mechanisms e.g. transverse cracks, blade failures can be prevented in the future by taken the right precautions in time. Utilizing new knowledge from this project that torsional loads are a key driver for the development of transverse cracks, it is expected that future blades will be tested taking torsional loads into account during certification.

History shows that it takes time to update certification standards and therefore it is most likely that manufactures will start to implement this together with test centres. Many wind turbine owners today are aware that they must clarify whether the turbine/blades they consider buying have passed additional testing and analysis in excess of what is required for the standard certification. Some wind turbine owners make technical due-diligences before making the decision on what turbine/blade to buy. Others work together with Bladena and other third companies to make a set of additional requirements, called “Owners Requirements”. The set of requirements are closely discussed with a wide range of manufactures including LM Wind Power and Nordex which have both been a part of this project.

Bladena
Universitetsparken 7
DK-4000 Roskilde
www.bladena.com

Cost and Reliability

The work from AAU lay a foundation for the industry to continue working with this field. EUDP has recently decided to support a new project (CORTIR) where more focus on risk and how to analyze this will be the main objective. Bladena will use the work which has been developed in this project and make a user-friendly Cost and Reliability tool named CAR-Tool. The tool will also include fracture mechanical models from DTU as well as structural understanding of blade failures developed in this project.

WTO Blade Group Network

The WTO Blade Group Network will continue in the new CORTIR project and EUDP is also financing a structured process working with full-value chain. Focus is to optimize the collaboration between WTOs, OEMs and Insurance companies. It is therefore of key importance that all three groups have decided to join the new CORTIR project, in total 23 partners.

Bladena
Universitetsparken 7
DK-4000 Roskilde
www.bladena.com

8 References

[1] F. M. Jensen, "Ultimate strength of a large wind turbine blade," Risø DTU, PhD Thesis, 2008.

[2] P. Brøndsted and R. P. Nijssen, Advances in wind turbine blade design and materials, Woodhead Publishing, 2013.

[3] F. M. Jensen, "Floor™ Patent owned by Bladena Aps". Patent WO 2008.086205, 2008.

[4] "Data Report: Full-scale test of a LM58.7m blade with edgewise fatigue loading," Energy Development and Demonstration Program (EUDP) RATZ project, 64015-0602, Roskilde, 2019.

[5] "Data Report: Full-scale test of a LM58.7m blade with combined static loading," Energy Development and Demonstration Program (EUDP) RATZ project, 64015-0602, Roskilde, 2019.

[6] "Data report: Full Scale Test SSP 34m blade, Combined static load," Energy Development and Demonstration Program (EUDP) Experimental Research, Phase 2 , Risø, 2010.

[7] DNV-GL, "Standard DNVGL-ST-0376: Rotor blades for wind turbines," DNV GL AS, 2015.

Bladena
Universitetsparken 7
DK-4000 Roskilde
www.bladena.com

Appendix A Cost & Reliability and Guide2Defect

Closing Activity Report

Guide2Defect ApS Activities performed under Work Package 12

The key role of Guide2Defect under the RATZ -EUDP project 64015-0602, work package 12, was to provide updated and statistically significant defect data for the cost tool to be prepared by Aalborg University, and based on inspection reports received from the participants and other relevant parties.

During the project, Guide2Defect has increased the size of the Guide2Defect Reference Data Base, both based on inspection reports received from the participants, but also reports analysed by our Indian partner, Rotortech. The Indian partners time has been paid for his customers and has hence not been included in this project. The total amount of data retrieved and analysed by Guide2Defect is summarised below (Table 3):

Table 3: Analysed inspection Reports under the RATZ project.

Inspection Reports	1701
Projects	48
Turbines	760
Blades	1596
Defects	9913

Task 12.1: Update of Defect Categories in G2D Database

Prior to the start of this project, Guide2defect has already established a first version of the defect tree used to categorize the defects. This first draft was prepared as part of a previous EUDP supported LEX project. During this project, Guide2Defect has reviewed and updated the underlying defect tree by:

- Review of defects to control the fit of the defect tree to the defects identified
- Discussions with project participants and Rotortech
- Desk research.

Bladena
Universitetsparken 7
DK-4000 Roskilde
www.bladena.com

Based on this work, the six additional defect catagories was added, and the defect tree is considered to be complete for now, but will require another review, once defects idenfied by NDT will begin to be included in the data base. None of such inspections were analysed during this project, but will soon be received via RotorTech in India. The data base has been updated with the additional defect catagories, and this hence satisfy the following deliverables:

- Deliverable 12.1.a: Top down defect threes for a) to d).
- Deliverable 12.1.b: Updated defect categories (as applicable) in G2D database.

The updated defect tree now comprised the following defect categories:

Figure 48: Updated defect tree.

Task 12.2: Acquisition and entering of inspection reports retrieved from participating owners in G2D Database

As part of the project, Guide2Defect has acquired inspection reports from the participating wind turbine owners but have also included inspections report retrieved via our Indian partner, RotorTech. This work has tripled the number of inspection report analyzed in Guide2defect. The inspection report retrieved from participating owners has been analyzed by the either Guide2Defect partners or our junior associates trained to perform the analysis.

Bladena
Universitetsparken 7
DK-4000 Roskilde
www.bladena.com

During this project, Guide2Defect has analyzed a total of 1701 inspection reports covering 1596 blades with a total of 9913 defects. The inspection report is distributed among the owners as per the below figure (Figure 49):

Project Code	Site Name	Turbine Family	Project Size	# of turbines	Owner	Count Turbines	Count Blades	Count - Inspection Reports	Count - Defects
33	Baillie	Nordex N90/2500	53	21	Statkraft	21	18	18	58
34	Sheringham Shoal	Siemens SWT-3.6-107	317	89	Statkraft	89	138	153	540
35	Alltwalis	Siemens SWT-2.3-93	23	10	Statkraft	10	18	18	369
36	Forest Creek I	Siemens SWT-2.3-93	87	38	E.ON	0	0	0	0
37	Forest Creek II	Siemens SWT-2.3-93	37	16	E.ON	0	0	0	0
38	Panther Creek I	GE 1.5	143	95	E.ON	28	84	84	866
39	Panther Creek II	GE 1.5	116	77	E.ON	0	0	0	0
40	Panther Creek III	GE 1.5	200	133	E.ON	0	0	0	0
41	Robin Rigg	Vestas V90/3000	174	58	E.ON	37	107	107	574
42	Kentish Flat I	Vestas V90/3000	90	30	Vattenfall AB	30	75	75	203
43	Stor-Rotliden I	Vestas V90/2000	80	40	Vattenfall AB	39	51	51	111
44	Stengårdsholma	Vestas V90/2000	20	10	E.ON	10	0	0	0
45	Champion (Roscoe I)	Siemens SWT-2.3-93	1265	55	E.ON	10	0	0	0
46	Roscoe	MWT-100-61	209	209	E.ON	17	0	0	0
47	Voskero	Vestas V52/850	60	7	Enel	7	21	1	3
48	Aspri Petra	NEG Micon NM52/900	20	22	Enel	22	66	66	83
49	Soros	NEG Micon NM52/900	12	13	Enel	13	39	39	41
50	Geraki	NEG Micon NM52/900	14	16	Enel	16	48	49	58
51	Monastiri I	Nordex N50/800	6	8	Enel	8	24	24	25
52	Monastiri II	NEG Micon NM52/900	11	12	Enel	12	36	36	40
53	Heliolousti I	NEG Micon NM44/750	8	10	Enel	10	30	18	19
54	Agios Kyrillos	Enercon E44/900	7	8	Enel	8	24	24	25
55	Koutsoutis	Enercon E44/900	12	13	Enel	13	39	39	41
56	Panagia Soumela	Gamesa G87/2000	14	7	Enel	7	21	21	26
57	Zoudochos Pigi	Gamesa G87/2000	24	12	Enel	12	36	36	36
58	Schkortleben	Siemens SWT-2.3-93	23	12	Engie	12	41	75	620
59	Mont de Bezard	Senvion MM82/2000	36	18	Engie	12	36	36	398
60	Haute-Lys	GE 1.5	375	25	Engie	25	47	70	466
61	East Lake St. Clair	Vestas V90/1800	100	55	Engie	54	1	1	1
62	Campagnes	Ecotecnia ECO 80/1670	8	5	Engie	5	15	15	435
63	Chemin des Haguenets	Senvion MM92/2000	28	14	Engie	14	39	43	282
64	Longchamps	Ecotecnia ECO 80/1670	835	5	Engie	5	12	12	273
65	Baleni	GE 2.5	50	20	Engie	20	60	120	1924
66	Rézentières-Vieillespesse	Nordex N90/2500	20	8	Engie	6	1	1	10
67	Craigengelt	Nordex N90/2500	20	8	Engie	8	24	24	217
68	Blantyre Muir	Senvion MM92/2000	6	3	Engie	6	18	18	134
69	Gemenele	Siemens SWT-2.3-101	48	21	Engie	21	63	63	864
70	Dabrowice	GE 2.75	36	13	Engie	13	39	39	189
71	Kerigaret	Acciona AW-1500/77	12	8	Engie	8	24	24	56
72	La Picoterie	Gamesa G90/2000	22	11	Engie	11	33	33	84
73	Tambours	Ecotecnia ECO 80/1670	8	5	Engie	5	15	15	334
74	Piontes Aux Roches	Vestas V90/1800	49	27	Engie	27	1	1	11
75	Kukru Wind Power Pvt Ltd	Gamesa G97/2000	50	25	Atria Power	25	75	75	224
76	Jamanwada	Suzlon S95/2100	53	25	Mytrah Energ	25	75	75	0
77	High Volts	NEG Micon NM80/2750	825	3	E.ON	3	0	0	0
78	Holmside Hill	NEG Micon NM80/2750	55	2	E.ON	2	0	0	0
79	Nipaniya	Inox DF100/2000	30	15	Mytrah Energ	15	45	45	41
80	G.V Palli Wind Power Projec	GE 1.7	26	15	Atria Power	15	45	45	161
81	Lamba	Nordex N27/200	1	4	Ineos	4	12	12	71
Totals						760	1596	1701	9913

Figure 49: Inspection reports analysed.

As part of this task, Guide2Defect should deliver two deliverables:

Deliverable 12.2.a: Updated baseline report to participating owners:
The baseline report was added to the owners' dash board and this was informed to the owners via mail dated January 10th, 2018.

Deliverable 12.2.b: Data report for financial models:

Bladena
Universitetsparken 7
DK-4000 Roskilde
www.bladena.com

Special dashboard with access to the relevant data was opened in the Guide2Defect, and access was given to Aalborg University on March 9th, 2018. Prior to this, the data – as they were at that time – was exported to a spread sheet, cleaned and organized, and forwarded to Aalborg University by mail dated January 8th, 2018.

Further to the deliverables, access has been given to Engie and Enel to dashboards with the same level of information as given to the participating owners. Engie has chosen to pay for an additional benchmark report, and this has been prepared outside this project.

Task 12.3: Vulnerability Analysis

The vulnerability analysis was not defined prior to the start of the project, and first task was hence to define, how the vulnerability analysis should be performed and what it should comprise. Guide2defect has carefully evaluated the context and has decided that the vulnerability analysis should combine the hit rate and the average time to reach the hit rate. Hit rate being defined – for each defect category – as the number of blades, which has been hit with defect grade 3 or higher of this particular defect. Bottom line, the higher hit rate, the higher vulnerability. The lower average clock hours, the stronger the vulnerability.

The project leadership decided to change focus of the analytical part of the project to transverse crack at the max chord section of the blades. This made the planned work in this task and the following task 12.4, 12.5 and 12.6 obsolete, and it was hence decided that Guide2Defect should focus the vulnerability analysis on the transverse cracks, but also should include the generic vulnerability analysis in the dashboards of the participating owners. This was confirmed in an email exchange between the work package leader and the project manager of the project dated August 20th, 2018.

As part of the work under this task, Guide2defect, had two deliverables:

Deliverable 12.3.a: Overall Vulnerability Analysis on the full population:
A full report for transverse cracks were sent to Bladena in mail dated November 5th, 2018. The report was prepared on turbine type level. The report was discussed at a meeting the following day.

Deliverable 12.3.b: Specific vulnerability analysis for each participating owner:
This has been incorporated in the dashboard on site and turbine level. This allows each participating owner to retrieve the analysis via their dashboard. The vulnerability is calculated for all defect categories.

Bladena
Universitetsparken 7
DK-4000 Roskilde
www.bladena.com

Task 12.7 Guide2Defect Workshop

It was decided that rather has having one work shop demonstrating the data base to owners, how has already been introduced to it, to execute a number of seminars presenting the findings and challenges in relation to the cost and reliability. 4 such seminars have been held.

Deliverable 12.7.a: G2D workshop with course material:

- Animation video describing and introducing the Guide2Defect data base.
- Ratz Nordic blade group work shop, June 16th, 2016 in Kolding
- Mid-term meeting, June 2nd, 2017 in Aalborg
- Offshore Energy LEP seminar on February 22nd, 2018 at DTU Wind Energy
- Codan Cost and Reliability Seminar, April 30th, 2018 in Aalborg.

Task 12.8 – Tool for optimal planning of blade inspections

This task has been executed by Aalborg University, and will be reported separately by them. Outside the delivery of data under task 12.2, Guide2defect has actively participated in the review and commenting of the tool prepared either via project meetings or via review of information provided.

As part of the project, Guide2Defect has included a simple first-generation repair cost calculation feature in the G2D including a repair catalogue with associated cost. This feature currently is only workable on reporting level based on a high degree of manual input and should be developed further. Further, as a response to the extensive use of drones and simple photo documentation, we have also updated the Guide2Defect data base with a direct input section, allowing drone operator to use Guide2Defect as an inspection report generator. All data received via Rotortech has been entered using the direct input section.

Conclusion

Guide2Defect has fulfilled its role and delivered all task in accordance with the plan with the adjustments agreed during the project with the project management. Outside the value given to particular the cost and reliability tool, the project has supported Guide2Defect in enlarging the population of the database, improved the dash boards, but also prepared the Guide2Defect for further expansion and development of the data base, also considering future use of AI and lower cost inspection options.

Prepared by:
Søren Horn Petersen
Work Package Manager; Partner, Guide2Defect

Bladena
Universitetsparken 7
DK-4000 Roskilde
www.bladena.com

Appendix B Fracture Mechanics

Tests on the DCB-UBM geometry are performed in both static and dynamic loads to derive the fracture toughness and the crack propagation rates at different mode-mixity phase angles.

One important advantage of this test setup is that the mode mixity is independent of the crack length, therefore it is possible to have a constant controlled crack propagation, in addition a single specimen can be tested repeatedly under multiple conditions. From an experimental perspective, this simplifies fracture testing as there arises no necessity to continuously monitor the crack length. The critical moment can be identified as the sudden departure in the slope of M vs. θ plot (Figure 50).

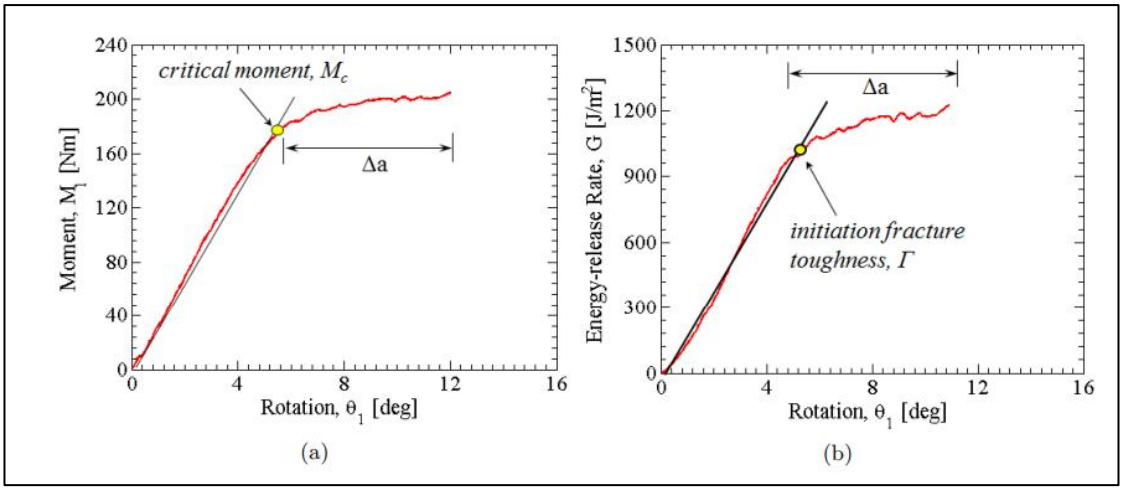

Figure 50: Typical moment (a) and energy-release rate (b) plots for DCB-UBM sandwich specimens. The initiation of fracture propagation and its relative toughness are highlighted.

The interface fracture toughness increased with mode-mixity phase angle and a phenomenological expression was utilized to express fracture toughness as a function of mode-mixity. The foam core specimens with E-glass face sheets showed fracture toughness values in the range 180 - 600 J/m^2 and the toughness values in predominant mode I and mixed mode conditions are comparable to the results obtained using the MMB and TSD test methods for similar materials tested in previous works.

Bladena
Universitetsparken 7
DK-4000 Roskilde
www.bladena.com

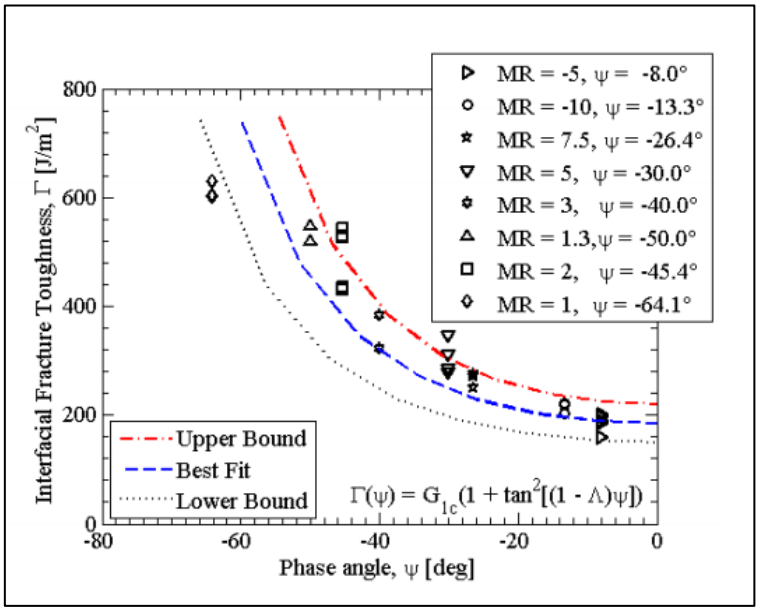

Figure 51: Interface fracture toughness of the PVC foam core E-glass sandwich material. The analytical fit law is superimposed to the experimental data points.

Fatigue growth rates are derived from experimental trials, these are conducted using an advanced method for accurate tracking of the energy release rate amplitude, allowing to reduce the number of samples needed and the time required for a full test plan. These tests are repeated for different mode-mixities as well. For all cases, the R value of the load spectrum is kept unchanged.

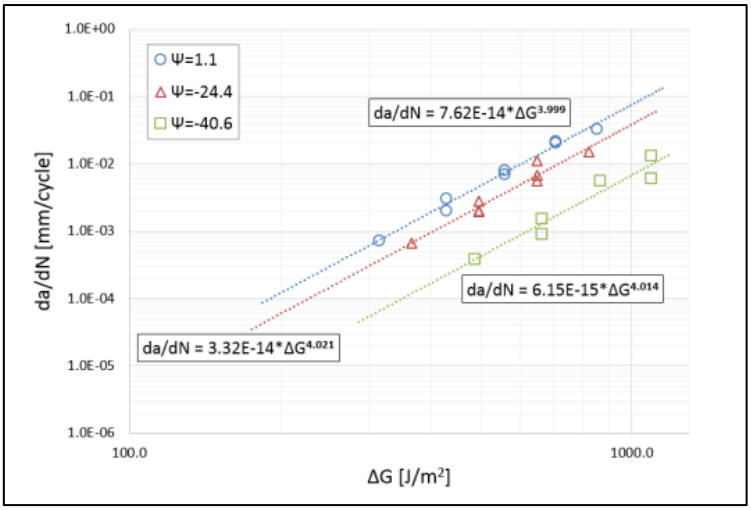

Figure 52: Crack growth rate versus cyclic energy release rate for different mode-mixities.

Bladena
Universitetsparken 7
DK-4000 Roskilde
www.bladena.com

The closed form solutions for the load case of this geometry are used to determine the energy release rates and the phase angle of the interface and populate the material data. These are additionally used to validate the numerical model using Linear Elastic Fracture Mechanics formulations. The numerical model is applied initially to coupon scale tests, but is then implemented in a more complex geometry representing a circular defect of arbitrary shape embedded in a flat panel subjected to various types of loads. The evaluation of the energy release rate is done for both cases invoking a submodel run, where the stress conditions around the crack tip are extracted and a detailed simulation is performed to extract the crack front shape. Then, the Crack Surface Displacement Extrapolation (CSDE) method is used to determine the conditions of the crack front. This method showed to give satisfactory results in sandwich specimens in multiple previous and current works, and will be applied to the large scale testing of the debonded SSP34 blade once experimental results are available.

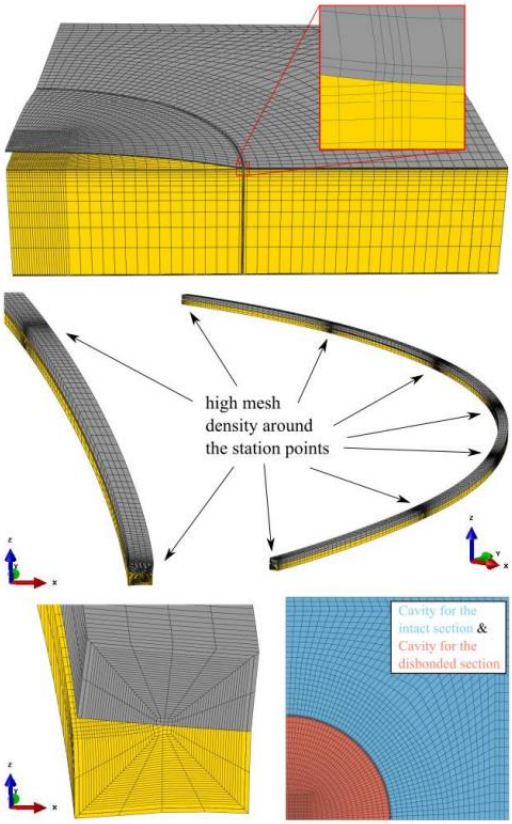

Figure 53: Finite element model of the disbanded foam core sandwich panel using a sub-modelling technique.

Bladena
Universitetsparken 7
DK-4000 Roskilde
www.bladena.com

February 2019

Appendix C Large-scale test (Journal paper)

Out-of-plane deformations of double-curved trailing edge sandwich panels in the root transition zone of a 34m wind turbine blade

Jacob P. Waldbjørn[1], Andrei Buliga[2], Christian Berggreen[1], Find M. Jensen[2]

[1]Department of Mechanical Engineering, Technical University of Denmark, Kgs. Lyngby, Denmark
[2]Bladena ApS, Universitetsparken 7, Roskilde, Denmark

Keywords: *Substructural scale testing, out-of-plane deformation, transition zone, transverse cracks, multi-axial control, 34m wind turbine blade*

Abstract

Transverse cracks on the double curved trailing edge panels within the max chord region and towards the root are one of the more increasing in field damages found on wind turbine blades. Believed to be root cause of these transverse cracks, the out-of-plane deformation of the double curved trailing edge pressure side panels – referred to here as the gauge zone – is evaluated on the inner 15m root section of a SSP 34m wind turbine blade – referred to here as the root section. Through a parametrical study, the free end of the root section is loaded in the quasi-static regime comprising two dofs including edgewise loading (Fy) and torsional moment (Mz) around the longitudinal axis of the blade. This particular load configuration is able to replicate the combined loading scenario to which the blade are exposed during real operational conditions. The root section is through a multi-scale numerical analysis found to be representative. A combination between Fy and Mz are found to generate the highest magnitude of out-of-plane deformation. A linear relation between each of the two dofs versus out-of-plane deformation in the gauge zone is identified. From these data, the out-of-plane deformation governed by a combination between the two dofs is found to follow the rule superposition.

Introduction

Wind turbines are progressively used as a substitute to fossil fuels enhancing the demand for larger and more efficient wind turbine blades. These demands yields for lighter, stronger and more reliable wind turbine blades that can withstand the highly dynamic forces governed by cyclic changes in gravity direction, centrifugal forces and changing wind conditions when sited both on- and offshore [1].

Wind turbine blades are usually made from composite materials including glass and carbon fibre reinforced plastics along with lightweight cores such as e.g. balsa, foam, etc. Hence, the ambition to improve the structural and operational performance within the industry of wind turbines has resulted in extensive research within design principles and material technology applied for wind turbine blades [2]. In these efforts, testing has primary been focusing on two length scales including laminate and structural scale testing [3]. A representation of the multi-scale approach for structural assessment of a wind turbine blade are illustrated in Figure 54.

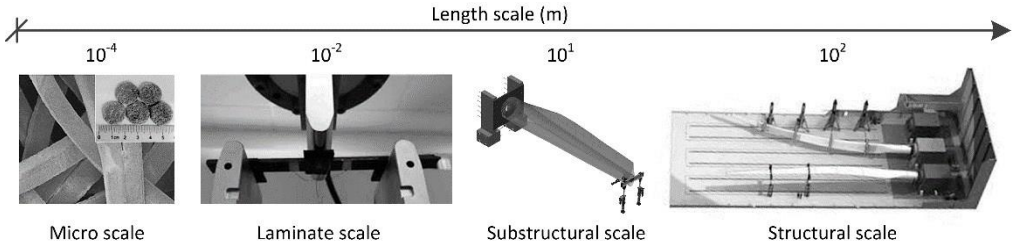

Figure 54: Schematic of the multiscale approach for structural assessment of composite materials and structures for wind turbine blades.

Structural scale testing provides valuable knowledge concerning the structural behavior, however it is time consuming and expensive to perform due to the large dimensions of the wind turbine blade [4], [5], [6], [7]. Here the wind turbine blade is tested according to standard certification prescription including two principle components; in flap wise and edgewise direction. This is a significant simplification compared to the actual forces acting on the blade during service, which include both torsion and bending in different directions at the same time, which is not reflected in the standard today.

In order to investigate the material characteristics of the individual materials in the composite structure, coupon testing on laminate scale is conducted [8]. Such tests are performed on specially designed specimens, resulting in idealized stress and strain states. Consequently, they do not account for the complex stress states and interactions, which often occur within structural scale testing, leading to advanced failure modes among these mixed mode delamination, crack propagation, etc. Such failures often initiate from joints, bearings and other critical details [9], [10] thereby weaken the structure locally, changing the structural response both on a local and global scale.

Substructural scale testing provide a service link between laminate and structural scale testing within the industry of wind energy [11]. The scope of this paper is to present and demonstrate a multi-axial test rig for substructural scale testing on the inner 15m root section of a 34m SSP wind turbine blade – referred to here as the root section. This setup enables structural assessment of the root and transition zone, which exhibits structural

Bladena
Universitetsparken 7
DK-4000 Roskilde
www.bladena.com

failure as a direct impact of the increased size of the wind turbine blade [3]. This hypothesis is from an operational perspective, supported by the Wind Turbine Owners (WTOs) who are reporting a gradually increasing amount of transverse cracks cf. Figure 55 [12]. Regardless of the blade make or model, the transverse cracks are located in the transition zone and max chord region. These cracks typically require extensive repairs up- or down tower which, depending on the severity, in both cases leads to loss of AEP due to downtime. The need to identify the root cause of these blade damages in the design phase is for that reason obvious [13].

Figure 55: Extract of a blade inspection report showing transverse cracks in the max chord region on an infield wind turbine blade.

These structural failures is, among others, believed to be governed by out-of-plane deformations in the large double curved trailing edge aerodynamic shell panels located in the transition zone from max. chord to the stiff cylindrical root region [14]. These deformations, often referred to as 3D longitudinal out-of-plane bending, leads to critical bending stresses in the area where the trailing edge panels are connected/kinked onto the stiff cylindrical root section, which is believed to be the primary source of damage in that region [15].

The out-of-plane deformation is primary triggered by the edgewise dominated loading, which have to carried by the large curved shell panels [3]. Furthermore, a torsional moment around the longitudinal axis of the wind turbine blade is governed by the flap wise deformation, which acts as an in-plane eccentricity to the edgewise load [15].

Here the root section is utilized to evaluate the out-of-plane deformation of the large double curved trailing edge aerodynamic shell panels on the pressure side within the root and transition zone of the SSP 34m blade – referred to here as the gauge zone. Through a servo hydraulic load train, capable of applying a discrete load at the free end of the root section, a combined edge wise load and torsional moment around the longitudinal axis of the blade is applied in the quasi-static regime. Through high-resolution 3D full field measurements by

Bladena
Universitetsparken 7
DK-4000 Roskilde
www.bladena.com

digital image correlation (DIC), the outof-plane deformation within the gauge zone is acquired and evaluated through a parametrical study.

Quantification of the structural effect in terms of out-of-plane deformations within the gauge zone governed by the mechanical constraints applied by the load train is performed through a multi scale approach using Finite Element (FE) modelling. Here the out-of-plane deformations is identified for i) the root section with the structural constraints governed by the load train and ii) the structural scale model of the "stand – alone" SSP34m blade – referred to here as the full blade. With equally applied section forces within the gauge zone of the root section and full blade, it is investigated whether the structural behavior in terms of out-of-plane deformations within the gauge zone are correlating between the two models.

Experimental test setup

A fatigue rated multi-axial test rig for structural assessment of the root section is established. A 3D illustration of the test setup including the load train and clamped support is presented in Figure 56:

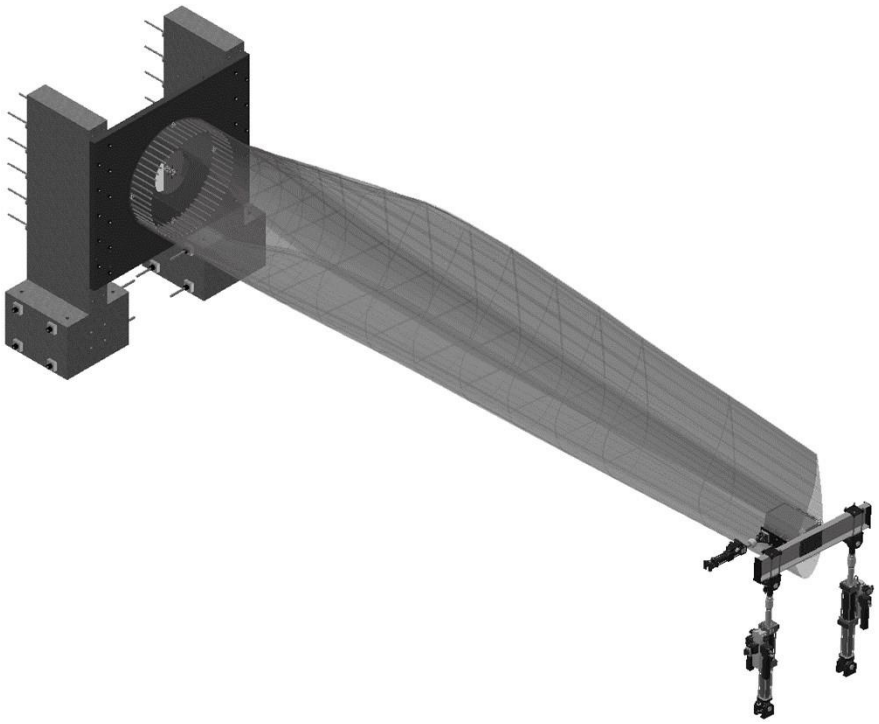

Figure 56: 3D illustration of test setup.

The clamped support of the root joint is governed through a mobile vertical strong wall. This vertical strong wall consists of two concrete towers mounted to the strong floor using

Bladena
Universitetsparken 7
DK-4000 Roskilde
www.bladena.com

pretensioned thread bars. A steel plate with a width, height and thickness of 3.4m, 2.8m and 0.120m respectively is attached to the concrete towers using pretensioned thread bars. The test specimen is connected to the center of the steel plate using 54 pretensioned M30 thread bars. All critical pretensioned thread bars in the mobile vertical strong wall are monitored through donut load cells of the type: K-181/N550-G31.

The load train is capable of applying a discrete load at the free end of the root section comprising three independently operated degrees-of-freedom (dofs) including: flap- and edge wise loading (Fx and Fy) along with a torsional moment (Mz) around the longitudinal axis of the blade. The servo hydraulic system is operated in load control with the format [Fx; Fy; Mz] through a PID controller of the type MTS FlexTest using the MTS 793 software. The coupling between the control point, located in the center of the load carrying box girder cf. Figure 57b, and the corresponding force of each of the actuators are defined through the MTS 793.15 Degree of Freedom Control software following the assumption of rigid body motion. Related coordinate system and notation is presented in Figure 57b. The load is transferred to the free end of the root section through a bulkhead, which is extending 750mm into the free end of the load carrying box girder, fixed to the inner surface of both spar caps using glue and thread bars. Attached to the bulkhead is a moment lever, which accommodates the swivels of actuator A and B with an eccentricity of 1808mm capable of inducing an edgewise load (Fy) and torsional moment (Mz). Actuator A and B is a MTS model 244.31S, each providing a force capacity of ±250kN with a static and dynamic stroke of 518.2mm and 508.0mm respectively. The hydraulic flow through the actuator is operated by two servo valves model MTS 252-25G-01 each with a capacity of 56 l/min. The displacement of the actuator is monitored by an internally mounted LVDT and the force measured by an MTS load cell model 611.22D-01 with a capacity of ±250kN. The flap wise loading (Fx) is induced through actuator C with the swivel attached to the installation plate on the pressure side of the wind turbine blade cf. Figure 57a. Actuator C is a MTS model 244.21 which provide a force capacity of ±50kN with a static and dynamic stroke of 401.3mm and 381.0mm respectively. A servo valve model MTS 252.23 G-01 operates the hydraulic flow through the actuator with a capacity of 19l/min. The displacement of the actuator is monitored by an internally mounted LVDT and the force measured by an MTS load cell model 661.20F-02 with a capacity of ±50kN.

Bladena
Universitetsparken 7
DK-4000 Roskilde
www.bladena.com

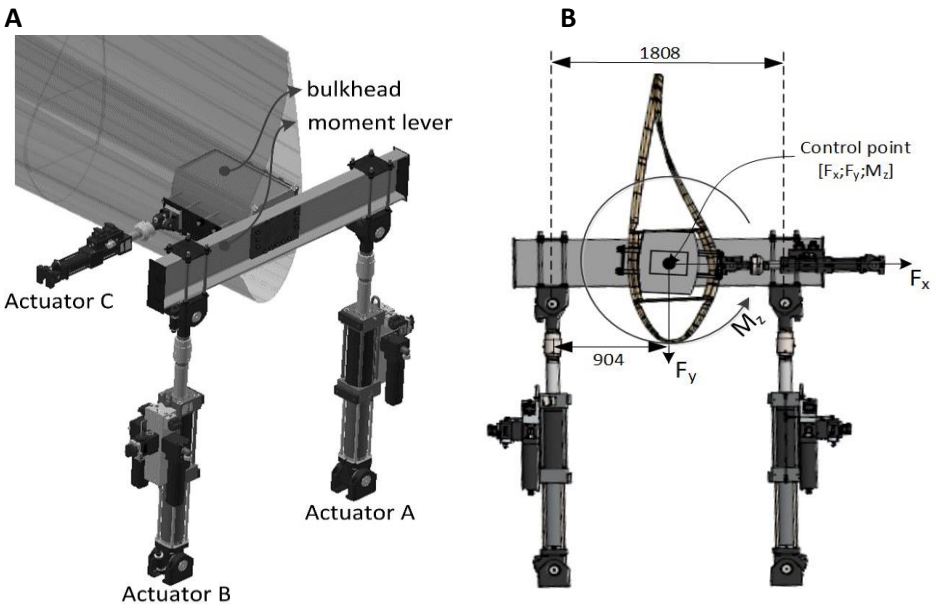

Figure 57: Test setup including: a) 3D illustration of the test setup and b) active coordinate system and notation.

The load train and clamped support presented in Figure 56 combine to form the fatigue rated test setup with a load capacity of ±50kN and ±100kN in the flap and edge wise direction respectively. Furthermore, a moment around the longitudinal axis of 100kNm can be introduced.

To avoid critical peeling stresses in the adhesive bond line connecting the trailing edge (TE) and leading edge (LE) panels with the spar caps, the free end of the root section is fully constrained against in-plane distortion. This is achieved by closing the cross section by installing plywood plates, which are over laminated using GFRP fabrics.

DIC measurements

The out-of-plane deformations within the gauge zone is evaluated on the pressure side of the root section through a full-field 3D DIC system of the type: Aramis 12M by Gesellschaft für Optische Messtechnik mbh (GOM GmbH). The white light camera setup and performance are presented in Table 4.

Table 4: Setup and performance of the 3D-DIC system.

DIC zone	1	2
Technique used	3D image correlation	3D image correlation
Subset	35x35px	40x40px
Shift	6px (83% overlap)	6px (85% overlap)

Bladena
Universitetsparken 7
DK-4000 Roskilde
www.bladena.com

Camera Field of View Measurement points	Dalsa Falcon2 FA-80-12M1H with an 12-bit, 4096x3072pixel CMOS (6.00µm pitch) censor and 24mm lens 2275x1630mm (4096x2663px) 10878	Dalsa Falcon2 FA-80-12M1H with an 12-bit, 4096x3072pixel CMOS (6.00µm pitch) censor and 24mm lens 2250x1764mm (4050x2882px) 9531
Displacement Spatial resolution *Resolution* In plane	 19.44mm, 35pixels 0.046mm, 0.082pixels	 22.23mm, 40pixels 0.045mm, 0.081pixels
Out of plane	0.091mm, 0.16pixels	0.090mm, 0.16pixels

The gauge zone is separated in two zones named: zone 1 and zone 2 cf. Figure 58a. The out-of-plane deformation is monitored through a number of discrete measurement points located along a transverse and longitudinal path cf. Figure 58b, c.

Bladena
Universitetsparken 7
DK-4000 Roskilde
www.bladena.com

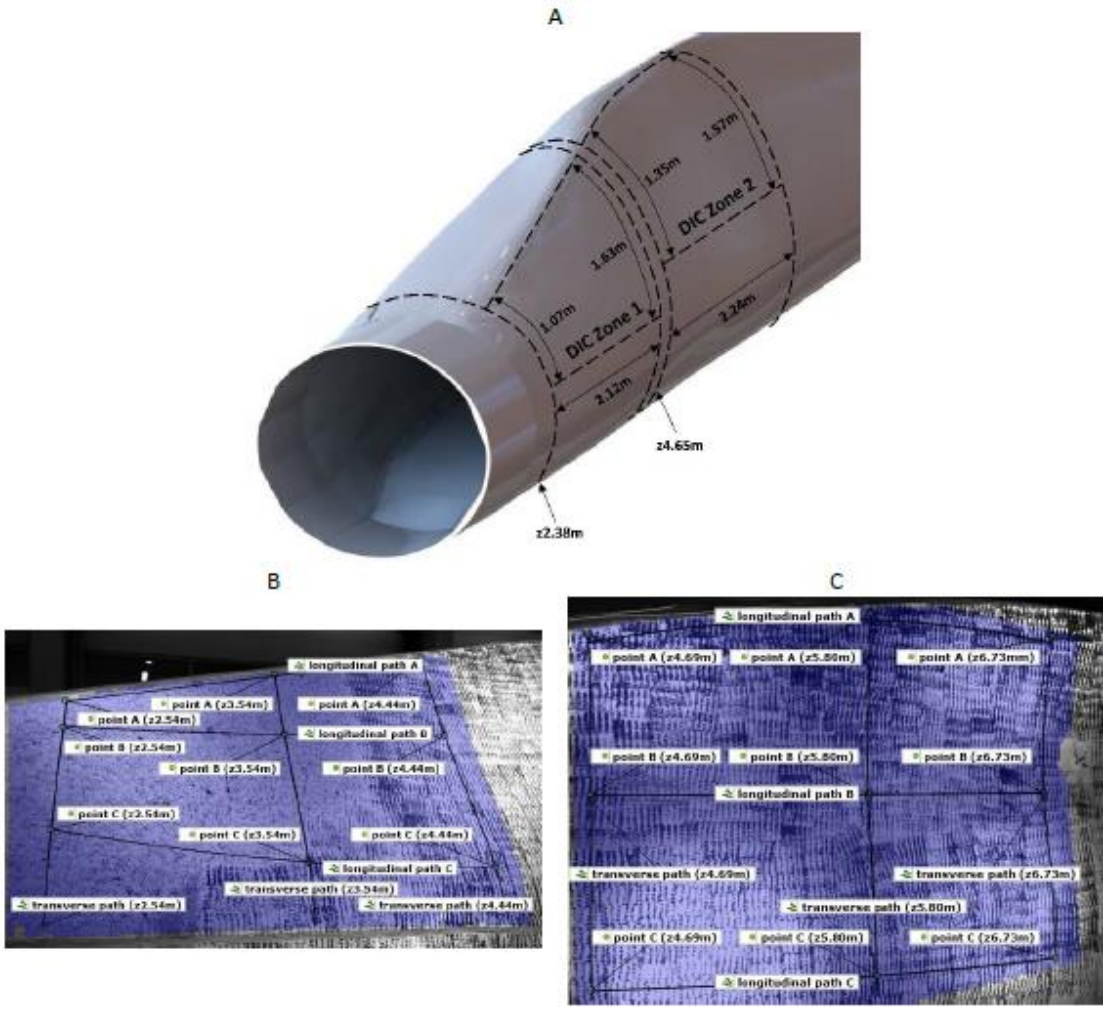

Figure 58: Location, dimension and labelling of DIC zone 1 and 2.

Considering A(z) and C(z) as stiff points, the relative out-of-plane deformation of point B(z) is derived with the longitudinal distance from the root z using the rigid nody removal method cf. Figure 59.

Bladena
Universitetsparken 7
DK-4000 Roskilde
www.bladena.com

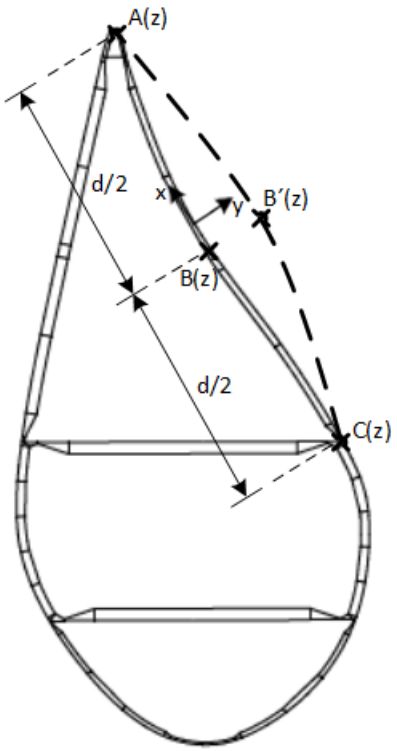

Figure 59: Principle of the rigid nody removal method.

Knowing the absolute measured deformation normal to the surface (along the y-axis cf. the local coordinate system in Figure 59) for each of the three points named A(z), B(z) and C(z), the out-of-plane deformation B´(z) is derived cf. eq. (1).

$$B'(z) = B(z) - \frac{A(z)+C(z)}{2} \quad (1)$$

The longitudinal path A, B and C cf. Figure 59b and Figure 59c are discretized in a finite number of points, which are aligned in the transverse direction with the longitudinal distance to the root z. Each group of aligned points represents a cross section in which the out-of-plane deformation B´(z) is derived cf. eq. (1). The transverse path is likewise discretized in a finite number of points, where point A(z) and C(z) is defined as the two outer points located at TE and after shear web respectively. The out-of-plane deformation B´(z) along the chord width x of each of the intermediate points are derived cf. eq. 1 in the trailing towards leading edge (TTL) direction.

Bladena
Universitetsparken 7
DK-4000 Roskilde
www.bladena.com

Multi-scale numerical assessment of the out-of-plane deformations

A numerical validation is performed to reveal whether the gauge zone exhibits a representative structural behavior in terms of out-of-plane deformation with the mechanical constraints applied at the free end of the root section. This is done through a numerical assessment of the structural behavior at substructural and structural scale. Here the numerical assessment at substructure scale represents the root section presented above while the assessment at structural scale represents the full blade. The purpose is to create a link from blade field operation conditions to the substructural test methodology. A full set of aero elastic loads for the full blade have been used as a starting point. It is assumed that rated wind speeds will be the dimensioning loads on the blade during normal operation.

A combined loading scenario considering the flap wise loads at rated wind speed together with the edgewise loads is used in a base load for simulations of the full blade. The edgewise loads are introduced in a distributed manner along the blade in the corners of the spar caps. Flap wise loads are introduced at ¼ distance from LE, where the aerodynamic center of the profile is located, in a distributed manner along the blade.

With equally applied section forces within the gauge zone of the root section and full blade, it is investigated whether the structural behavior in terms of out-of-plane deformations within the gauge zone are correlating between the two models. The loads applied on the test specimen are introduced using a rigid bulkhead simulated using an RBE2 MPC, with an offset, to account for the eccentricity revealed by the combined edgewise load Fy and moment around the longitudinal axis of the blade Mz.

$$error = \frac{|B'(z)_{substructure} - B'(z)_{structure}|}{|\max(B'(z)_{substructure})|} \times 100 \qquad (2)$$

Non-linear simulations are carried out and the out-of-plane deformations of the panels within the gauge zone of the root section and full blade are evaluated, see Figure 58. The relative discrepancy between the out-of-plane deformation of the gauge zone within the root section and full blade is derived cf. eq. (2).

Bladena
Universitetsparken 7
DK-4000 Roskilde
www.bladena.com

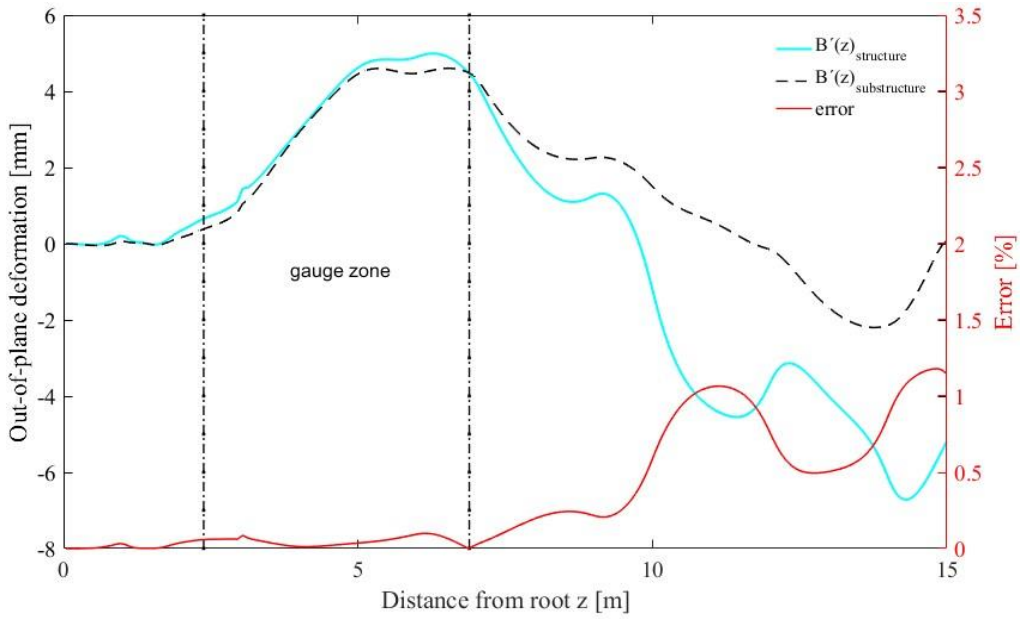

Figure 60: Comparison of the out-of-plane deformation obtained on a the full blade when loaded with aeroelastic loads vs the root section using the substructural load configuration.

The out-of-plane deformations seen in Figure 60 exhibits clear similarities between the two models. The results within the gauge zone correlates with an error of up to 0.1%. When moving towards the tip end of the root section, the measured out-of-plane deformations start to deviate significantly from the full blade due to the artificial constraints induced by the rigid bulkhead, see Figure 57a.

Results and discussion

The out-of-plane deformation B´(z) within the gauge zone of the root section is evaluated in the quasi-static regime comprising two dofs including: edgewise loading (F_y) and torsional moment (M_z). Flap wise loading named F_x will remain zero throughout the entire test campaign. Through 20 load configurations, a parametrical study is conducted with the peak-to-peak loads given in Figure 61a. From P_{ip}^{2} through P_{ip}^{10} each of the two dofs are operated in-phase (ip) cf. Figure 61b, while P_{oop}^{2} through P_{oop}^{10} are operated with a phase shift of 90 degree cf. Figure 61c – referred to here as out-of-phase (oop). The load configuration P^{1} and P^{11} are operated in a single dof configuration covering edgewise load (Fy) or torsional moment (Mz) respectively. Covering 49 equally distributed load steps forming a triangular waveform comprising 3 periods, both dofs are fully reversed loaded cf. Figure 61 b and c.

Bladena
Universitetsparken 7
DK-4000 Roskilde
www.bladena.com

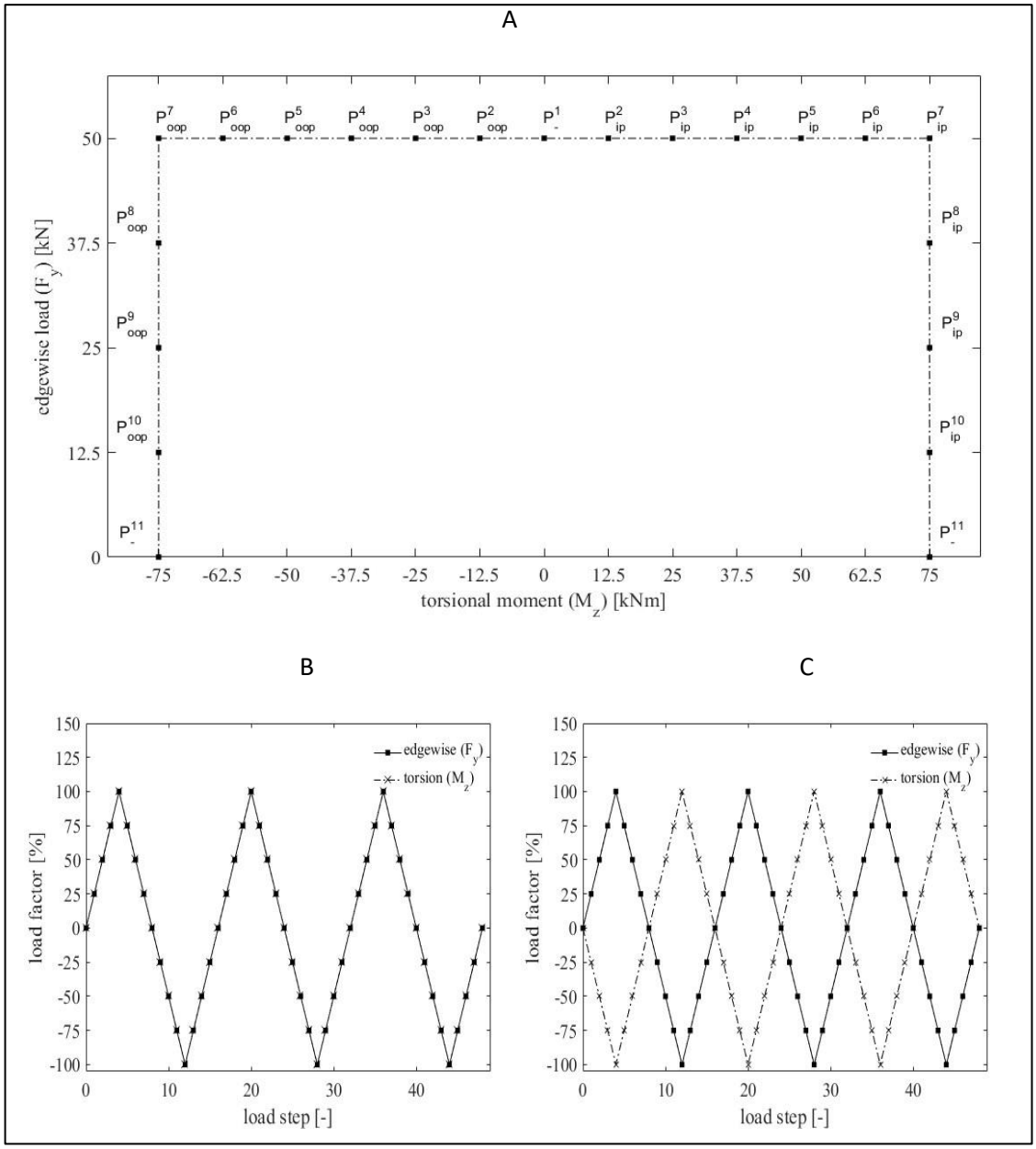

Figure 61: Load configuration including: a) parametrical study, b) in-phase and c) out-of-phase load steps.

The peak-to-peak out-of-plane deformation B´(z) acquired for the extrema load configuration named: P_{-}^{1}, P_{ip}^{7}, P_{oop}^{7}, P_{-}^{11} are presented in Table 5.

Bladena
Universitetsparken 7
DK-4000 Roskilde
www.bladena.com

Table 5: Key results concerning out-of-plane deformations acquired for load configuration: P_{-}^{1}, P_{ip}^{7}, P_{oop}^{7}, P_{-}^{11}

Load config. [-]	F_y [kN]	Mz [kNm]	Dist. From root z [m]	Peak-to-peak out-of-plane deformation B'(z) [mm]
P_{-}^{1}	50 -50	0 0	5.18 4.16	-5.27 4.28
P_{ip}^{7}	50 -50	75 -75	6.30 6.30	-2.96 2.16
P_{oop}^{7}	50 -50	-75 75	4.44 4.12	-8.37 7.57
P_{-}^{11}	0 0	75 -75	4.14 4.14	2.82 -3.20

Based on Table 5 the highest magnitude of out-of-plane deformation B´(z) is achieved within load configuration P_{oop}^{7}. For that reason, the equivalent out-of-plane deformation B´(z) along the longitudinal path B and transverse path located throughout zone 1 and 2 cf. Figure 58b, c is presented in Figure 62 and Figure 63respectively.

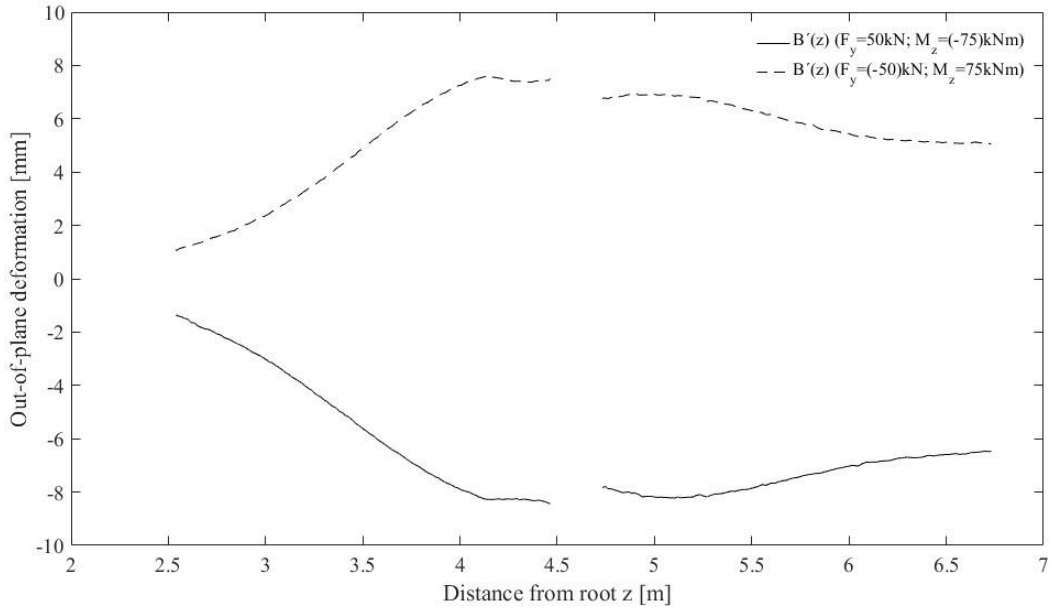

Figure 62: Peak-to-peak out-of-plane deformation in the longitudinal direction for load configuration P_{oop}^{7}

Bladena
Universitetsparken 7
DK-4000 Roskilde
www.bladena.com

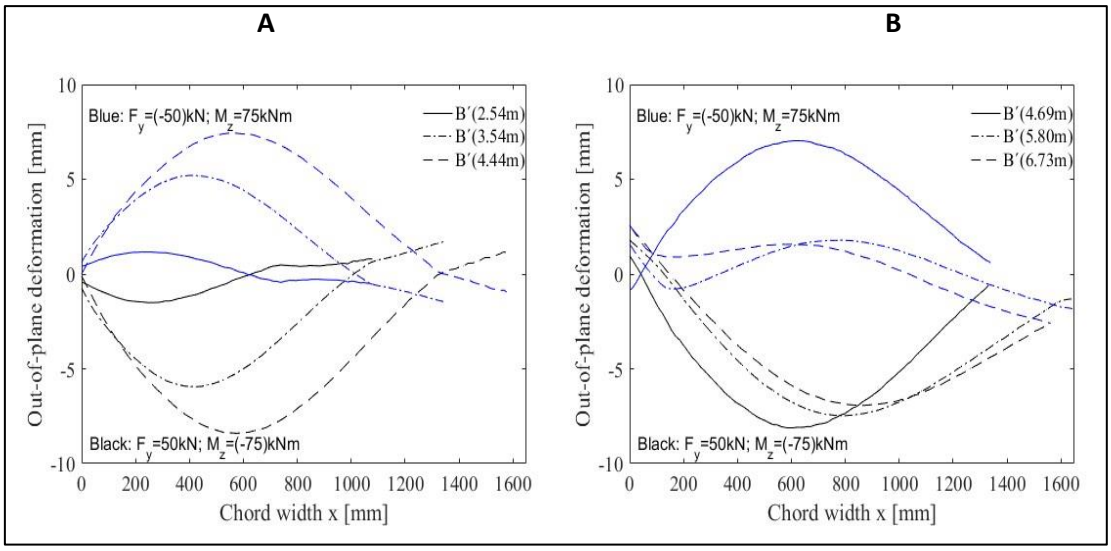

Figure 63: peak-to-peak out-of-plane deformation in the transverse direction for load configuration P_{oop}^{7} including: a) zone 1 and b) zone 2.

Following a triangular load pattern cf. Figure 61b within load configuration $P_{\_}^{1}$ (M_z = 0kNm), the out-of-plane deformation B´(z) of point B within zone 1 and 2 as a function of the edgewise load (F_y) is investigated cf. Figure 64.

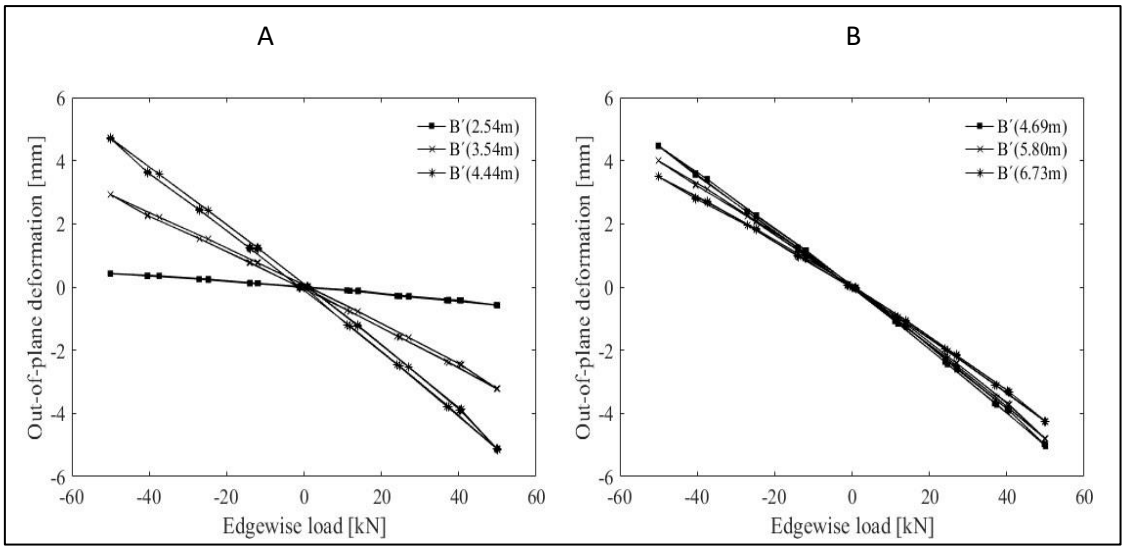

Figure 64: Out-of-plane deformation in point B as a function of edgewise loading when subjected to $P_{\_}^{1}$: a) zone 1 and b) zone 2.

Likewise is the out-of-plane deformation B´(z) of point B within zone 1 and 2 investigated as a function of the torsional moment (M_z) cf. Figure 62, following the triangular load pattern cf. Figure 61b within load configuration $P_{\_}^{11}$ (F_y = 0kN).

Bladena
Universitetsparken 7
DK-4000 Roskilde
www.bladena.com

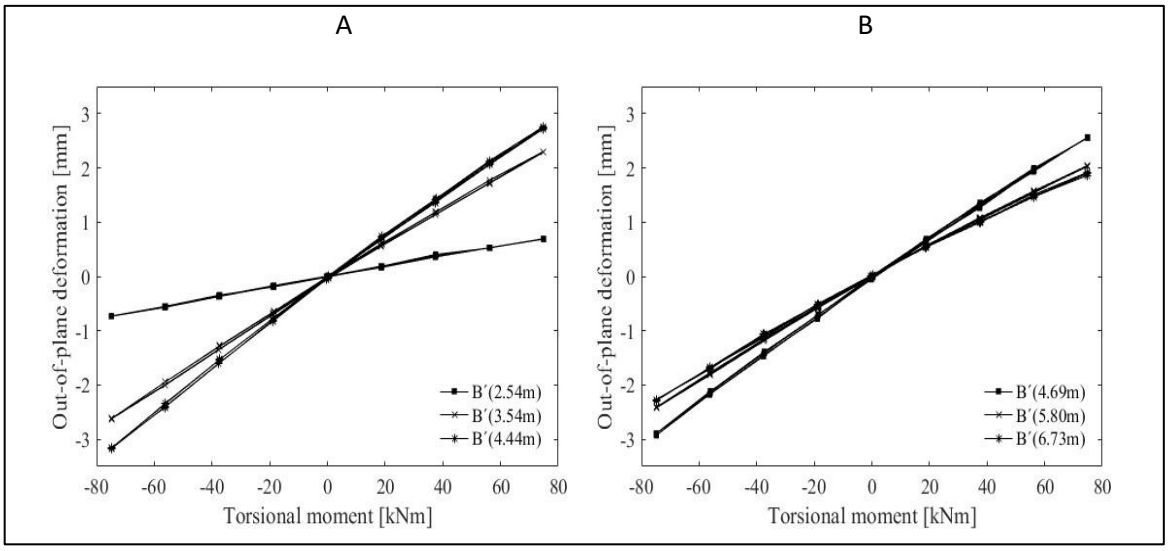

Figure 65: Out-of-plane deformation in point B as a function of torsional moment when subjected to $\underline{P}^{11}$: a) zone 1 and b) zone 2.

From Figure 64 and 65 a linear relation is identified between a varying torsional moment (Mz) and edgewise load (Fy) versus out-of-plane deformation B´(z) measured in point B within zone 1 and 2. Therefore, the out-of-plane deformation for a load configuration comprising both edgewise loading (Fy) and torsional moment (Mz) around the control point is approximated from $\underline{P}^{1}$ and $\underline{P}^{11}$ through superposition. This hypnosis's is tested in the following by comparing the actual measured out-of-plane deformation through DIC $B'(z)_{msd}$ with the approximated out-of-plane deformation from $\underline{P}^{1}$ and $\underline{P}^{11}$ through superposition $B'(zz)_{spt}$. The peak-to-peak out-of-plane deformation acquired at point B is presented in Figure 66 as a function of a varying edgewise load (P_{ip}^{7} through P_{ip}^{11} and P_{oop}^{7} through P_{oop}^{10}). A dashed cyan line represents the equivalent out-of-plane deformation derived through superposition.

Bladena
Universitetsparken 7
DK-4000 Roskilde
www.bladena.com

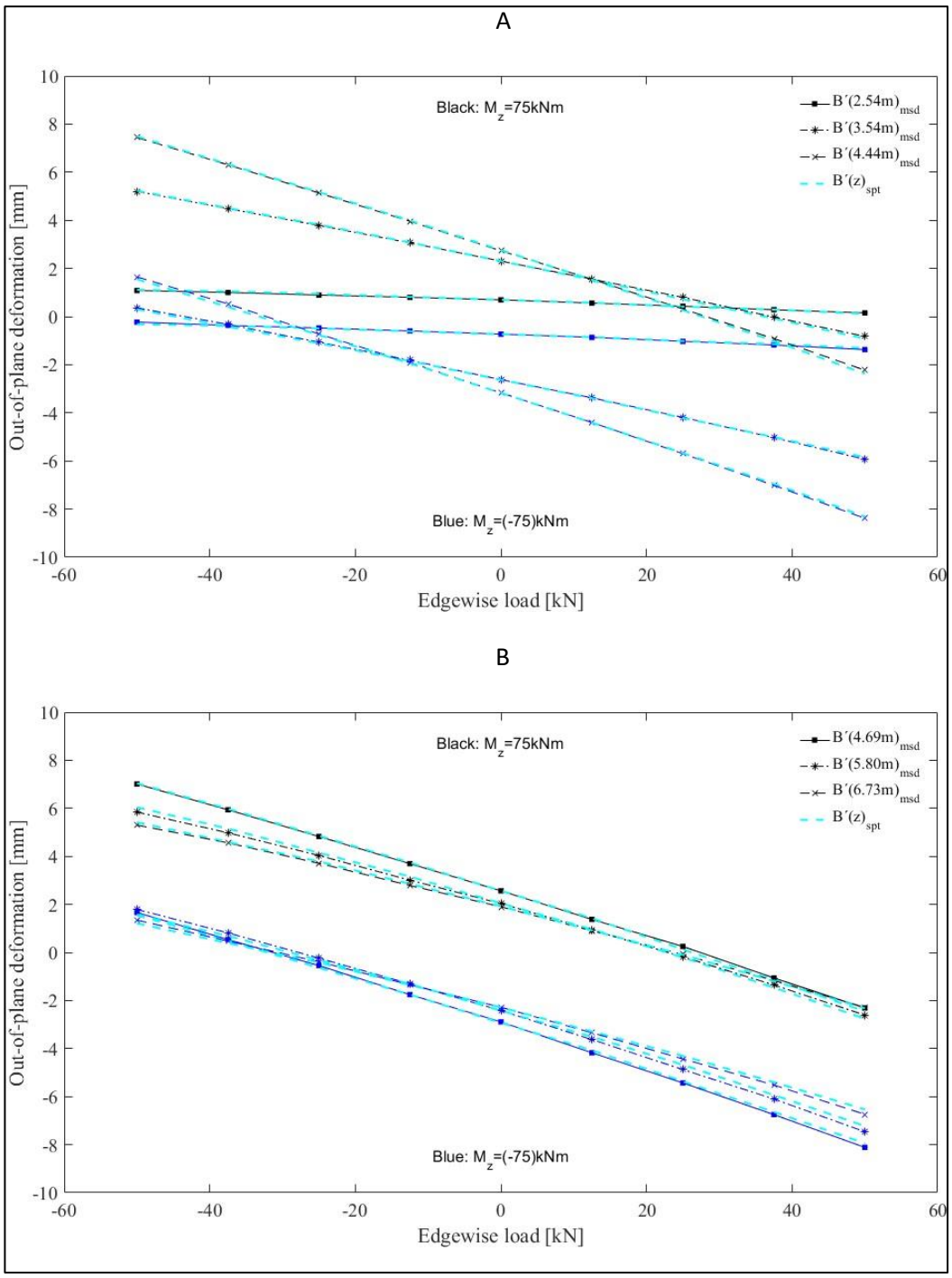

Figure 66: Peak-to-peak out-of-plane deformation in point B for a varying edgewise load: a) zone 1 and b) zone 2.

Bladena
Universitetsparken 7
DK-4000 Roskilde
www.bladena.com

Furthermore, the peak-to-peak out-of-plane deformation $B'(z)_{msd}$ is acquired at point B and presented in Figure 67 as a function of a varying torsional moment (P_{ip}^{1} through P_{ip}^{7} and P_{oop}^{2} through P_{oop}^{7}). A dashed cyan line represents the equivalent out-of-plane deformation $B'(zz)_{spt}$ derived through superposition.

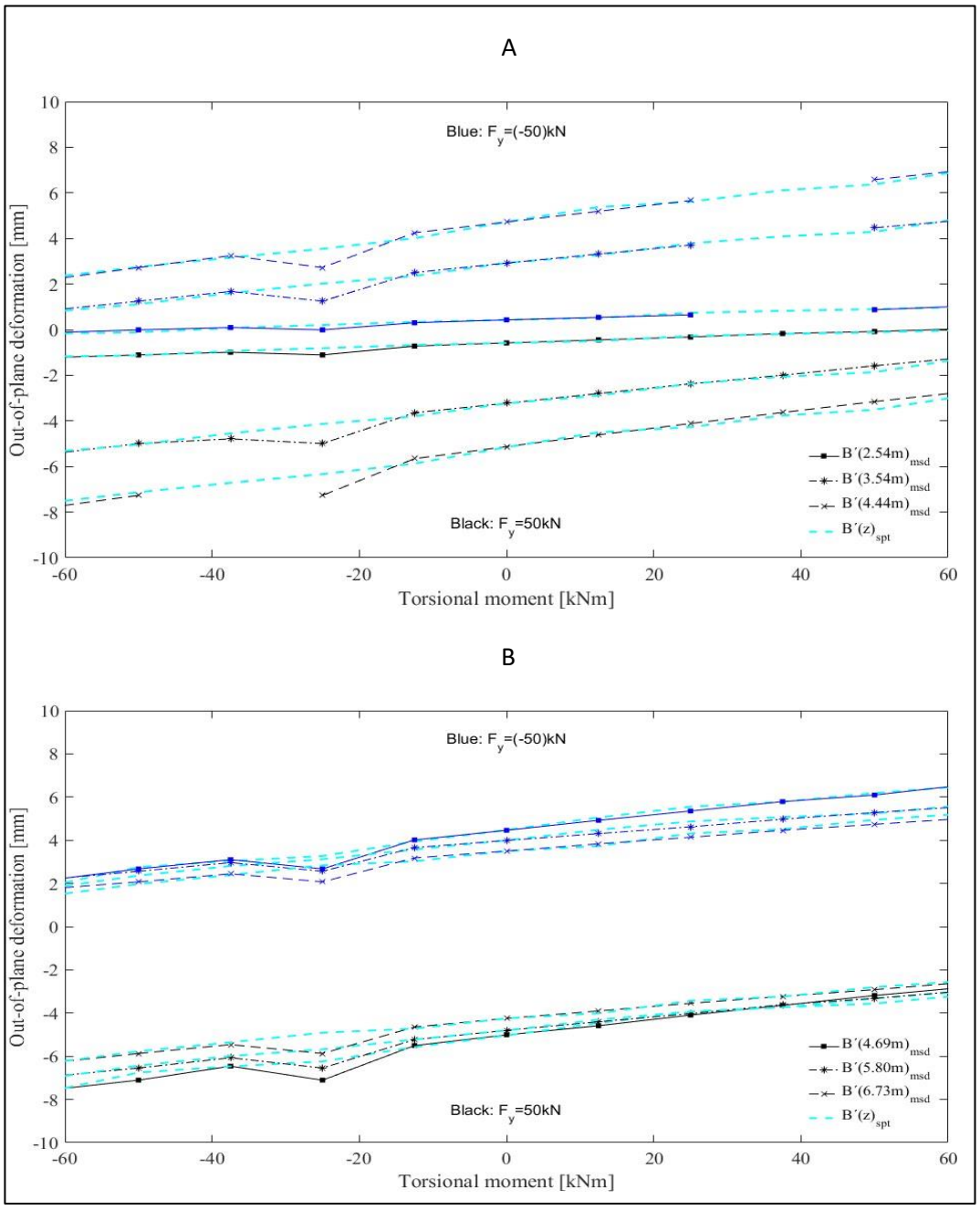

Figure 67: peak-to-peak out-of-plane deformation in point B for a varying torsional moment: a) zone 1 and b) zone 2

Bladena
Universitetsparken 7
DK-4000 Roskilde
www.bladena.com

The relative discrepancy between the actual measured out-of-plane deformation $B'(z)_{msd}$ and the approximated out-of-plane deformation derived from $\boldsymbol{P}_{-}^{\boldsymbol{1}}$ and $\boldsymbol{P}_{-}^{\boldsymbol{11}}$ through superposition $B'(z)_{spt}$ is quantified according to eq. (2).

$$error = \frac{|B'(z)_{msd} - B'(z)_{spt}|}{|\max(B'(z)_{msd})|} \times 100 \qquad (3)$$

Separating the 20-load configurations in Figure 61a into four load groups identified in the legend of Figure 68, the root-mean-square (RMS) error of eq. (3) for each point B with the longitudinal distance from the root z is presented in Figure 68.

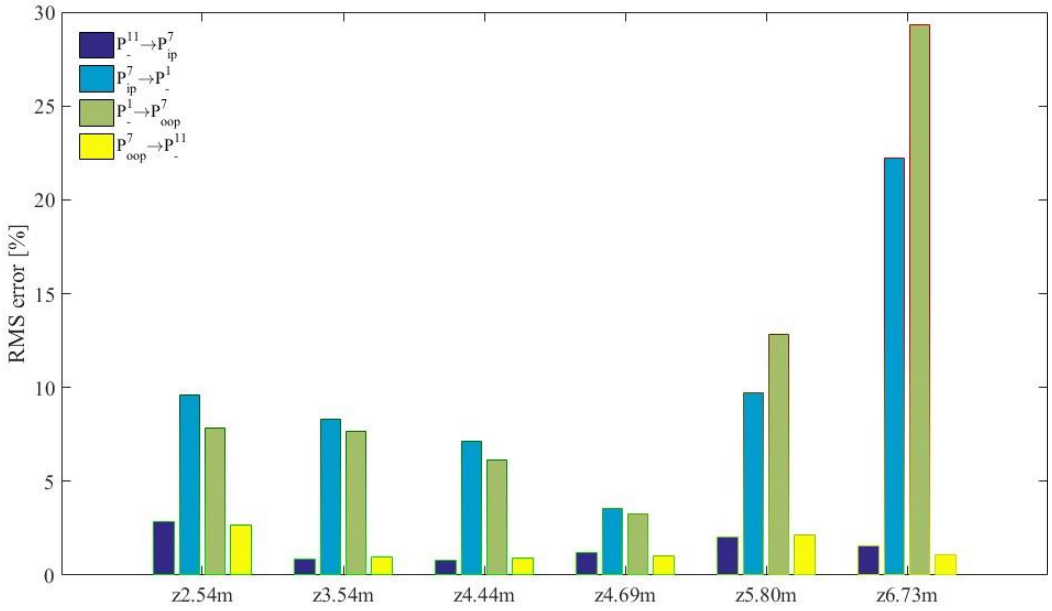

Figure 68: Root-mean-square error at point B´(z) when covering all load configurations with

The load configuration with a constant torsional moment (M_z) comprise a significant improved correlation between $B'(z)_{msd}$ and $B'(z)_{spt}$ relative to the load configuration with a constant edgewise load (F_y). The reason is most likely the poor linear relation seen in Figure 67, which is significant at M_z = 25kNm.

Conclusion

As a service link between laminate and structural scale testing within the industry of wind energy, a multi-axial test rig for substructural testing was demonstrated on the inner 15m root section of an SSP34m wind turbine blade. Through a servo hydraulic load train connected to the free end of the substructure, the blade was subjected to two independently operated dofs including edgewise loading and torsional moment around the longitudinal axis of the blade. This setup enabled structural assessment of the root and transition zone on

Bladena
Universitetsparken 7
DK-4000 Roskilde
www.bladena.com

which a gradually amount of transverse cracks were reported from blade inspection reports regardless of blade make or model. Leading to critical bending stresses in the area where the trailing edge panels are connected/kinked into the stiff cylindrical root section, 3D longitudinal out-of-plane bending were investigated within the large double curved trailing edge aerodynamic shell panels located in the transition zone from max chord to the stiff cylindrical root region. Through a multi-scale approach covering i) the inner 15m root section of the SSP34m blade with the mechanical constraints exhibited within the experimental substructure and ii) the structural scale model of the SSP34m blade, the mechanical response in terms of out-of-plane displacements within the gauge zone were evaluated using FE-modelling. With identical section forces within the gauge zone of the substructural and structural scale model, the results within the gauge zone correlation with an error of up to 0.1%. Through high-resolution 3D full field DIC measurements, the out-of-plane deformations within the gauge zone were acquired and evaluated through a parametrical study. Here an out-of-plane deformation within the gauge zone of up to 8.37mm were identified governed by the combined load configuration P_{oop}^{7}, located 4.44m from the root. When operating each of the two dofs independently, a linear relation between a varying edgewise load and torsional moment vs out-of-plane deformation within the gauge zone were identified. This observation indicated that the out-of-plane deformation observed is triggered by the geometry of the shell structure and not instability, which is a non-linear phenomenon. Furthermore, it was found that the out-of-plane deformations governed by a combination of edgewise loading and torsional moment could be derived through the rule of superposition.

Acknowledgement

The authors would like to acknowledge the financial support by the Energy Technology Development and

Demonstration program (EUDP) under the grant number: 64013-0115. Furthermore, the authors acknowledge the Villum Center for Advanced Structural and Material Testing (CASMaT), Technical University of Denmark (DTU) for supplying laboratory facilities and technical support.

Bladena
Universitetsparken 7
DK-4000 Roskilde
www.bladena.com

References

[1] S. Singh, "Wind power: Future lies within," in 7th India International Conference on Power Electronics, Patiala, 2016.

[2] O. T. Thomsen, "Sandwich Materials for Wind Turbine Blades - Present and Future," Journal of Sandwich Structures and Materials, vol. 11, no. 1, pp. 7-26, 2009.

[3] F. M. Jensen, "Ultimate Strength of Large Wind Turbine Blade," Department of Civil Engineering, Technical University of Denmark, Kgs. Lyngby, 2008.

[4] H. F. Zhou, H. Y. Dou, L. Z. Qin, Y. Chen, Y. Q. Ni and J. M. Ko, "A review of full-scale structural testing of wind turbine blades," Renewable and Sustainable Energy Reviews, vol. 33, pp. 177-187, 2014.

[5] F. M. Jensen, B. Falzon, J. Ankersen and H. Stang, "Structural testing and numerical simulation of a 34m composite wind turbine blade," Elsevier, Composite Structures, vol. 76, no. 1-2, pp. 52-61, 2006.

[6] H. G. Lee and J. Park, "Static test until structural collapse after fatigue testing of a full-scale wind turbine blade," Composite Structures, vol. 136, pp. 251-257, 2016.

[7] O. C. T. Lars, E. Lund and T. T. Ole, "Structural collapse of a wind turbine blade. Part A: Static test and equivalent single layered models," Composites Part A: Applied Science and Manufacturing, vol. 41, no. 2, pp. 257-270, 2010.

[8] P. Brøndsted, H. Lilholt and A. Lystrup, "Composite materials for wind power turbine blades," Annual Review of Materials Research, vol. 35, no. 1, pp. 505-538, 2005.

[9] H. S. Wang, C. L. Hung and F. K. Chang, "Bearing failure of bolted composite joints .1. Experimental characterization," Journal of Composite Materials, vol. 30, no. 12, pp. 1284-1313, 1996.

[10] R. Karakuzu, B. M. Icten and Ö. Tekinsen, "Failure behavior of composite laminates with multi-pin loaded holes," Journal of Reinforced Plastics and Composites, vol. 29, no. 2, pp. 247-253, 2010.

[11] M. E. Asl, C. Niezrecki, J. Sherwood and P. Avitabile, "Application of structural similitude theory in subcomponent testing of wind turbine blades," in 29th Annual Technical Conference of the American Society for Composites, La Jolla, 2014.

[12] C. IVS, "Guide2Defects," Guide2Defect, 06 January 2016. [Online]. Available: www.guide2defect.com. [Accessed 17 December 2018].

Bladena
Universitetsparken 7
DK-4000 Roskilde
www.bladena.com

[13] NaN, "Global Wind Service," Global Wind Service, 6 January 2008. [Online]. Available: https://globalwindservice.com/. [Accessed 14 January 2019].

[14] A. Buliga, "Energy Workshops," Bladena A/S, 20 August 2018. [Online]. Available:

https://energyworkshops.sandia.gov/wind-workshops/2018-2/. [Accessed 29 August 2018].

[15] F. M. Jensen, M. Werk, A. Buliga, C. Berggreen, J. P. Waldbjoern, J. D. Sørensen, Y. Yang and E. S. Jensen, "Root and Transition zone (RATZ) and reduction O&M cost of WT blades," Bladena A/S, Roskilde, 2019.

Bladena
Universitetsparken 7
DK-4000 Roskilde
www.bladena.com

Appendix D Data report: Full-scale test of LM58.7m blade with fatigue loads

D1. Acknowledgements

Bladena and partners would like to acknowledge the Energy Development and Demonstration Program (EUDP) for financial support under the grant number: 64015-0062 RATZ Project. Furthermore, acknowledgment goes to LM Wind Power who has donated a LM58.7m blade to be used in the full-scale test and demonstration performed in the project.

Bladena
Universitetsparken 7
DK-4000 Roskilde
www.bladena.com

D2. Introduction

The current report describes an edgewise fatigue test that was performed on the LM58.7m blade under the frame of the EUDP RATZ project, while the entire experiment was executed at Blaest test center. It is a part of a series of blade tests performed in order to investigate the Root Area Transition zone which will become even more critical in terms of structural defects as the wind turbines keep increasing in size.

Figure 69: Full scale fatigue test. The clamps are mounted on the different sections of the blade to apply the appropriate load.

The focus with the current test is to investigate the fatigue strength of the transition zone, under edgewise fatigue loading. The current experiment focuses to a Proof-of-concept investigation of the Bladena patented Floor™ solution (Figure 70).

Bladena
Universitetsparken 7
DK-4000 Roskilde
www.bladena.com

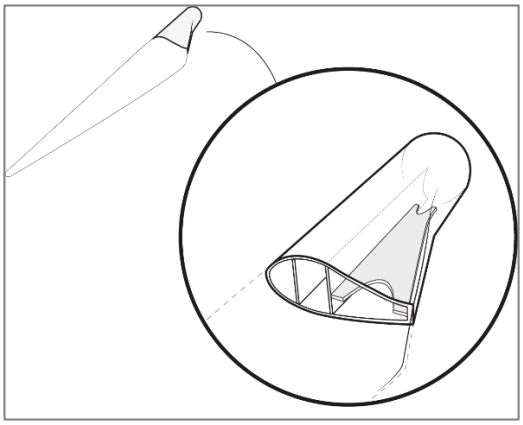

Figure 70: The Floor™ solution

After the Floor™ technology was retrofitted, the crack growth stopped. This was also documented in the "*Root Area Transition Zone – RATZ and Reduction O&M cost of WT blades, EUDP project 64015-0062 – Final Report*". Finally, as part of the damage investigation on the blade, various NTDs were performed to examine the blade and evaluate potential damages.

D3. Experimental procedure

In the current chapter the test conditions and configurations are explained. As already mentioned, the blade was exposed to a pure edgewise fatigue test with a total of 2,950,539 million cycles. The blade was positioned with the suction side facing the floor of the test hall as it is illustrated in Figure 69.

The Floor™ product

Because of the complex geometry of the Root-Transition zone, critical edgewise shear forces are developing at this area which can lead to critical failures of the blade. By considering the importance of this area in terms of structural performance, it becomes apparent that a retrofit solution could increase the structural capacity and minimize the likelihood of failure occurrence. With respect to the latter, the Floor™ can be described as a horizontal shear web between the trailing edge and the aft shear web which can result to the mitigation of risk of damages and failures in this region. For the current fatigue test, the Floor™ was installed from 3m until 9m from the blade root. A visual illustration of the Floor™ is depicted in Figure 71, while the installation on the LM58.7m blade is depicted in Figure 72.

Bladena
Universitetsparken 7
DK-4000 Roskilde
www.bladena.com

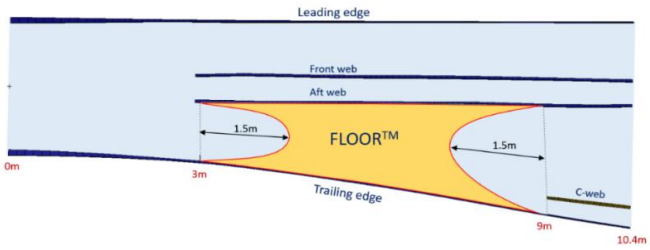

Figure 71: The Floor™ in the LM58.7m blade started 3m from blade root and ended just before the start of the C-web 9m from blade root. In each end of the Floor™ a "fish-mouth" was introduced to reduce local stress concentrations.

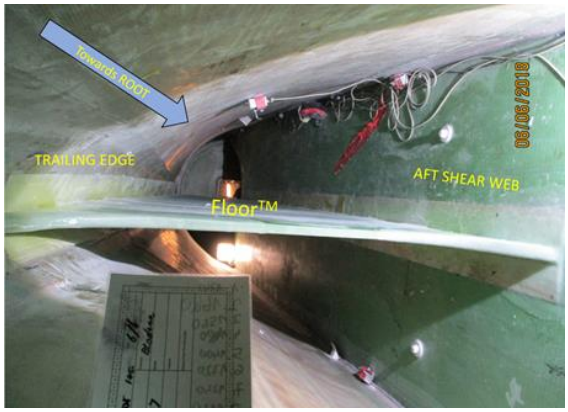

Figure 72: The Floor™ is designed to be retrofitted in the Root-transition zone of a wind turbine area between the aft shear web and the trailing edge. Here can be seen the first prototype of a Floor™ retrofitted in the LM58.7m blade.

Experiment's pre-conditions and focus

Before the initiation of the test the blade has undergone a thorough inspection to ensure that no design flaws have been found. Indeed, none major flaws were found and therefore the blade was considered un-damaged.

Finally, the focus was mainly centered in the transition zone area as it is performed under the RATZ EUDP project. However, regular observations have been done during the test to evaluate the structural integrity throughout the fatigue test.

D4. Load configuration

Load application for fatigue test

The fatigue loads are applied by exciting the blade near its natural frequency using an eccentric mass powered by an electrical motor. By adjusting the eccentric mass and placing additional masses on the blade (if needed) the measured strains (and inferred bending moment) can be matched to the edgewise target bending moments. Both the fatigue exciter and the additional masses are to be attached to the blade using clamps. The measured strains

Bladena
Universitetsparken 7
DK-4000 Roskilde
www.bladena.com

are calibrated to the applied bending moment by undertaking a static calibration pull before, during and after the edgewise fatigue tests.

Exciter placed under the blade	Mass added under the blade
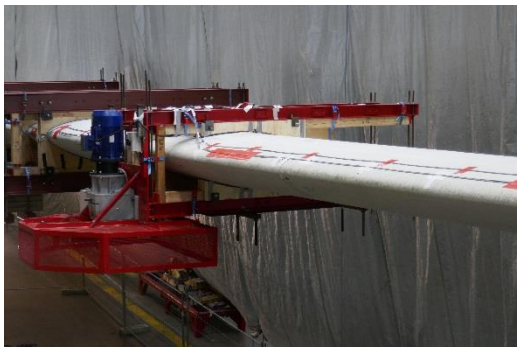	

Figure 73: Test configuration and load application.

As it can be seen from Figure 73, during the edgewise fatigue test the LM58.7m blade was tested horizontally with the suction side facing the floor of the test hall. It is intended due to the limited time to relatively fast reach a high load level. As already mentioned, the blade was tested with and without the Floor™ technology. The test without Floor™ will then be running until failure is observed in the transition zone. After failure has occurred and damage growth has been observed, the Floor™ will be installed and the same load level will be applied.

Loads level

The LM58.7m blade was tested at the Blaest Test Center in full-scale fatigue. The blade was positioned hanging from a vertical concrete block with the suction side facing the floor. Five clamps at 20m, 28m, 32m and 56m from blade root carries added masses and an exciter are placed at the clamp 32m from blade root. The blade was excited in edgewise fatigue. The edgewise fatigue load has been increased compared to the certification load to decrease the number of fatigue cycles. The test is started at a load level 16% higher than tested in certification. The increase in load is due to a reduction in the number of cycles. When the number of cycles is cut in half, the load level must increase with 8%. The number of cycles has been reduced from 6 million cycles in the original certification test to 1.5 million cycles in the RATZ project. This means that with the applied load the blade is designed for 1.5 million cycles in certification.

It should be stated that at 760960 cycles the load level is increased with 20%. This changes the number of test cycles that is the equivalent to the designed certification test (number of

Bladena
Universitetsparken 7
DK-4000 Roskilde
www.bladena.com

cycles), it would need to be calculated to know if the damage developed before or after the certification test would have been reached.

Clamps, exciter and mass offset

The blade is loaded with mass added at four wooden clamps and an exciter at one of the clamps.

Desciption	Z-position [m]	Total mass at clamp* [kg]
Clamp	20	6000
Clamp	28	1800
Clamp + Exiter	32,4	1600
Clamp	56.3	50
* The total mass at clamps are the mass of the clamp plus the added mass at the clamp plus in one case the mass of the exciter.		

Table 6: Added masses as these were implemented on the wooden clamps.

Both the exciter and the added masses are placed under the blade (at suction side, facing the floor). This was done to introduce an added torsion in the blade due to the offset of masses. No significantly effect of the mass offset was documented, and the test can be thought of as a pure edgewise fatigue test.

The exciter and added mass at one of the clamps can be seen in Figure 73.

D5. Measurements

The current chapter presents all the results obtained from the full-scale fatigue test. The results are categorized in two main groups, where the first one refers to the ASM measurements while the second group refers to the strain development at different blade sections and locations.

Deformation measurements (ASMs)

During the fatigue test different cross sections were chosen to measure the blade's load deformation responses e.g. panel bending. With that in mind, different positions were chosen on both the rear and main box to evaluate the overall displacements, while all the notations are illustrated in Figure 74. It should be noted that in the Figure 74 (left) all notations are presented (Positions A, B, C, D and E) while through the rest of this report the notations for the measurement positions are kept constant for every cross section.

Bladena
Universitetsparken 7
DK-4000 Roskilde
www.bladena.com

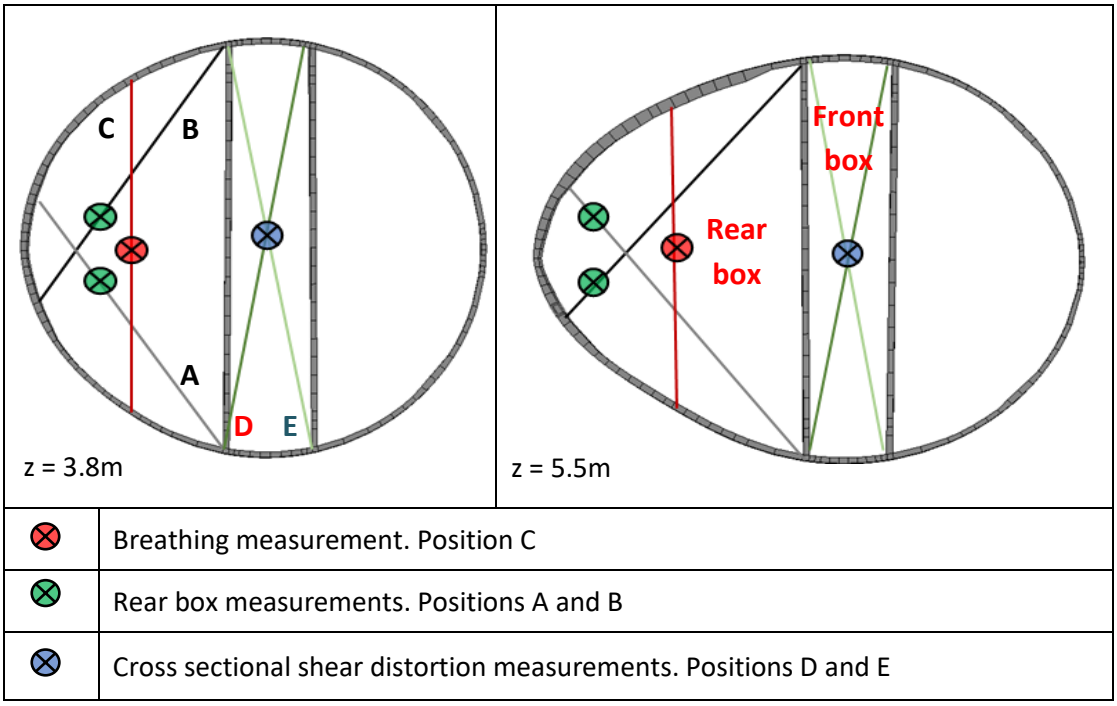

⊗	Breathing measurement. Position C
⊗	Rear box measurements. Positions A and B
⊗	Cross sectional shear distortion measurements. Positions D and E

Figure 74: Cross sections at the transition zone at the sections z=3.8m and z=5.5m. The measurement positions and the relative notations are illustrated.

The first group of measurements that will be presented herein refers to the investigation of the cross-sectional shear distortion before the Floor™ technology is implemented. This is done by measuring through positions "A, B" for the rear box and "D, E" for the main box. From the following figures (Figure 75) it can be concluded that the displacements around the diagonal B, decrease along the blade's length. On the other hand, the displacements along the diagonal A indicate an increasing trend until z=8m, but after that point they follow a descending trend as approaching the tip of the blade.

Bladena
Universitetsparken 7
DK-4000 Roskilde
www.bladena.com

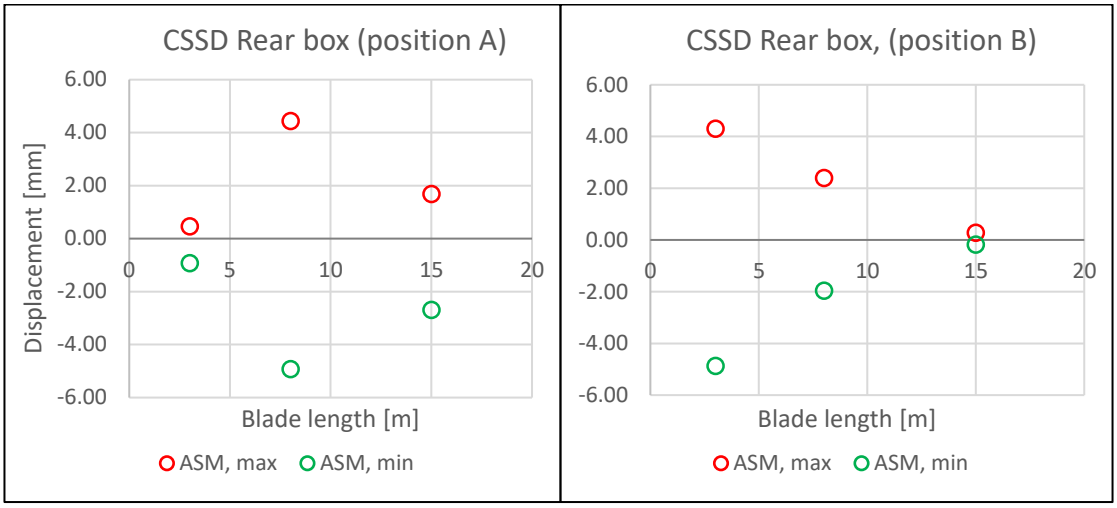

Figure 75: Cross sectional shear distortion measurements at position A (left) and position B (right). The second group of measurements refers to the cross-sectional shear distortion of the main box.

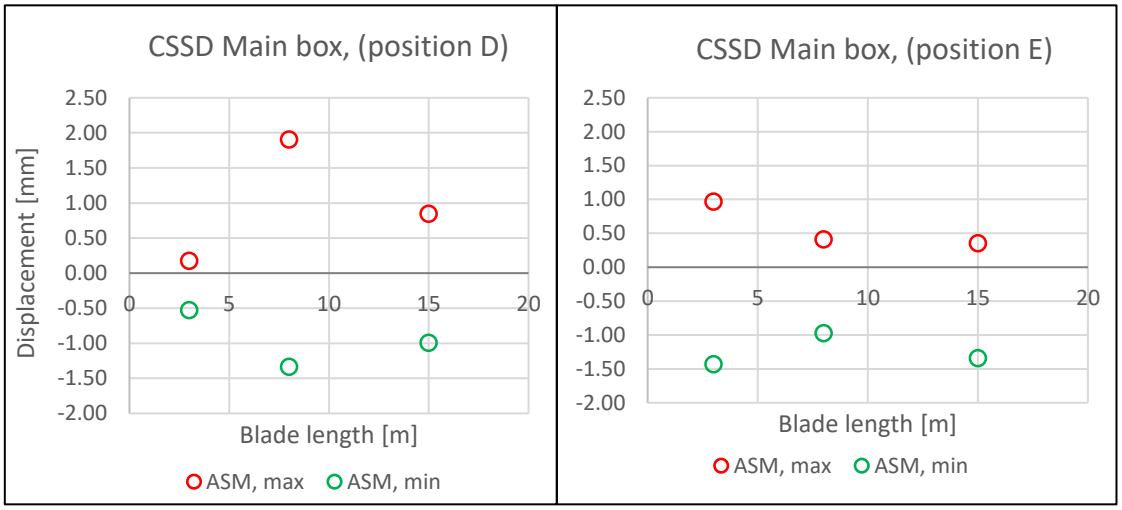

Figure 76: Cross sectional shear distortion measurements at position D (left) and position E (right).

Aiming to the overall analysis of the cross-sectional movement, the “breathing” between the pressure and suction side is also visualized in Figure 77 for different sections along the blade.

Bladena
Universitetsparken 7
DK-4000 Roskilde
www.bladena.com

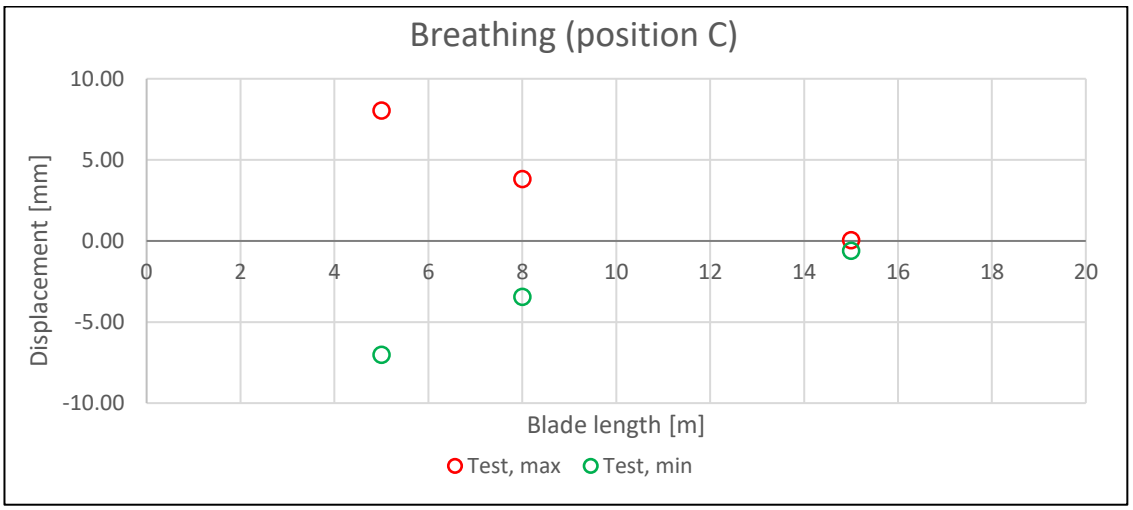

Figure 77: Breathing measurement before the Floor installation.

In addition to the panels' relative movement i.e. breathing, in Figure 78 a comparison is made between the breathing measurements for both with and without the Floor™ solution. The depicted sections are located at z=5m and z=8m, as both points are inside the range of the Floor's implementation which is installed from 3m to 9m. It becomes apparent that the Floor™ has great influence on the breathing at the trailing edge panel, especially at 5m, where the resulted deformation has been decreased by 24%.

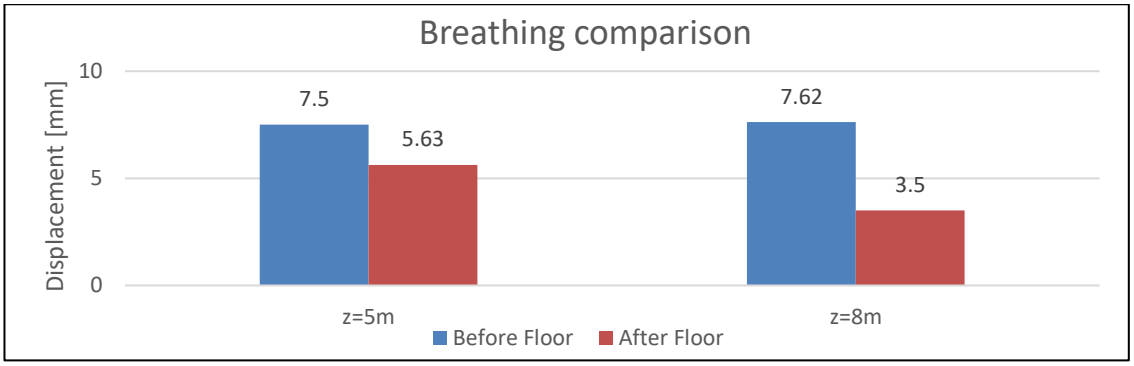

Figure 78: Breathing between PS and SS at trailing edge with and without the Floor™ solution.

During the stage where the blade was "as-is" an additional measurement was introduced to capture the longitudinal displacement between the trailing edge and the fore aft shear web, as this is illustrated in Figure 79.

Bladena
Universitetsparken 7
DK-4000 Roskilde
www.bladena.com

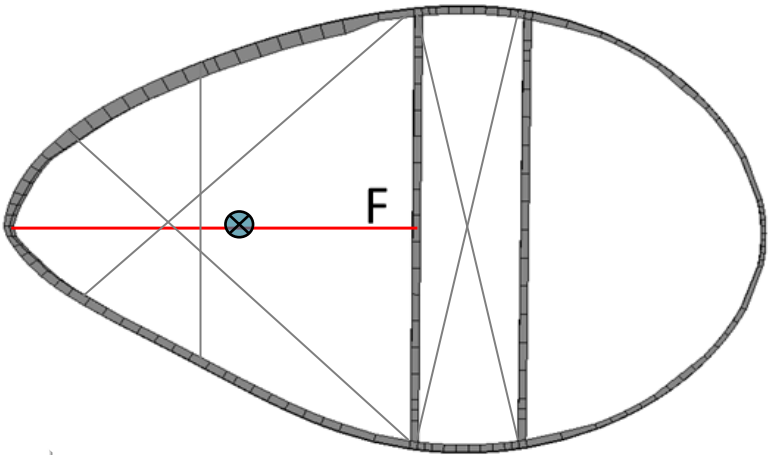

Figure 79: Rear box horizontal displacement. ASM placement from the trailing edge to the fore aft shear web. The presented cross section is located at z=7.5m.

In Figure 80, the horizontal displacement along the F direction is illustrated for three different locations at z=3m, z=7.3m and z=9m. While the displacements until z=7.3m follow a rather constant trendline, at z=9m there is a sudden increase. This can be justified by taking into account the geometry of the Floor™, which at z=7.3m reshaped in the "fish mouth" as this presented in Figure 71.

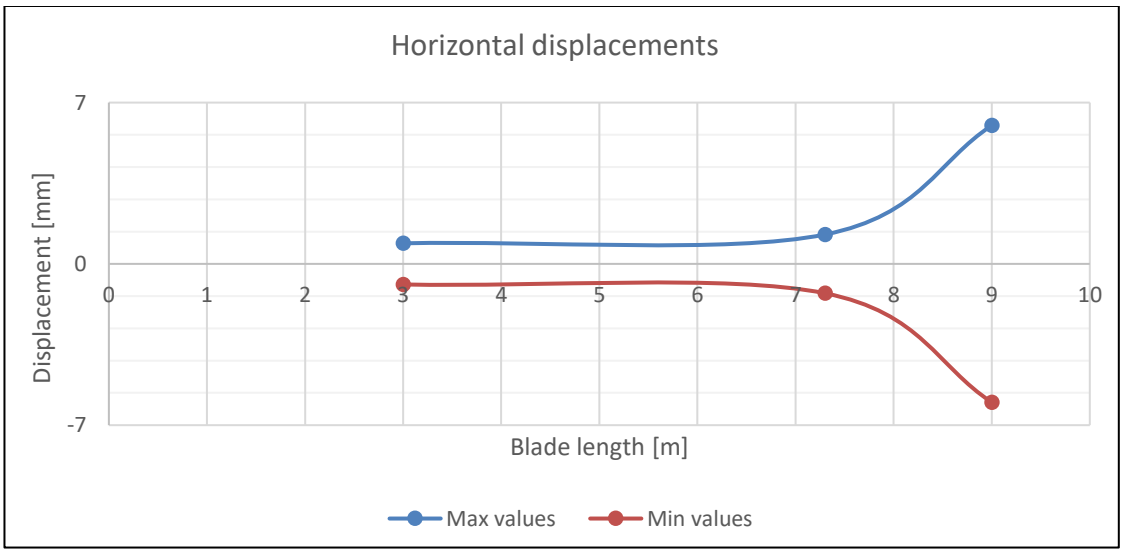

Figure 80: Longidutinal displacements along different sections of the blade, located at z=3m; 7.3m; 9m

Bladena
Universitetsparken 7
DK-4000 Roskilde
www.bladena.com

Strain (strain gauges)

Longitudinal strain on leading edge (LE) and trailing edge (TE)

In terms of developing strains at the trailing and leading edge, multiple sections were chosen along the blade to evaluate its response and the influence that the Floor™ technology may have. In Figure 81 the strain gauges at leading edge are illustrated, while a comparison is being made between the different load levels as well as after the Floor™ has been installed. As it was expected, the strains do not seem to get affected by the presence of the Floor™, while the highest difference is resulted between the different load levels of 100% and 120%.

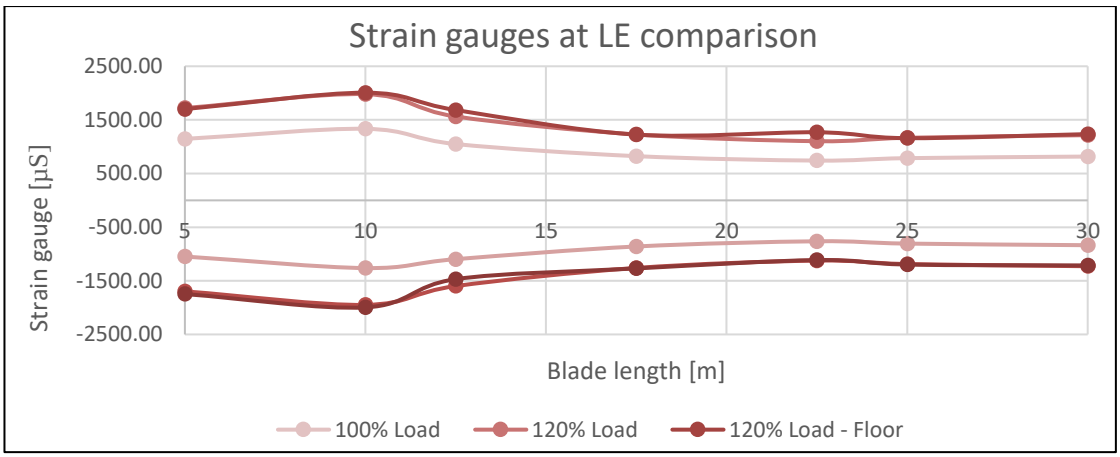

Figure 81: Straing gauges at leading edge for different load levels and comparison with Floor™.

Similarly, in Figure 82 the strain gauges at the trailing edge are depicted. Again, the Floor does not influent the resulted strains, while the highest impact is from the load increase.

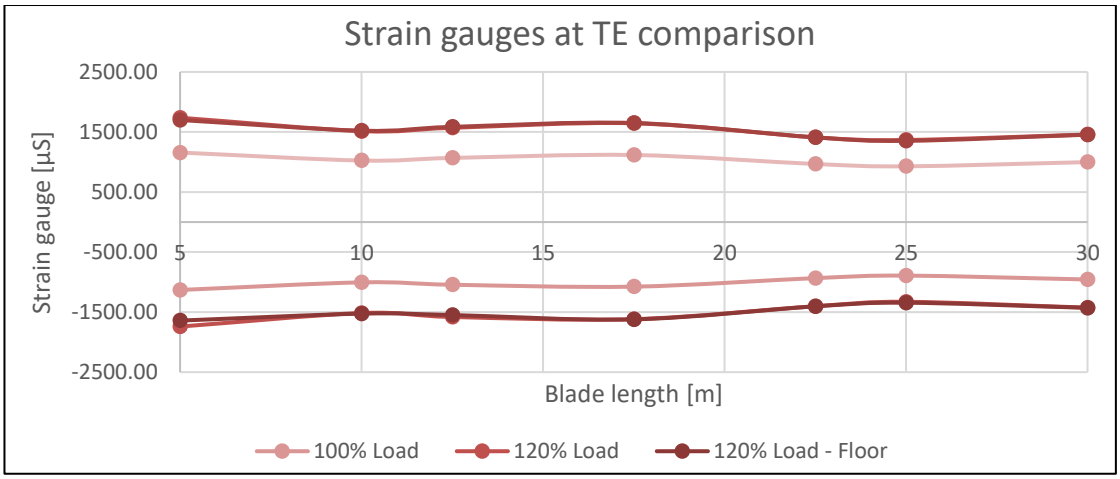

Figure 82: Strain gauges at trailing edge for different load levels and comparison with Floor™.

Bladena
Universitetsparken 7
DK-4000 Roskilde
www.bladena.com

Digital image correlation

In addition to the aforementioned measurements, digital image correlation was also used to further evaluate the structural behavior of the blade in terms of deformations both local and global. The measurements were applied before but also after the Floor™ was installed, while all the DIC measurements were performed by DTU Mech under the guidance of Bladena.

Digital image correlation (DIC) is an optical non-contact method to measure 3D coordinates for the evaluation of 3D surfaces, 3D motion and deformation. In order to capture the blade's deformations, different sections were utilized and painted to describe discrete image areas, which can be determined with subpixel accuracy by analyzing the image information. In Figure 83 there is an illustration of a reference section of the blade which was painted for that reason.

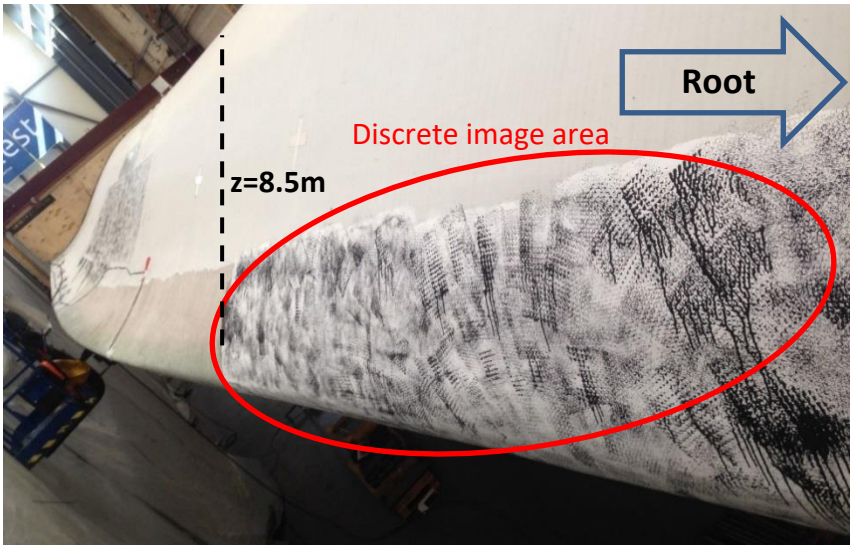

Figure 83: Painted patterns at the trailing edge for DIC measurements located at z=8.5m.

Selected sections and results

In Table 7 the different sections on the blade that were selected for DIC measurements are presented. The max chord and transition zone were the main points of interest as it is expected to result in increased panel deformations. Moreover, the transition zone was evaluated in both LTT (Leading Toward Trailing edge) and TTL (Trailing Toward Leading edge) directions.

Table 7: Blade's locations for DIC measurements.

Location on blade	Distance from blade root
Max chord	12.5-16.5m
Transition zone	5.5-8.5m

Bladena
Universitetsparken 7
DK-4000 Roskilde
www.bladena.com

Max chord

At the first scenario where the Floor™ is not installed, the max chord area was selected at the trailing edge panel on the pressure side and from 54cm from the trailing edge with a width of approximately 1.5m at the max chord area and 1m wide in the rest of the area, starting at 12.5m from the blade root and until z=16.5m.

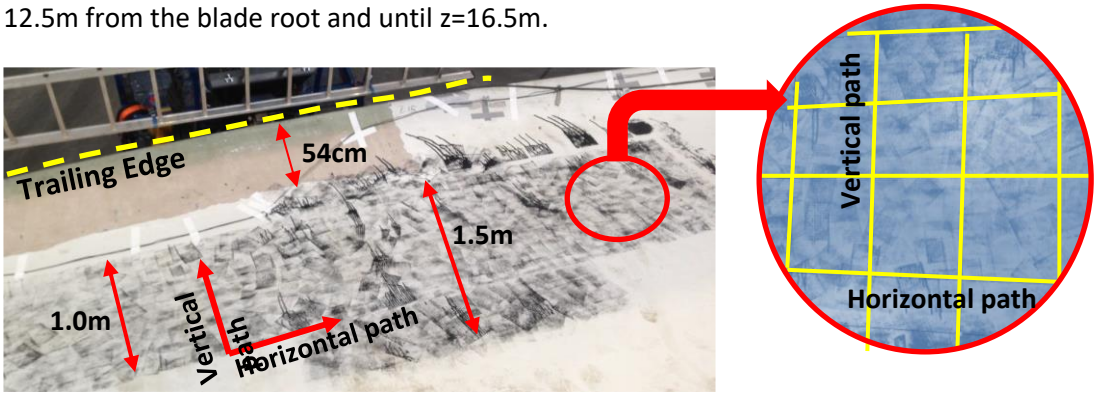

Figure 84: Max chord area - DIC painted pattern representation and generated canvas according to DIC technique.

Having prepared the area, a canvas is created with horizontal and vertical paths (see Figure 84) and different pictures are captured when the blade is at maximum locations in both LTT and TTL directions. These images are then interpreted and according to the different points and their relative movements an overall local out-of-plane deformation can be extracted with respect to the entire length of the selected area. With that in mind, the resulted out-of-plane deformations of the trailing edge panel at the max chord area and without the Floor™ reinforcement, are illustrated in Figure 85.

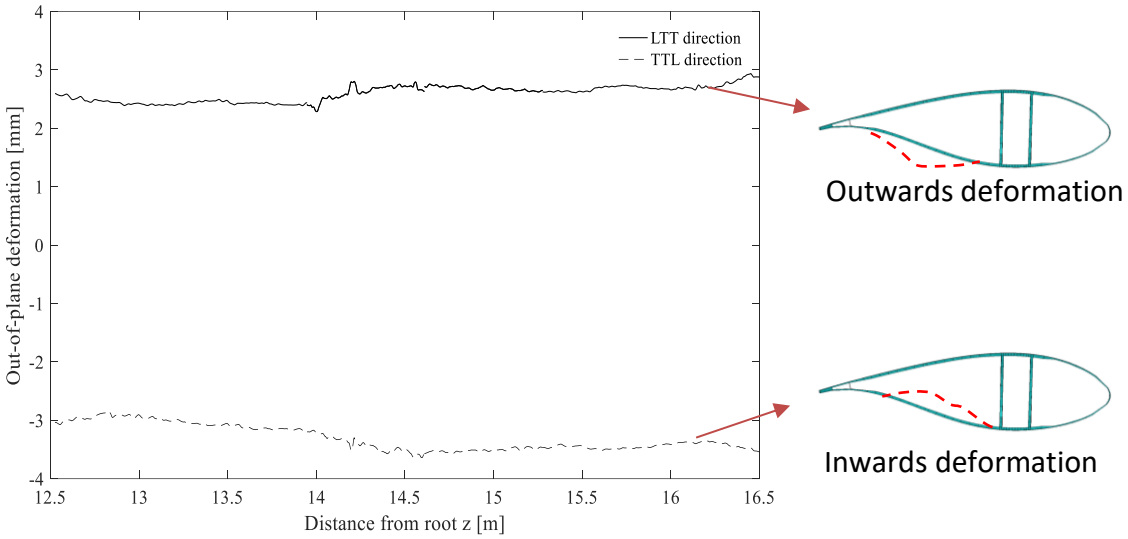

Figure 85: Out-of-plane deformations of the max chord area before the Floor™ installation.

Bladena
Universitetsparken 7
DK-4000 Roskilde
www.bladena.com

In terms of the second scenario where the Floor™ is now installed, the painted area has been expanded and it is illustrated in Figure 86.

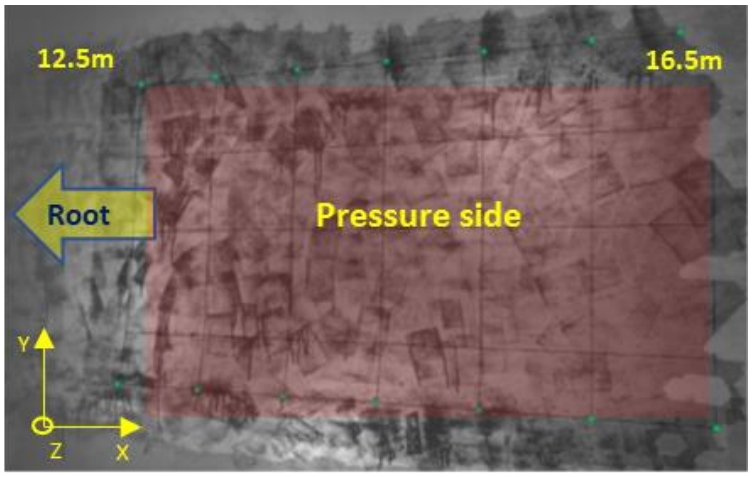

Figure 86: Max chord area - DIC representation when the Floor™ is installed.

Similar to the above, the resulted out-of-plane deformations in case the Floor™ is implemented are depicted in Figure 87.

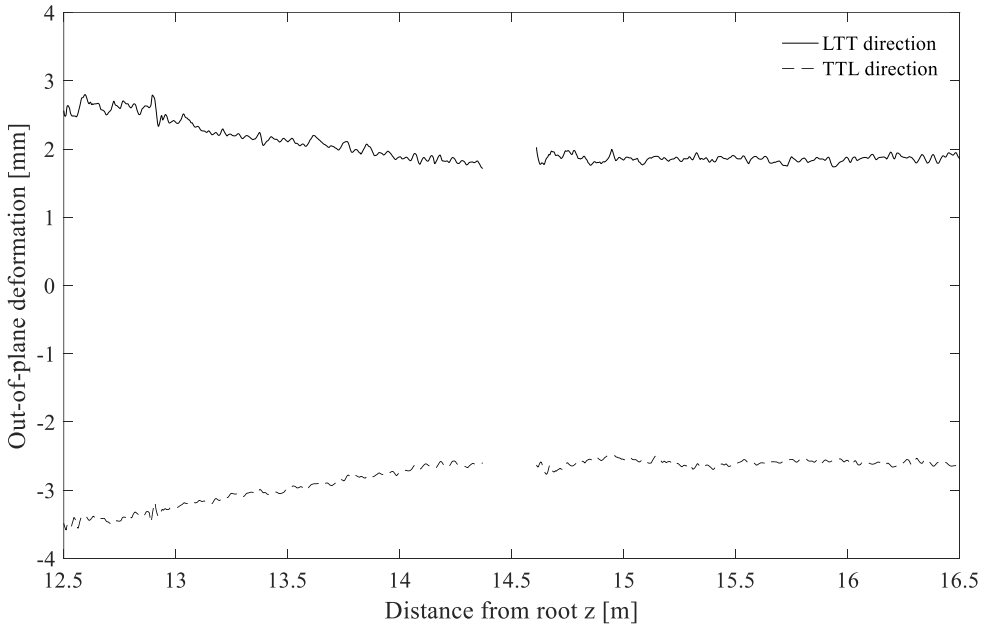

Figure 87: Out-of-plane deformations of the max chord area after the Floor™ installation.

From Figure 85 and Figure 87 it can be observed the influence of the Floor™ in the resulted deformations. While on one hand the deformation in the LTT direction is rather steady with a

Bladena
Universitetsparken 7
DK-4000 Roskilde
www.bladena.com

slight increase after the max chord center line, when the Floor™ is installed the respective deformation is slightly decreasing in a rather consistent manner along the entire length. In terms of the TTL deformations the pattern is again similar. In the case before the Floor™ the deformations after the max chord point (z=14.5m) are increasing, while on the other hand after the Floor™ installation, the deformations are steadily decreasing along the length of the examined area. To sum up, the influence of the Floor™, although it is located at the transition zone, seems to have some positive impact in the movement response of the blade even when the area under investigation is located at the max chord area.

Transition zone

The transition zone area was selected between pressure and suction side with a width of approximately 1.2m as visualized in Figure 88. Similar to the max chord area, the painted area was converted into a canvas with respect to the longitudinal and transverse paths of the desired area.

Figure 88: Transition area representation.

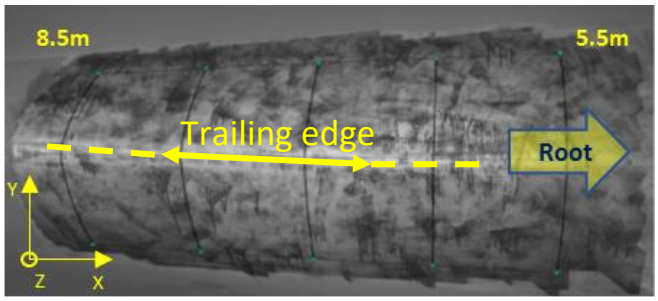

Figure 89: DIC representation and illustration of the reference system. The Z-direction represents the out-of-plane deformation and it is parallel to the chord of the blade, with the positive direction pointing outwards.

Bladena
Universitetsparken 7
DK-4000 Roskilde
www.bladena.com

Having prepared the area, digital images were captured before and after the installation of the Floor™ to investigate the influence that has on the resulted out-of-plane deformations. Therefore, in Figure 90 and Figure 91.

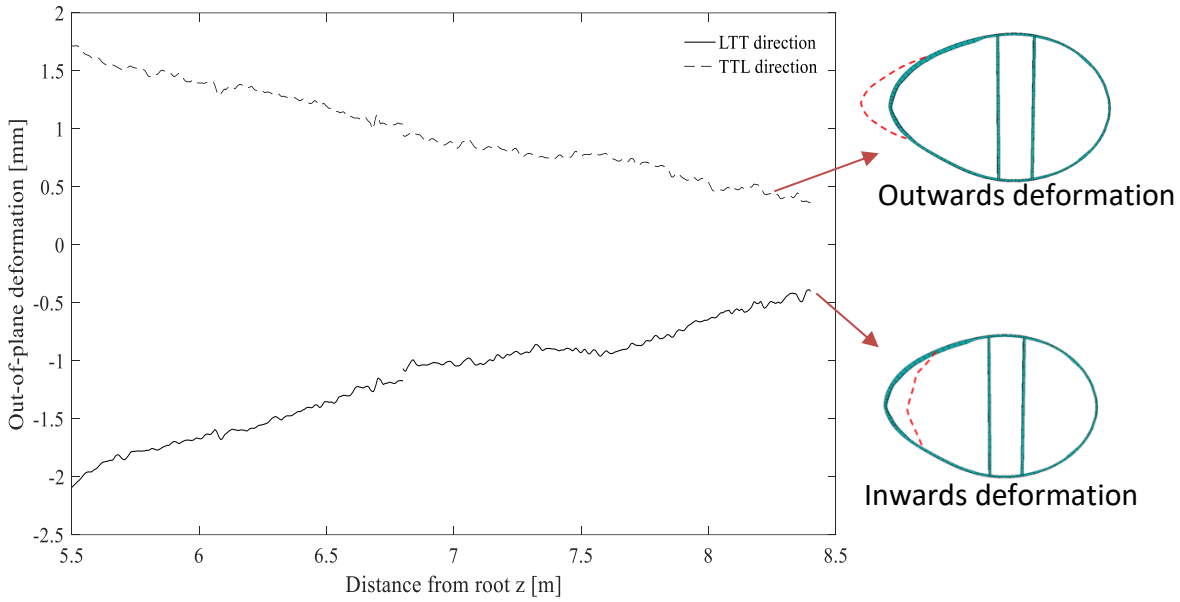

Figure 90: Out-of-plane deformations of the transition zone area before the Floor™ installation.

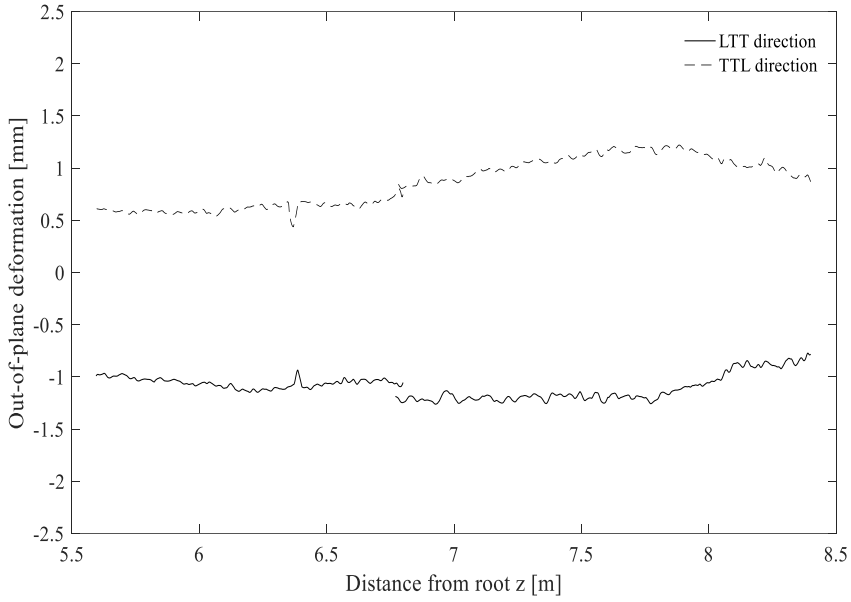

Figure 91: Out-of-plane deformations of the transition zone area after the Floor™ installation.

Bladena
Universitetsparken 7
DK-4000 Roskilde
www.bladena.com

As it can be depicted, once more the Floor™ impacts the resulted deformations, however in the transition zone the influence is much greater, which was expected as it is installed at z=3m until z=9m. This time, the out-of-plane deformations are lower both in terms of maxima but also in terms of development trend for both the LTT and TTL direction. In case of the former, in the absence of the Floor™ (Figure 90), the resulted deformations begin from approximate 1.8mm and decrease until 0.5mm at the end of the longitudinal path. After the Floor™ is installed (Figure 91), the deformations are developing in a rather constant manner, while the peak magnitude is decreased to 0.5mm with a fluctuation up to 1.2mm. Moreover, with respect to the TTL direction, the behavior is similar as the Floor™ limits the out-of-plane deformation to develop around a rather stable value of 1mm which is 50% lower from the case where the Floor™ is not installed.

Finally, by analyzing the behavior of both max chord and transition zone, it can be concluded that there are no indications of buckling in any of the panels. This can be justified by observing the pattern of the resulted deformations which do not appear to follow a nonlinear trend, but instead they vary rather linearly along the length of the examined areas.

D6. Non-destructive testings and visual inspections

To further evaluate the structural behavior of the blade in terms of damages, a series of NTDs were applied and numerous visual inspections were made before, during and after the fatigue test to evaluate the structural integrity of the blade and keep a track of progress regarding the defects.

Visual inspections

At first, a thorough visual inspection was made on the entire blade to ensure that no damages are present and to also evaluate if there are any obvious manufacturing defects. Having confirmed that the blade was completely undamaged with none major flaws the fatigue test was began.

The second visual inspection was made at the points that there were indications of potential damages according to the preliminary study of FEM calculations. Indeed, after the first 1.800.000 cycles the first damaged areas were observed at the trailing edge and z=8m. After that point, aiming to the evaluation of the damage growth, the fatigue test was continued for an addition of 190.000 cycles and the damage growth was evaluated once more. Indeed, the damage was developing while the load cycles were increasing, while a new damage appeared at z=6.15m and at 1,902,000 cycles. At this point, the Floor™ was installed and no further damage growth was observed. Until the end of the fatigue test the damaged area has been constantly observed through a GoPro with photos between 1minute intervals. All the damages observed are depicted through Figure 92 and Figure 93. To sum up, the

Bladena
Universitetsparken 7
DK-4000 Roskilde
www.bladena.com

reinforcement of the Floor™ had a great effect in terms of structural performance as after the installation all the damages stopped growing, while no more defects were detected.

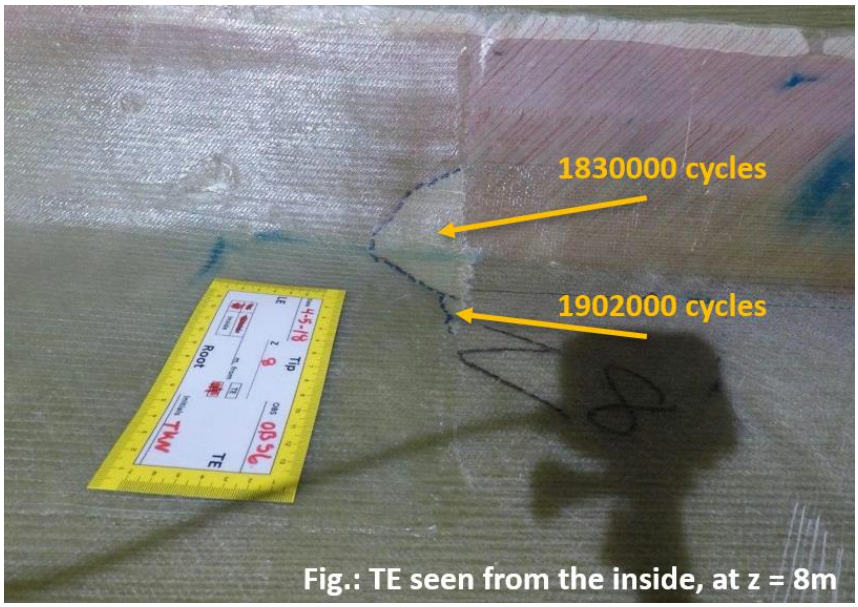

Figure 92: Trailing edge seen from the inside of the blade at z = 8m.

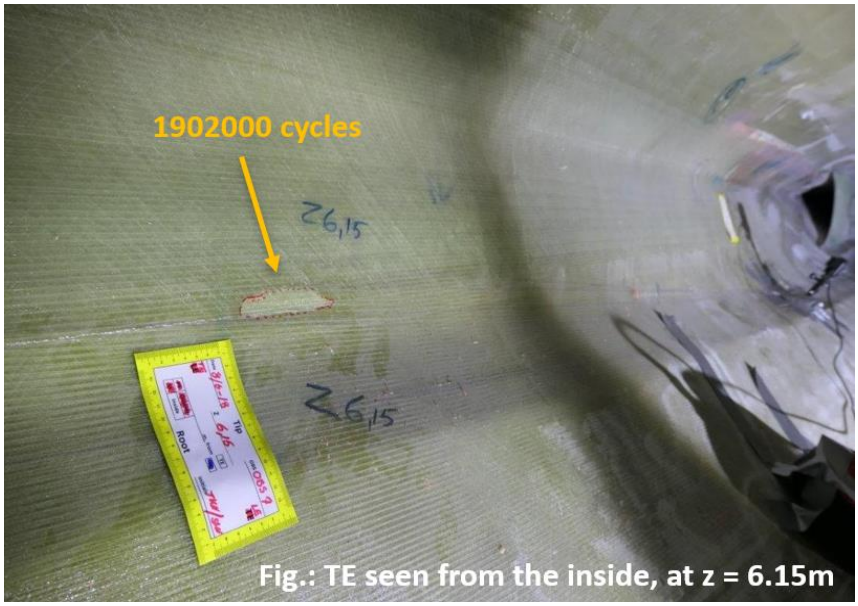

Figure 93: Trailing edge seen from the inside of the blade at z = 6.15m.

Bladena
Universitetsparken 7
DK-4000 Roskilde
www.bladena.com

Thermographic photos

In addition to the visual inspections, a thermographic inspection has been also done on the blade to detect any damages. While the materials are under stress and close to a failure, the temperature is increased which can lead to either find the source of the damage or to detect a damage that may not be visible. Based on the following figures (Figure 94, Figure 95), it can be observed that at the areas where damages occurred the temperature was also increased.

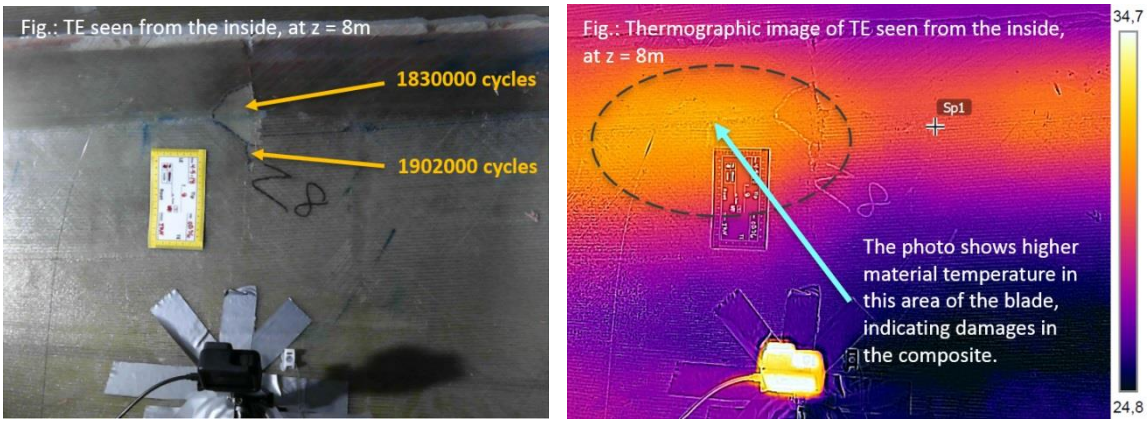

Figure 94: Thermographic image of the damages area at z=8m.

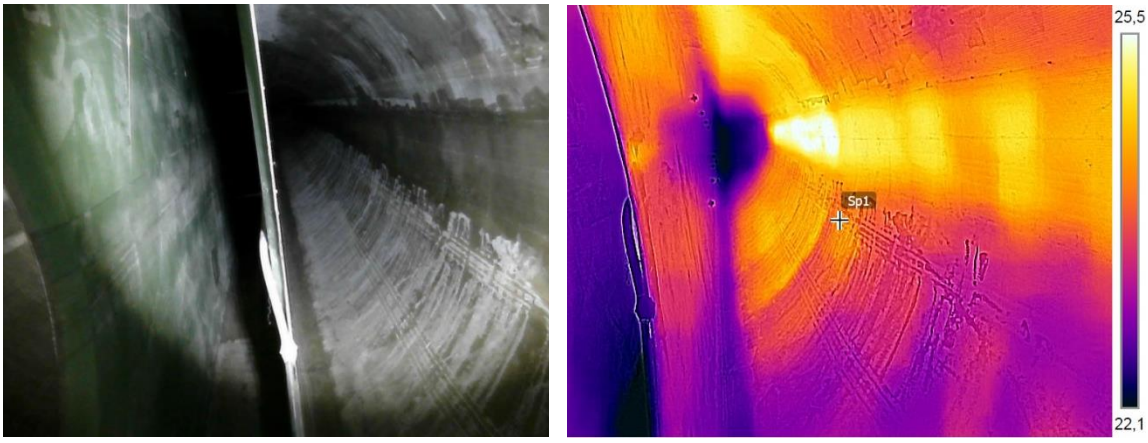

Figure 95: Thermographic image of the damages area at z=8m.

Bladena
Universitetsparken 7
DK-4000 Roskilde
www.bladena.com

NDT scanning by force

Force Technology performed two NDT scans on the blade to firstly see if a damage in the transition trailing edge area could be detected and secondly to see if the damage growth proceeded after Floor™ was installed. In Table 8 the two inspections dates and the relative findings are presented, while in Figure 96 the sections on the blade where the damages occurred are illustrated.

Date	Findings
15. June 2018	The first scan found damages in the TE area at 6.15m and at 8m
25. July 2018	The damages last found were again scanned and no damage growth were detected.

Table 8: Inspection dates and findings

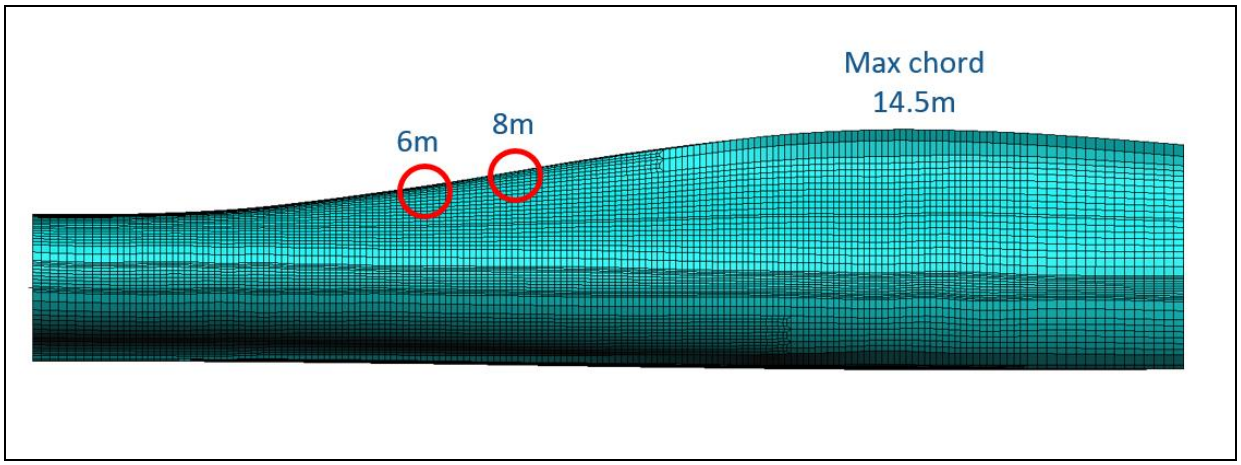

Figure 96: Damages were found by NDT scans at the trailing edge on the transition zone at 6.15m and at 8m.

Conclusion of the NDT scans

According to the inspection report from Force Technology two main points were observed:

1. Indications (lamination or crushed) were found between 6.1m to 6.35m and 7.5m to 7.85m. This was approximately the same on both examination dates.
2. There has been very limited variation of the indications found between the measurements, and any potential growth is within the uncertainty of manual measurements.

The one-page report and conclusion received by Force Technology after the completion of the two NDT scans, can be read in D7.

Bladena
Universitetsparken 7
DK-4000 Roskilde
www.bladena.com

Figure 97: Damage detected

Figure 98: No damage

Bladena
Universitetsparken 7
DK-4000 Roskilde
www.bladena.com

D7. NDT report by Force Technology

Field Report
UT/Polymers and composites

FORCE TECHNOLOGY

Division for Inspection and Testing

DANAK Reg. No.	Enclosure No.	FORCE id./FORCE order No. 118-31651.00000001		Report No. 01	Page of 1-1
Client order No.	Periode of examination/date. 29-06. 25-07-2018	Technician (Init.) CAJ	Certificate No. 0306-N3-U7	Assistant (Init.)	Certificate No.
Client BLADENA		Contractor CLIENT			
Owner		Location BLAEST, Aalborg Øst havn.			
Object LM58,7M Blade, Scanning of TE. from 5.30m to 8.30m.				Drawing No./Rev.No.	
				Material Fiberglass	

☒ **Manual thickness** ☐ **Automated Ultrasonic Examination** ☐ **Adhesive bonded joints**

Material I & II (only for adhesive bonded joints)	Adhesive type (only for adhesive bonded joints)
Equipment - Type / Reg. No. UT-POD/UFKA-01	Probes Type / Reg. No. M2008/UAX14
Thickness meter Reg. No.	Thermometer Reg. No.

Test blocks
Calibration performed on Blade

Specific Procedure
FCS.247. REV.2013

Acceptance criteria

☒ Operator check of ultrasonic probes carried out	Temperature measured on surface of object: 18
Reference system	Speed velocity (mean val. 4 pt.) 2700 M/S

Extent of examination
Scanning of TE. from 5.30m to 8.30m.

Result of examination
Indications (lamination or crushed) where found between 6,1m to 6,35m and 7,5m to 7,85m. This was approximately the same on both examination dates. Conclusion is there has been very limited growth of the indications found between the measurements, and any potential growth is with in the uncertainty of manuel measurements.

Enclosure
☐ Reference scan ☐ Screen dump ☐ Prints ☒ Other

☒ Copy delivered to Name: Find Mølholt Jensen	Firm:	Technician (date/sign.) 27-08-2018 Carl Jørgensen FORCE F 1451
Appr. by client ☐ Copy delivered to Date/sign.	Appr. by owner/repres. ☐ Copy delivered to Date/sign.	Appr. by cert. auth. ☒ Copy delivered to Date/sign.

573-1-1-en-en

Figure 99: Field report as this was condacted by Force Technology.

Bladena
Universitetsparken 7
DK-4000 Roskilde
www.bladena.com

D8. LM Wind Power dynamic fatigue moment

The target dynamic test moment (load = 100%) has been taken from the document received by LM Wind Power ("LM 58.7 P2 - fatTestPlanOverview.xlsx").

Distance from root	Dynamic test moment (range)
[m]	[kNm]
0.00	10227.9
1.00	9907.3
3.50	9105.9
6.00	8305.2
8.50	7506.5
11.00	6711.7
13.50	5923.1
16.00	5170.2
18.50	4469.4
21.00	3828.3
23.50	3273.3
26.00	2738.4
28.50	2251.4
31.00	1891.9
33.50	1558.4
36.00	1252.4
38.50	974.8
41.00	728.9
43.50	519.8
46.00	348.45
48.50	213.32
51.00	112.61
53.50	45.25
55.90	10.17
57.70	0.81
58.45	0.02

Table 9: Dynamic test moments as these were developed along the blade's length.

Bladena
Universitetsparken 7
DK-4000 Roskilde
www.bladena.com

D9. Tri-axial strain gauges

In addition to the longitudinal strain gauges, different measurements were captured also for tri-axial strains with orientations of 0°, 45 ° and 90 ° degrees. In F… there is an overall presentation of the resulted tri-axial strains located at pressure and suction side but also at the trailing and leading edge.

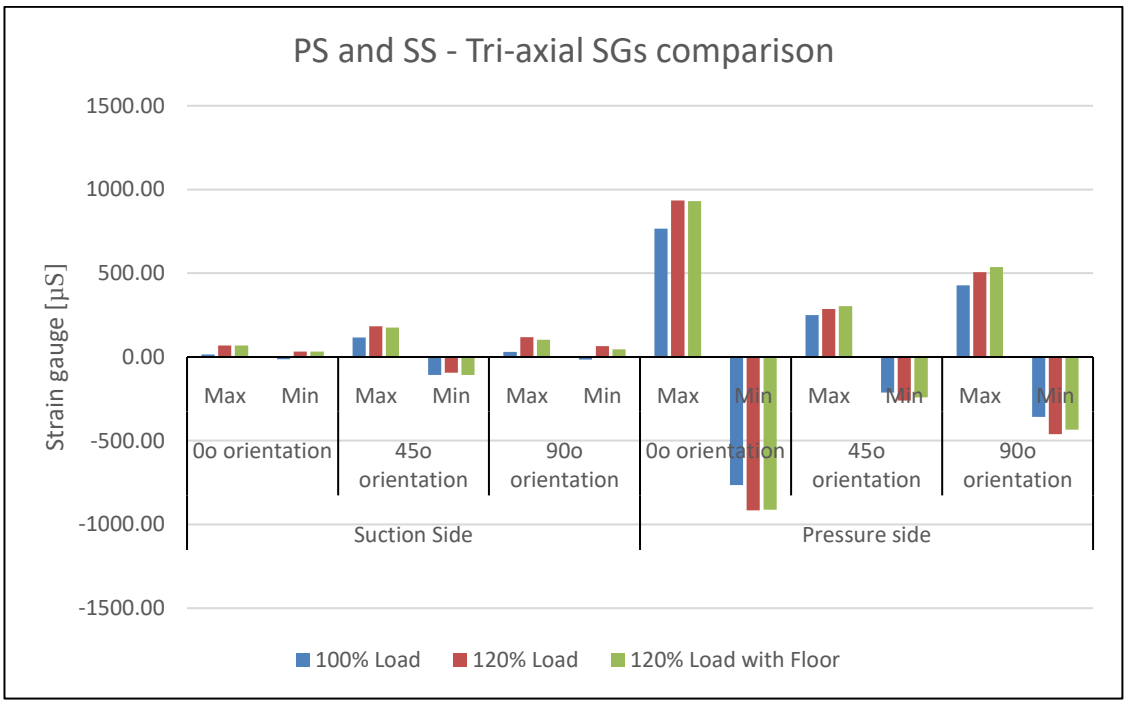

Figure 100: Tri-axial strain gauges at pressure and suction side located at the root of the blade (z=1m).

Bladena
Universitetsparken 7
DK-4000 Roskilde
www.bladena.com

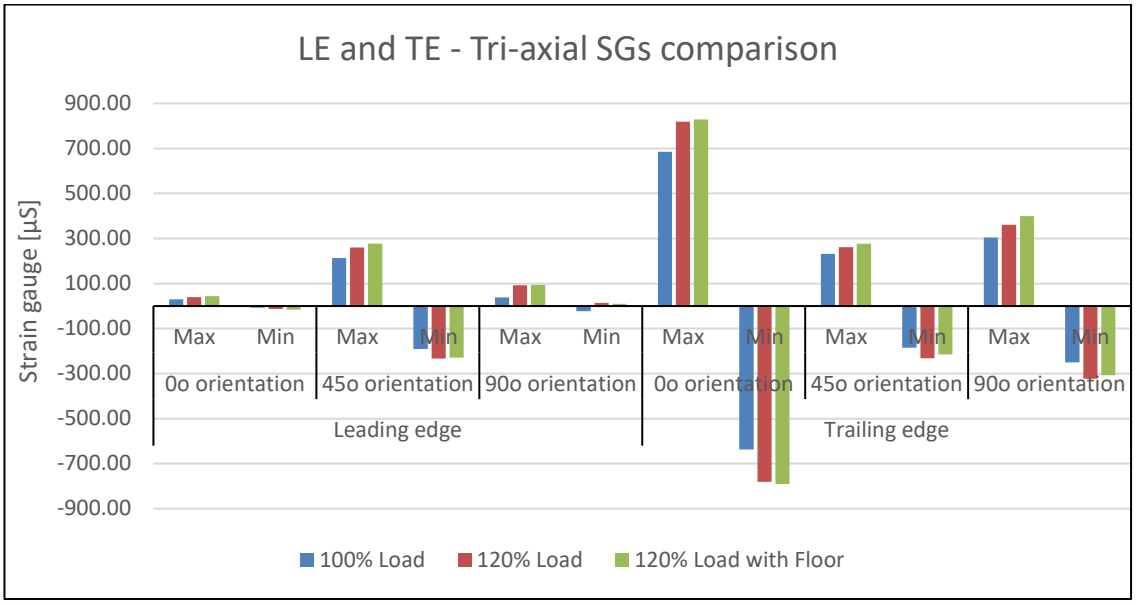

Figure 101: Tri-axial strain gauges at leading and trailing edge located at the root of the blade (z=1m).

Bladena
Universitetsparken 7
DK-4000 Roskilde
www.bladena.com

February 2019

Appendix E Data report: Full-scale test of LM58.7m blade with combined static loads

E1. Acknowledgements

Bladena and partners would like to acknowledge the Energy Development and Demonstration Program (EUDP) for financial support under the grant number: 64015-0062 RATZ Project. Furthermore, acknowledgment goes to LM Wind Power who has donated a LM58.7m blade to be used in the full-scale test and demonstration performed in the project.

Bladena
Universitetsparken 7
DK-4000 Roskilde
www.bladena.com

E2. Introduction

The test described in this report is part of a series of blade tests done under the EUDP RATZ project and performed at Blaest Test Center. For more information on the work, results and conclusions obtained during the RATZ project, including from this test, see "*Root Area Transition Zone – RATZ and Reduction O&M cost of WT blades, EUDP project 64015-0062 – Final Report*". At the time of this static test presented in the current report, the blade has already undergone a high-load edgewise fatigue test with the purpose of demonstrating the positive effects of Bladena's Floor™ technology. For more information on the fatigue test see "*Data Report, EUDP RATZ Project: Full-scale test of a LM58.7m blade with edgewise fatigue loading*".

The first objective of this static test has been to evaluate the structural performance the LM58.7m blade in combined loading evaluate the structural performance reinforcement constellations of the trailing edge. The focus has been in the midspan area with respect to out-of-plane deformations of the trailing edge panel and buckling of the trailing edge in the midspan area. Furthermore, the test has been used to investigate if D-Stiffeners® can replace the built-in C-web as the trailing edge reinforcement. The purpose of replacing D-Stiffeners® instead of a C-web is to minimize the cost of production, as well as counter for new HSE-rules making the current way of manufacturing the C-web impossible, due to inner overlamination of bondlines. The test was also performed with no reinforcement of the trailing edge. See Table 10.

Table 1: Tests description

Test number	Reinforcement type
Test 1	C-webs
Test 2	D-stiffeners
Test 3	No reinforcement
Test 4	Load offset

The second objective of the test has been to show that a large blade can be tested in a static test with high combined loading. This falls under the standardization work package of the RATZ report and might be used by owners in the future when deciding which test a new blade has to undergo. Several conditions have been set up for the test: 1) The combined load is the most critical load direction and a combination of flap and edge. 2) The clamps for the load application points are all in the outer 40% of the blade to allow the transition zone and midspan area to locally deform freely (e.g. panel bending and trailing edge buckling). 3) Two load setups, one with the force applied on the blade shear center and one with the forces offset towards leading edge creating torsion in the blade has been performed and are evaluated against one another. See the test setup in Figure 102. Finally, a comprehensive

Bladena
Universitetsparken 7
DK-4000 Roskilde
www.bladena.com

comparison is also being made between the different reinforcement solutions, while the measurements presented were performed for proof of concept of D-stiffener® and its structural performance as a replacement of C-webs®.

Figure 102: The LM58.7m blade is fixed at the root and hanging angled to ensure that the test pull towards the floor is in the right direction (combined load) according to the blade. Four clamps have been distributed in the outer 40% of the blade to apply the load.

Bladena
Universitetsparken 7
DK-4000 Roskilde
www.bladena.com

E3. Experimental procedure

This chapter gives a short description of the test conditions and load configurations. As already mentioned, the blade was imposed in four different static tests. At first, C-web was used as reinforcement type. Secondly, the C-web was removed, and D-stiffeners were installed along the midspan area, while for the final two tests, both reinforcements have been removed. In figures 2a and 2b, C-web and D-stiffener are illustrated respectively.

Subfigure 2a: C-web

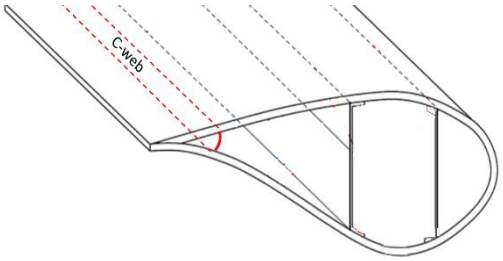

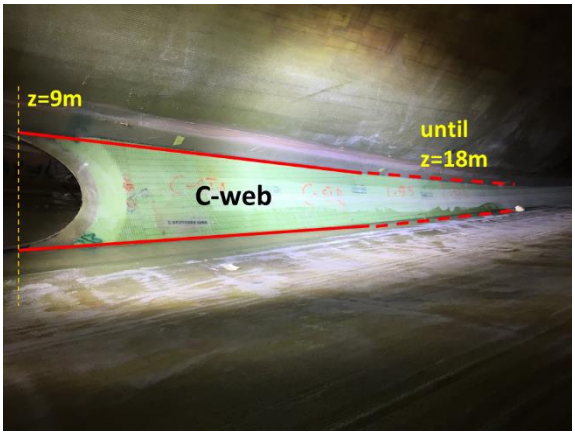

Subfigure 2b: D-stiffeners

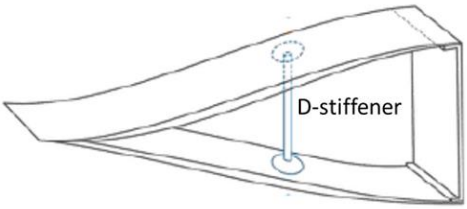

Figure 103: D-stiffeners and C-web visualization

Bladena
Universitetsparken 7
DK-4000 Roskilde
www.bladena.com

Finally, the D-stiffeners were installed at specific positions along the midspan area starting at 9.4m from the blade root and until 24m. With respect to every section, the D-stiffeners were placed at specific locations from the trailing edge. Each one of these positions are presented in Table 11.

Table 11: Locations of D-stiffeners

Position from root [m]	Distance from TE [m]
9.4-11	0.7
11-18	0.8
18-19.5	0.75
19.5-21	0.7
21-22.5	0.6
22.5-24	0.5

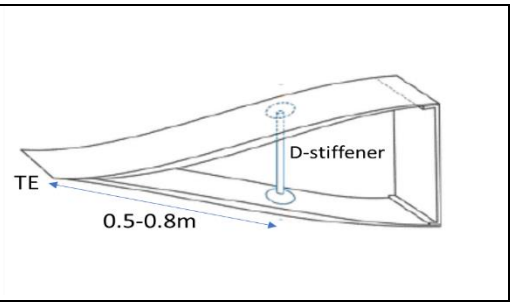

Loading configuration

For the purposes of the current project, the load that was applied to the blade was a combined flap and edgewise load, while in the final test (Test 4) torsion has been also introduced by applying an offset to the shear center.

In terms of forces, four different sections were chosen with different force magnitude. Figure 104, demonstrates the acting force at an arbitrary blade section and its subcomponents and how these are imposed with respect to both flap and edgewise direction.

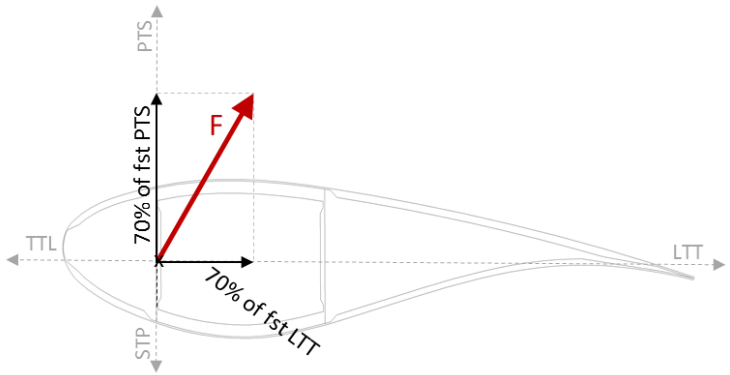

Figure 104: Derivation of applied force to the two directions.

This current report documents measurements from different static tests under combined loading. The combined loading has been applied at four different sections of the blade, through wire pulls, while different configurations have been tested containing different reinforcement types and loading scenarios.

Bladena
Universitetsparken 7
DK-4000 Roskilde
www.bladena.com

For the combined load test, the blade was mounted on the test rig as shown in Subfigure 4a. The load configuration included wooden clamps, designed accordingly to the respective section of the blade. Finally, steel panels were used around the wooden clamps, in order to attach a steel wire and apply the desired force for every section individually. In Subfigure 4c, it can be observed the entire experiment configuration with the steel wires and how these apply forces to the respective blade sections. Moreover, Subfigure 4b depicts the applied forces as these are imposed to the different sections. For simplicity reasons, for the rest of this report the clamps where the load is applied will be called as “Clamp 1”, “Clamp 2”, “Clamp 3”, “Clamp 4” starting at the tip of the blade and towards the root.

Subfigure 4a: Mounting of the blade

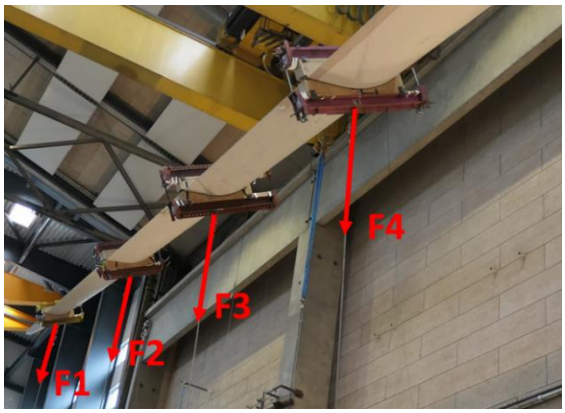

Subfigure 4b: Acting forces at the different sections

Subfigure 4c: Experiment configuration

Figure 105: Experiment setup

Bladena
Universitetsparken 7
DK-4000 Roskilde
www.bladena.com

Finally, all the forces were applied through steel wires (Figure 105c) that were connected to clamps at specified sections of the blade. However, because the usage of clamps restricts the local deformation, all the forces were applied at the 40% of the blade length towards the tip, while the rest of the blade was free of clamps in order to capture any local deformations. The acting forces with respect to the length of the blade is illustrated in Figure 106, while the exact force magnitude and location are presented in Table 12.

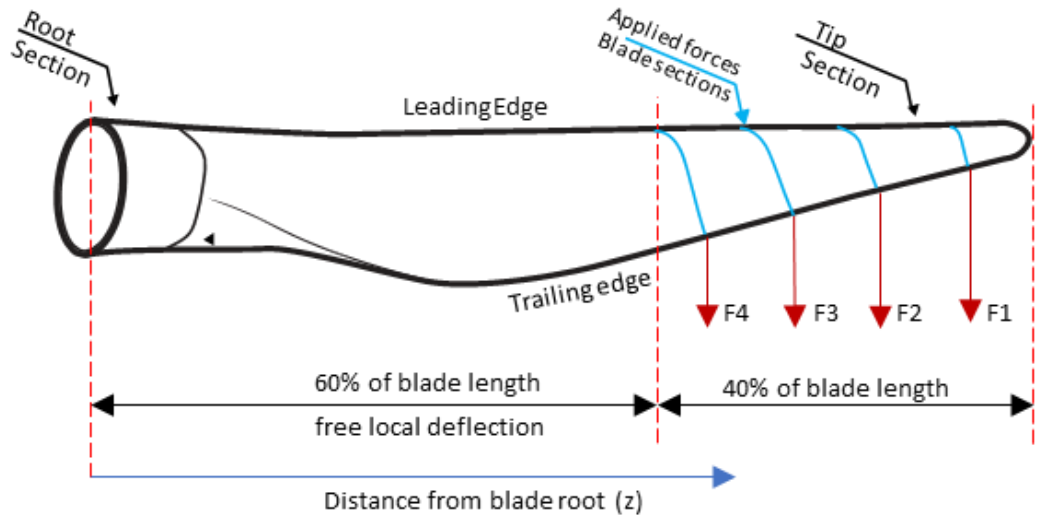

Figure 106: Blade geometry and applied forces

Table 12: Magnitude and location of applied forces

Blade section	Force applied [kN]	Force applied [Tn]
z = 39m	74	7.6
z = 44m	61	6.2
z = 49m	29	3.0
z = 55m	11	1.1

Bladena
Universitetsparken 7
DK-4000 Roskilde
www.bladena.com

Load offset

In order to introduce a torsion at the blade, an offset of the acting force was applied for all clamps, except of the one that is closest to the tip of the blade (Clamp 1). This is better visualized in Figure 107, while the actual load configuration and how the offset was applied is visualized through pictures in Appendix A (Table 17). It should be stated that the offset of the applied force for all the cases was introduced towards the leading edge. With respect to the second clamp, the offset was equal to 30.4cm, while for the cases of the third and fourth clamp the offset was 36.8cm and 31.0 cm respectively. In Table 13 the offset distances for each clamp and test are presented.

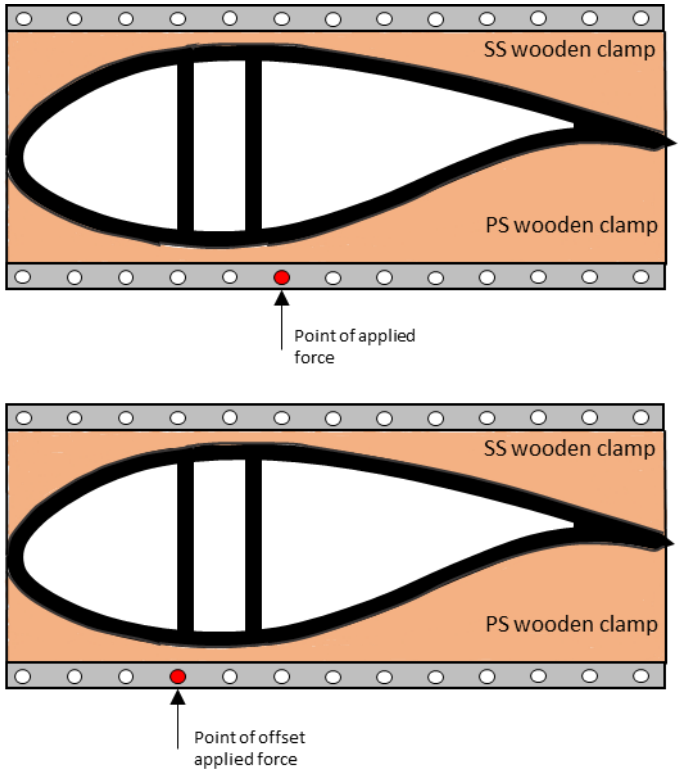

Figure 107: Schematically illustration of the loading offset.

Table 13: Offset distances. The reference point for all distances and movement points is the one closest to the trailing edge

	Original position (Tests 1,2,3)	Offset position (Test4)	Difference (mm)
Clamp1 (z = 55m)	1st hole	1st hole	0
Clamp2 (z = 49m)	6th hole	10th hole	304
Clamp3 (z = 44m)	9th hole	13th hole	368
Clamp4 (z = 39m)	9th hole	14th hole	310

Bladena
Universitetsparken 7
DK-4000 Roskilde
www.bladena.com

Applied loads on the wires

Having defined the test configuration and the way the load is applied to the different blade sections, in Figure 108 the loading at the wires is depicted for the different sections placed at 55m, 49m, 44m and 39m from the blade root respectively. It can be observed that the loadings are in accordance with the theoretical force that should be applied. Hence, it can be concluded that the experiment procedure is in compliance to the theoretical calculations and it was performed accurately.

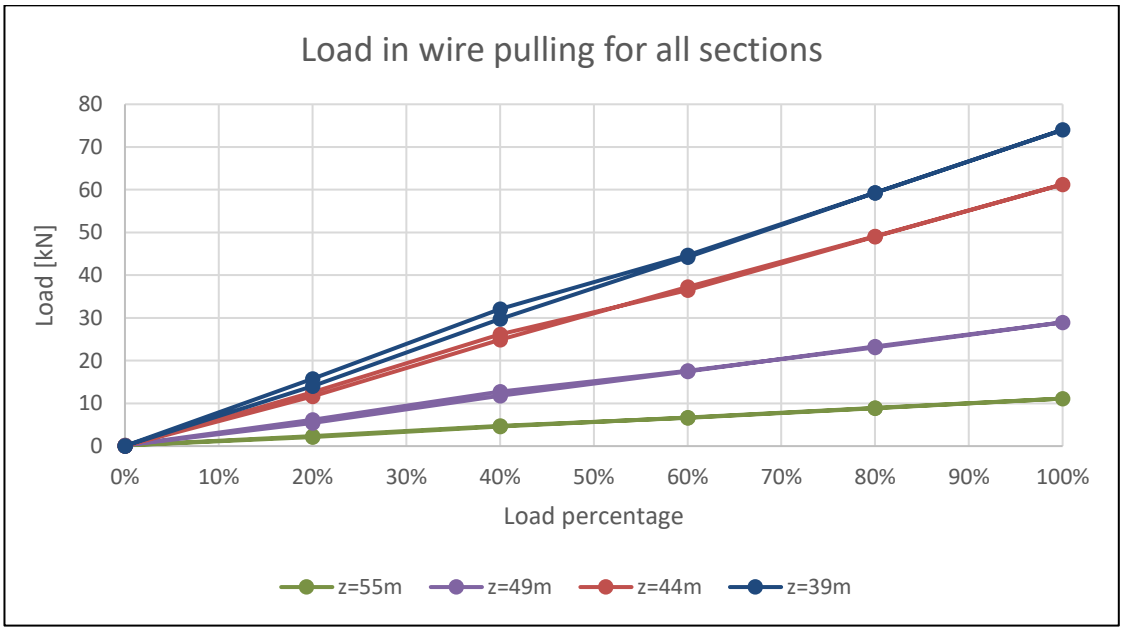

Figure 108: Load in wire pulling for every section of applied force

E4. Measurements

Global deflection

In order to capture the global deflection of the blade three different sections were chosen as reference points. The blade tends to deflect towards the floor but also sideways due to the combined load configuration. This is better visualized through Figure 176 in Appendix A. In addition, the deflection is measured using draw-wire displacement sensors which are positioned to be perpendicular on the respective section at 100% load. The positions of the sensors are based on theoretic deflection calculations. The respective sections were the measurement devices were implemented are illustrated in Table 14.

Bladena
Universitetsparken 7
DK-4000 Roskilde
www.bladena.com

Table 14: Measurement points for the blade's deflection under loading

Blade section	Description	Unit
D58.7m	Blade deflection "towards the floor", z=58.7m	mm
D41.5m	Blade deflection "towards the floor", z=41.5m	mm
D28m	Blade deflection "towards the floor", z=28.0m	mm

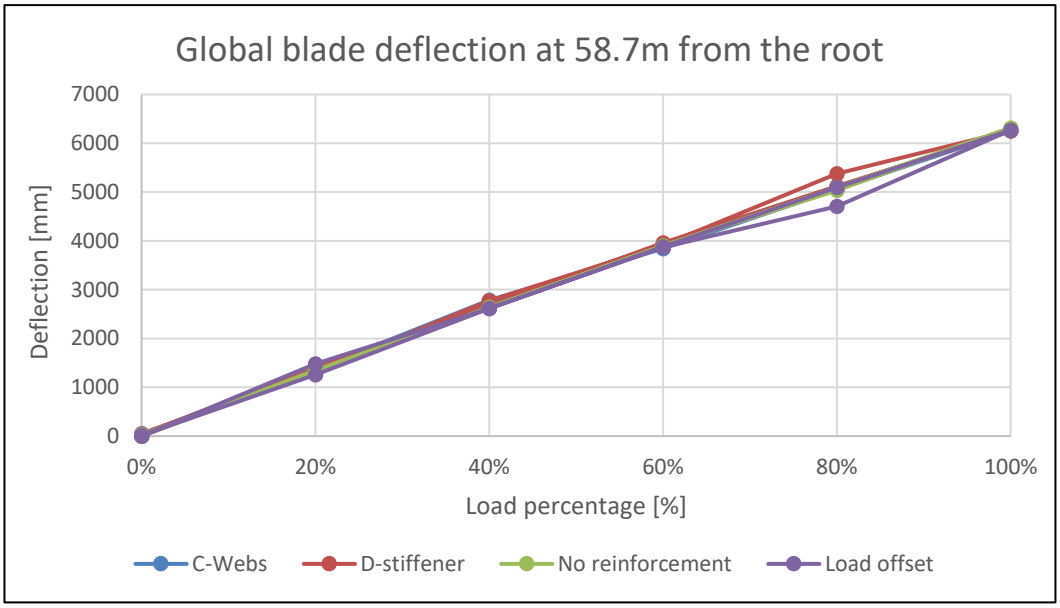

Figure 109: Global deflection at 58.7m from the root

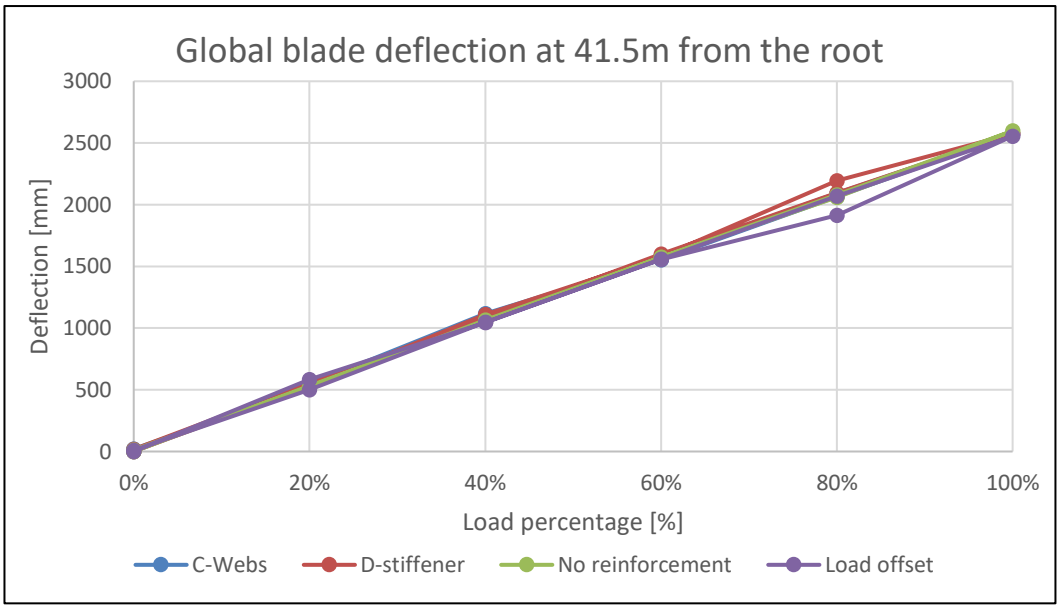

Figure 110: Global deflection at 41.5m from the root

Bladena
Universitetsparken 7
DK-4000 Roskilde
www.bladena.com

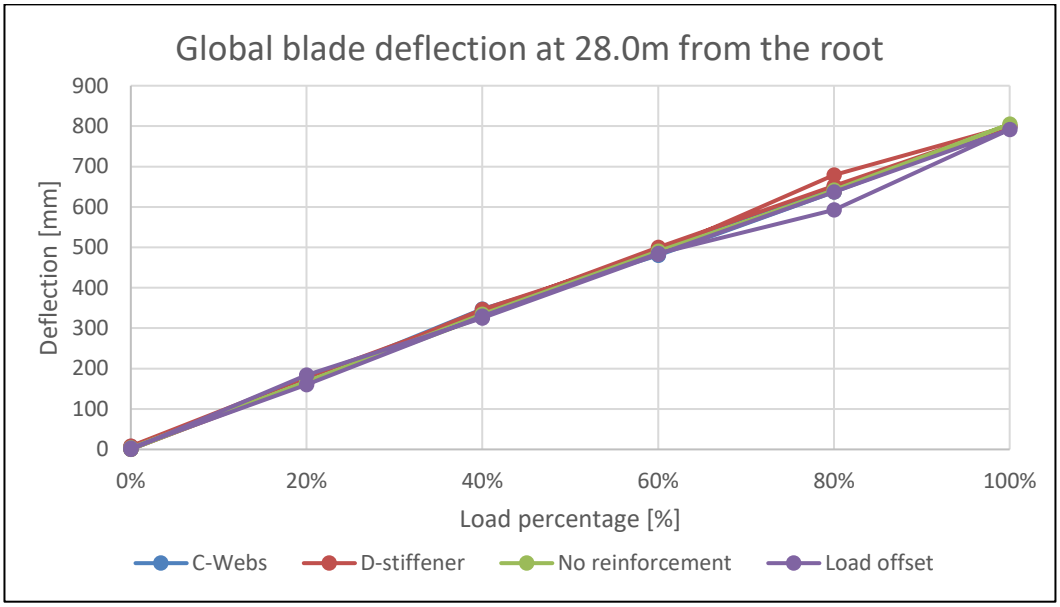

Figure 111: Global deflection at 28.0m from the root

Inclination measurements

The inclination angle that the airfoil at a specific section is directed is illustrated in Figure 112. Moreover, in Figure 113 the measured inclination angle is depicted for three different blade sections of z=40, 24 and 1m from the blade root respectively. It becomes evident that the offset of the load contributes to the blade twist, as for all sections, the load offset, results to the highest inclination angle. Finally, it can be concluded that the section which is located at 40m from the blade root, results to the highest inclination independently of the Test configuration.

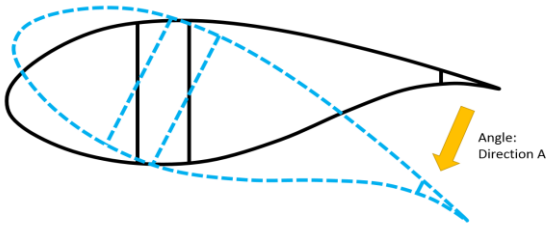

Figure 112: Direction of the inclination angle.

Bladena
Universitetsparken 7
DK-4000 Roskilde
www.bladena.com

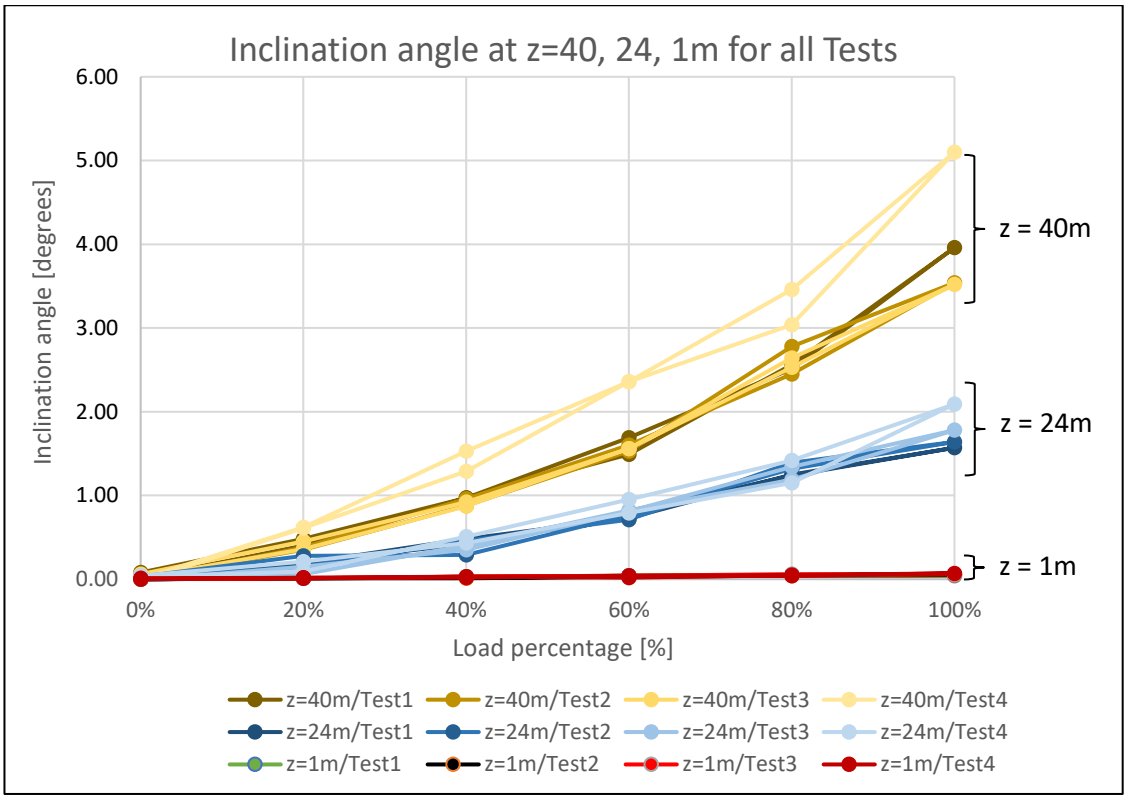

Figure 113: Inclination angle for different blade sections for all tests.

Panel deformations

The aim of this category of measurements is to capture the independent movement of the panels, which can further be translated in the relative distance that the two panels have been moved from each other. The exact measuring methodology is illustrated through Table 15, where it can be seen the different measurement points for both the suction and pressure side. In the following section, different measurements will be illustrated, for both the suction and pressure side. Following the same concept, cameras have also been placed inside the blade, aiming to the observation of the panel's deformation and potential failures that may not be visible from the outside. Finally, all the measurements are compared in terms of the different configurations, in order to clarify the influence of the various reinforcement types. In the current report, the measurements that are illustrated refer to three different sections located at 16.4m, 17.2m and 18m. It should also be stated that at sections of 16.4m and 18m a comparison is made only between the Tests 3 and 4.

Bladena
Universitetsparken 7
DK-4000 Roskilde
www.bladena.com

Table 15: Measurement points at different blade sections.

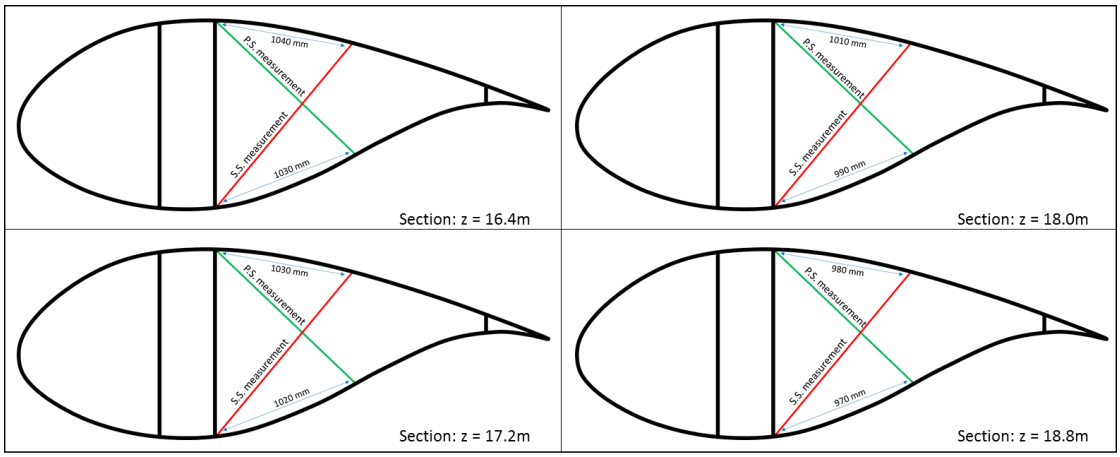

As it can be observed from Figure 114 and Figure 115 it is evident that the movement between the panels is highly dependent on the reinforcement type. For instance, the displacement of the pressure side maximizes when the loading is applied with the abovementioned offset. Second displacement in order is originated on the case where there is not any type of reinforcement and the loading is acting normally. Moreover, the lowest displacement is observed in the case of D-stiffeners followed by the C-webs. Finally, it should be noted that the displacement order remains constant for the whole duration of loading as well as unloading.

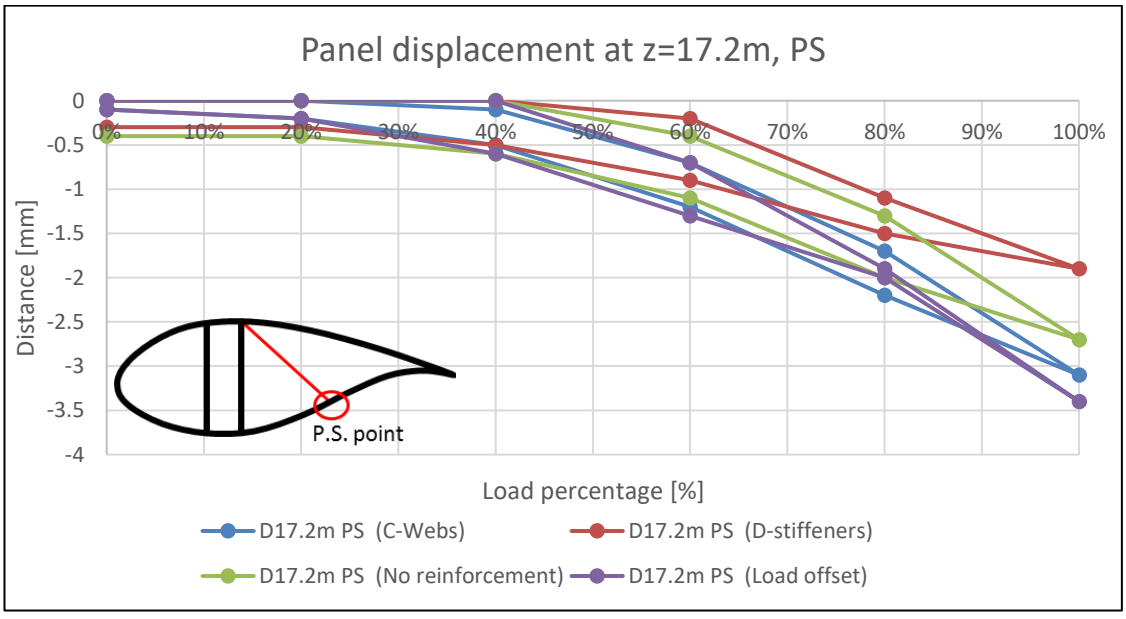

Figure 114: Measured distance at the Pressure-Side at 17.2m from the root

Bladena
Universitetsparken 7
DK-4000 Roskilde
www.bladena.com

The suction side shown in Figure 115, follows a slightly different pattern. The maximum displacement for the suction side is originated from the case of no reinforcement, while the load offset leads to insignificant results. In addition, both D-stiffeners and C-webs behave in a similar way as the maximum distance measured is identical.

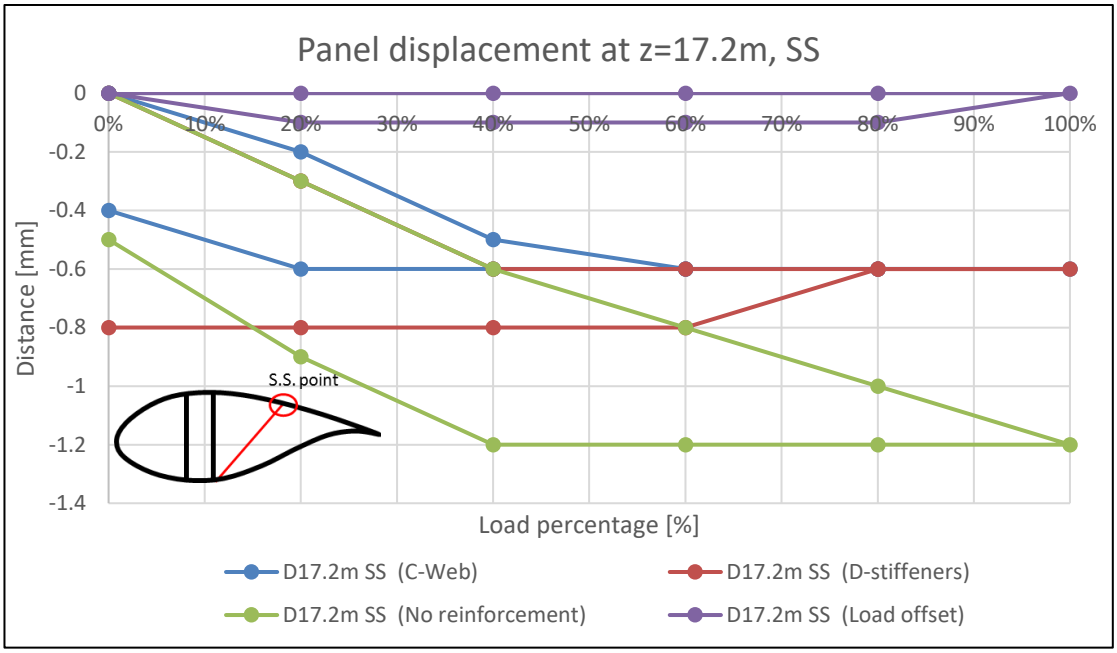

Figure 115: Measured distance at the Suction-Side at 17.2 from the root

Similar results are observed also for the sections that are located at 16.4 and 18.0m from the blade root in Figure 116. At 16.4m from the blade root, the maximum distance comes from the Load offset which is higher than the case where all the reinforcement types are removed. An interesting observation can be made when examining the distances at z=18.0m. Although the load offset leads to the maximum deflection, the behaviour is different until the load reaches its full capacity. More specifically, in the range of 20%-65%, the maxima originates from Test3.

Finally, in Figure 117, the maximum deflection in pressure and suction side are presented for two different sections located at 16.4m and 18.0m from the blade root. It can be concluded that for both tests (Test 3 and 4) the pressure side results in higher deformations than the suction side. However, while the suction panel seems to deform around zero, at 18m from the blade root it seems to deform higher than any other section.

Bladena
Universitetsparken 7
DK-4000 Roskilde
www.bladena.com

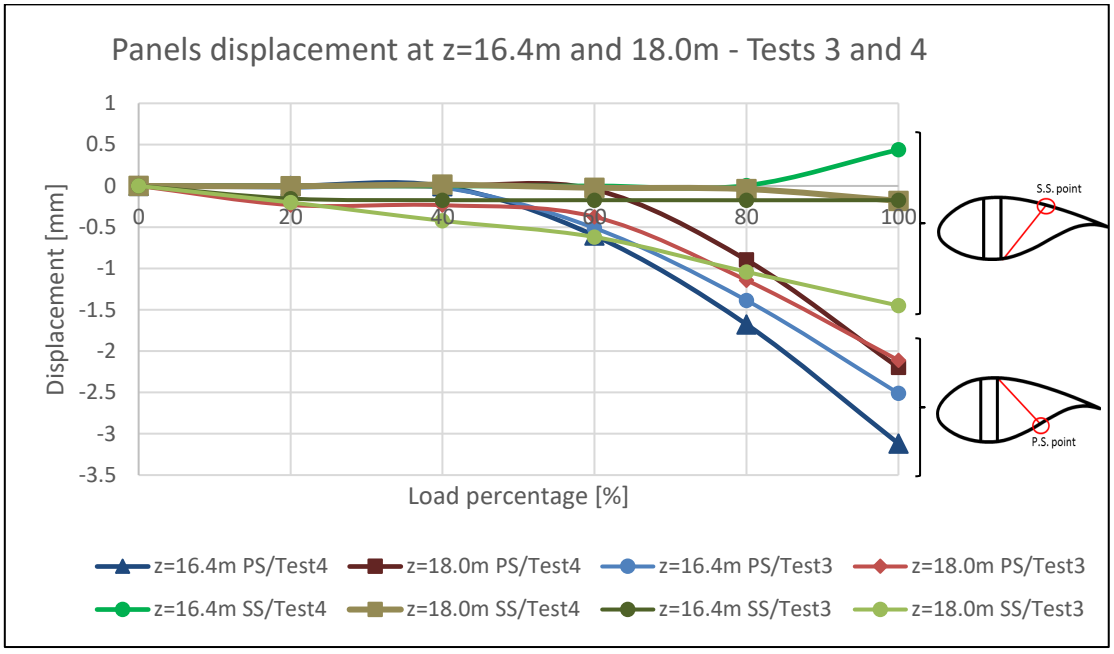

Figure 116: Panels displacement for Tests 3 and 4 for both PS and SS, at z=16.4m and 18.0m

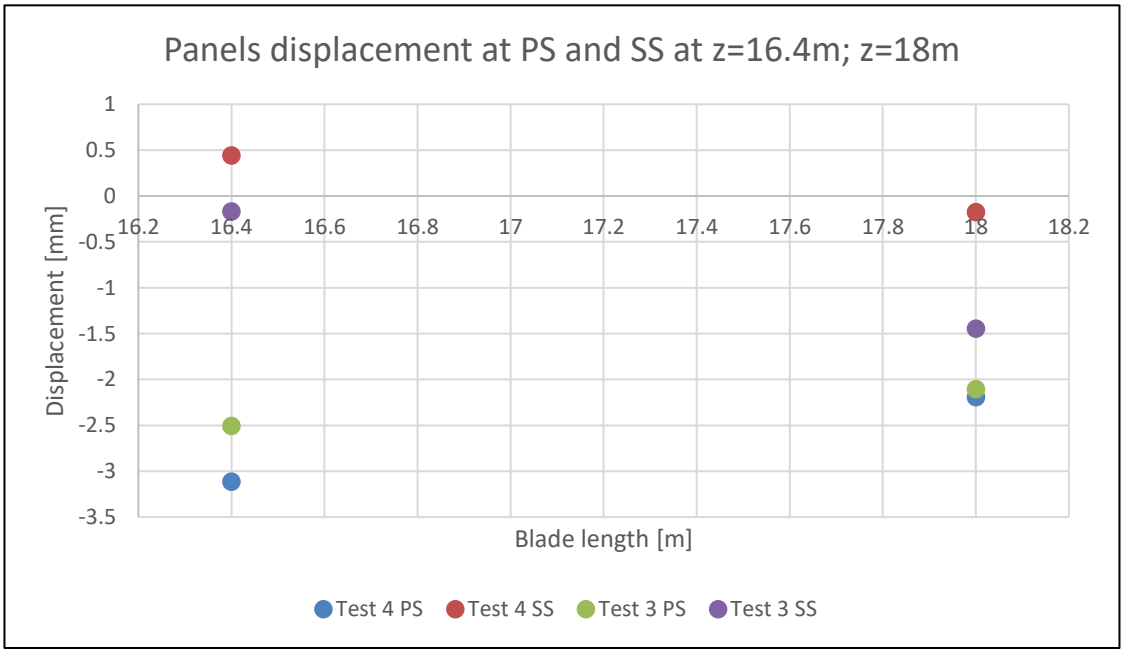

Figure 117: Maximum panels' displacement for different sections for Tests 3 and 4

Bladena
Universitetsparken 7
DK-4000 Roskilde
www.bladena.com

Finally, the panels behaviour is further evaluated through Figure 118, where the Pressure and Suction sides are illustrated together in case where C-webs are implemented. It can be depicted that the pressure side results in increased deformations along the length of the blade, while the suction side deforms in a rather consistent manner with limited variations.

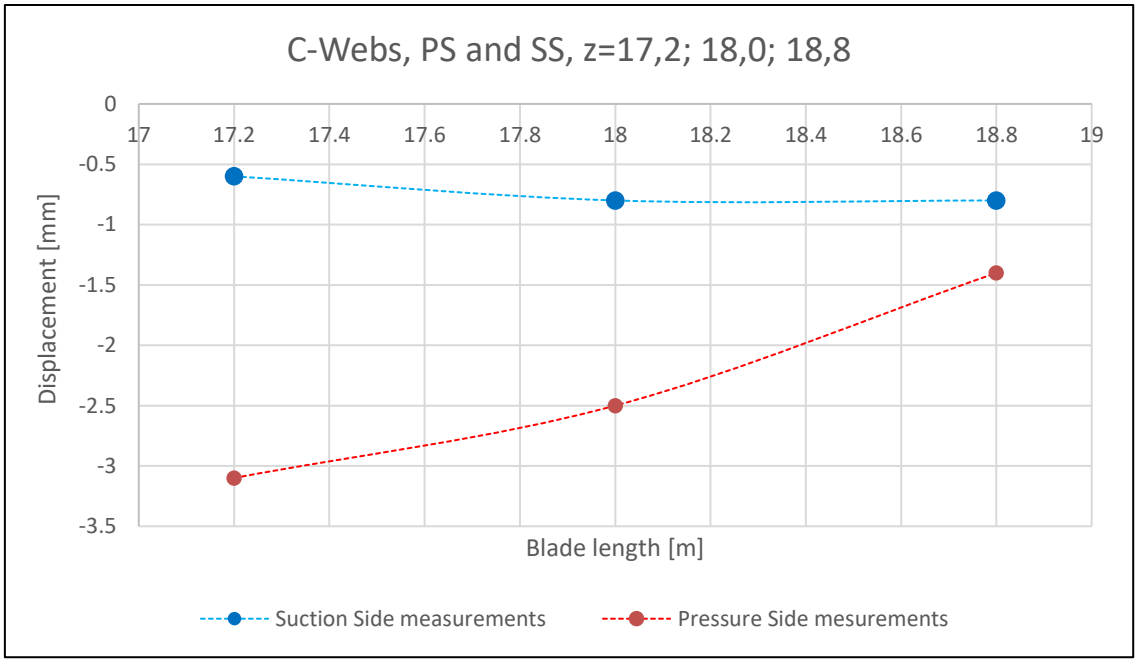

Figure 118: Maximum deflection for different sections with C-webs

Back-to-back strain gauges

The strain gauges are separated in three different categories depending on their orientation and placement. In the current section, all the strain gauges that are placed back-to-back and at 4cm from the trailing edge, for both the pressure and suction side, are presented. The orientation of the measuring device is zero degrees as they are placed on the longitudinal direction of the blade and in order to capture the uni-axial strain. The overall description and maximum values of all the strain gauges are presented at Table 16, in Additional Results.

The configuration of the uni-axial strain measurement procedure is illustrated in Figure 119.

Bladena
Universitetsparken 7
DK-4000 Roskilde
www.bladena.com

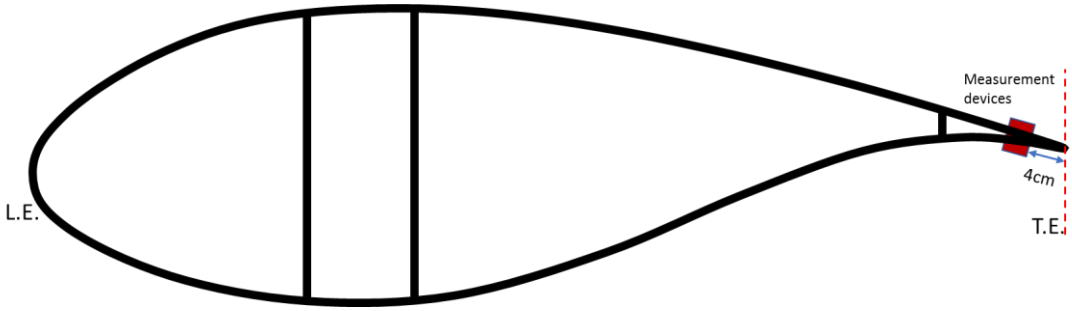

Figure 119: Placement of uni-axial strain, back-to-back, measurement devices

The purpose of the back-to-back strain gauges is to detect any potential buckling behavior of the trailing edge. In order to investigate if buckling occurs, it is important to analyze the strain gauges in different sections of the blade. As a non-linear phenomenon, buckling is detected by observing nonlinear behavior in the development of strains along the blade length. With that said, in the following figures, a group of strain gauges at specific locations are presented, aiming to the investigation of any potential nonlinearities.

From Figures 19-22, it can be observed that independently of the experiment configuration, the strains until 100% load develop in linear manner throughout every loading intervals. This can be further justified in Figure 130 through Figure 143 in Additional Results, where the strains behave linear in every blade section. Therefore, it can be concluded that buckling does not occur in any test.

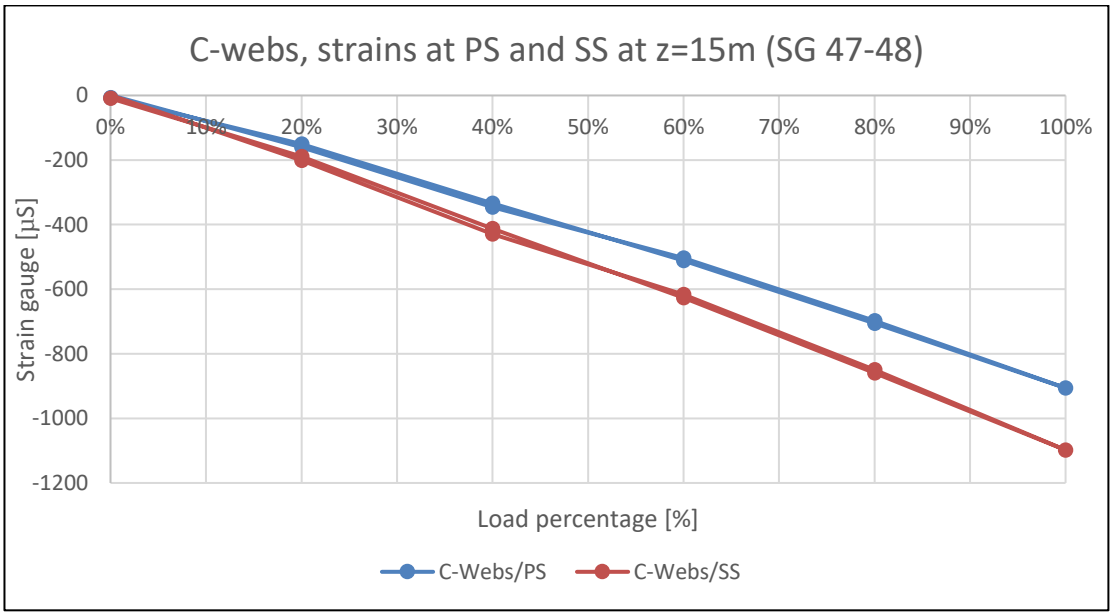

Figure 120: Strain gauges at pressure and suction side in case of C-Webs

Bladena
Universitetsparken 7
DK-4000 Roskilde
www.bladena.com

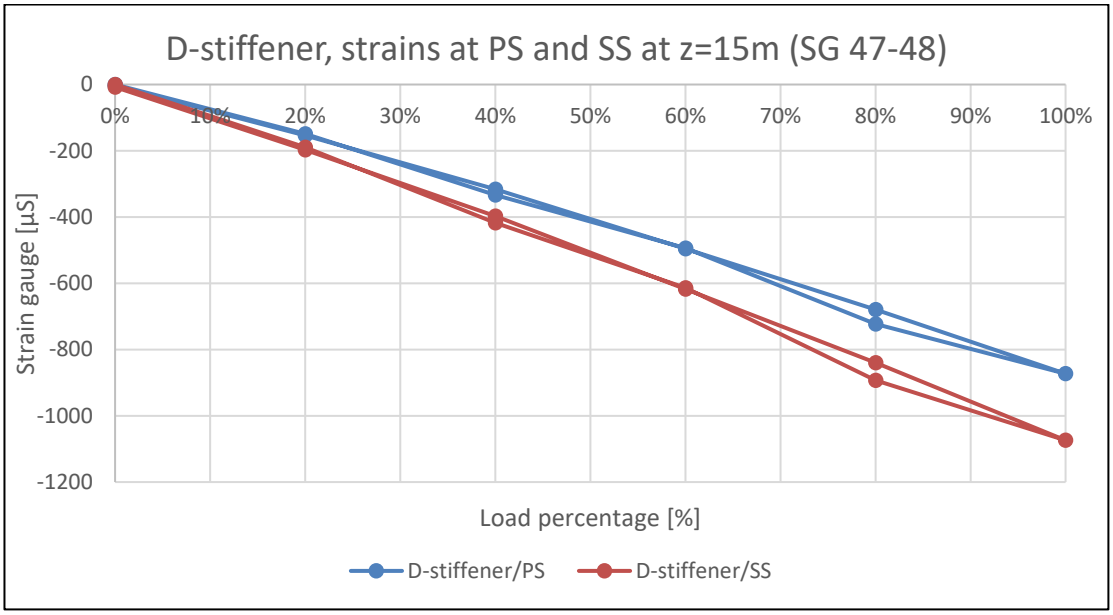

Figure 121: Strain gauges at pressure and suction side in case of D-stiffeners

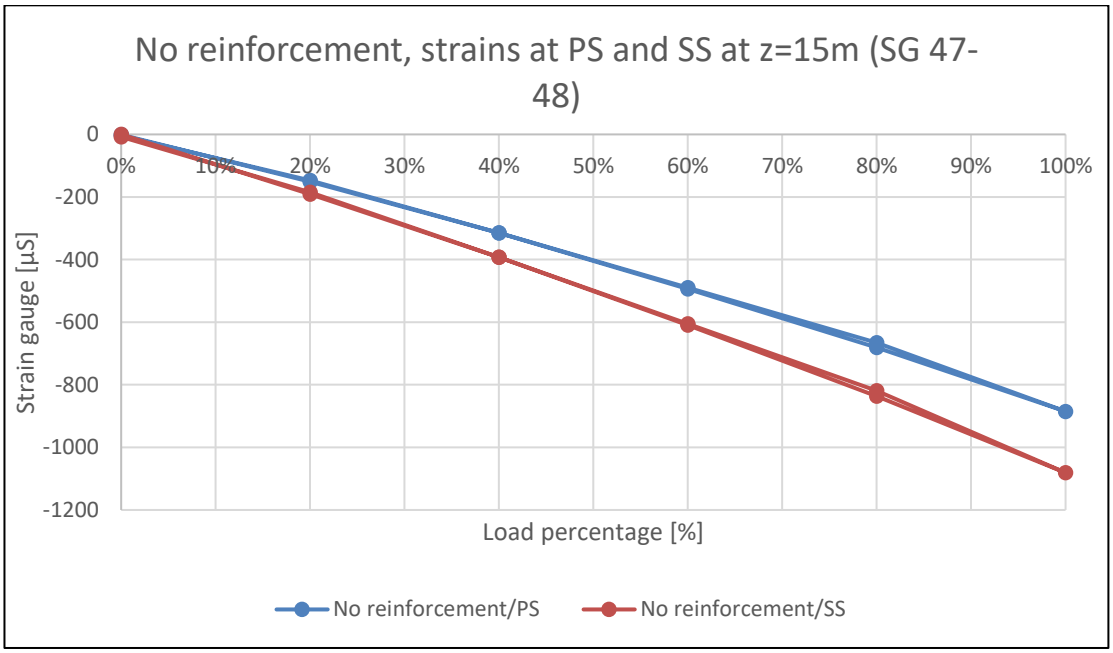

Figure 122: Strain gauges at pressure and suction side in case of no reinforcement

Bladena
Universitetsparken 7
DK-4000 Roskilde
www.bladena.com

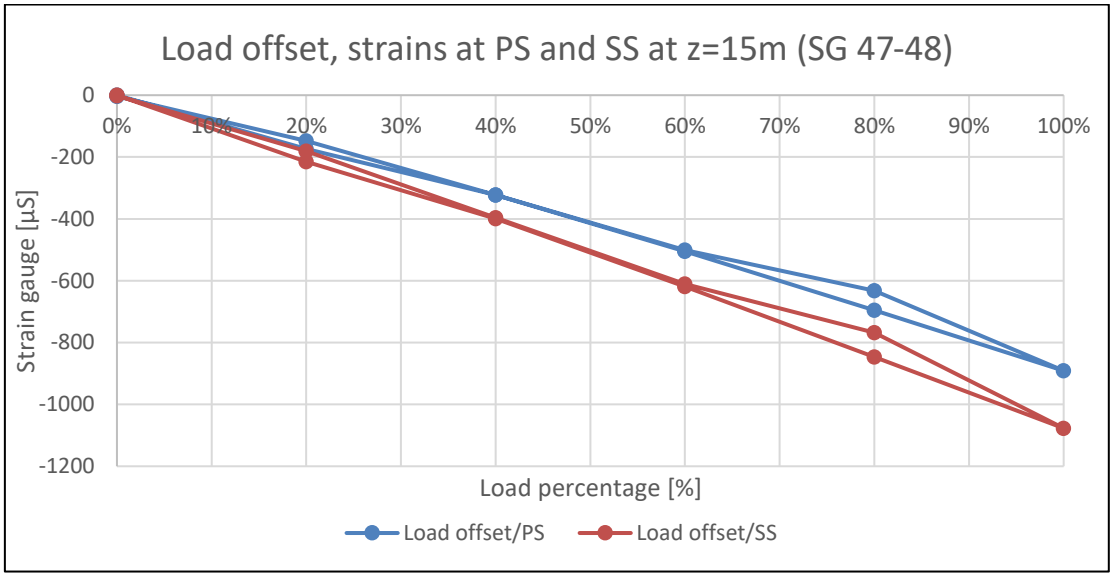

Figure 123: Strain gauges at pressure and suction side in case of the load offset

Longitudinal strain gauges

Similar to the back-to-back strains, in the following lines the different tri-axial strain and torsion gauges are presented. More specifically, in Figure 124 the measurement configuration is presented, while in Figure 125, Figure 126 the longitudinal strains are presented for the leading and trailing edge respectively. As it can be observed from the figures, the experiment configuration does not influence the strain behavior or magnitude as in any case the strain follows a linear increase with respect to the acting load. In addition, the leading and trailing edge behave in a different way as the trailing edge is in compression while the leading edge is in tension. This is better visualized in Figure 127 and Figure 128, where the longitudinal strains along the length of the blade is presented for both the trailing and leading edge.

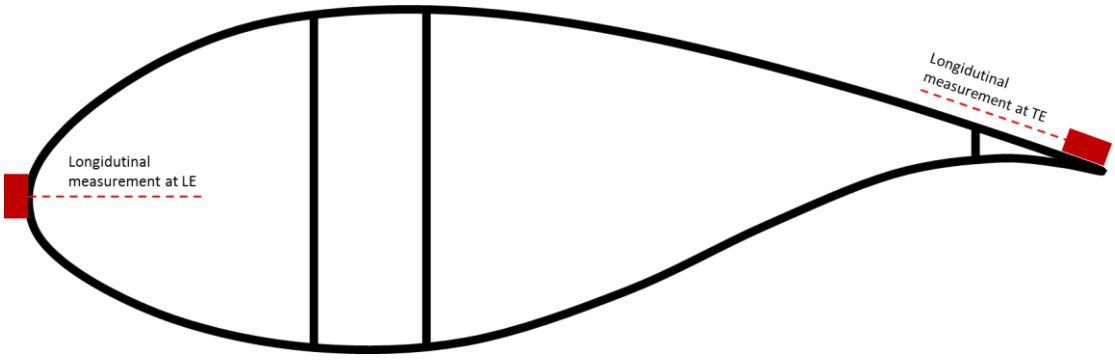

Figure 124: Placement of longitudinal measurement devices

Bladena
Universitetsparken 7
DK-4000 Roskilde
www.bladena.com

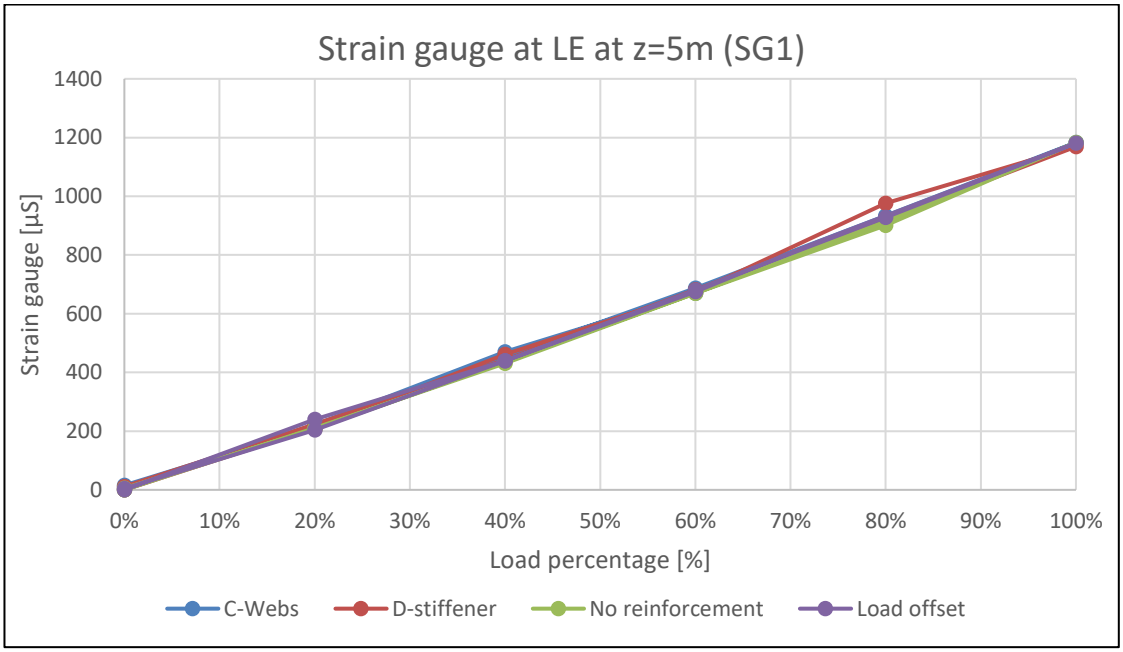

Figure 125: Uni-axial strain gauge for all the different configurations at z=5m

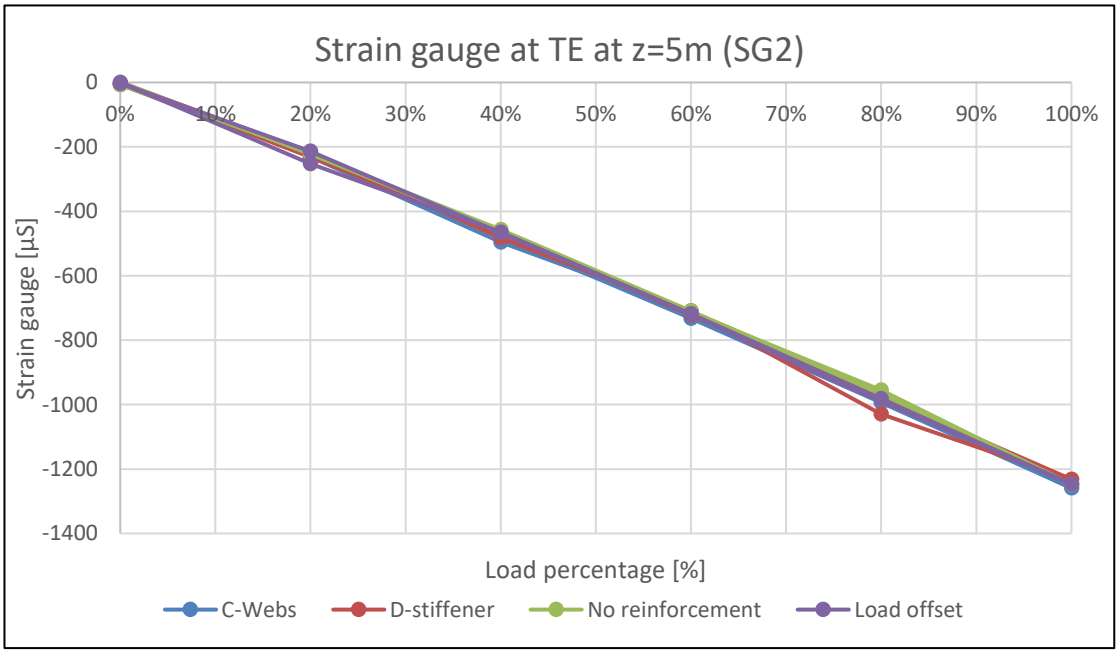

Figure 126: Uni-axial strain gauge for all the different configurations at z=5m

Bladena
Universitetsparken 7
DK-4000 Roskilde
www.bladena.com

As it can be concluded from the following figures (26 and 27), the blade behaves as it was expected. By observing the strains along the length of the blade, the trailing edge is in compression along the entire length, while the leading edge is in tension. Taking also into account the direction of the combined load, as this is illustrated in Figure 104, this behaviour for both TE and LE is justified. In addition, in Figure 127 the variation among the different tests is illustrated, where it can be concluded that the different configurations do not affect the strain magnitude with respect to the leading and trailing edge.

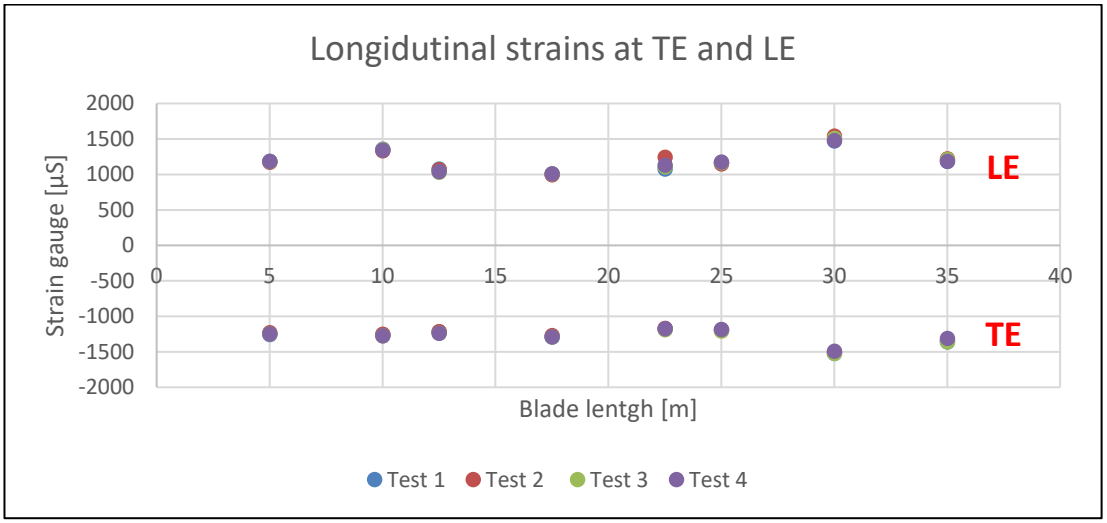

Figure 127: Longidutinal strain along the blade length for all tests

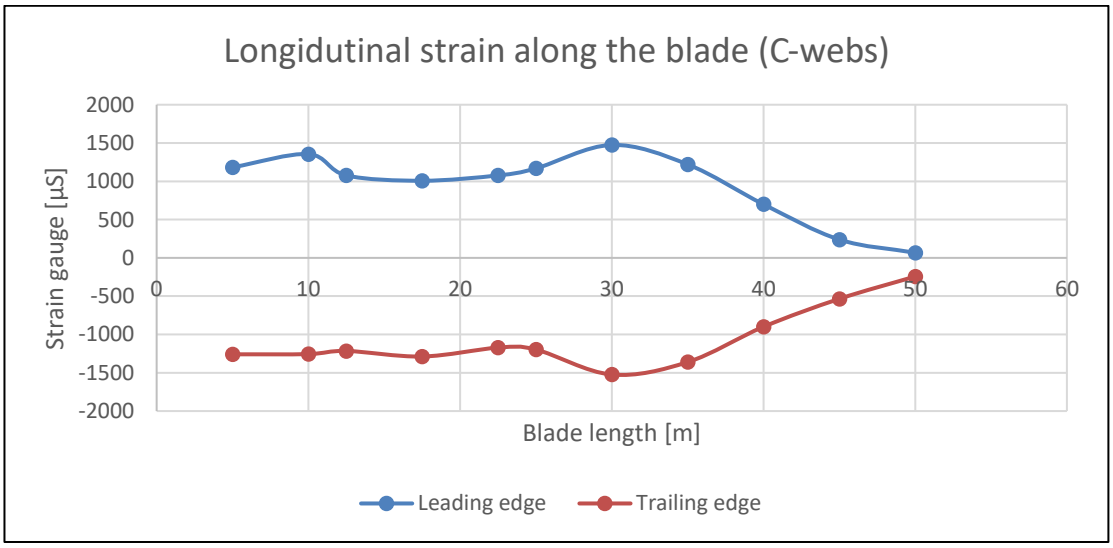

Figure 128: Longidutinal strain along the blade length for C-webs

Bladena
Universitetsparken 7
DK-4000 Roskilde
www.bladena.com

E5. Additional results

Strain gauges summary and graphs

Table 16: Summary of Strain gauges

SG No	Z distance [m]	Uni- or triaxial	Position	Orientation	Strain gauge [µS] Test1	Strain gauge [µS] Test2	Strain gauge [µS] Test3	Strain gauge [µS] Test4
1	5	Uni-axial	L	0°	1183	1169	1183	1181
2	5	Uni-axial	T	0°	-1259	-1232	-1248	-1247
3	10	Uni-axial	L	0°	1355	1334	1350	1340
4	10	Uni-axial	T	0°	-1256	-1254	-1273	-1276
5	12,5	Uni-axial	L	0°	1077	1068	1031	1039
6	12,5	Uni-axial	T	0°	-1215	-1217	-1238	-1239
7	17,5	Uni-axial	L	0°	1007	995	1010	1009
8	17,5	Uni-axial	T	0°	-1288	-1271	-1291	-1288
9	22,5	Uni-axial	L	0°	1077	1244	1107	1128
10	22,5	Uni-axial	T	0°	-1172	-1173	-1189	-1175
11	25	Uni-axial	L	0°	1168	1149	1168	1173
12	25	Uni-axial	T	0°	-1197	-1189	-1205	-1186
13	30	Uni-axial	L	0°	1475	1539	1507	1479
14	30	Uni-axial	T	0°	-1524	-1505	-1524	-1493
15	35	Uni-axial	L	0°	1221	1200	1213	1186
16	35	Uni-axial	T	0°	-1361	-1341	-1361	-1311
17	40	Uni-axial	L	0°	9806	-9806	-9806	-9806
18	40	Uni-axial	T	0°	-9806	-9806	-9806	-9806
19	45	Uni-axial	L	0°	239	-9806	-9806	-9806
20	45	Uni-axial	T	0°	-535	9806	9806	9806
21	50	Uni-axial	L	0°	67	65	72	41
22	50	Uni-axial	T	0°	-243	-239	-246	-214
23	1	Tri-axial	S	0°	9806	9806	9806	9806
24	1	Tri-axial	S	45°	6	5	5	17
25	1	Tri-axial	S	90°	493	456	457	435
26	1	Tri-axial	L	0°	559	544	556	559
27	1	Tri-axial	L	45°	336	332	336	337
28	1	Tri-axial	L	90°	-311	-306	-312	-310

Bladena
Universitetsparken 7
DK-4000 Roskilde
www.bladena.com

29	1	Tri-axial	P	0°	816	821	835	813
30	1	Tri-axial	P	45°	308	311	314	301
31	1	Tri-axial	P	90°	-442	-447	-453	-441
32	1	Tri-axial	T	0°	-500	-497	-506	-502
33	1	Tri-axial	T	45°	-51	-49	-50	-55
34	1	Tri-axial	T	90°	263	262	268	266
35	1	Tri-axial	S	Torsion	-9806	-9806	-9806	-9806
36	1	Tri-axial	L	Torsion	-9806	-9806	-9806	-9806
37	1	Tri-axial	P	Torsion	-9854	-9854	-9854	-9854
38	1	Tri-axial	T	Torsion	-9806	-9806	-9806	-9806
39	24	Tri-axial	S	Torsion	-9806	-9806	-9806	-9806
40	24	Tri-axial	S	0°	-2040	-2042	-2064	-2014
41	24	Tri-axial	P	Torsion	-9806	-9806	-9806	-9806
42	24	Tri-axial	P	0°	2728	2725	2758	2694
43	30	Tri-axial	S	Torsion	-9806	-9806	-9806	-9806
44	30	Tri-axial	S	0°	-2322	-2317	-2348	-2308
45	30	Tri-axial	P	Torsion	-9806	-9806	-9806	-9806
46	30	Tri-axial	P	0°	2632	2630	2661	2612
47	15	Uni-axial	P - 4cm from TE	0°	-906	-873	-885	-891
48	15	Uni-axial	S - 4cm from TE	0°	-1098	-1074	-1081	-1077
49	16	Uni-axial	P - 4cm from TE	0°	-961	-957	-980	-985
50	16	Uni-axial	S - 4cm from TE	0°	-483	-457	-459	-459
51	17	Uni-axial	P - 4cm from TE	0°	-1045	-1031	-1028	-1038
52	17	Uni-axial	S - 4cm from TE	0°	-1186	-1172	-1185	-1184
53	18	Uni-axial	P - 4cm from TE	0°	-970	-940	-928	-932
54	18	Uni-axial	S - 4cm from TE	0°	-1195	-1156	-1177	-1173
55	19	Uni-axial	P - 4cm from TE	0°	-1010	-1000	-1012	-1013
56	19	Uni-axial	S - 4cm from TE	0°	-1141	-1130	-1146	-1141
57	20	Uni-axial	P - 4cm from TE	0°	-1027	-1019	-1037	-1037
58	20	Uni-axial	S - 4cm	0°	-1202	-1201	-1216	-1209

Bladena
Universitetsparken 7
DK-4000 Roskilde
www.bladena.com

			from TE					
59	21	Uni-axial	P - 4cm from TE	0°	-937	-932	-950	-950
60	21	Uni-axial	S - 4cm from TE	0°	-1131	-1131	-1147	-1138
61	22	Uni-axial	P - 4cm from TE	0°	-958	-957	-974	-970
62	22	Uni-axial	S - 4cm from TE	0°	-1074	-1076	-1092	-1080
63	23	Uni-axial	P - 4cm from TE	0°	-907	-897	-912	-909
64	23	Uni-axial	S - 4cm from TE	0°	-1126	-1122	-1138	-1126
65	24	Uni-axial	P - 4cm from TE	0°	-836	-825	-839	-833
66	24	Uni-axial	S - 4cm from TE	0°	-1070	-1063	-1078	-1062
67	25	Uni-axial	P - 4cm from TE	0°	-808	-800	-813	-799
68	25	Uni-axial	S - 4cm from TE	0°	-1120	-1111	-1126	-1107
69	16,5	Uni-axial	P - 4cm from TE	0°	-997	-985	-998	-1003
70	16,5	Uni-axial	S - 4cm from TE	0°	-1128	-1124	-1139	-1139
71	17,5	Uni-axial	P - 4cm from TE	0°	-1067	-1071	-1056	-1065
72	17,5	Uni-axial	S - 4cm from TE	0°	-1130	-1132	-1146	-1145
73	18,5	Uni-axial	P - 4cm from TE	0°	-1063	-1035	-1045	-1047
74	18,5	Uni-axial	S - 4cm from TE	0°	-1096	-1062	-1071	-1064
75	19,5	Uni-axial	P - 4cm from TE	0°	-1014	-1008	-1023	-1024
76	19,5	Uni-axial	S - 4cm from TE	0°	-1142	-1142	-1156	-1150

Bladena
Universitetsparken 7
DK-4000 Roskilde
www.bladena.com

Uni-axial strain gauges

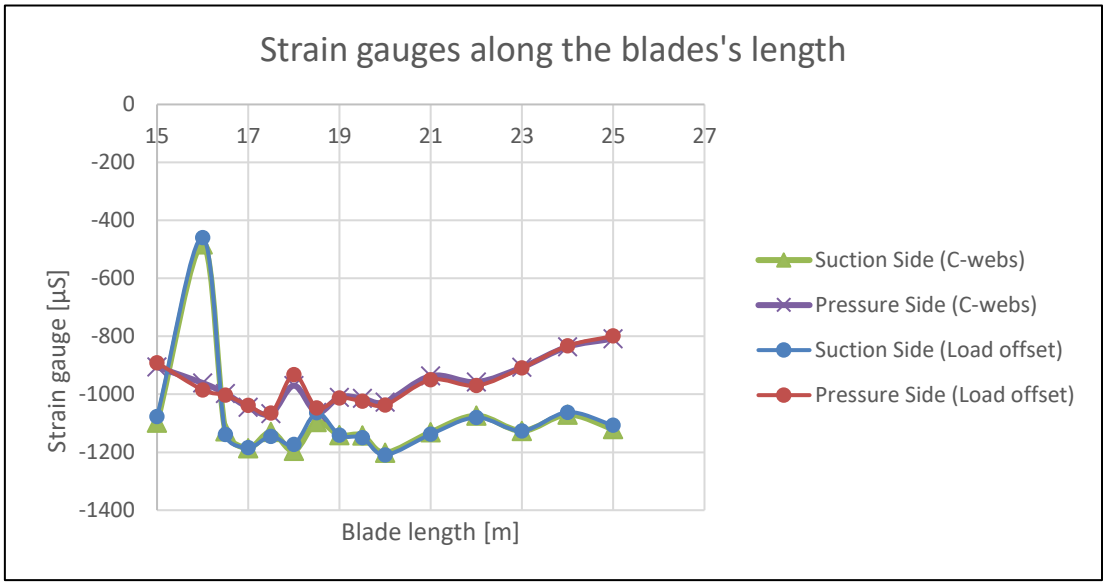

Figure 129: Back-to-back strain measurements along the blade

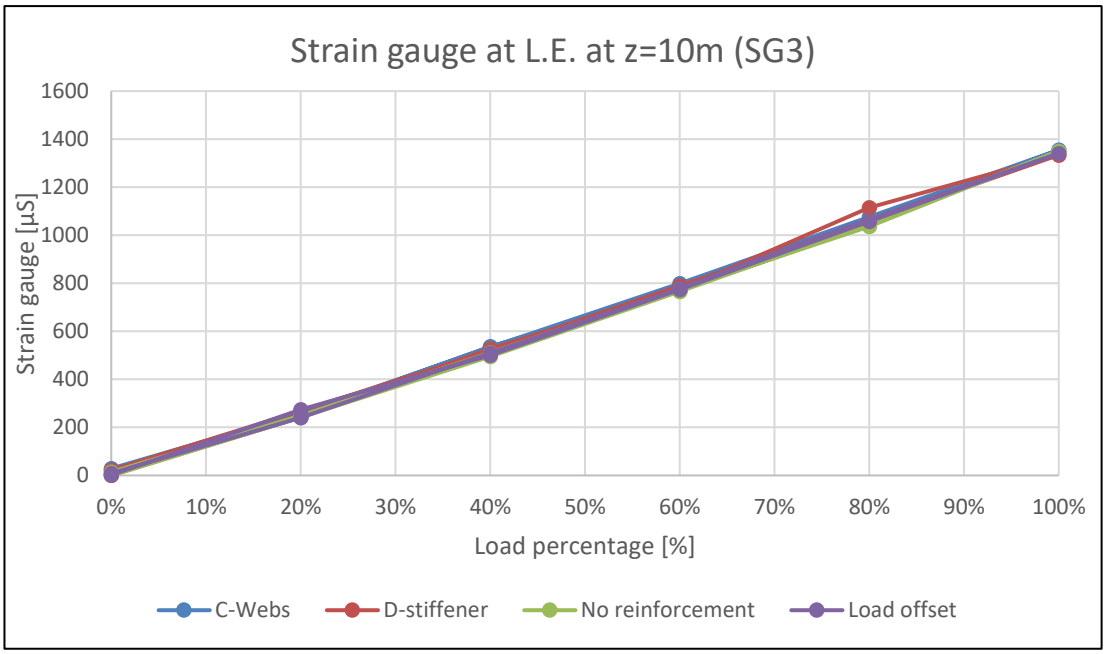

Figure 130: Uni-axial strain gauge for all the different configurations at z=10m

Bladena
Universitetsparken 7
DK-4000 Roskilde
www.bladena.com

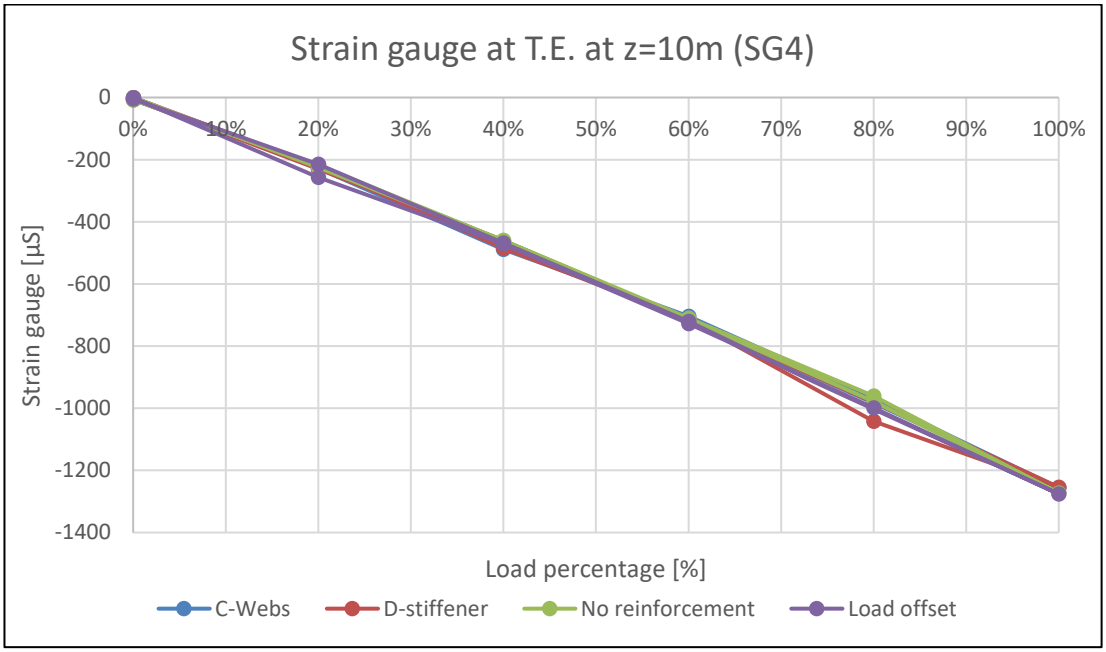

Figure 131: Uni-axial strain gauge for all the different configurations at z=10m

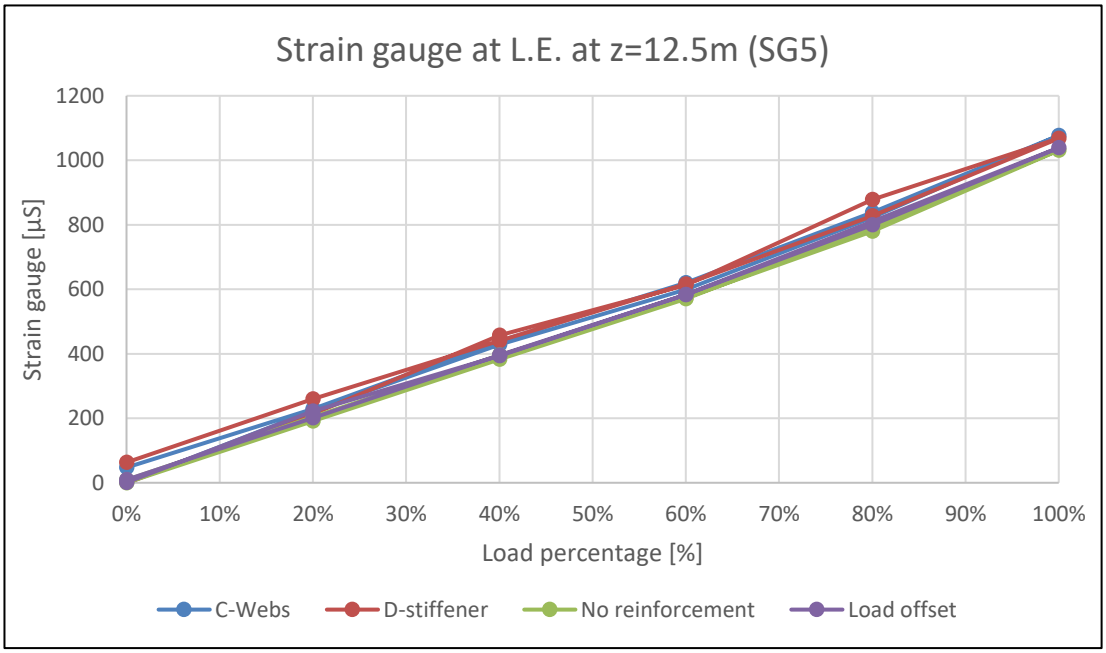

Figure 132: Uni-axial strain gauge for all the different configurations at z=12.5m

Bladena
Universitetsparken 7
DK-4000 Roskilde
www.bladena.com

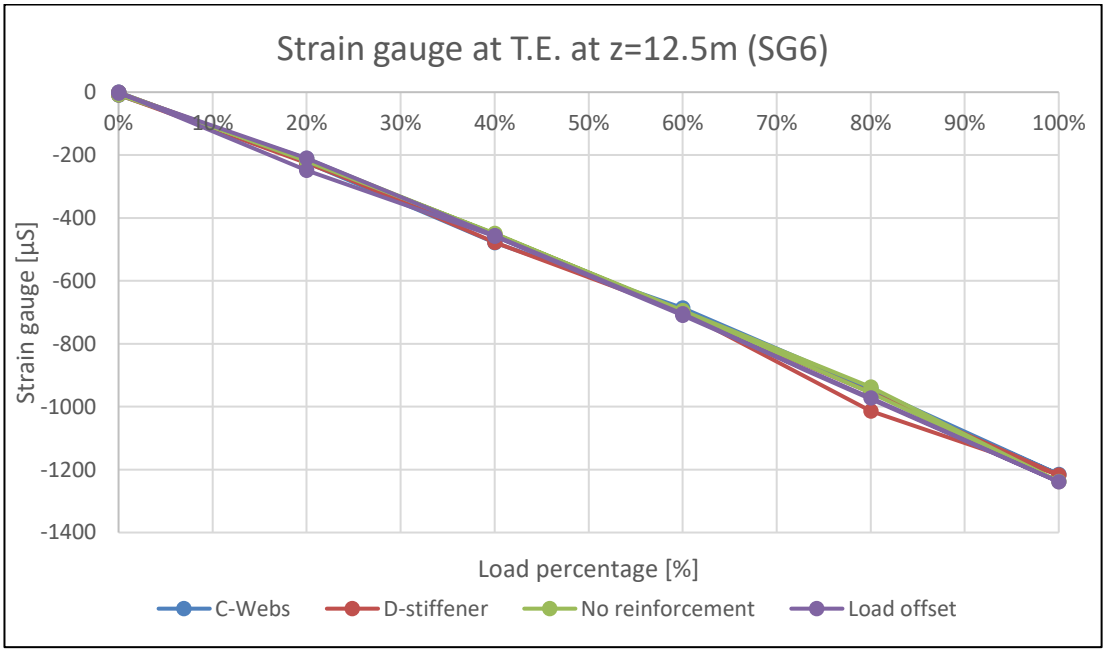

Figure 133: Uni-axial strain gauge for all the different configurations at z=12.5m

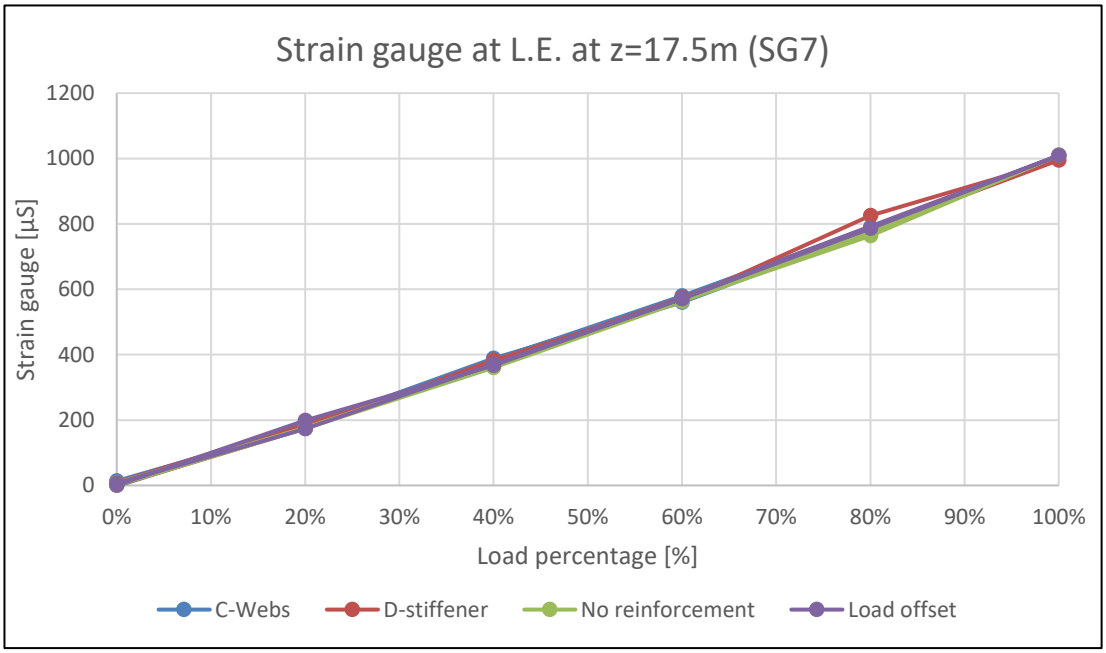

Figure 134: Uni-axial strain gauge for all the different configurations at z=17.5m

Bladena
Universitetsparken 7
DK-4000 Roskilde
www.bladena.com

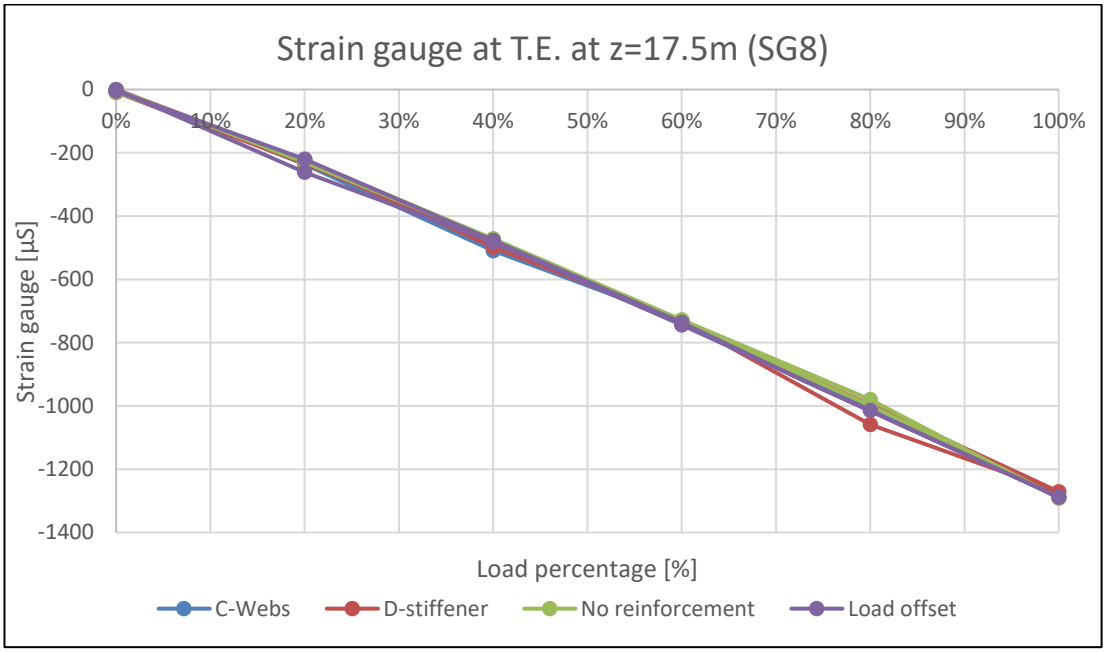

Figure 135: Uni-axial strain gauge for all the different configurations at z=17.5m

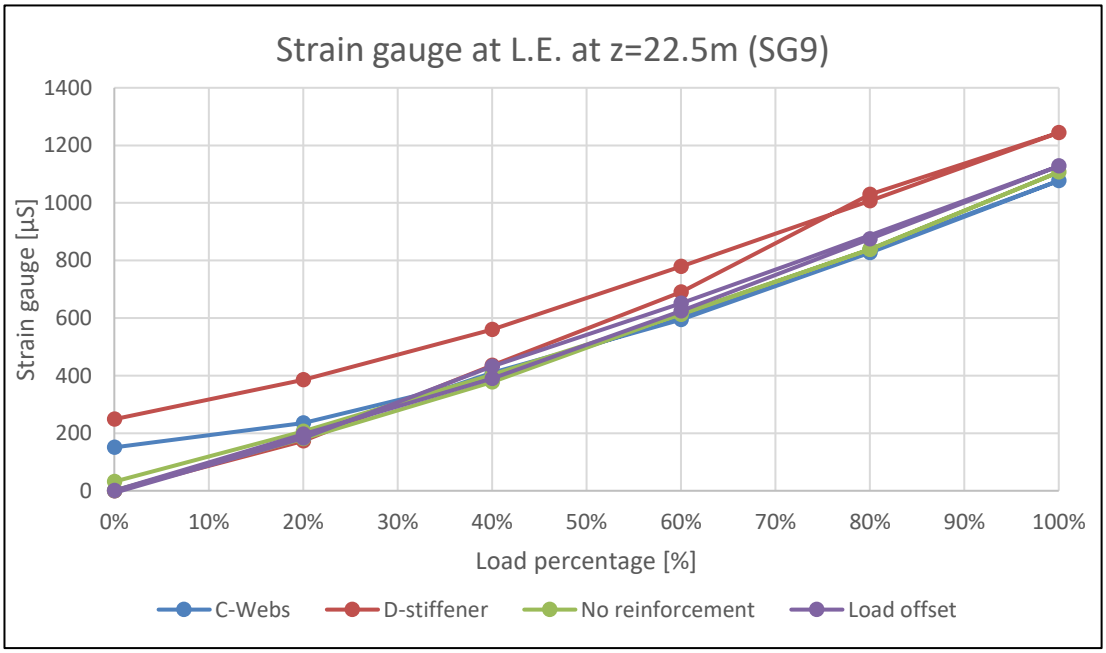

Figure 136: Uni-axial strain gauge for all the different configurations at z=22.5m

Bladena
Universitetsparken 7
DK-4000 Roskilde
www.bladena.com

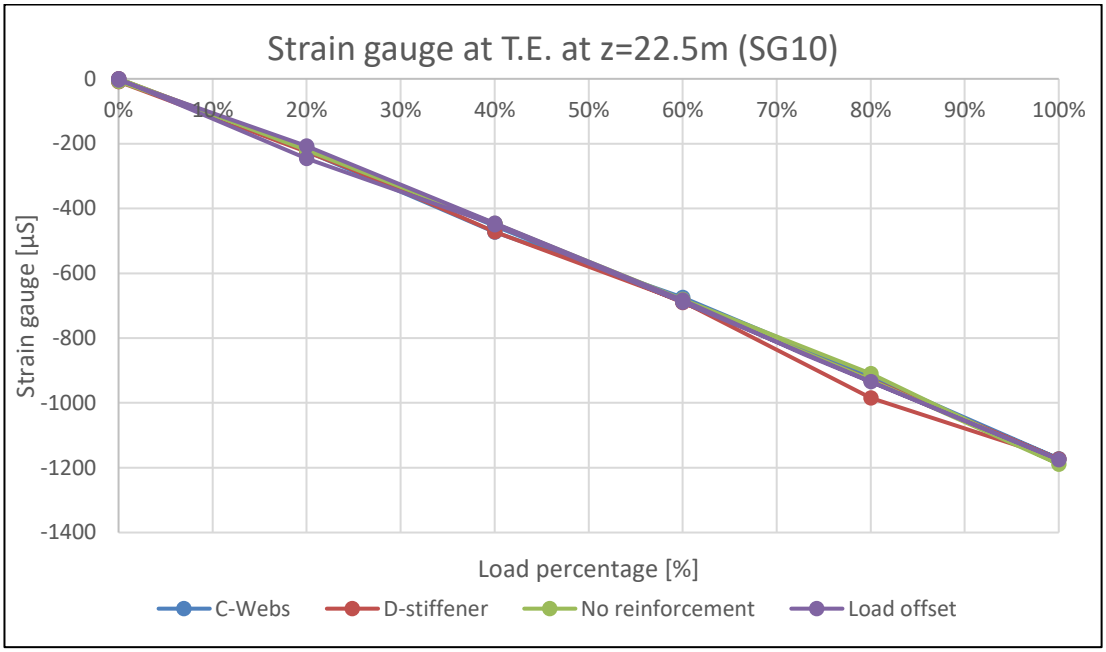

Figure 137: Uni-axial strain gauge for all the different configurations at z=22.5m

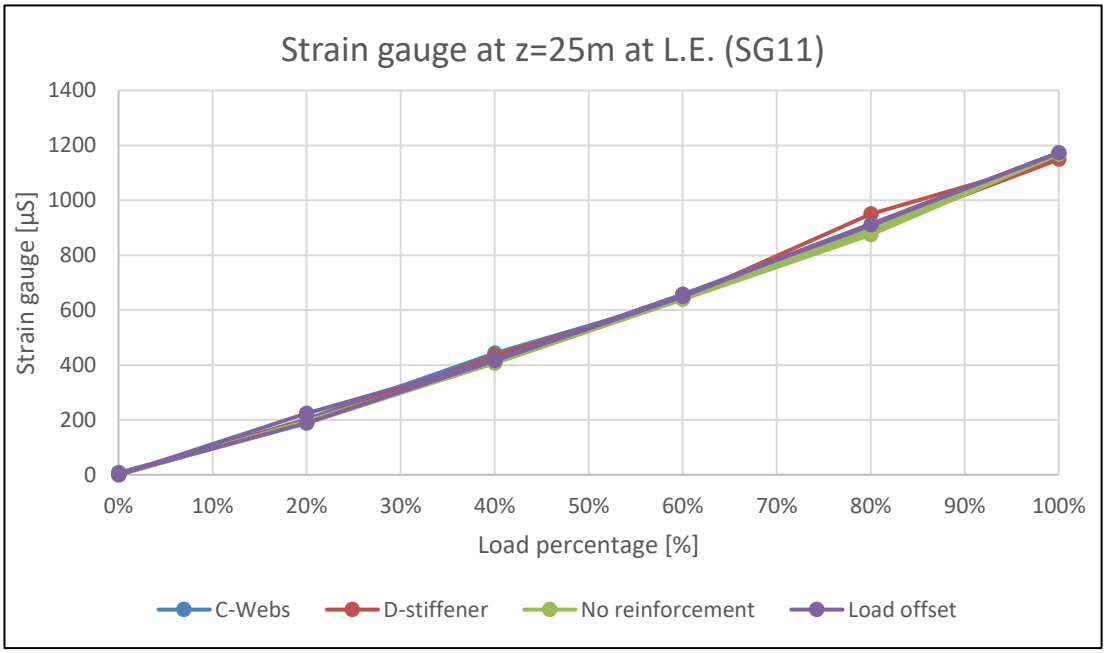

Figure 138: Uni-axial strain gauge for all the different configurations at z=25m

Bladena
Universitetsparken 7
DK-4000 Roskilde
www.bladena.com

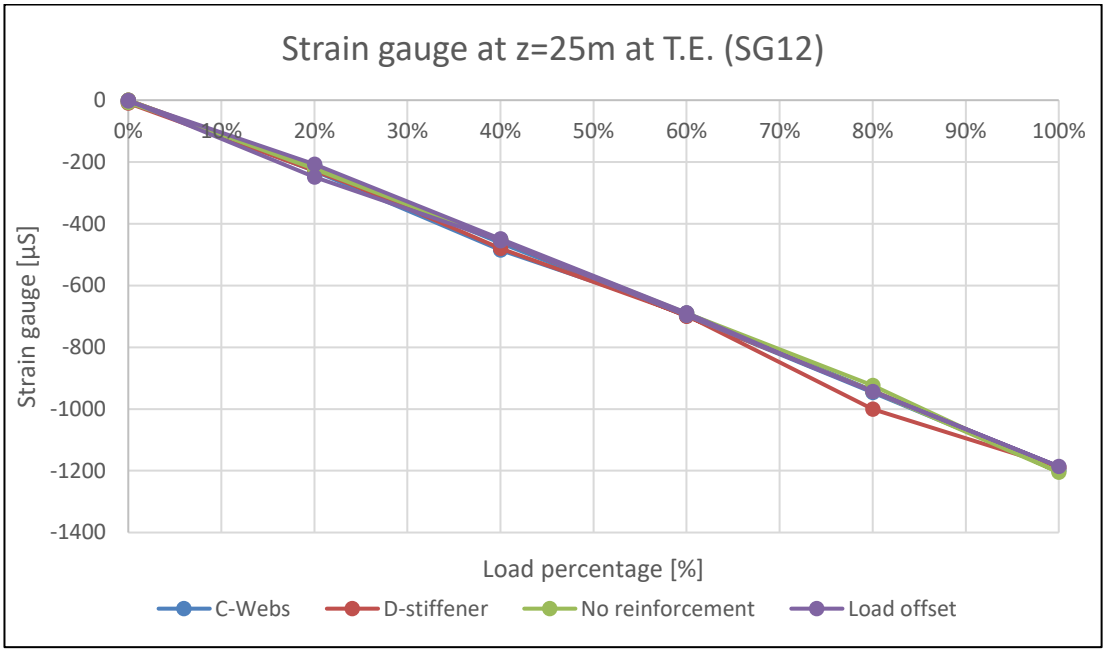

Figure 139: Uni-axial strain gauge for all the different configurations at z=25m

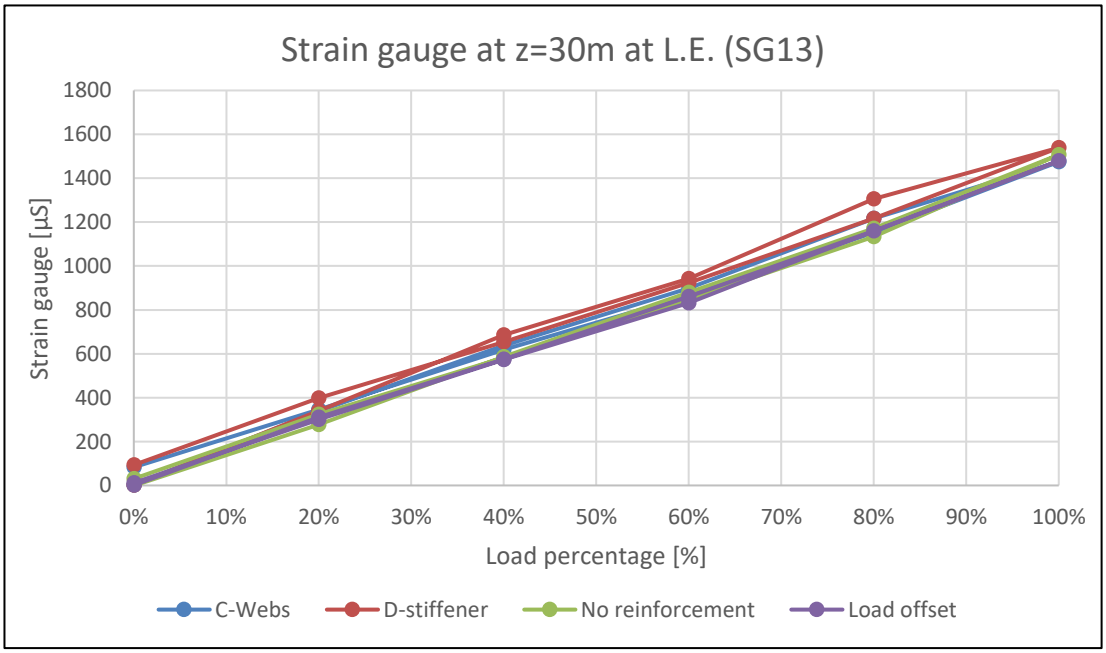

Figure 140: Uni-axial strain gauge for all the different configurations at z=30m

Bladena
Universitetsparken 7
DK-4000 Roskilde
www.bladena.com

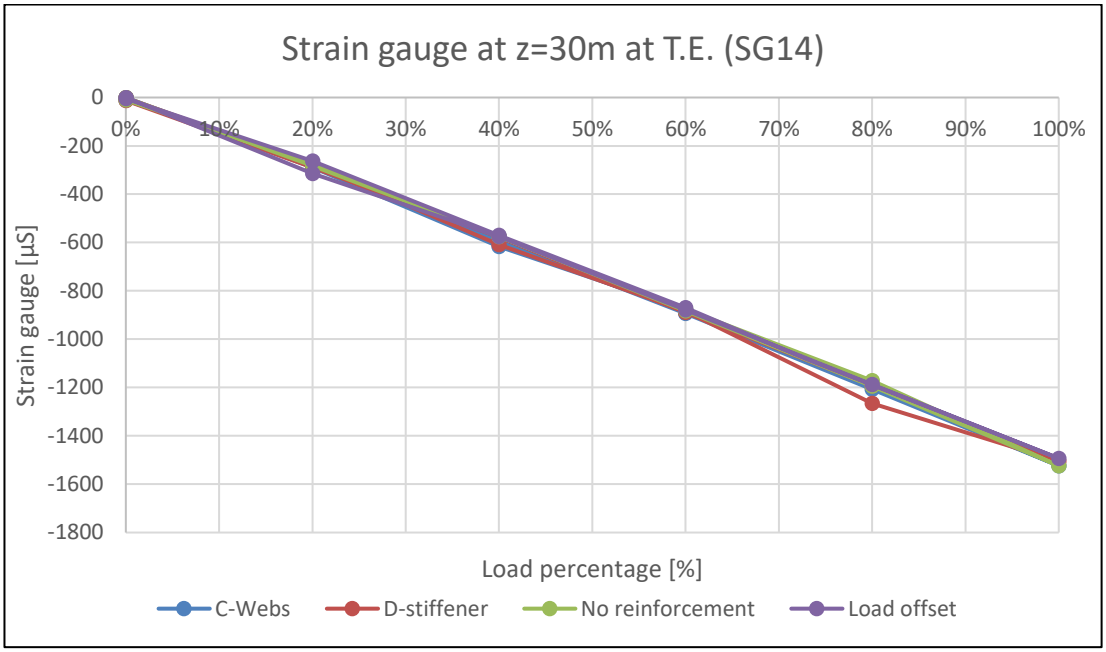

Figure 141: Uni-axial strain gauge for all the different configurations at z=30m

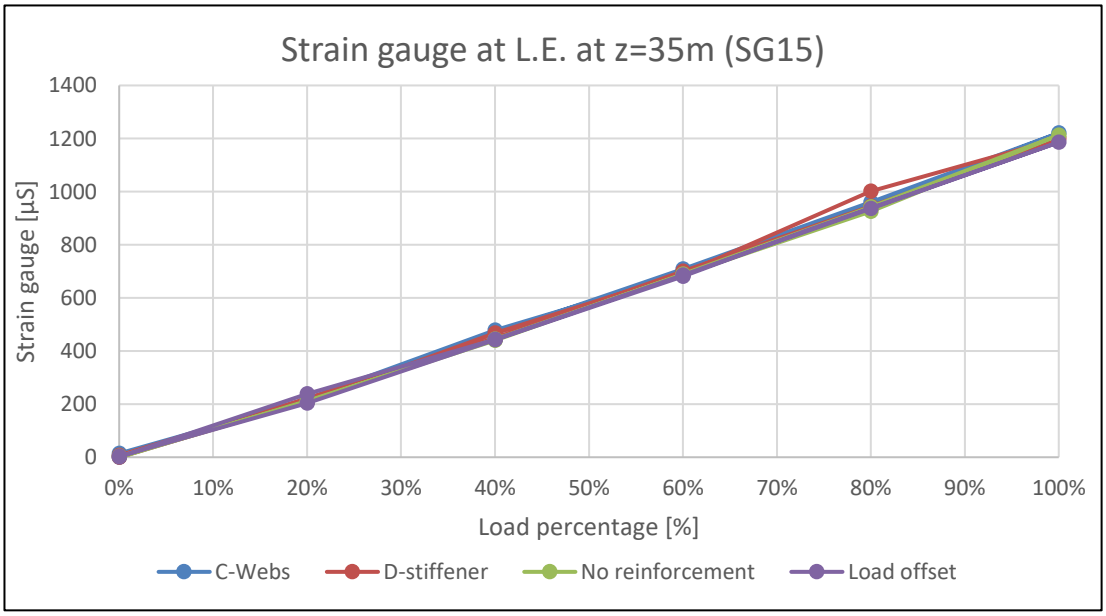

Figure 142: Uni-axial strain gauge for all the different configurations at z=35m

Bladena
Universitetsparken 7
DK-4000 Roskilde
www.bladena.com

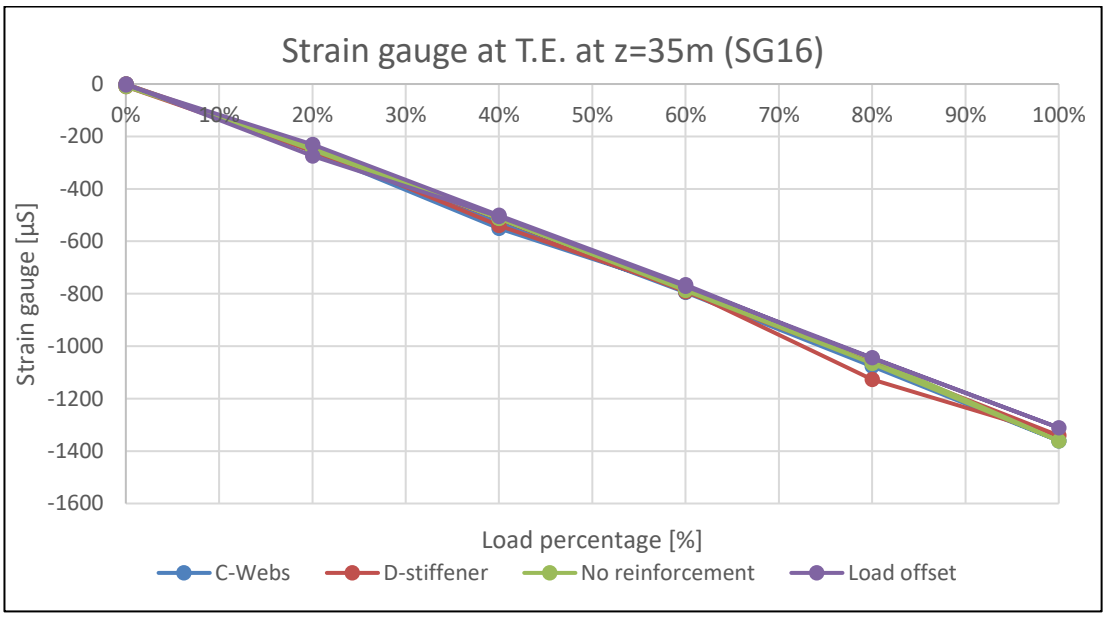

Figure 143: Uni-axial strain gauge for all the different configurations at z=35m

Tri-axial strain gauges

In order to capture the strain development in terms of three different orientations (0, 45 and 90 degrees) a tri-axial strain gauge was placed at 1m from the blade root. The orientations and the placement of the measurement devise is illustrated in Figure 144. Moreover, from Figure 145, becomes evident that the strain gauges which are placed at the leading and trailing edge behave in a rather similar pattern. In terms of the former, at 0° and 45° degrees orientation it is under tension, while at 90° degrees the strains indicate compression. Regarding the latter, the pattern is different as at 0° and 45° degrees the trailing edge is under compression, while at 90° degrees it is under tension. Furthermore, although the strains' magnitude is rather similar, at 45° degrees the trailing edge indicate strains close to zero, while the leading edge at 45° degrees results to strain of approximately 340µS.

Bladena
Universitetsparken 7
DK-4000 Roskilde
www.bladena.com

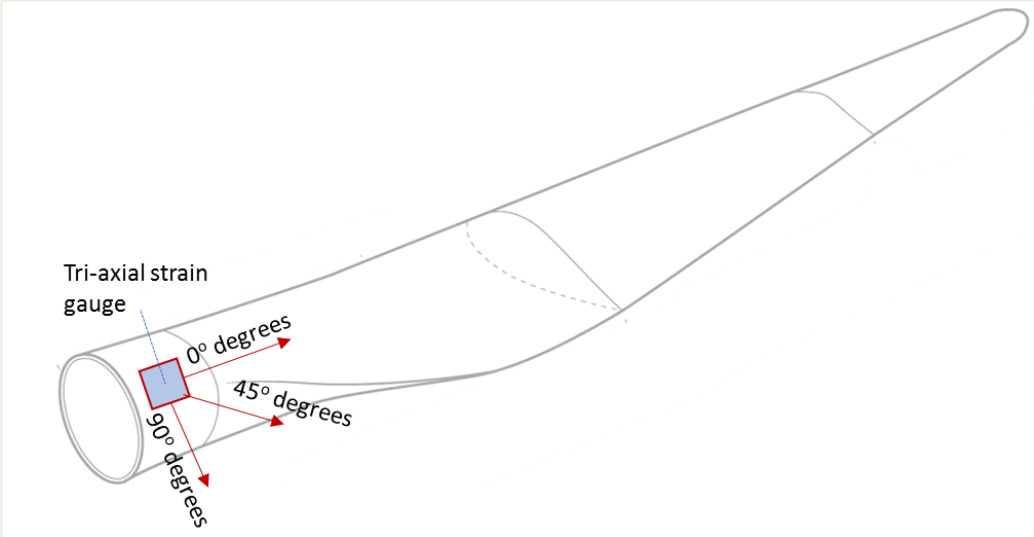

Figure 144: Tri-axial strain gauge orientations

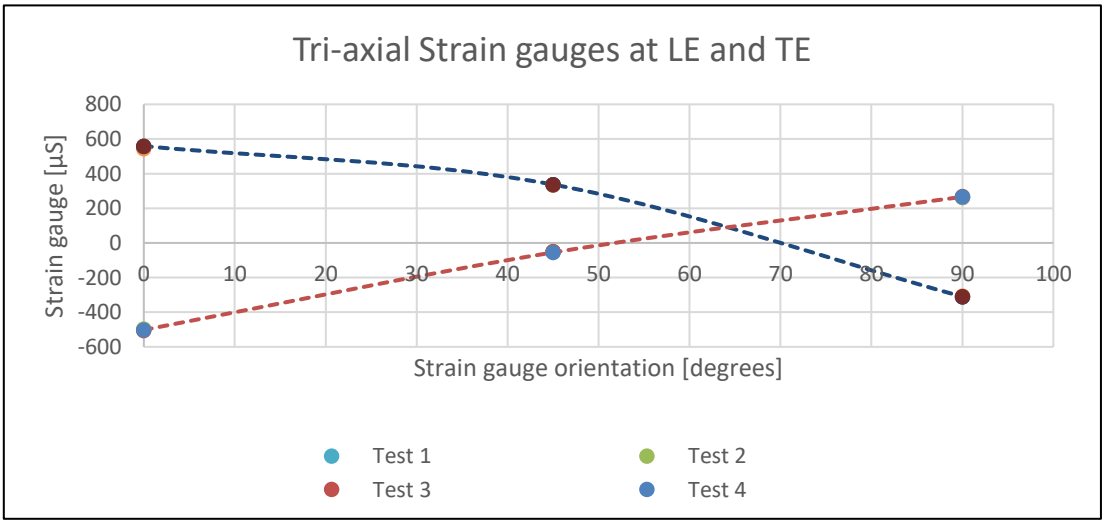

Figure 145: Tri-axial strain gauges at LE and TE at R=1m, for all tests and with orientations of 0°, 45° and 90°.

Similar to the LE and TE, the tri-axial strain gauges which were placed at PS and SS are depicted in Figure 146 for every test. In terms of the pressure side, at 0 and 45 degrees, the strains indicate that is under tension, while at 90 degrees it converts into compression.

However, this not the case for the suction side. According to the resulted strains, the suction side is in tension independently from the orientation of the measured strain. More specifically, at 0 and 45 degrees is under tension, while at 90 degrees the resulted strain is approaching zero.

Bladena
Universitetsparken 7
DK-4000 Roskilde
www.bladena.com

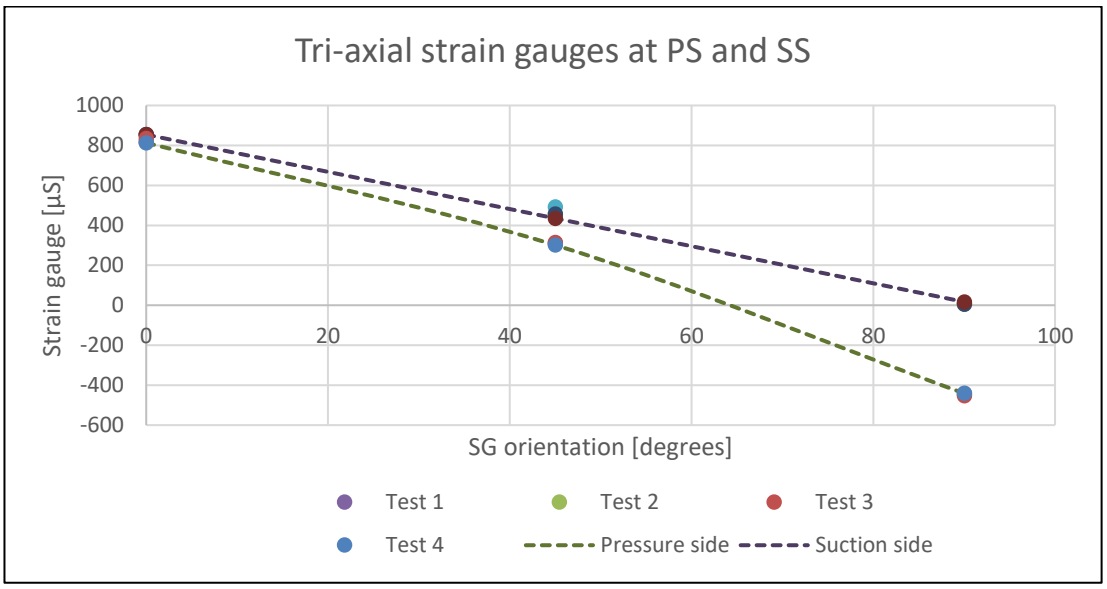

Figure 146: Tri-axial strain gauges at PS and SS at R=1m, for all tests.

In addition, in the following figures there is an illustration of the resulted strains for both the pressure and suction side, but also for the trailing and leading edge. This time, the strains are presented with respect to the load intervals until the 100% loading. According to these figures, a similar linear pattern is observed for every location and measurement's orientation, while it is evident that the different experiment configurations do not greatly affect the resulted strains in every direction and location of the strain measurement device.

It should be stated, that in the following results some microstrain measurements are approaching the ten thousand limit value. However, at approximately 10k microstrain, either the strain gauge or the DAQ channel is defected, thus the respective measurements should be disregarded. This applied for all the measured microstrains captured during the tests.

Bladena
Universitetsparken 7
DK-4000 Roskilde
www.bladena.com

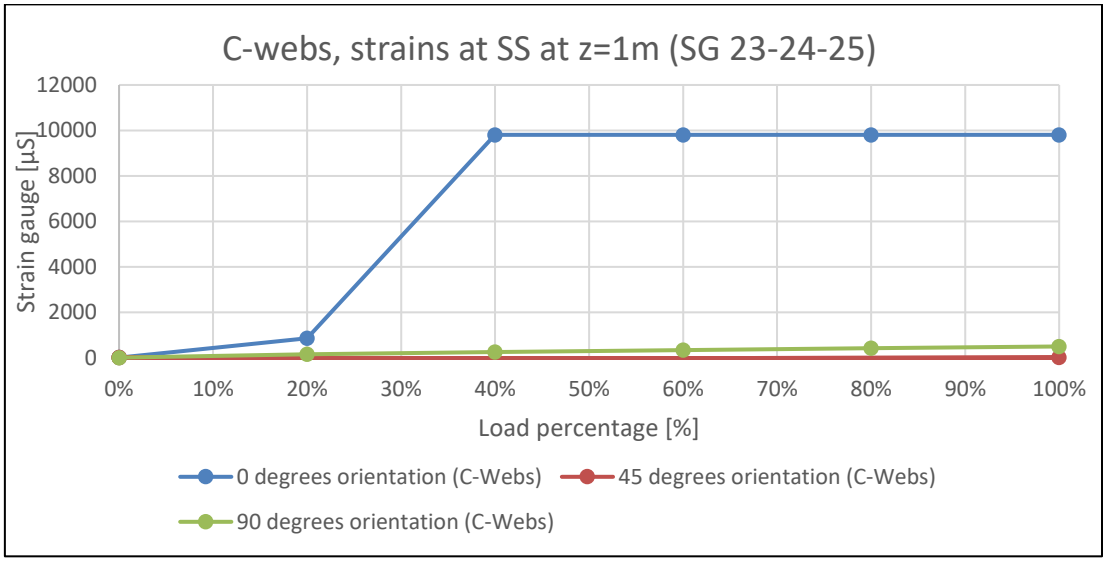

Figure 147: Tri-axial strain gauges at suction side in case of C-webs

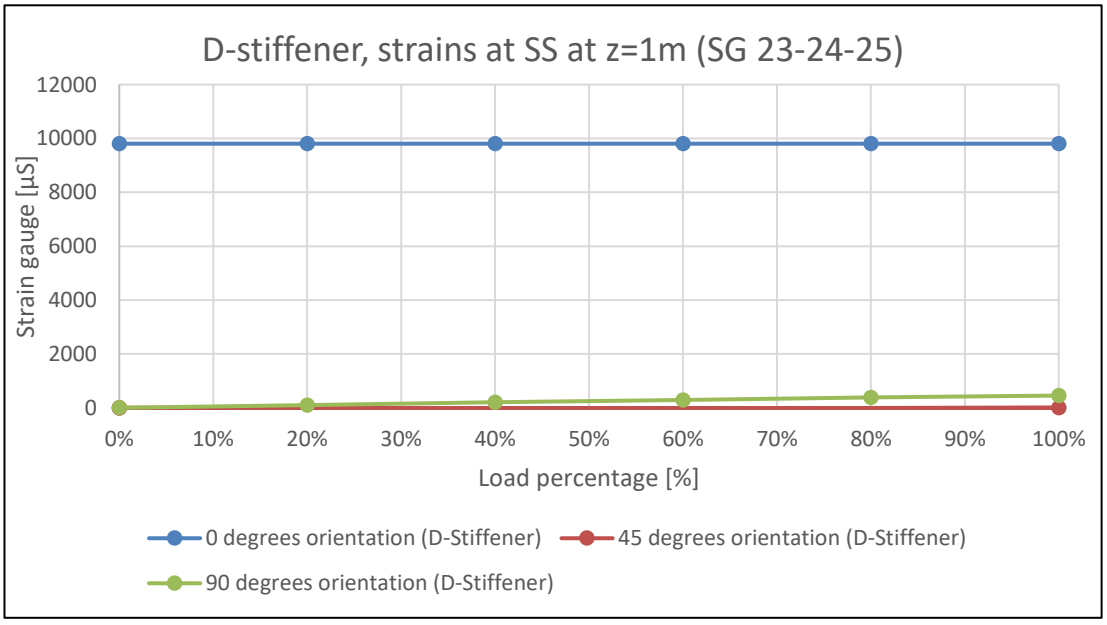

Figure 148: Tri-axial strain gauges at suction side in case of D-stiffeners

Bladena
Universitetsparken 7
DK-4000 Roskilde
www.bladena.com

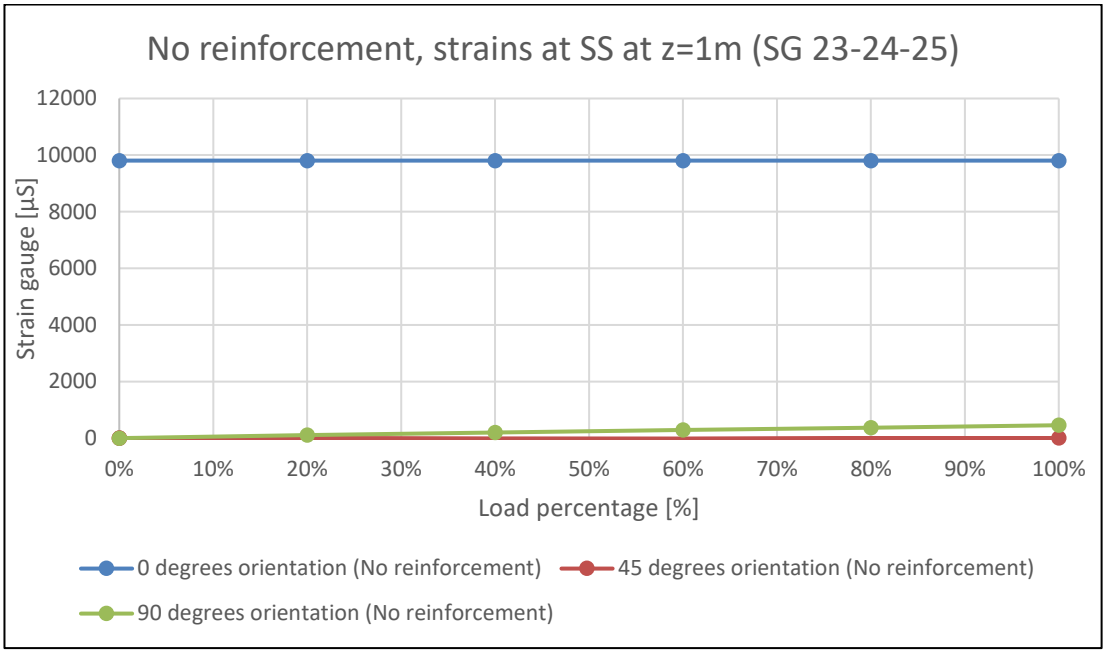

Figure 149: Tri-axial strain gauges at suction side in case of No reinforcement

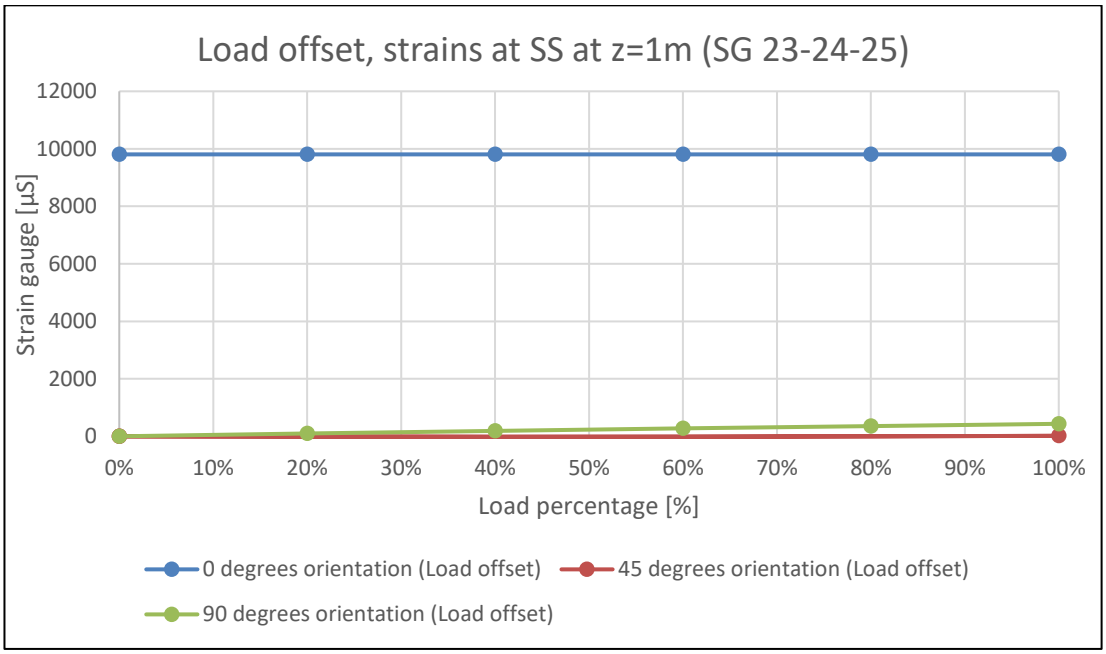

Figure 150: Tri-axial strain gauges at suction side in case of load offset

Bladena
Universitetsparken 7
DK-4000 Roskilde
www.bladena.com

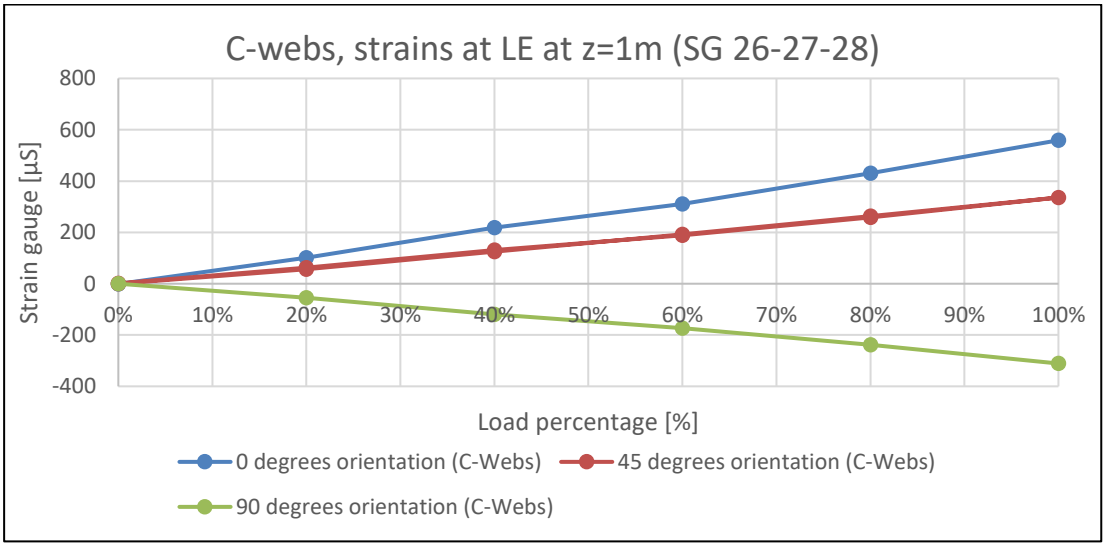

Figure 151: Tri-axial strain gauges at the leading edge in case of C-webs

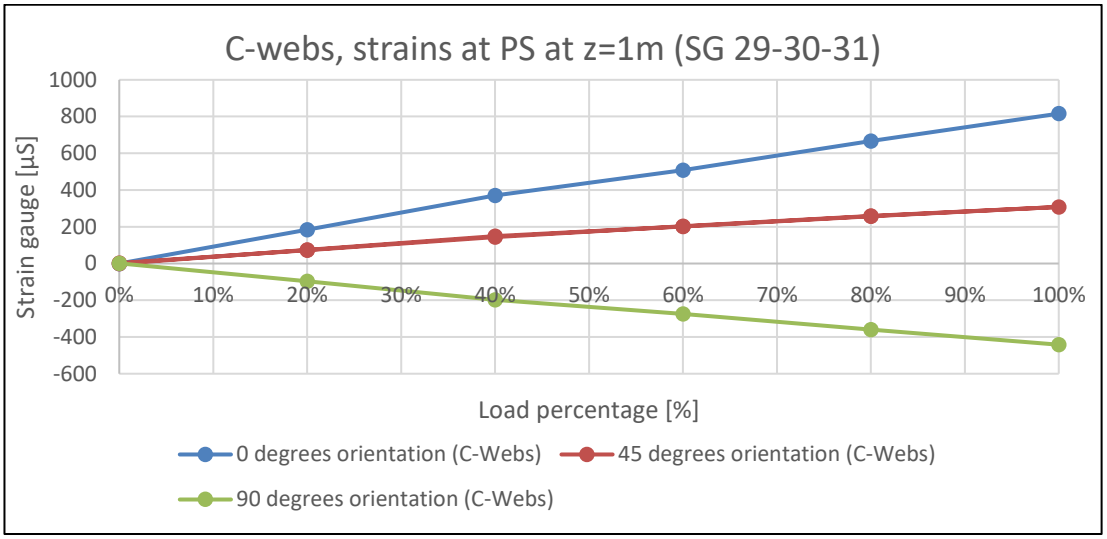

Figure 152: Tri-axial strain gauges at the pressure side in case of C-webs

Bladena
Universitetsparken 7
DK-4000 Roskilde
www.bladena.com

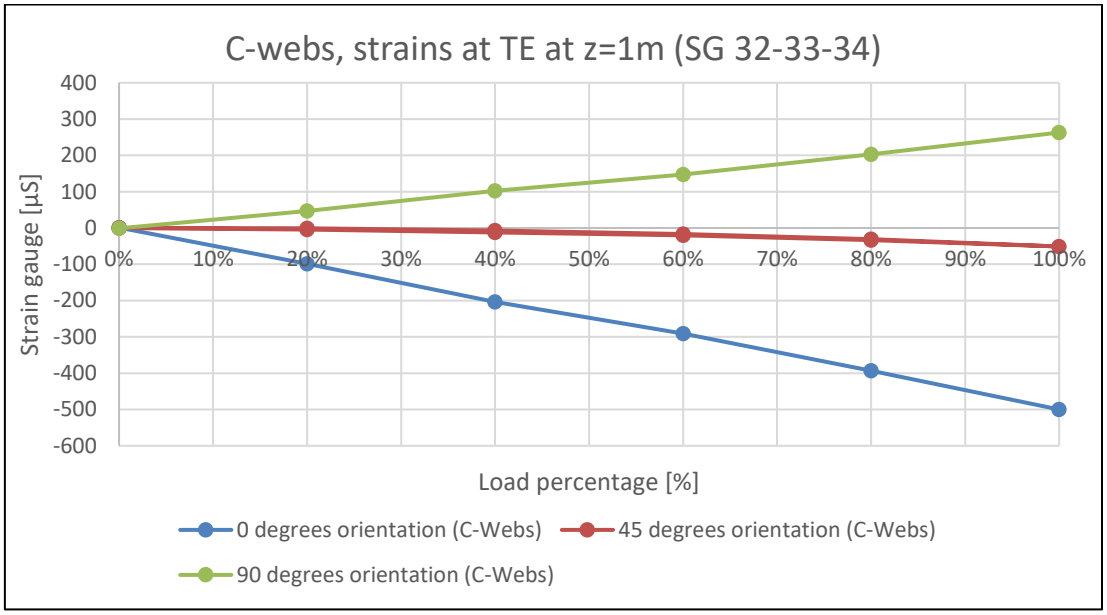

Figure 153: Tri-axial strain gauges at the trailing edge in case of C-webs

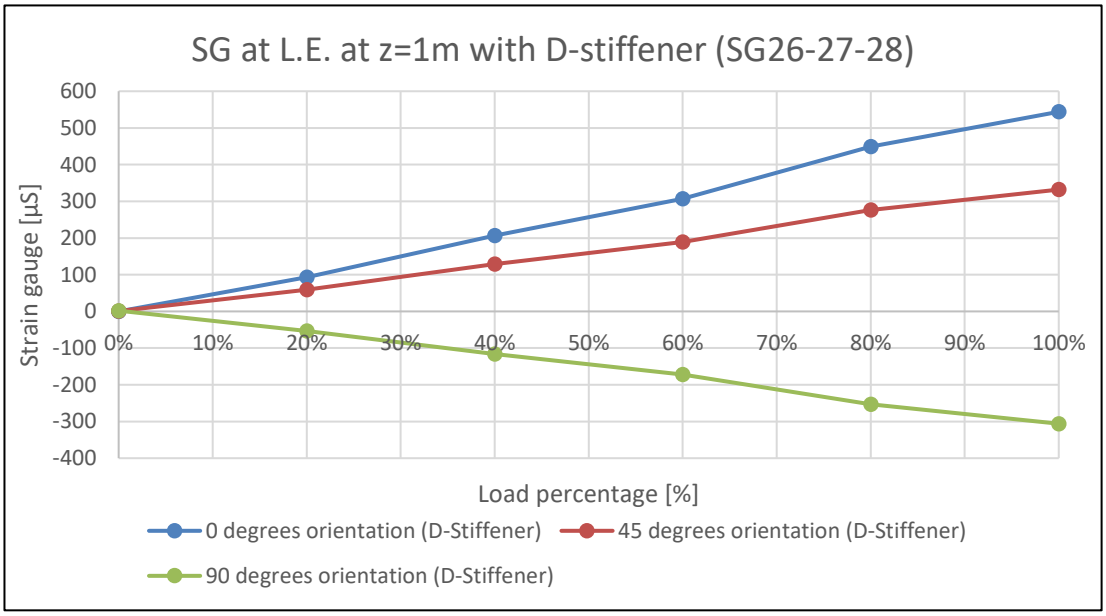

Figure 154: Strain gauges at the leading edge, with D-stiffeners at z=1m

Bladena
Universitetsparken 7
DK-4000 Roskilde
www.bladena.com

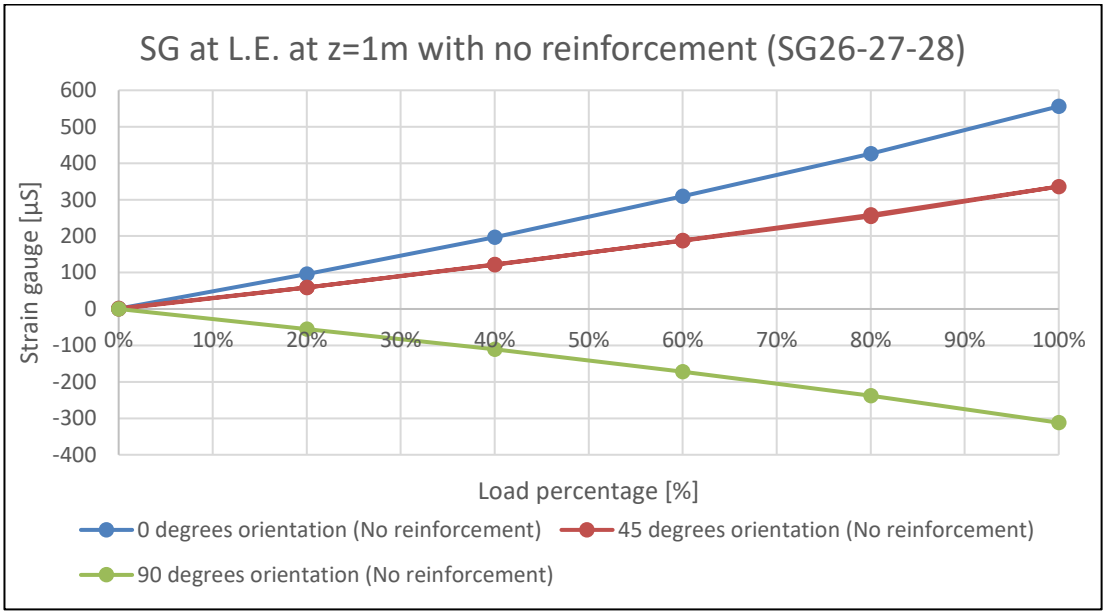

Figure 155: Strain gauges at the leading edge, with No-reinforcement at z=1m

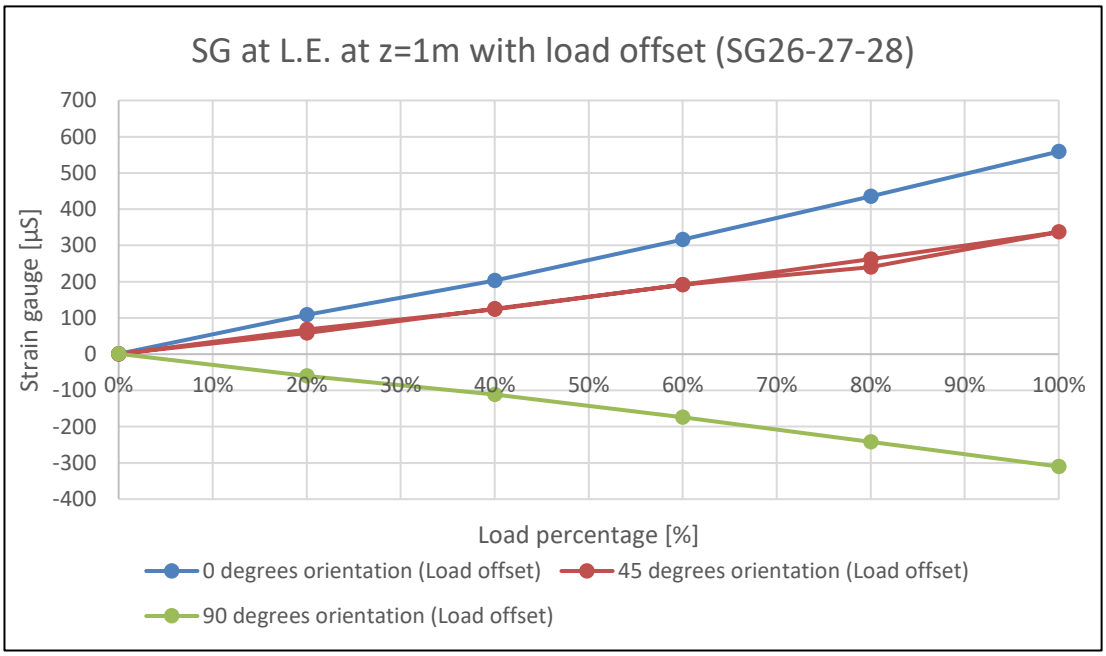

Figure 156 : Strain gauges at the leading edge, with load offset at z=1m

Bladena
Universitetsparken 7
DK-4000 Roskilde
www.bladena.com

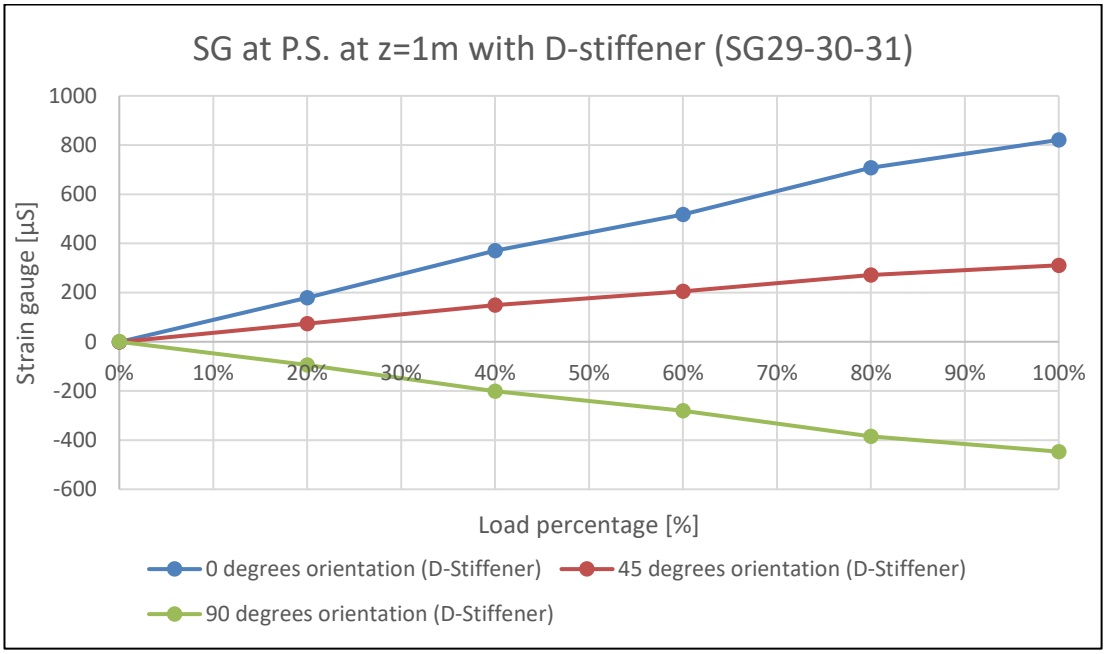

Figure 157: Strain gauges at the pressure side, with D-stiffeners at z=1m

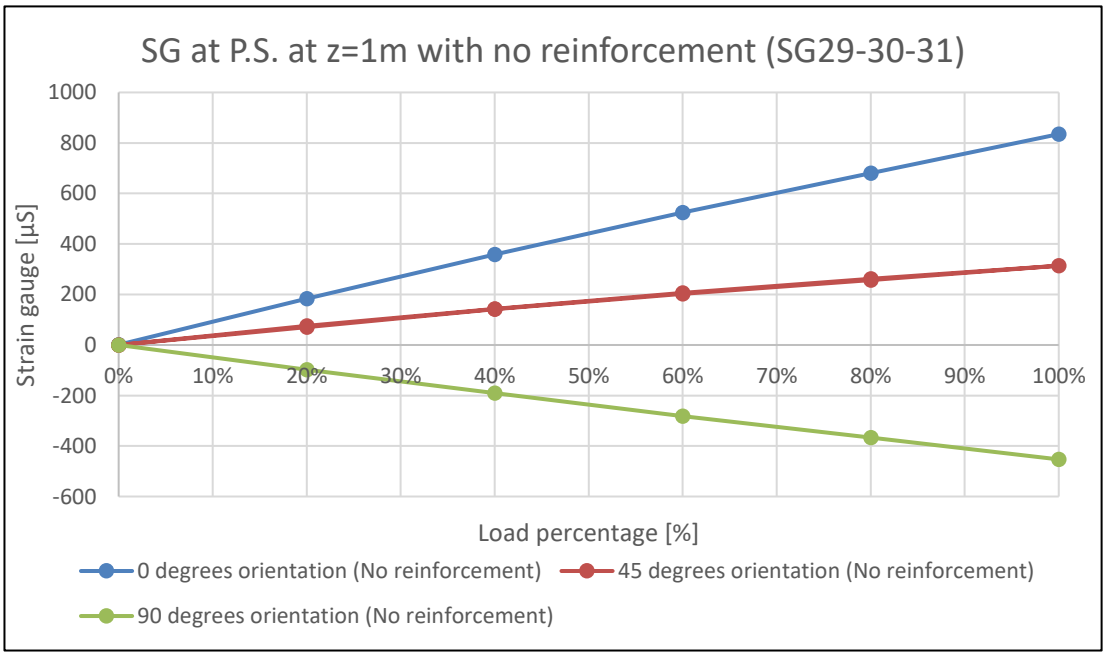

Figure 158: Strain gauges at the pressure side, with No reinforcement at z=1m

Bladena
Universitetsparken 7
DK-4000 Roskilde
www.bladena.com

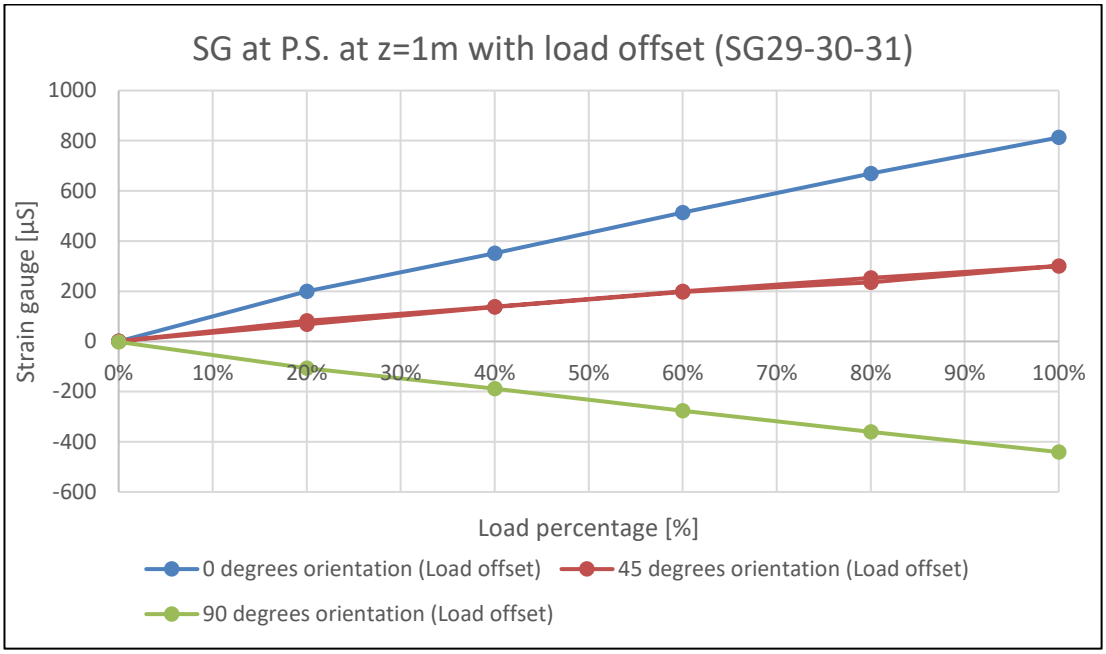

Figure 159: Strain gauges at the pressure side, with load offset at z=1m

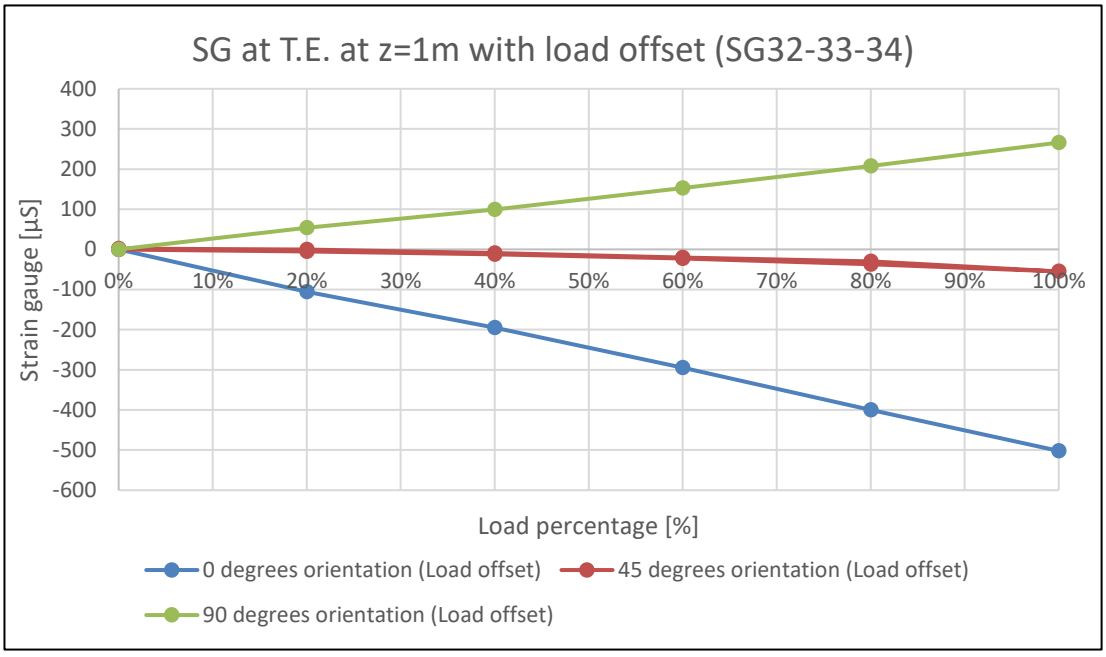

Figure 160: Strain gauges at the trailing edge, with load offset at z=1m

Bladena
Universitetsparken 7
DK-4000 Roskilde
www.bladena.com

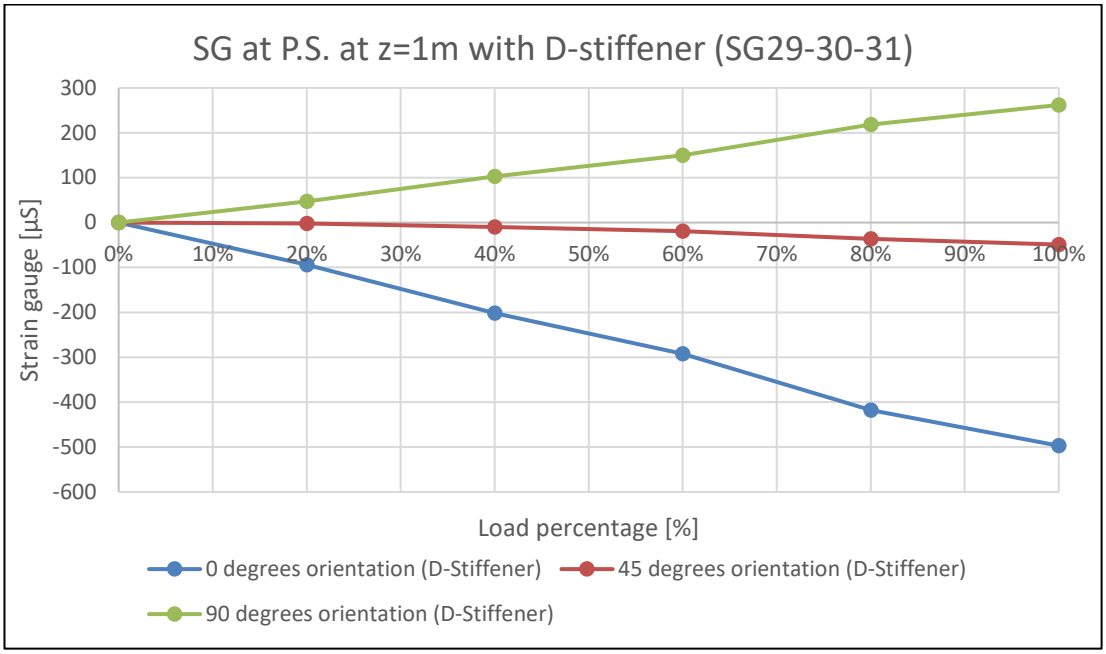

Figure 161: Strain gauges at the trailing edge, with D-stiffeners at z=1m

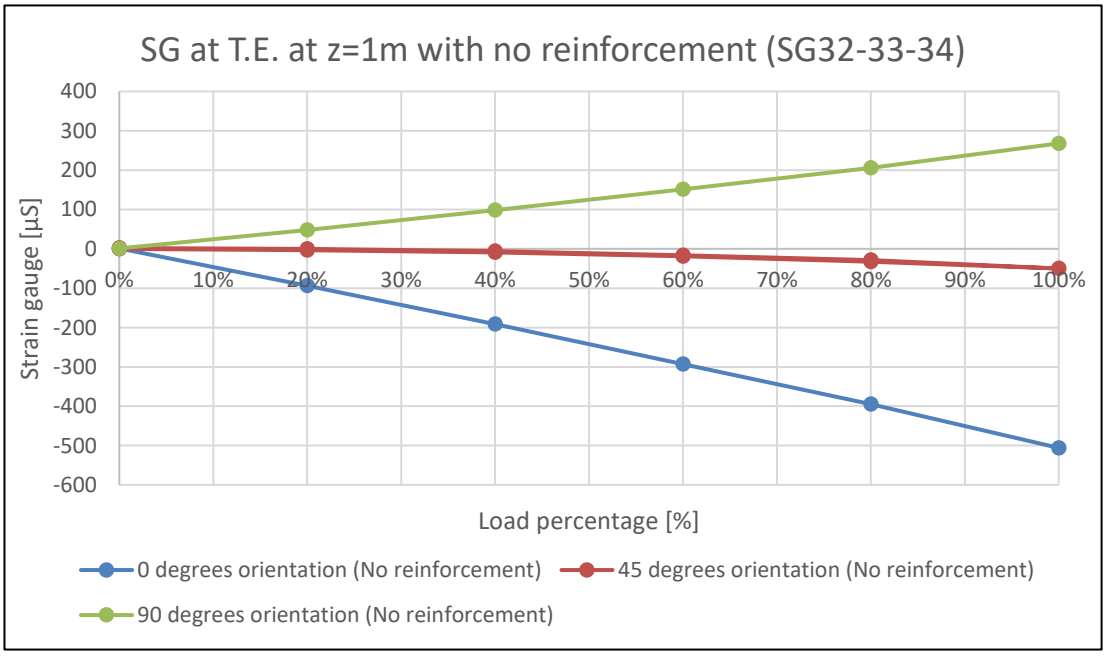

Figure 162: Strain gauges at the trailing edge, with no reinforcement at z=1m

Bladena
Universitetsparken 7
DK-4000 Roskilde
www.bladena.com

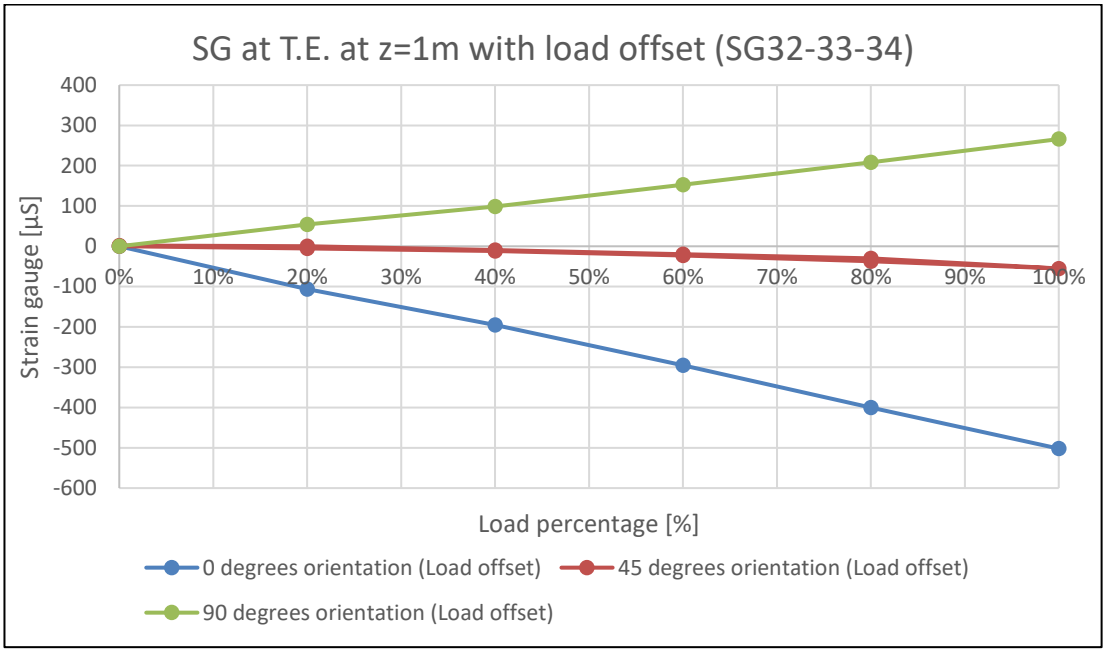

Figure 163: Strain gauges at the trailing edge, with load offset at z=1m

Back-to-back strain gauges

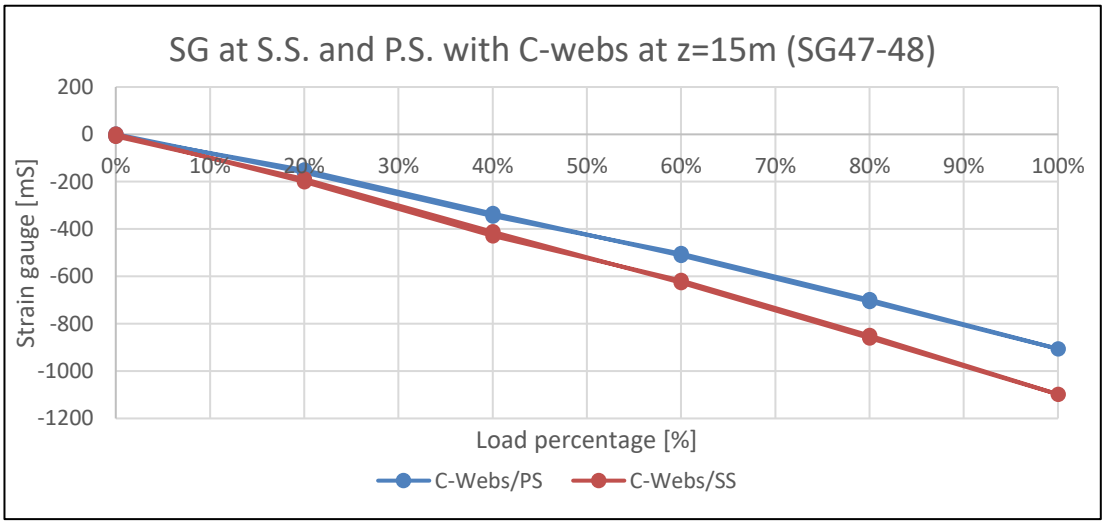

Figure 164: Strain gauges at the pressure and suction side, with C-webs at z=15m

Bladena
Universitetsparken 7
DK-4000 Roskilde
www.bladena.com

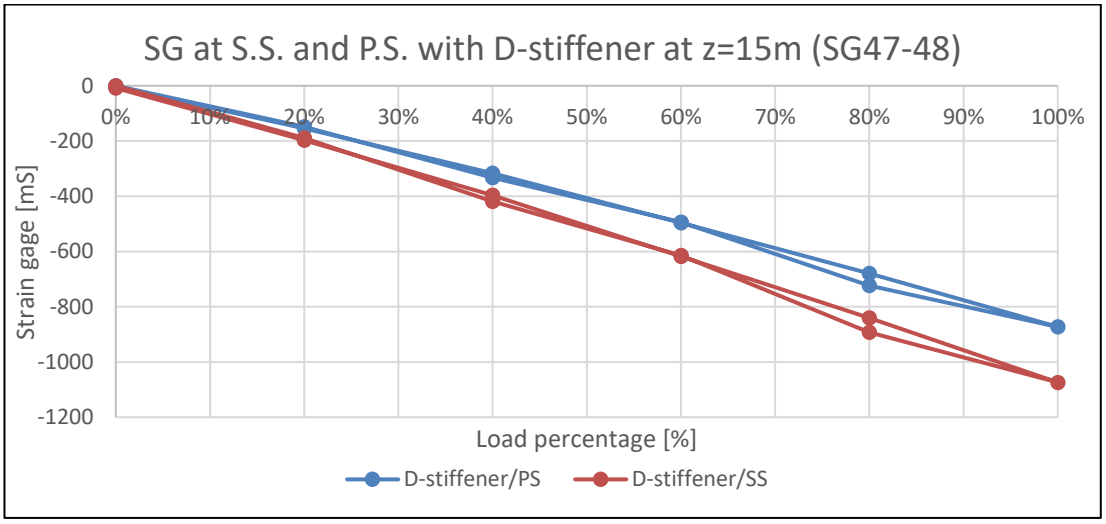

Figure 165: Strain gauges at the pressure and suction side, with D-stiffener at z=15m

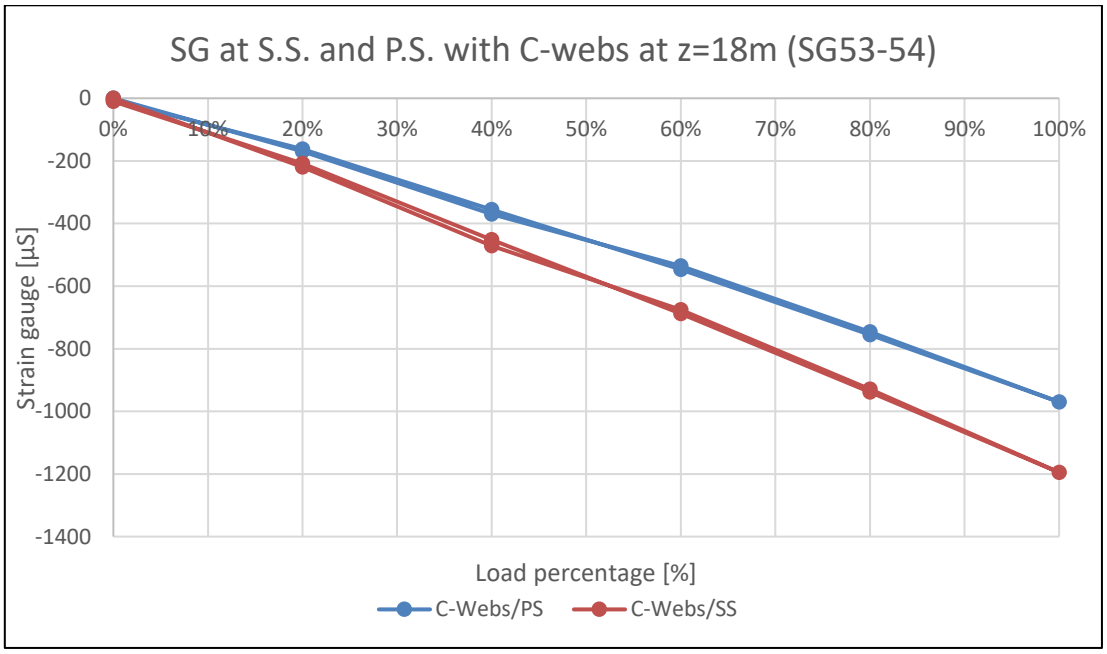

Figure 166: Strain gauges at the pressure and suction side, with C-webs at z=18m

Bladena
Universitetsparken 7
DK-4000 Roskilde
www.bladena.com

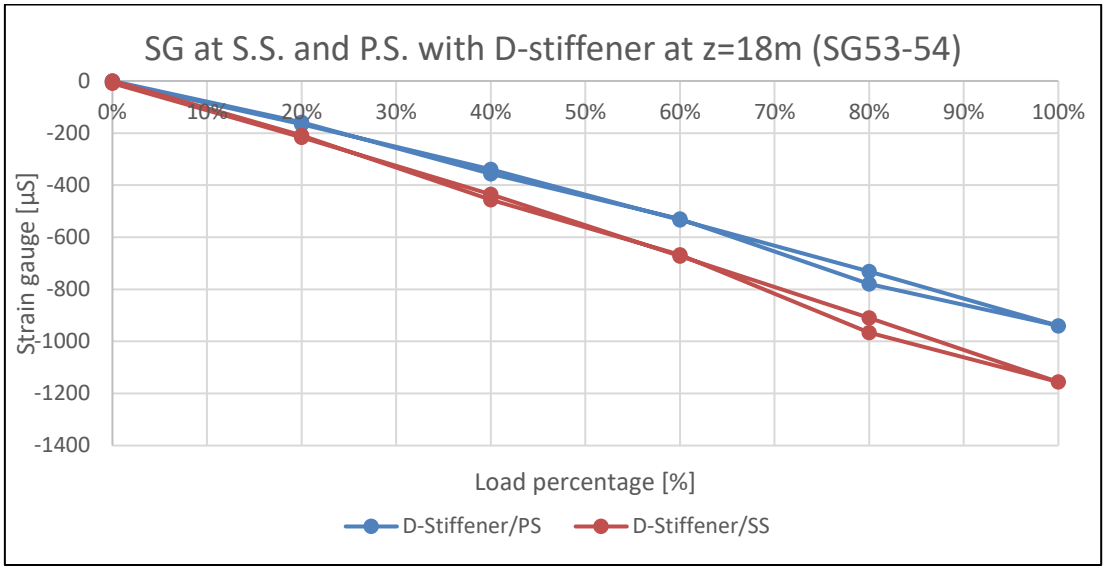

Figure 167: Strain gauges at the pressure and suction side, with D-stiffeners at z=18m

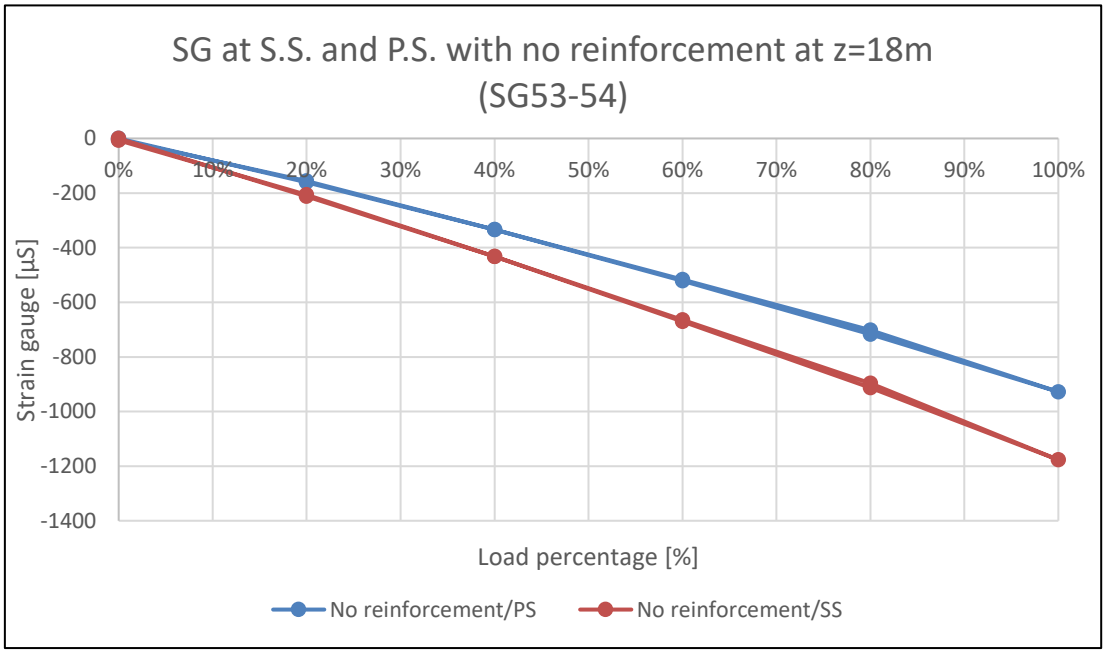

Figure 168: Strain gauges at the pressure and suction side, with No reinforcement at z=18m

Bladena
Universitetsparken 7
DK-4000 Roskilde
www.bladena.com

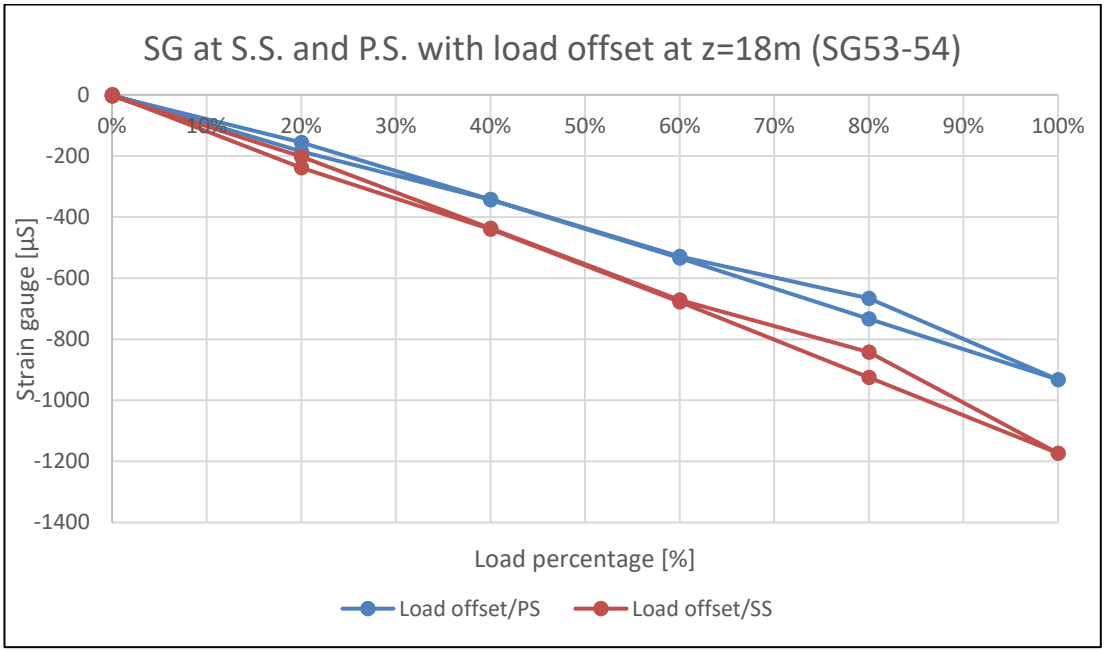

Figure 169: Strain gauges at the pressure and suction side, with load offset at z=18m

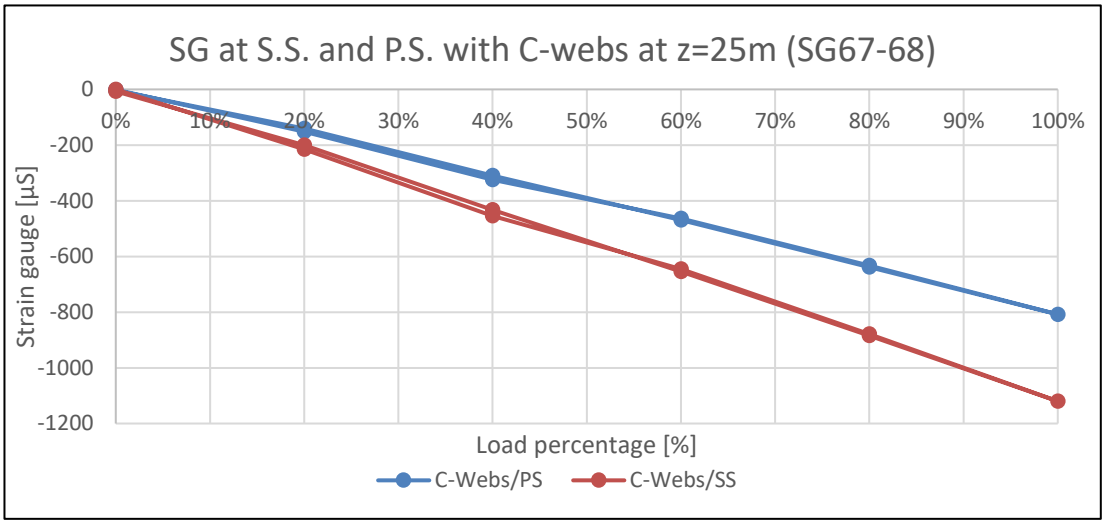

Figure 170: Strain gauges at the pressure and suction side, with C-webs at z=25m

Bladena
Universitetsparken 7
DK-4000 Roskilde
www.bladena.com

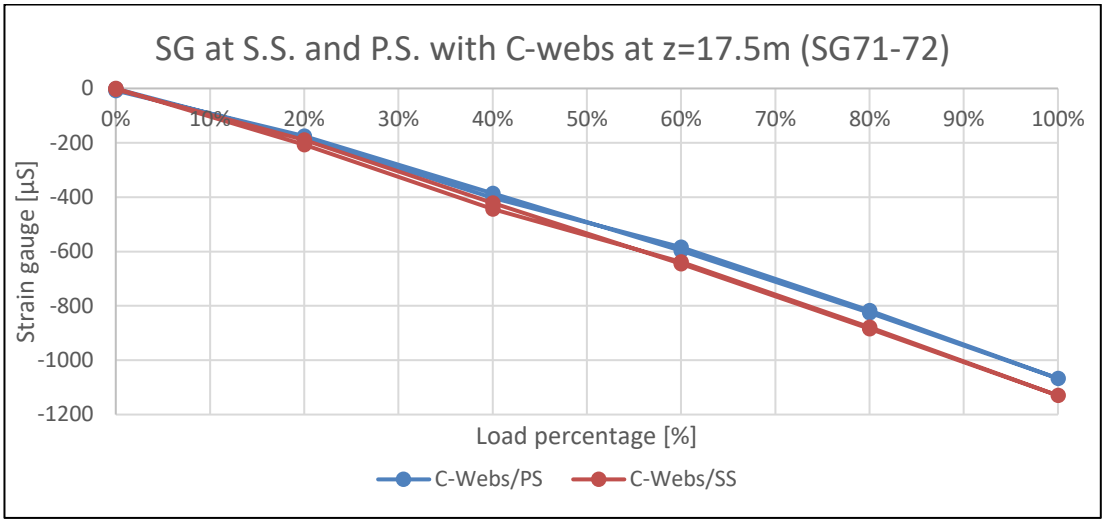

Figure 171: Strain gauges at the pressure and suction side, with C-webs at z=17.5m

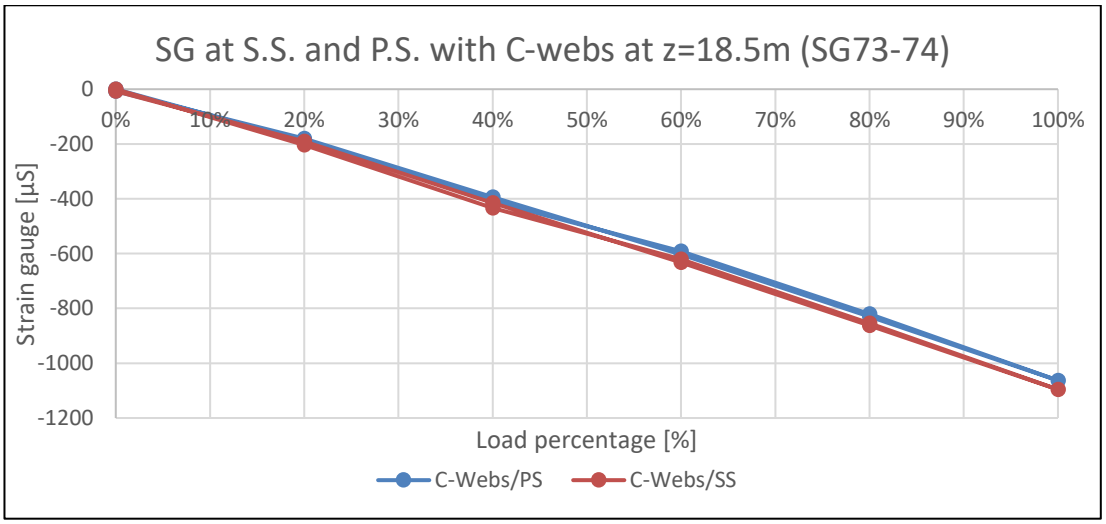

Figure 172: Strain gauges at the pressure and suction side, with C-webs at z=18.5m

Bladena
Universitetsparken 7
DK-4000 Roskilde
www.bladena.com

E6. Experiment photos

Table 17: Load offset positions

Original position	Offset position
Z=39m	
	
Z=44m	
	
Z = 49m	
	
Z = 55m	
	

Bladena
Universitetsparken 7
DK-4000 Roskilde
www.bladena.com

Figure 173: Blade root mounted on the test rig

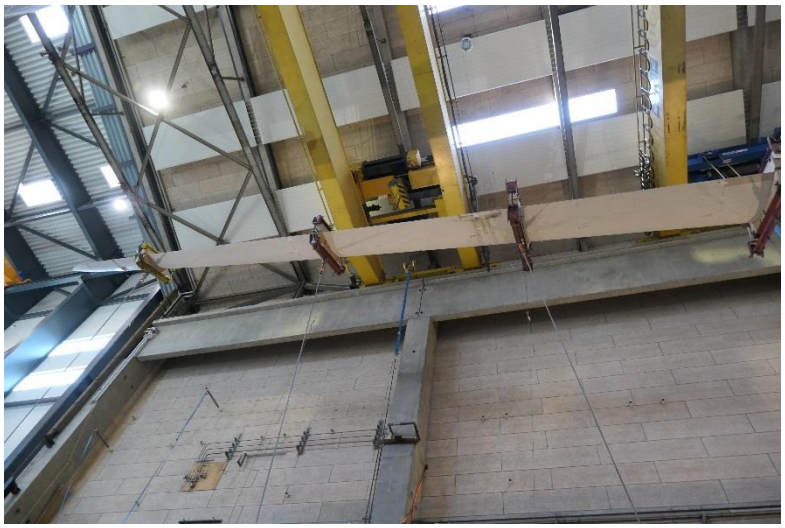

Figure 174: Steel wires applying the desired forces

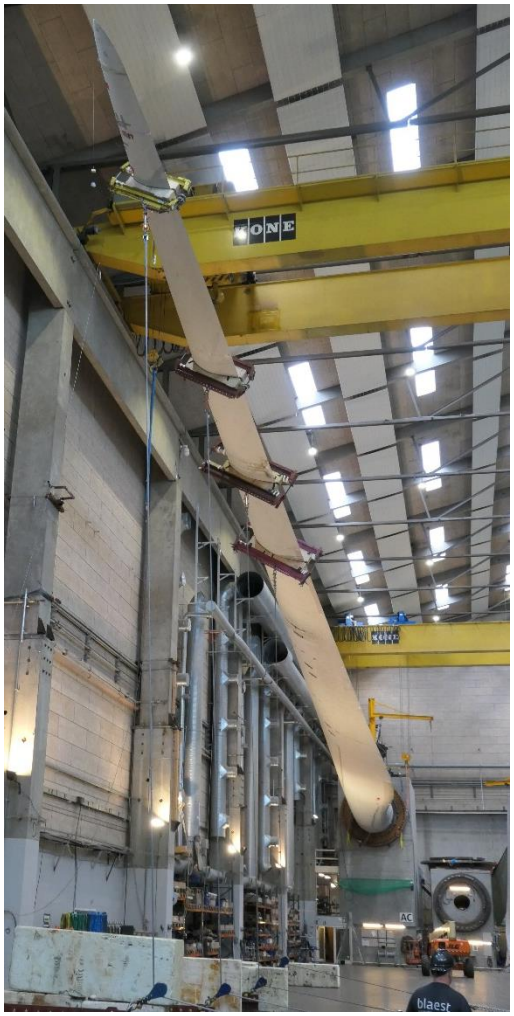

Figure 175: Experiment configuration

Bladena
Universitetsparken 7
DK-4000 Roskilde
www.bladena.com

Figure 176: Blade deflection under loading

Bladena
Universitetsparken 7
DK-4000 Roskilde
www.bladena.com